KINETIC INVESTIGATIONS OF HETEROGENEOUSLY CATALYZED REACTIONS ON THE Ru(001) AND Pt(110)-(1×2) SURFACES

Thesis by
Yongkui Sun

In Partial Fulfillment of the Requirements
for the Degree of
Doctor of Philosophy

California Institute of Technology
Pasadena, California 91125

1989

(Submitted September 20, 1989)

To my family.

Acknowledgments

Coming to the United States to study at Caltech is one of most important and most memorable experiences in my life. I am grateful to Professors Tian Zhaowu and Cai Qirui, and the late Professor Earl Muetterties, for encouraging me to apply and recommending me to Caltech. I am also grateful to Boning, Paula, Jim Engstrom, Roxy, Travis, Jim Stoos, Pat and John, whose help and friendship made the first few months of my stay at Pasadena much easier. I remember clearly when Jim Stoos told me about the nitty-gritty of the banking systems here and showed me how to write my first personal check; and when Paula and Pat celebrated my first birthday in the United States the night before the Placement Examination.

I would like to express my most sincere gratitude to my research advisor, Henry Weinberg, for his valuable advice on my research, and for his time and patience (Thank Buddha!) in critical reading of all my scientific manuscripts over the years. His comments on my manuscripts have not only made my technical papers more presentable and helped improve my English proficiency, but also stimulated me to think more and gain more insight into the science of surface chemistry.

It has been a pleasure to work with John Vajo and Wilman Tsai, both of them offered me a great deal of help when I first started my research projects. I would like to thank John Vajo in particular for being a collaborator as well as a good friend. We often shared ideas and had stimulating discussions on research, as well as on other things. I have also enjoyed numerous discussions with Buddie Mullins on varieties of subjects. He has also been a good friend whom I can always trust and turn to for advice, both professional and personal. Playing table tennis with John Parmeter, and softball with Dale Johnson, were as enjoyable as discussing science with them. Chunyu Chan and Tom Jachimowski assisted me in a number of projects, for which I am grateful. Over the years I have had the pleasure of

interacting with other members of Weinberg's research group: Hway-Chuan Kang, Youqi Wang, Jim Engstrom, Brad Anton, Brian Toby, Greg Gajda, Steve George, Udo Schwalke, Eric Hood, Jenna Zinck, Malina Hills and Phil Szuromi, from whom I have learned much in one way or another.

I owe much to many others at Caltech, including Kathy Lewis, Chic Nakawatase, Tony Stark, Guy Duremberg, John Yehle, Tom Dunn, Gabor Faludi, and Dave Malerba for their assistance that was necessary for the completion of this thesis; and also to Tony Skjellum, who helped me on quite a few occasions, debugging computer programs.

Many thanks are also due to all my friends outside Caltech, who have made my life in Pasadena more enjoyable. Most of all I would like to thank Lily for her friendship, understanding and support, and for the fun and joy we have shared over the past four years. At a moment like this I can not help remembering my high school math teacher, Li Mingru, and physics teacher, Fan Huizhen, who introduced me to the fascinating world of science, to them I am most grateful. Finally, I would like to thank my parents, and both brothers, for their love and constant encouragement, and I dedicate this thesis to them.

Abstract

The initial probabilities of activated, dissociative chemisorption of methane and ethane on Pt(110)-(1×2) have been measured. The surface temperature was varied from 450 to 900 K with the reactant gas temperature constant at 300 K. Under these conditions, we probe the kinetics of dissociation via trapping-mediated (as opposed to 'direct') mechanism. It was found that the probabilities of dissociation of both methane and ethane were strong functions of the surface temperature with an apparent activation energies of 14.4 kcal/mol for methane and 2.8 kcal/mol for ethane, which implys that the methane and ethane molecules have fully accommodated to the surface temperature. Kinetic isotope effects were observed for both reactions, indicating that the C-H bond cleavage was involved in the rate-limiting step. A mechanistic model based on the trapping-mediated mechanism is used to explain the observed kinetic behavior. The activation energies for C-H bond dissociation of the thermally accommodated methane and ethane on the surface extracted from the model are 18.4 and 10.3 kcal/mol, respectively.

The studies of the catalytic decomposition of formic acid on the Ru(001) surface with thermal desorption mass spectrometry following the adsorption of DCOOH and HCOOH on the surface at 130 and 310 K are described. Formic acid (DCOOH) chemisorbs dissociatively on the surface via both the cleavage of its O-H bond to form a formate and a hydrogen adatom, and the cleavage of its C-O bond to form a carbon monoxide, a deuterium adatom and an hydroxyl (OH). The former is the predominant reaction. The rate of desorption of carbon dioxide is a direct measure of the kinetics of decomposition of the surface formate. It is characterized by a kinetic isotope effect, an increasingly narrow FWHM, and an upward shift in peak temperature with θ_T, the coverage of the dissociatively adsorbed formic acid. The FWHM and the peak temperature change from 18 K and 326 K at $\theta_T = 0.04$ to

8 K and 395 K at $\theta_T = 0.89$. The increase in the apparent activation energy of the C-D bond cleavage is largely a result of self-poisoning by the formate, the presence of which on the surface alters the electronic properties of the surface such that the activation energy of the decomposition of formate is increased. The variation of the activation energy for carbon dioxide formation with θ_T accounts for the observed sharp carbon dioxide peak. The coverage of surface formate can be adjusted over a relatively wide range so that the activation energy for C-D bond cleavage in the case of DCOOH can be adjusted to be below, approximately equal to, or well above the activation energy for the recombinative desorption of the deuterium adatoms. Accordingly, the desorption of deuterium was observed to be governed completely by the desorption kinetics of the deuterium adatoms at low θ_T, jointly by the kinetics of deuterium desorption and C-D bond cleavage at intermediate θ_T, and solely by the kinetics of C-D bond cleavage at high θ_T. The overall branching ratio of the formate to carbon dioxide and carbon monoxide is approximately unity, regardless the initial coverage θ_T, even though the activation energy for the production of carbon dioxide varies with θ_T. The desorption of water, which implies C-O bond cleavage of the formate, appears at approximately the same temperature as that of carbon dioxide. These observations suggest that the cleavage of the C-D bond and that of the C-O bond of two surface formates are coupled, possibly via the formation of a short-lived surface complex that is the precursor to to the decomposition.

The measurement of steady-state rate is demonstrated here to be valuable in determining kinetics associated with short-lived, molecularly adsorbed precursor to further reactions on the surface, by determining the kinetic parameters of the molecular precursor of formaldehyde to its dissociation on the Pt(110)-(1×2) surface.

Overlayers of nitrogen adatoms on Ru(001) have been characterized both by thermal desorption mass spectrometry and low-energy electron diffraction, as well as chemically via the postadsorption and desorption of ammonia and carbon monoxide.

The nitrogen-adatom overlayer was prepared by decomposing ammonia thermally on the surface at a pressure of 2.8×10^{-6} Torr and a temperature of 480 K. The saturated overlayer prepared under these conditions has associated with it a $(\frac{\sqrt{247}}{10} \times \frac{\sqrt{247}}{10})R22.7^\circ$ LEED pattern, has two peaks in its thermal desorption spectrum, and has a fractional surface coverage of 0.40. Annealing the overlayer to approximately 535 K results in a rather sharp $(\sqrt{3} \times \sqrt{3})R30^\circ$ LEED pattern with an associated fractional surface coverage of one-third. Annealing the overlayer further to 620 K results in the disappearance of the low-temperature thermal desorption peak and the appearance of a rather fuzzy p(2×2) LEED pattern with an associated fractional surface coverage of approximately one-fourth. In the low coverage limit, the presence of the $(\sqrt{3} \times \sqrt{3})R30^\circ$-N overlayer alters the surface in such a way that the binding energy of ammonia is increased by 20% relative to the clean surface, whereas that of carbon monoxide is reduced by 15%.

A general methodology for the *indirect* relative determination of the absolute fractional surface coverages has been developed and was utilized to determine the saturation fractional coverage of hydrogen on Ru(001). Formaldehyde was employed as a bridge to lead us from the known reference point of the saturation fractional coverage of carbon monoxide to unknown reference point of the fractional coverage of hydrogen on Ru(001), which is then used to determine accurately the saturation fractional coverage of hydrogen. We find that $\theta_{\mathrm{H}}^{sat} = 1.02\ (\pm 0.05)$, *i.e.*, the surface stoichiometry is $\mathrm{Ru} : \mathrm{H} = 1 : 1$. The relative nature of the method, which cancels systematic errors, together with the utilization of a glass envelope around the mass spectrometer, which reduces spurious contributions in the thermal desorption spectra, results in high accuracy in the determination of absolute fractional coverages.

TABLE OF CONTENTS

Chapter 1.

Introduction

The quest for gaining the ability to control the activity and the selectivity of solid surfaces towards chemical transformations of molecules on the solid surfaces has been motivating surface scientists to probe kinetics, dynamics and mechanisms of gas-solid interactions in ever more precise details (**1-5**). The activity and selectivity of a surface for a chemical reaction are ultimately dictated by the multi-dimensional potential energy surface that describes the gas-solid interaction in quantum mechanical details, which up to now remains as 'black box' due to its extreme complexity. The reactivity of a surface reaction, one important output of the 'black box,' can be expressed as a function of a set of input variables, both macroscopic and microscopic ones. Examples of these variables are surface and gas temperatures, reactant pressure, translational and internal energies of the incident molecules, angle of incidence and orientation of the incident molecules, the surface geometric and electronic structures, and the modification of them due to electronegative and electropositive adsorbates. Over the years with the advent of new technologies for surface scientists, the understanding of the gas-solid chemical interactions progresses significantly as one becomes able to control precisely, and measure changes in reactivity and selectivity caused by variation of, more and more of these variables, especially the microscopic ones.

Kinetic measurement, both transient and steady state, has been and remaines as one of the most powerful means of probing the nature of the chemical interactions between gas-phase molecules and surfaces and assessing effects of the input variables on the reactivity and selectivity of the surface reaction. Kinetic information concerning the most fundamental and technologically important surface processes obtained on well-characterized transition metal surfaces, including atomically flat, atomically rough, stepped and kinked, and adsorbate-modified surfaces, has provided us with tremendous insights into the mechanisms of the chemical transformations on the surfaces, and sheds light on the factors that affect the activity and selectivity of various catalysts. The latter is of extreme significance since the control of these factors is the ultimate goal of the heterogeneous catalysis. Some of these most fundamental and technologically important surface chemical reactions are dissociative chemisorption of nitrogen (**6-8**) and methane (**3**), oxidation of carbon monoxide (**1, 2**), reduction of nitric oxide (**9**), oxidation of hydrogen (**10**), and methanation from carbon monoxide and hydrogen (**11**).

The activity and selectivity of a transition metal surface toward a surface chemical reaction can be strongly altered by the geometric structure of surface, such as the dissociative chemisorption of nitrogen on the low-index surfaces of tungsten (**7**) and hydrogenolysis of alkanes on nickel surfaces (**4**). On the other hand, certain reactions are surface-structure insensitive, such as the methanation reaction of hydrogen and carbon monoxide on nickel surfaces (**4**). Surface additives, both electropositive (**12**) and electronegative (**13**), can alter dramatically the activity and selectivity of a transition metal surface, resulted from both geometric blocking of specific binding or reaction sites and modification of the electronic structures of the catalytic surfaces. The potential energy surface that describes the interaction of gas phase molecules and the surface is modified by the presence of the surface additives in such a way that the activation energy of the desired reaction is either lowered or increased. Accordingly, the reaction is said to be promoted or poisoned by the additives. Often the surface species generated *during* a catalytic surface reaction are found to influence profoundly the selectivity of the surface. For instance, acetic acid undergoes both dehydration that leads to the formation carbon monoxide and water and dehydrogenation that leads to the formation of carbon dioxide and hydrogen on a initailly clean platinum polycrystalline wire (**14**). The reactions deposits atomic carbon on the surface. As the surface carbon adatoms build up, the reaction the leads to the formation of carbon dioxide and carbon monoxide becomes gradually poisoned. It comes finally to a stop, while another reaction pathway, the dehydration of the acetic acid to produce ketene and water is activated, as the surface is covered by a monolayer of carbon (**14**).

This thesis, which describes kinetic investigations of mechansims of chemically catalyzed reactions on the atomically flat, close-packed (001) surface of ruthenium and highly corrugated, reconstructed (110)-(1×2) surface of platinum, is basically composed of three sections, each of which aims at an understanding of different, but closely related aspects of the heterogeneous catalysis.

The first section consists of Chapter 2 in which the kinetics of the trapping-mediated, activated dissociative chemisorption of methane and ethane on the Pt(110)-(1×2) surface are examined. The mechanisms by which a gas molecule dissociatively chemisorbs on a surface are often classified into two types, namely, trapping-mediated and direct mechanisms. In the trapping-mediated mechanism, the gas molecules lose a sufficient fraction of their incident kinetic energy to become trapped and thermally accommodated to the surface temperature. The trapped molecules can either desorb back into gas phase, or they can locate a minimum barrier in the potential energy surface and chemisorb. In the case of methane and ethane on the Pt(110)-(1×2) surface, the trapped molecules may be considered to be physically adsorbed, and the chemisorption is dissociative involving C-H bond cleavage. The observed probability of dissociative chemisorption is a convolution of a dynamical factor (the trapping probability) and a kinetic factor (the relative rates of dissociation vs. desorption from the physically adsorbed state). The former decreases precipitously with increasing incident translational energy (or gas "temperature") (**15**) but is a rather weak function of the surface temperature (**16, 17**). The latter can be rather sensitive to the surface temperature, depending upon the energetics associated with the two competing pathways for the trapped molecules (**5**). The rate associated with the direct mechanism, however, is not a strong function of the surface temperature. The overall rate of dissociative chemisorption can be expressed as the sum of a trapping-mediated component and a direct component. Depending upon the reaction conditions, one of the two components may be dominant in the overall rate, making it possible to investigate the kinetics and dynamics of the two reaction channels separately. In this case, the pressures of the reactants were so chosen that the gas temperature was maintained at 300 K whereas the surface temperature was varied, in order to probe the kinetics of the dissociative chemisorption via trapping-mediated mechanism. Note that in the case where the temperature of the reactant changes in unison with the surface temperature, not only the component via the direct mechanism would increase but also would the trapping probability of the reactant decrease when the surface temperature is increased, making the analysis of the overall probability of dissociation much more complicated.

Chapters 3 through 8 constitute the second section of this thesis. It describes kinetic and mechanistic studies of reactions of small oxygen-containing organic molecules, formic acid and formaldehyde in particular, on the Ru(001) and Pt(110)-(1×2) surfaces and a couple of applications resulted from these studies. Formic acid reacts on Ru(001) via two pathways, dehydration and dehydrogenation. The decomposition of formic acid is a convenient model catalytic system for studying the kinetics and mechansim of a *branching* reaction on surfaces. Both steady-state and transient decomposition rates were measured for isotopically labeled and non-labeled formic acid, to establish a reaction mechanism in terms of elementary surface reactions. When a decomposition reaction reaches steady state at sufficiently high surface temperature, surface processes such as desorption of reaction products become so fast that they disappear from the overall rate expression. The rate becomes dictated by the kinetics associated with the molecular precursor to its decomposition. This provides us with means of measuring the kinetic parameters associated with the elementary reaction of the molecular precursor, which are often too difficult to be obtained due to its extremely low concentration on the surface. An application of this principle is demonstrated for the decomposition of formaldehyde on the Pt(110)-(1×2) surface, in which kinetic parameters associated with the elementary reaction of molecularly adsorbed formaldehyde are obtained.

Finally, characterizations of surface overlayers of hydrogen and nitrogen adatoms on Ru(001) are the subject of the third section which consists of Chapters 9 and 10. Hydrogen adatoms are involved in numerous numbers of important catalytic reactions. In spite of the large number of studies concerning hydrogen adsorption on the Ru(001) surface, the fundamental question of what is the absolute saturation fractional coverage of hydrogen adatoms is yet to be answered accurately and unambiguously. The coverage obtained with traditional means has associated with it, a large uncertainty. A general methodology for the *indirect* relative determination of the absolute fractional coverage is described in this section and applied in the case of hydrogen on Ru(001). The absolute fractional coverage of hydrogen is determined *accurately* to be unity, *i.e*, one atomic hydrogen per ruthenium atom. This implies that half of the three-fold sites on the surface are empty at saturation. These three-fold sites stop to be populated either due to an altered kinetics of hydrogen dissociation by the presence of hydrogen adatoms on the surface in such a way that the dissociation stops, or due to unfavorable energetics of populating the other half of the three-fold sites on the surface. Which is the case remains to be determined.

To describe fully the kinetics of a surface catalytic reaction, one must take into account effects of various reaction-generated surface species, on the kinetic parameters of adsorption and desorption of reactants and products, as well as elementary steps involved in the overall reaction. Nitrogen adatoms was found to be the most abundant surface species in a number of industrially important catalytic reactions including ammonia synthesis, nitric oxide reduction and the synthesis of hydrogen cyanide. Despite its importance, little is known concerning the nature of its overlayers on Ru(001) including the chemical effects on the chemisorptive properties on the Ru(001) surface. In this section is described a characterization of overalyers of nitrogen with thermal desorption mass spectrometry, low-energy electron diffraction, as well as chemical probes such as the postadsorption and desorption of carbon monoxide and ammonia, which interact qualitatively differently with the surface.

REFERENCES

1. G. Ertl, in *Solvay Conference on Surface Science*, eds., F. W. de Wette, Springer-Verlag, Heidelberg, 1988, p. 322.
2. G. Ertl, in *Catalysis Science and Technology*, eds., J. R. Anderson and M. Boudart, Vol. 4, Springer-Verlag, New York, 1983, p. 209.
3. G. Ehrlich, in *Chemistry and Physics of Solid Surfaces*, eds., R. Vanselow and R. F. Howe, Springer-Verlag, Heidelberg, 1988, p. 1.
4. D. W. Goodman and J. E. Houston, *Science* **236**, 403 (1987).
5. W. H. Weinberg, in *Kinetics of Interface Reactions*, eds., M. Grunze and H. J. Kreuzer, Springer-Verlag, Heidelberg, 1987, p. 94.
6. G. Ertl, S. B. Lee and M. Weiss, *Surface Sci.* **114**, 515 (1982).
7. J. Lee, R. J. Madix, J.E. Schlaegel and D. J. Auerbach, *Surface Sci.* **143**, 626 (1984), and references therein.
8. C. T. Rettner, H. Stein and E. H. Schweizer, *J. Chem. Phys.* **89**, 3337 (1988).
9. E. F. Egelhoff, Jr., in *The Chemical Physics of Solid Surfaces and Heterogeneous Catalysis*, eds., D. A. King and D. P. Woodruff, Vol. 4, Elsevier, Amsterdam, Oxford, 1982, p. 397.
10. P. R. Norton, in *The Chemical Physics of Solid Surfaces and Heterogeneous Catalysis*, eds., D. A. King and D. P. Woodruff, Vol. 4, Elsevier, Amsterdam, Oxford, 1982, p. 27.
11. R. D. Kelley and D. W. Goodman, in *The Chemical Physics of Solid Surfaces and Heterogeneous Catalysis*, eds., D. A. King and D. P. Woodruff, Vol. 4, Elsevier, Amsterdam, Oxford, 1982, p. 427.
12. H. P. Bonzel, *Surface Sci. Reports* **8**, 43 (1988).
13. M. P. Kiskinova, *Surface Sci. Reports* **8**, 359 (1987).
14. J. J. Vajo, Y. -K. Sun and W. H. Weinberg, *J. Phys. Chem.* **91**, 1153 (1987).

15. C. T. Rettner, E. K. Schweizer and C. B. Mullins, *J. Chem. Phys.* **90**, 3800 (1989).

16. C. T. Rettner, H. Stein and E. H. Schweizer, *J. Chem. Phys.* **89**, 3337 (1988).

17. C. T. Rettner, E. H. Schweizer, H. Stein and D. J. Auerbach, *Phys. Rev. Letters* **61**, 986 (1988).

CHAPTER 2.

Kinetics of Dissociative Chemisorption of Methane and Ethane on Pt(110)-(1×2)

[This chapter consists of an article coauthored with W. H. Weinberg]

ABSTRACT

The initial probability of dissociative chemisorption P_r of methane and ethane on the highly corrugated, reconstructed Pt(110)-(1×2) surface has been measured in a microreactor by counting the number of carbon atoms on the surface following the reaction of methane and ethane on the surface which was held at various constant temperatures between 450 and 900 K during the reaction. Methane dissociatively chemisorbs on the Pt(110)-(1×2) surface with an apparent activation energy of 14.4 kcal/mol and an apparent preexponential factor of 0.6. Ethane chemisorbs dissociatively with an apparent activation energy of 2.8 kcal/mol and an apparent preexponential factor of 4.7×10^{-3}. Kinetic isotope effects were observed for both reactions. The fact that P_r is a strong function of surface temperature implies that the dissociation reactions proceed via a trapping-mediated mechanism. A model based on a trapping-mediated mechanism is used to explain the observed kinetic behavior. Kinetic parameters for C-H bond dissociation of the thermally accommodated methane and ethane are extracted from the model.

1. INTRODUCTION

The dissociative chemisorption of a gas-phase molecule on a solid surface is a complicated process that occurs on a multi-dimensional potential energy surface. The mechanisms by which a gas molecule dissociatively chemisorbs on a surface are often classified into two types, namely, trapping-mediated and direct mechanisms (**1-5**). In the trapping-mediated mechanism, the gas molecules lose a sufficient fraction of their incident kinetic energy to become trapped and thermally accommodated to the surface temperature. The trapped molecules can either desorb back into gas phase, or they can locate a minimum barrier in the potential energy surface and chemisorb. In the case of methane and ethane on the Pt(110)-(1×2) surface, the trapped molecules may be considered to be physically adsorbed, and the chemisorption is dissociative involving C-H bond cleavage. The observed probability of dissociative chemisorption is a convolution of a dynamical factor (the trapping probability) and a kinetic factor (the relative rates of dissociation vs. desorption from the physically adsorbed state). The former decreases precipitously with increasing incident translational energy (or gas "temperature") (**5, 6**) but is a rather weak function of the surface temperature (**4**). The latter can be rather sensitive to the surface temperature, depending upon the energetics associated with the two competing pathways for the trapped molecules (**2**). The rate associated with the direct mechanism, however, is not a strong function of the surface temperature. The overall rate of dissociative chemisorption can be expressed as the sum of a trapping-mediated component and a direct component. Depending upon the reaction conditions, one of the two components may be dominant in the overall rate, making it possible to investigate the kinetics and dynamics of the two reaction channels separately. This has been demonstrated explicitly for the dissociative chemisorption of nitrogen on the W(100) surface (**4**) and ethane on the

Ir(110)-(1×2) surface (**5**).

The activation of C-H bonds in alkanes for subsequent functionalization is an extremely important chemical process. An understanding of the chemical interactions of methane and ethane, the two simplest alkanes, with initially clean transition metal surfaces is likewise very important. While there have been a number of molecular beam investigations of the direct, dissociative chemisorption of methane on a variety of transition metal surfaces including W(110) (**7**), Ir(110)-(1×2) (**8, 9**), Pt(111) (**10, 11**), Ni(111) (**12**) and Ni(110) (**13**), less work has been concerned with dissociative chemisorption on well-characterized surfaces via the trapping-mediated mechanism (**14**). The goal of the work reported here is to measure the probability of dissociative chemisorption of methane and ethane via the trapping-mediated mechanism and to interpret the results microscopically.

2. EXPERIMENTAL DETAILS

The experiments were performed in a microreactor that has been described previously (**15, 16**). The microreactor has a volume of 30 cm^3 and is connected to an ion-pumped UHV chamber which has a base pressure of 3×10^{-10} Torr. The reactant pressures were measured by a Baratron gauge. Both sides of the Pt(110) crystal were polished and the surfaces were cleaned initially by argon ion sputtering *in situ* in the microreactor. The (110) surface has a total area of 0.8 cm^2 (both sides). Two high purity platinum wires (0.010 in. in diameter and 0.2 in. in length) were spot welded to the edge of the crystal and were clamped onto two 0.24-cm-diameter copper leads that support the crystal and allow it to be heated resistively. The temperature of the crystal was measured with a 0.003-in.-diameter W-5% Re/W-26% Re thermocouple, which was spot welded to the crystal. The crystal was cleaned between experiments by heating to 950 K for 5 min in 5×10^{-4} Torr of O_2 flowing through the microreactor, and subsequently in 5×10^{-4} Torr of

H_2 for another 5 min to remove surface oxygen. Thermal desorption spectra of CO from the surface are in good agreement with the previously published ones (**17**), verifying the validity of our cleaning procedures.

The microreactor was operated in a batch mode when studying the dissociation of methane ($^{13}CH_4$) on Pt(110)-(1×2) at low surface temperatures ($\leq$ 740 K), since the probability of dissociative chemisorption is very low. In this mode the crystal was held at a constant temperature, and a methane "pressure jump" was created by rapidly opening and then closing the inlet valve. The transient part of the pressure profile is shorter than five seconds, which is less than 15% of the *minimum* batch reaction time. Thus we have a well-defined reaction condition (i.e., surface temperature and reactant pressure). The methane was allowed to react in the sealed reactor for a period of time τ, followed by immediate cooling of the crystal and pump-out of the contents of the reactor. The number of carbon-13 adatoms on the surface N_c, which is directly proportional to the probability of dissociation, was determined by counting the number of $^{13}CO_2$ molecules mass spectrometrically during oxygen titration of the carbon-13 adatoms. No ^{13}CO was observed under the titration conditions. The pressure of methane and the value of τ were chosen in a such way that the coverage of carbon-13 adatoms is above the detection limit of the titration method and below 10% of a monolayer. The initial probability of dissociative chemisorption at a surface temperature T, P_r(T), was calculated by extrapolation to zero-carbon coverage using the following relation

$$P_r(T) = \frac{N_c}{n\tau F}, \tag{1}$$

where n is the number of carbon atoms in the reactant molecule, and F is the impingement rate of reactant molecules.

For the dissociative chemisorption of methane at high surface temperatures ($>$ 740 K) and ethane in the entire temperature range studied (345 to 715 K), the experimental procedure was the same as that described above except that the reactor was operated in a flow mode in which the reactant continuously flows through the reactor for a period of time τ at a flow rate that is much greater than the reaction rate in order to maintain low conversions of methane (at a pressure of approximately 1×10^{-4} Torr) and ethane (at a pressure of 5×10^{-6} Torr) in the reactor. Unlabeled ethane (C_2H_6) rather than carbon-13 labeled ethane was used since it was found in the experiments with the carbon-13 labeled methane that the signal of $^{12}CO_2$ due to oxidation of background CO is negligibly small compared with that of $^{13}CO_2$. Hence the carbon labeling was not necessary.

Both the carbon-13 labeled methane ($^{13}CH_4$, 99 atom $\%^{13}C$) and deuterated methane (CD_4, 99 atom %D) were obtained from Icon Services, the ethane (C_2H_6, 99.99%) from Matheson, and the deuterated ethane (C_2D_6, 98 atom %D) from Cambridge Isotopes. All gases were manipulated in a gas manifold that was pumped by a diffusion pump and had a base pressure below 1×10^{-7} Torr.

3. RESULTS AND DISCUSSION

The logarithm of the measured initial probability of dissociative chemisorption P_r of $^{13}CH_4$ on the Pt(110)-(1×2) surface is plotted as a function of reciprocal surface temperature in Fig. 1, where P_r is represented by filled circles. The diagram is divided into three different regimes (by the two vertical dashed lines), i.e., low- (below 510 K), intermediate- (510 to 740 K) and high-temperature (above 740 K) regimes. In the low-temperature regime, P_r increases with increasing surface temperature more rapidly than it does in the intermediate surface temperature regime. In the high-temperature regime, P_r first levels off and then decreases slightly with increasing surface temperature. Only in the intermediate-temperature regime is P_r the true initial dissociative chemisorption probability of $^{13}CH_4$ on the Pt(110)-(1×2) surface. In the low-temperature regime, the measured value of P_r is decreased due to adsorption of CO from the background, and in the high-temperature regime it is decreased due to the diffusion of carbon into the bulk of the platinum (**16**). Taking into account appropraite corrections for these processes caused all data to agree with those measured at intermediate-temperatures, cf. Fig. 1. The slope of the straight line in Fig. 1 corresponds to an apparent activation energy of 14.4 kcal/mol and an apparent preexponential factor of 0.6, i.e., we find

$$P_r = k_{app}^{(0)} e^{-E_{app}/k_B T}, \tag{2}$$

where $k_{app}^{(0)} = 0.6$ and $E_{app} = 14.4$ kcal/mol.

The initial probability of dissociative chemisorption of CD_4 was also measured and was found to be consistently lower than that of $^{13}CH_4$. Assuming the same value of the preexponential factor as for $^{13}CH_4$, the apparent activation energy for the dissociative chemisorption of CD_4 is 15.6 kcal/mol. (**16**). The observation of this kinetic isotope effect is expected since C-H bond cleavage is the rate-limiting step in the decomposition of the methane.

Ethane dissociates on the Pt(110)-(1×2) surface more readily than methane. The initial probability of dissociative chemisorption of C_2H_6 and C_2D_6 were measured at a pressure of 5×10^{-6} Torr. Since the reactant pressure was much lower than it was in the methane experiment, there is negligible background adsorption of CO in this case. The results of the measurements are shown in Fig. 2 in the form of an Arrhenius plot. The data are well-described by Eq. (2) with an apparent activation energy of 2.8 kcal/mol and an apparent preexponential factor of 4.7×10^{-3}. Deuterated ethane reacts on the surface with a rate that is approximately 2.5 times slower than that of C_2H_6, with an apparent activation energy of 3.5 kcal/mol and the same preexponential factor as that of C_2H_6.

Since all of the experiments were carried out at reactant pressures below 10^{-2} Torr, the temperature of the reactants should be nearly equal to the wall temperature of the reactor (approximately 300 K) rather than the surface temperature of the single crystal (**14**). The probability of direct, dissociative chemisorption of a Maxwell-Boltzmann gas of methane or ethane at 300 K is negligibly small compared to our measured values. Furthermore, the fact that P_r is a strong function of surface temperature and can be described by Eq. (2) indicates that the dissociation reactions are proceeding via a trapping-mediated mechanism. Consider, for example, the case of methane. A trapped methane molecule can either desorb or dissociate on the surface, i.e.,

$$\mathrm{CH_4(g)} \underset{\mathbf{k_d}}{\overset{\zeta\mathrm{F}}{\rightleftharpoons}} \mathrm{CH_4(a)}$$

$$\mathrm{CH_4(a)} \xrightarrow{\mathbf{k_r}} \mathrm{C(a)} + 2\mathrm{H_2(g)}.$$

Assuming a pseudo-steady state for $^{13}\mathrm{CH_4(a)}$, one finds that the probability of dissociation is given by (**2**)

$$P_r = \frac{\zeta k_r}{k_r + k_d}, \tag{3}$$

where ζ is a thermal average of the trapping probability of methane, and k_d and k_r are the rate coefficients of the two competing processes, i.e., desorption and reaction of the trapped methane molecules on the surface. Since $k_d \gg k_r$ for methane on the Pt(110)-(1×2) surface, Eq. (4) may be rewritten as

$$P_r \simeq \zeta \frac{k_r}{k_d}. \tag{4}$$

Assuming that both k_d and k_r are of the Arrhenius form $k_i^{(0)} e^{-E_i/k_B T}$ and that ζ is independent of the surface temperature (**4**), one would expect a straight line when $\ln P_r$ is plotted vs. 1/T with the slope being $-(E_r - E_d)/k_B$ and the intercept being $\ln(\zeta k_r^{(0)}/k_d^{(0)})$. Hence, our measured apparent activation energies for the dissociative chemisorption of methane (14.4 kcal/mol) and ethane (2.8 kcal/mol) represent the activation energy with respect to an energy zero that is the alkane in the gas phase. The activation energy with respect to the bottom of the physically adsorbed well E_r

is simply equal to the measured activation energy plus the activation energy for desorption E_d of the physically adsorbed alkane, i.e., $E_r = E_{app} + E_d$. Since the values of E_d for methane and ethane are approximately 4 and 7.5 kcal/mol, respectively (**16**), the values of E_r for methane and ethane on this surface are approximately 18.4 and 10.3 kcal/mol, respectively. Furthermore, if the preexponential factors of the desorption rate coefficients of methane and ethane from the physically adsorbed well are $10^{13}\ s^{-1}$ and ζ is taken to be unity (**5**), then the preexponential factors of the rate coefficients for dissociation on this surface are $6 \times 10^{12}\ s^{-1}$ for methane and $4.7 \times 10^{10}\ s^{-1}$ for ethane.

4. SUMMARY

The initial probabilities of dissociative chemisorption of methane and ethane on the highly corrugated, reconstructed Pt(110)-(1×2) surface have been measured. The surface temperature was varied with the reactant gas temperature maintained constant at 300 K. Under these conditions we probed the kinetics of trapping-mediated dissociation. Dissociative chemisorption is activated for both methane with an apparent activation energy of 14.4 kcal/mol, and ethane with an apparent activation energy of 2.8 kcal/mol. These activation energies are measured with respect to the alkane in the gas phase. The activation energies measured with respect to the bottom of the physically adsorbed well (i.e., the activation energies of the elementary surface reactions) are approximately 18.4 kcal/mol for methane and 10.3 kcal/mol for ethane.

Acknowledgment: This work was supported by the Office of Basic Energy Sciences of the Department of Energy (Grant DE-FG03-89ER14048). Additional support was provided by the Donors of the Petroleum Research Fund of the American Chemical Society (Grant PRF 19819-AC5-C).

REFERENCES

1. P. Kisliuk, *J. Phys. Chem. Solids* **3**, 95 (1957); **5**, 78 (1958).
2. W. H. Weinberg, in *Kinetics of Interface Reactions*, Eds., M. Grunze and H. J. Kreuzer, Springer-Verlag, Heidelberg, 1987, p. 94.
3. S. G. Brass and G. Ehrlich, *J. Chem. Phys.* **87**, 4285 (1987).
4. (a) C. T. Rettner, H. Stein and E. H. Schweizer, *J. Chem. Phys.* **89**, 3337 (1988).

   (b) C. T. Rettner, E. H. Schweizer, H. Stein and D. J. Auerbach, *Phys. Rev. Letters* **61**, 986 (1988).
5. C. B. Mullins and W. H. Weinberg, *J. Chem. Phys.* (submitted).
6. C. T. Rettner, E. K. Schweizer and C. B. Mullins, *J. Chem. Phys.* **90**, 3800 (1989).
7. C. T. Rettner, H. E. Pfnür and D. J. Auerbach, *Phys. Rev. Letters* **25**, 2716 (1985).
8. A. V. Hamza, H. -P. Steinrück and R. J. Madix, *J. Chem. Phys.* **86**, 6506 (1987).
9. C. B. Mullins and W. H. Weinberg, to be published.
10. G. R. Schoofs, C. R. Arumainayagam, M. C. McMaster and R. J. Madix, *Surface Sci.* **215**, 1 (1989).
11. A. C. Luntz and D. S. Bethune, *J. Chem. Phys.* **90**, 1274 (1989).
12. M. B. Lee, Q. Y. Yang and S. T. Ceyer, *J. Chem. Phys.* **87**, 2724 (1987).
13. A. V. Hamza and R. J. Madix, *Surface Sci.* **179**, 25 (1987).
14. T. M. Beebe, Jr., D. W. Goodman, B. D. Kay and J. T. Yates, Jr., *J. Chem. Phys.* **87**, 2305 (1987).
15. J. J. Vajo, W. Tsai and W. H. Weinberg, *Rev. Sci. Instrum.* **56**, 1439 (1985).
16. Y. -K. Sun and W. H. Weinberg, to be published.

17. C. M. Comrie and R. M. Lambert, *J. Chem. Soc. Faraday Trans. I* **72**, 325 (1975).

Figure Captions

Fig. 1: Arrhenius plot of the apparent initial dissociative chemisorption probability, P_r^{app} (●), of $^{13}CH_4$ on the Pt(110)-(1×2) surface. Two vertical dashed lines divide the diagram into three different regimes. The solid line is a fit to the data in the intermediate temperature regime with $E_{app} = 14.4$ kcal/mol. The data at both low and high temperatures fall on this same line when suitably corrected (see text).

Fig. 2: Arrhenius plot of the initial dissociative chemisorption probability of C_2H_6 (●) and C_2D_6 (○) on Pt(110)-(1x2). The apparent activation energies are 2.8 and 3.5 kcal/mol, respectively.

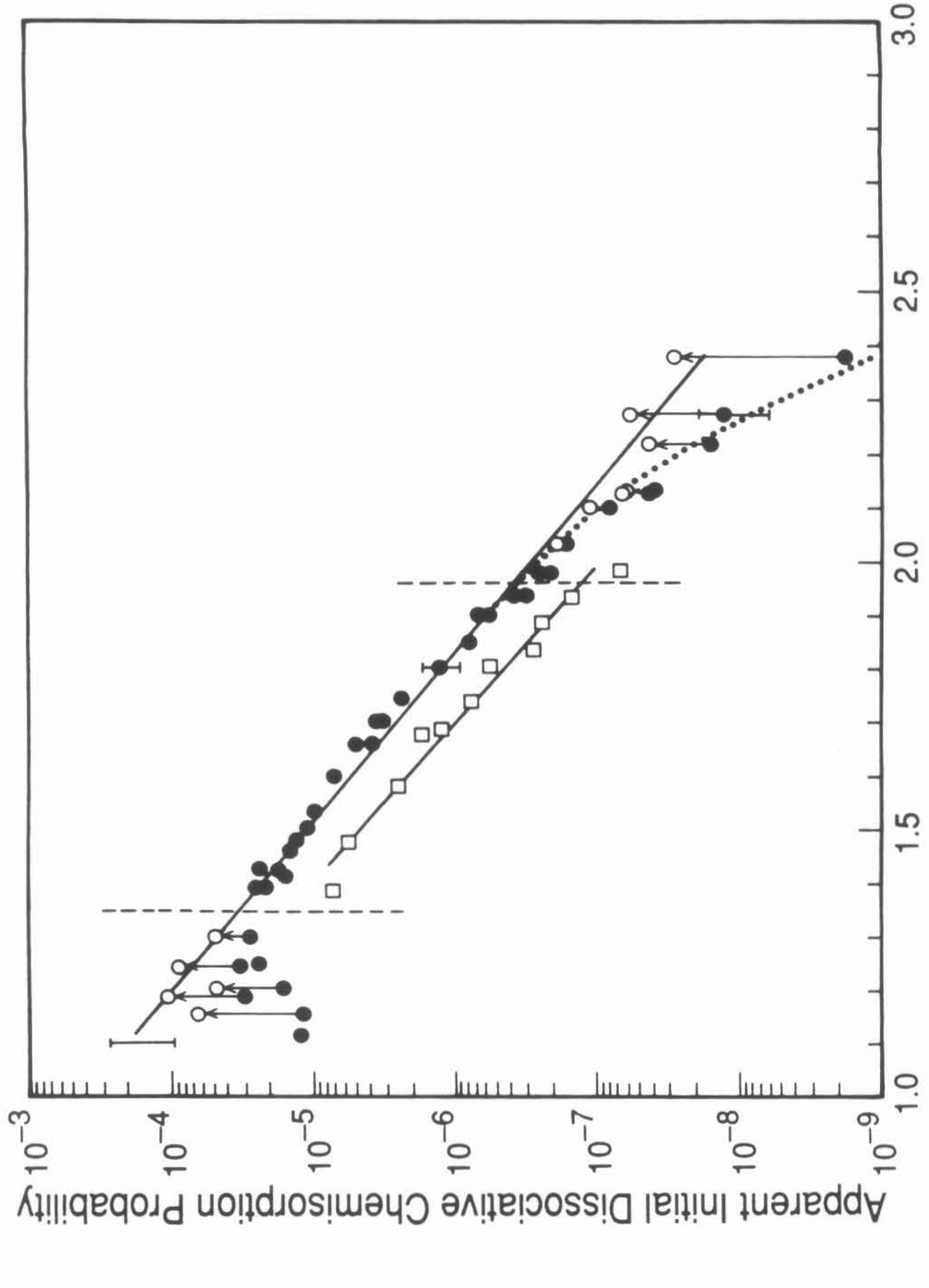
Apparent Initial Dissociative Chemisorption Probability
10^{-3}
10^{-4}
10^{-5}
10^{-6}
10^{-7}
10^{-8}
10^{-9}
1.0
1.5
2.0
2.5
3.0
$\frac{1000}{T}$, K^{-1}

Figure 1

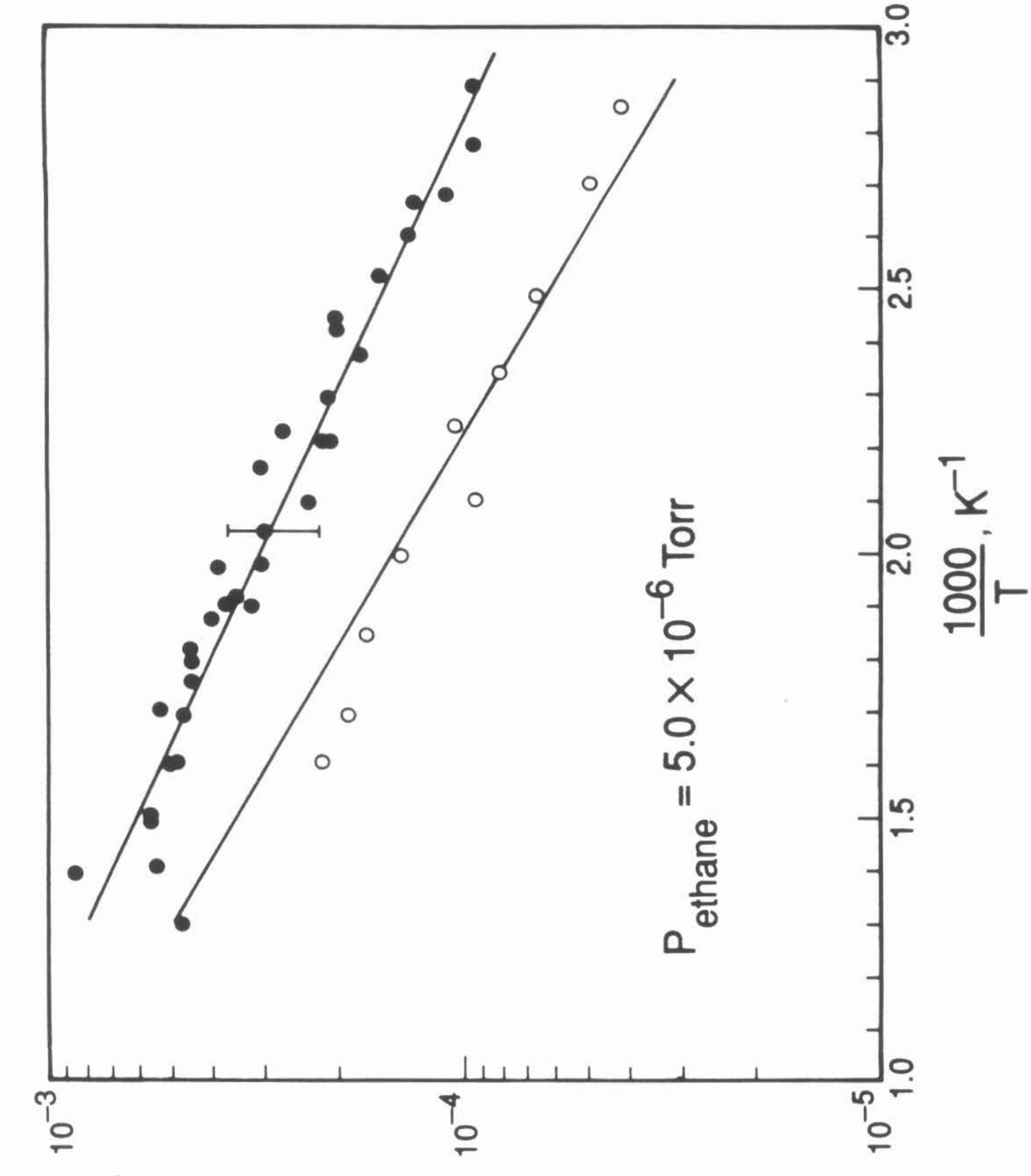

Initial Dissociative Chemisorption Probability
10^{-3}
10^{-4}
10^{-5}
1.0
1.5
2.0
2.5
3.0
$\frac{1000}{T}$, K^{-1}
$P_{ethane} = 5.0 \times 10^{-6}$ Torr

Figure 2

CHAPTER 3.

Kinetics and Mechanism of Formic Acid Decomposition on Ru(001)

[This chapter was published as a paper by Y. -K. Sun, J. J. Vajo, C. -Y. Chan and W. H. Weinberg in *Journal of Vacuum Science and Technology A* **6**, 854 (1988).]

Summary Abstract: Kinetics and mechanism of formic acid decomposition on Ru(001)

Y.-K. Sun, J. J. Vajo,[a)] C.-Y. Chan, and W. H. Weinberg
Division of Chemistry and Chemical Engineering, California Institute of Technology, Pasadena, California 91125

(Received 7 December 1987; accepted 13 January 1988)

The steady-state rate of decomposition of formic acid on Ru(001) has been measured as a function of surface temperature, parametric in the pressure of formic acid. The products of the decomposition reaction are CO_2, H_2, CO, and H_2O, i.e., both dehydrogenation and dehydration occur on Ru(001). A similar product distribution has been observed on Ni(110),[1] Ni(100),[2] Ru(100),[3] Fe(100),[4] and Ni(111)[5] surfaces; whereas only dehydrogenation to CO_2 and H_2 occurs on the Cu(100),[6] Cu(110),[7] and Pt(111)[8] surfaces. Only reversible adsorption and desorption of formic acid is observed on the less reactive Ag(110) surface at low temperatures,[9] whereas the more reactive Mo(100) surface is oxidized by formic acid at low temperatures with the products of this reaction being H_2, CO, and H_2O (Ref. 10). We report here the confirmation of earlier observations of the occurrence of both dehydrogenation and dehydration of formic acid on Ru(001),[11,12] and more importantly, we provide a detailed mechanistic description of the steady-state decomposition reaction on this surface in terms of elementary steps.

Details concerning both the UHV system that was employed in this work[13] as well as crystal preparation and cleaning[14] have been presented previously. The formic acid was introduced onto the Ru(001) surface through a directional beam doser consisting of a multichannel array of capillaries, and the ratio of the "beam pressure" of formic acid at the surface when the crystal was in front of the doser to the background pressure of formic acid in the UHV chamber was > 40. Under our experimental conditions, the incident formic acid was predominantly in monomer form. The rate of decomposition of the formic acid was measured by a multiplexed quadrupole mass spectrometer (UTI-100C) as the Ru(001) surface was positioned in and out of the formic acid beam with the surface temperature held constant. The measurements were carried out at surface temperatures between 350 and 800 K and for formic acid pressures of 7.3×10^{-7} and 2.1×10^{-6} Torr.

Arrhenius plots of the rate of decomposition of formic acid on Ru(001) are shown in Fig. 1 from which it is clear that there are two quite distinct kinetic regimes, labeled I and II in the figure. At relatively low surface temperatures between 360 and 400 K (regime II), the reaction rate is zero order in formic acid pressure with apparent activation energies of 16.0 ± 0.3 kcal/mol for CO_2 and H_2 production, and 15.0 ± 1.0 kcal/mol for CO and H_2O production. At temperatures above 500 K (regime I) the reaction rate becomes first order in formic acid pressure with apparent activation energies of -1.3 ± 0.2 kcal/mol for CO_2 and H_2 production, and -0.2 ± 0.3 kcal/mol for CO and H_2O production. The logarithm of the ratio of the rate of production of CO_2 and H_2 ($\equiv R_{CO_2}$) to that of CO and H_2O ($\equiv R_{CO}$) is plotted as a function of reciprocal surface temperature in Fig. 1(b). It is apparent that the rate of dehydrogenation is two to three times greater than that of dehydration in regime II, and five to eight times greater in regime I.

The kinetics of dehydrogenation of DCOOH were measured and compared with those of HCOOH. They are essentially the same in regime I. At relatively low temperatures (regime II), however, the apparent activation energy for DCOOH is 17.1 ± 0.3 kcal/mol, compared to 16.0 ± 0.3 kcal/mol for HCOOH. The absolute rate of dehydrogenation of HCOOH in regime II is greater than that of DCOOH.

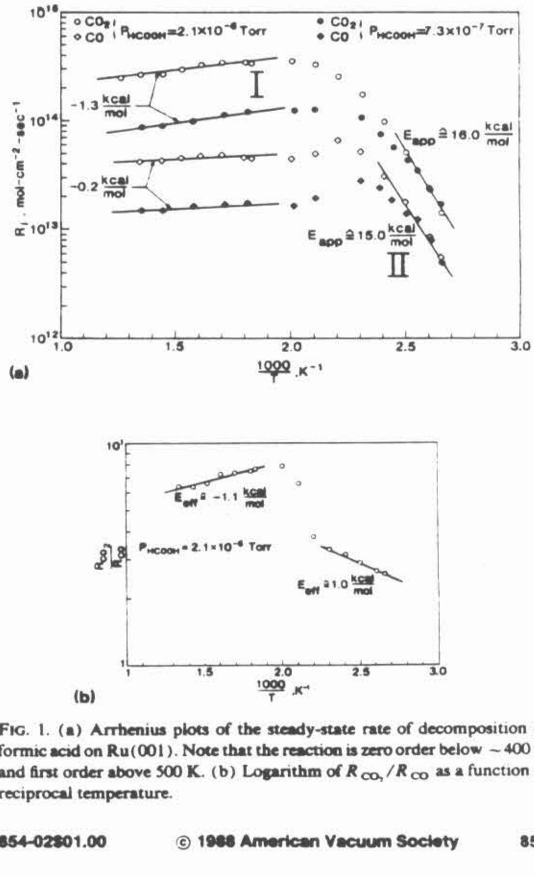

FIG. 1. (a) Arrhenius plots of the steady-state rate of decomposition of formic acid on Ru(001). Note that the reaction is zero order below ~400 K and first order above 500 K. (b) Logarithm of R_{CO_2}/R_{CO} as a function of reciprocal temperature.

This difference in the kinetics of dehydrogenation of DCOOH and HCOOH is due to a kinetic isotope effect, and indicates that C–H bond cleavage is involved in the rate-limiting step under these conditions. A third kinetic regime (regime III, not shown in Fig. 1) was observed below 370 K for the dehydrogenation of DCOOH. The rate is zero order in formic acid pressure in regime III with an apparent activation energy of 29.0 ± 0.6 kcal/mol.

A bidentate formate species has been identified by electron energy-loss spectroscopy to be the stable intermediate upon adsorption of formic acid on Ru(001) at 90 K with subsequent annealing to between 200 and 375 K.[11,12] Chemisorbed carbon monoxide and oxygen adatoms were observed spectroscopically on the surface after annealing to higher temperatures. The observation of the isotope effect for C–H bond cleavage together with the fact that formate is a stable intermediate clearly indicate that formate decomposition is the rate-limiting step in kinetic regime II.

Additional insight into the reaction mechanism can be gained if one has knowledge of the coverages of the various surface species during the steady-state reaction. Transient thermal desorption measurements carried out during the steady-state reaction[15] allow the determination of DCOO, D, H, and CO coverages during the steady-state decomposition of DCOOH. For pressures of DCOOH near 10^{-6} Torr, the hydrogen coverage is much smaller than that of deuterium in kinetic regimes II and III. Furthermore, the thermal desorption spectra of D_2 and CO_2 from DCOOH adsorbed at 300 K have the same shape and peak temperature. These facts imply that the formation of D_2 and CO_2 are governed by the same rate-limiting step, the decomposition of surface formate. The evolution of D_2 is reaction limited, whereas that of H_2 is desorption limited. The formate coverage (and thus the D coverage) remains essentially constant in kinetic regime III and decreases with increasing temperature in regime II with an activation energy given by $k_B d(\ln \theta_{\mathrm{DCOO}})/d(T^{-1}) = -13.3 \pm 1.0$ kcal/mol($\equiv E_{\theta_{\mathrm{DCOO}}}$). The activation energy E for the elementary reaction DCOO(a) $\rightarrow CO_2(g) + D(a)$, the apparent activation energy of dehydrogenation E_{app}, and $E_{\theta_{\mathrm{DCOO}}}$ are related by $E_{\mathrm{app}} = E - E_{\theta_{\mathrm{DCOO}}}$. Since $E_{\theta_{\mathrm{DCOO}}} \simeq 0$ in regime III, the apparent activation energy measured in this regime is the reaction barrier for formate to decompose via C–D bond cleavage ($E = E_{\mathrm{app}} = 29.0 \pm 0.6$ kcal/mol). Utilizing the value $E_{\mathrm{app}} = 17.1 \pm 0.3$ kcal/mol from regime II yields $E = 30.4 \pm 1.3$ kcal/mol, which agrees well with the value obtained from regime III (29.0 ± 0.6 kcal/mol). These results together with the kinetic isotope effect observed in regime II imply that the rate in regime III is also limited by the decomposition of formate.

The fact that the dissociative chemisorption of formic acid is irreversible was confirmed by reacting a mixture of HCOOH and D_2 of which the molar ratio was 1:2 and observing no mass 47 (HCOOD) as a reaction product under any conditions. The important fact that a secondary reaction leading to CO_2 via the oxidation of CO does not occur was established by carrying out the decomposition reaction at 500 K on a Ru(001) surface on which a half-monolayer of ^{18}O was predosed. The only initially observed reaction products were H_2, $C^{16}O^{16}O$, and $H_2^{18}O$. As the ^{18}O was depleted from the surface, $C^{16}O$ was also observed as a reaction product; in no case was $C^{16}O^{18}O$ detected, ruling out the secondary oxidation of CO on Ru(001) during the steady-state decomposition of formic acid.

The transition region seperating kinetic regimes I and II occurs between approximately 425 and 475 K, and it is characterized both by the desorption of chemisorbed CO from Ru(001) and by the accumulation of oxygen adatoms on the surface. Auger electron spectroscopic data revealed that the concentration of oxygen adatoms is negligible below 425 K during the steady-state reaction, and approaches a quarter-monolayer as the temperature increases above 475 K. The presence of oxygen leads to an enhancement in the rate of production of CO_2 relative to CO.

To summarize, for formic acid pressures near 10^{-6} Torr, there are three distinct kinetic regimes in the steady-state decomposition reaction on Ru(001): regime I above 500 K, regime II between 360 and 400 K, and regime III below 370 K. At relatively low surface temperatures (regimes II and III) the rate is limited by the decomposition of surface formate; whereas at high temperatures, the rate is limited by the formation of formate from molecularly adsorbed formic acid. The low-temperature regimes are characterized by a Ru(001) surface that is essentially saturated with reaction intermediates. The coverage of CO remains approximately constant in regimes II and III and decreases above 425 K. The formate coverage is relatively constant in regime III and decreases rapidly in regime II. The surface hydrogen coverage is insignificant compared to those of CO and formate. The high-temperature regime is characterized by a surface on which there is a steady-state concentration of oxygen adatoms approaching a quarter-monolayer. The latter selectively enhances the rate of dehydrogenation (CO_2 and H_2 production) relative to dehydration (CO and H_2O production). A detailed account of this work, including mechanistic modeling, will be presented elsewhere.[16]

Acknowledgment: This work was supported by the National Science Foundation under Grant No. DMR-8500789.

[a)] Present address: SRI International, Menlo Park, CA 94025.

[1] J. L. Falconer and R. J. Madix, J. Catal. **31**, 47 (1978).

[2] J. B. Benziger and R. J. Madix, Surf. Sci. **79**, 394 (1979).

[3] L. A. Larson and J. T. Dickenson, Surf. Sci. **84**, 17 (1979).

[4] J. B. Benziger and R. J. Madix, J. Catal. **65**, 49 (1980).

[5] J. B. Benziger and G. R. Schoofs, J. Phys. Chem. **88**, 4439 (1984).

[6] B. A. Sexton, Surf. Sci. **88**, 319 (1979).

[7] D. H. S. Ying and R. J. Madix, J. Catal. **61**, 48 (1980).

[8] N. R. Avery, Appl. Surf. Sci. **11/12**, 774 (1982).

[9] B. A. Sexton and R. J. Madix, Surf. Sci. **105**, 177 (1981).

[10] S. L. Miles, S. L. Bernasek, and G. L. Gland, Surf. Sci. **127**, 271 (1983).

[11] N. R. Avery, B. H. Toby, and W. H. Weinberg, Surf. Sci. **122**, L578 (1982).

[12] N. R. Avery, B. H. Toby, and W. H. Weinberg, J. Electron Spectrosc. **29**, 233 (1983).

[13] J. L. Taylor, D. E. Ibbotson, and W. H. Weinberg, J. Chem. Phys. **69**, 4298 (1978).

[14] G. E. Thomas and W. H. Weinberg, J. Chem. Phys. **70**, 954 (1979).

[15] W. Tsai and W. H. Weinberg, J. Phys. Chem. **91**, 5302 (1987).

[16] Y.-K. Sun, J. J. Vajo, C.-Y. Chan, and W. H. Weinberg (to be published).

CHAPTER 4.

Catalytic Decomposition of Formic Acid on Ru(001): Transient Measurements

[This chapter consists of an article coauthored with W. H. Weinberg.]

ABSTRACT

The kinetics of the decomposition of formic acid on Ru(001) have been investigated with thermal desorption mass spectrometry following the adsorption of DCOOH and HCOOH at both 130 and 310 K. Formic acid (DCOOH) dissociatively chemisorbs on the surface not only via O-H bond cleavage to form a formate and a hydrogen adatom but also via C-O bond cleavage to form a CO, a deuterium adatom and an hydroxyl, with the second reaction being much slower than the first. The saturation fractional coverage of the dissociatively chemisorbed formic acid is 0.47 following adsorption at 130 K, and 0.89 following adsorption at 310 K. Thermal desorption spectra of CO_2 are direct probe of kinetics of the C-D bond cleavage of the formate and are characterized by a kinetic isotope effect, a narrow peak width, and an upward shift in the peak temperature with increasing surface coverage of the formate. The latter indicates an increasing apparent activation energy for the C-D bond cleavage with increasing formate coverage, which results in self-accelerating decomposition kinetics that cause the observed sharp peak in the production of CO_2. Although the apparent activation energy for the C-D bond cleavage reaction varies strongly with the formate coverage, the relative yields of CO_2 and CO are independent of the formate coverage and are approximately 1 : 1. This observation, together with the observation that the formation of water which results from C-O bond cleavage of the formate appears at approximately the same temperature as that of CO_2 formation, suggests that the cleavage of the C-D and C-O bonds of the formate might not be independent. It is possible that a complex is formed on the surface which is a precursor to the C-D and C-O bond cleavage reactions.

1. INTRODUCTION

Molecules that contain multiple types of bonds may react on a transition metal surface in a number of ways, leading to the formation of different products. An identification of the reaction intermediates and the determination of the reaction pathways and their corresponding kinetics are essential for an understanding of the catalytic properties of the surface. Of even more importance, perhaps, is an understanding of the factors that can influence the selectivity of the surface, since the control of the selectivity is one of the primary goals in catalysis. On transition metal surfaces such as Ni(110) (**1-5**), Ni(100) (**6**), Ni(111) (**7**), Fe(100) (**8**), Ru(100) (**9**) and Ru(001) (**10-13**), formic acid decomposes via two pathways, namely, dehydrogenation which leads to the production of CO_2 and H_2, and dehydration which leads to the production of CO and H_2O. On the other hand, only dehydrogenation occurs on the Cu(100) (**14**), Cu(110) (**15**) and Pt(111) (**16**) surfaces. Only reversible adsorption and desorption of formic acid are observed on the less reactive Ag(110) surface at low temperatures (**17**), whereas the more reactive Mo(100) surface is oxidized by formic acid at low temperatures with the other products of this reaction being H_2, CO and H_2O (**18**). The decomposition of formic acid is a convenient model catalytic system for studying the kinetics and mechanism of a *branching* reaction on surfaces.

For the decomposition of formic acid that leads only to the production of CO_2 such as on the Cu(100) (**14**), Cu(110) (**15**) and Pt(111) (**16**) surfaces, the reaction mechanisms are well-established. Formic acid chemisorbs dissociatively on these surface to produce a hydrogen adatoms and a formate. The formate decomposes via C-H bond cleavage to form a CO_2 and a hydrogen adatom. For the decomposition on formic acid that leads to the production of both CO_2 and CO such as on the Fe(100) (**8**) surface, the reaction mechanism is also clear. Similarly, formic acid chemisorbs dissociatively on the surface to produce a formate and a hydrogen adatom. The formate, however, decomposes not only via C-H bond cleavage to produce CO_2 but also via C-O bond cleavage to form CO, oxygen and hydrogen adatom. In thermal desorption experiments (**8**), no water was observed to desorb from the surface. Oxygen adatoms remain on the surface. The relative yield of CO_2 to CO is approximately $1:1$, implying that the surface formate has approximately equal overall probabilities to undergo C-H and C-O bond cleavage reactions. In addition to the production of CO_2 and CO, water was also observed to desorb from the Ni(110) (**1-5**), Ni(100) (**6**), Ni(111) (**7**), Ru(100) **9**) and Ru(001) (**10**) surfaces in studies of the decomposition of formic acid with thermal desorption mass spectrometry. The reaction mechanism(s) of the formic acid decomposition, however, remain ambiguous and some of those that have been proposed are inconsistent with the experimental observations. Due to the similarity in the product distribution, it is helpful to review briefly pertinent results on the low-index surfaces of nickel, Ru(100) and Ru(001) surfaces.

The decomposition of HCOOH on Ni(110) was studied by McCarty, et al. using thermal desorption mass spectrometry, following adsorption of HCOOH at 240 K (**1**). It was found that the desorption spectra of H_2 consist of a desorption-limited peak centered at 310 K and a reaction-limited peak centered at 380 K. The former was controlled by the kinetics of recombinative desorption of hydrogen adatoms on the surface, whereas the latter was governed by the rate of decomposition of a surface intermediate that contain hydrogen atoms. The decomposition of DCOOH was later studied on the same surface following adsorption at 310 K (**2, 3**). At exposures greater than 0.5 L, CO_2 and D_2 desorbed from the surface with nearly identical and very narrow peaks at 390 K. The narrow peak was explained by an autocatalytic mechanism (**2, 3**). Neither H_2 nor HD were observed to desorb following adsorption at this temperature which is above that for the desorption-limited extrusion of hydrogen from the surface. The acidic hydrogen was *proposed* to desorb from the surface as H_2O via a *bimolecular* dehydration of DCOOH which led to the formation of a surface anhydride (**2, 3**). It was suggested that the anhydride decomposed to equal numbers of CO_2, CO and D_2 product molecules, i.e.,

$$2\mathrm{DCOOH(a)} \xrightarrow{<310\mathrm{K}} \mathrm{DCOOOCD(a)} + \mathrm{H_2O(g)}, \tag{1}$$

and

$$\mathrm{DCOOOCD(a)} \xrightarrow{390\mathrm{K}} \mathrm{D_2(g)} + \mathrm{CO(a)} + \mathrm{CO_2(g)}. \tag{2}$$

The same mechanism was also proposed on Ni(100) (**6**). The experimentally observed numbers of CO_2, CO and D_2 product molecules on Ni(110) were found to be approximately equal (**1-5**), but the formic anhydride was not observed spectroscopically following the adsorption of DCOOH at 310 K (**4**). Only formate and CO were identified on the surface. Hence, the mechanism embodied by Eqs. (1) and (2) was modified such that instead of forming the anhydride, formic acid (DCOOH) dehydrates *bimolecularly* to form H_2O, formate (DCOO) and formyl (DCO) (**4, 5**). The formyl would decompose to CO and deuterium adatoms at very low surface temperature. For example, it decomposes on the Ru(001) surface at 120 K (**19**). This modified mechanism predicts that the desorption-limited peak of H_2 in the studies by McCarty et al. (**1**) would consists of the carbon-bonded hydrogen only. It is probably fair to state that the mechanism of formic acid decomposition on Ni(110) remains uncertain.

A similar mechanism as Eqs. (1) and (2) was proposed for the decomposition of HCOOH on Ru(100), based upon the observation that H_2O desorbed from the surface and the numbers of H_2, CO and CO_2 that were produced were approximately equal following the adsorption of HCOOH at 100 K (**9**). The proposed mechanism, however, is inconsistent with the observation that the relative yield of

H_2 and CO_2 was not identical for different adsorption temperatures. It should also be noted that no formic anhydride was observed on the Ru(001) surface as judged by electron energy loss spectroscopy, following the adsorption of HCOOH at 80 K and subsequent annealing to various surface temperatures (**10, 11**).

The decomposition of HCOOH was recently investigated on Ni(111) surface (**7**). Substantial differences were observed in the thermal desorption spectra of H_2, CO and CO_2 following the adsorption of monomeric and dimeric of formic acid at 250 K. For the adsorption of the monomer, two H_2 peaks were observed at 350 and 400 K. The CO_2 production appears at the same temperature as the high-temperature H_2. For the adsorption of dimer, only one sharp H_2 peak was observed which coincides with that of CO_2 at 365 K. The kinetic behavior of the formic acid monomer was explained by dissociative adsorption of HCOOH to form formate and a hydrogen adatom. That of the formic acid dimer, however, was explained by a dehydration of the dimer at 250 K, which would deposit formate, CO and hydrogen adatoms on the surface. The hydrogen adatoms should desorb in a desorption-limited peak, which was not observed (**7**). The authors did not explain the discrapancy between the proposed mechanism and the observations.

A careful mass spectrometric study of the decomposition of formic acid on the Ru(001) surface following the adsorption of DCOOH and HCOOH on the surface at both 130 and 310 K is reported here. The quantatative measurements allow us to describe more completely the kinetics and mechanism of formic acid decomposition on Ru(001).

2. EXPERIMENTAL DETAILS

The experiments were carried out in an ion-pumped (200 l/s) stainless steel, ultrahigh vacuum chamber equipped with quadrupole mass spectrometry, Auger electron spectroscopy, and low-energy electron diffraction (**20**). The base pressure of the belljar was below 7×10^{-11} Torr of reactive gases. The Ru(001) surface (0.8 cm in diameter) was cut from a single crystalline ruthenium boule by spark erosion. It was polished to within 0.5° of the (001) orientation and mounted on a manipulator by two 0.010-in. tantalum wires spotwelded on the back of the crystal. The Ru(001) crystal could be heated resistively, and cooled conductively by liquid nitrogen. The temperature of the Ru(001) surface was measured by a 0.003 in. W/5%Re – W/26%Re thermocouple spotwelded to the back of the crystal. Since the Ru(001) crystal was heated by a programmable DC power supply, the measured thermocouple potential could deviate from the electromotive force (EMF) of the thermocouple by an offset due to a potential drop across part of the crystal if the two thermocouple wires are not in direct contact with each other at the surface, even though they both are in good contact with the crystal. Thus, in addition to ensuring good electric contact with the crystal, thermocouple potentials with the DC current flowing in both directions were also measured. Only when they were equal did we consider that the spotwelding was sufficiently good, and the potential measured is the EMF of the thermocouple. The surface was cleaned by argon ion sputtering, followed by oxygen cleaning. The latter was performed routinely each day by cycling the temperature of the crystal between 400 and 1100 K in 7×10^{-8} Torr of oxygen backfilled into the belljar. Chemisorbed oxygen was removed by annealing the crystal to over 1600 K (**21**). The cleanliness of the surface was verified by Auger electron spectroscopy.

The surface temperature was controlled using a previously described control scheme (**22**) that was implemented with an IBM PC/XT microcomputer with a Data Translation 2805 data aquisition board. The EMF of the thermocouple was measured with a Hewlett-Packard 3455A digital voltmeter at a rate of 25 readings/s, and the readings are transferred to the computer though a GPIB interface (National Instruments). The computer controls the DC power supply to heat the crystal.

This controller allows the crystal temperature to follow a predefined temperature profile: a linear ramp when measuring thermal desorption spectra, and a staircase function when measuring rates of decomposition at steady state. The computer software performs temperature control, mass spectrometric multiplexing and mass spectrometric signal measurements simultaneously.

Formic acid was introduced from a storage bulb onto the Ru(001) surface through a directional beam doser consisting of a type 304 stainless-steel plate with collimated hole structures (Brunswick Corporation). The hole diameters are 0.1 mm; the thickness of the plate is 1.3 mm; and the open area of the plate is 50%. The diameter of the plate is 9 mm, slightly larger than that of the Ru(001) single crystal, in order to render the pressure profile more uniform across the Ru(001) surface. The Ru(001) surface is parallel to and 3 mm from the doser when the crystal is in front of the beam doser. The crystal so positioned intercepts approximately 50% of the formaldehyde flowing through the doser (**23**). Under our experimental conditions, the incident formic acid was predominantly in monomeric form (**7**).

The absolute flow rate of formic acid through the doser was determined by the rate of the pressure drop in the formic acid storage bulb, measured by a Baratron manometer. The cryopanel in the UHV system was cooled by liquid nitrogen, and the ion gauge was turned off during thermal desorption measurements in order to decrease the background pressure. All thermal desorption spectra were measured with the mass spectrometer enclosed in a glass envelope, which reduces spurious contributions to the thermal desorption spectra (**24, 25**). The glass envelope has an orifice with a diameter of 3 mm. During measurements of the thermal desorption spectra, the surface was positioned 3 mm from the orifice. To analyze quantitatively the branching ratio of the formic acid decomposition to CO and CO_2, it is necessary to measure the ratio of the mass spectrometric sensitivities of CO (γ_{CO}) and CO_2 (γ_{CO_2}) that desorb from the surface. The mass spectrometric sensitivity γ_i is so defined that the rate R_i at which species i enters the glass envelope and the mass spectrometric intensity I_i are related by $R_i = I_i gamma_i$. It was determined that $\gamma_{CO} : \gamma_{CO_2} = 1.00 : 1.24$, using procedures that have been described previously (**26**).

Formic acid (HCOOH, 98%) was obtained from Aldrich Chemical Company, and formic-d$_1$ acid (DCOOH, 95% in H_2O and 99.2 atom %D) was from MSD Isotopes. All samples were purified by several freeze-pump-thaw cycles.

3. EXPERIMENTAL RESULTS

Formic acid was adsorbed on the Ru(001) surface at 130 and 310 K. It was observed to undergo both dehydrogenation that leads to the formation of CO_2 and H_2 and dehydration that produces CO and H_2O. Both formic acid (HCOOH) and formic-d$_1$ acid (DCOOH) were employed. The formic-d$_1$ acid was used to distinguish the carbon-bonded from the oxygen-bonded hydrogen atoms. At a surface temperature of 130 K and at exposures below 1.5 L, only decomposition products were observed to desorb from the surface upon heating. As the exposure was increased, molecular formic acid was also observed to desorb from the surface. The mass spectrometric intensities were recorded at m/e ratios of 2 (H_2^+), 3 (HD^+), 4 (D_2^+), 18 (H_2O^+), 19 (HDO^+), 20 (D_2O^+), 28 (CO^+) and 44 (CO_2^+) during measurements of the thermal desorption spectra from the decomposition of DCOOH. Approximately 0.07 (± 0.02) monolayer of oxygen adatoms remained on the surface, as determined by Auger electron spectroscopy, after thermal desorption experiments following a saturation exposure (> 1.5 L) of DCOOH at 130 K.

3.1 Adsorption of Formic Acid at 130 K

3.1.1 Production of CO_2 and CO

Shown in Figs. 1 (a) and 1 (b) are the mass spectrometric intensities of masses 44 and 28 as a function of the surface temperature following the adsorption of DCOOH at a surface temperature of 130 K for various exposures. In Fig. 1 (a) the peaks above 300 K are due to CO_2, whereas those below 250 K are due to a cracking fragment of molecularly desorbing DCOOH. In Fig. 1 (b) the peaks above 400 K are due to CO, the peaks between 300 and 400 K are due to a cracking fragment of desorbibg CO_2, and those below 250 K are due to a cracking fragment of molecularly desorbing DCOOH. The observed cracking pattern of the desorbing CO_2 is somewhat unusual in that the ratio of the mass spectrometric intensity at $m/e = 28$ due to fragmentation of CO_2 to that of the parent peak intensity is 0.58, much greater than the value of 0.18 stated in the manual of our UTI mass spectrometer. Removal of the glass envelope around the mass spectrometer results in a ratio that agrees with the value of 0.18. This unusual cracking pattern may result from higher density of vibrationally and/or electronically excited CO_2 molecules in the glass envelope. The 'hot' CO_2 would have a higher cross section to fragment to CO^+ upon ionization.

The selectivity of the Ru(001) surface in the decomposition of formic acid to form CO_2 and CO and its dependence on θ_T, the total coverage of the dissociatively chemisorbed formic acid, was measured quantitatively. This coverage θ_T is the sum of the *effective* fractional coverages of the desorbed CO_2 ("$\theta_{\mathrm{CO_2}}$") and CO ("θ_{CO}"). The quantitative measurements require a determination of the absolute mass spectrometric sensitivities of CO_2 ($\gamma_{\mathrm{CO_2}}$) and CO (γ_{CO}) that desorb from the surface and enter the orifice of the glass envelope in which the mass spectrometer is housed. As we noted in the experimental section, we found that

$$\gamma_{\mathrm{CO_2}} : \gamma_{\mathrm{CO}} = 1.00 : 1.24. \qquad (3)$$

To obtain the ratio of the *effective* fractional surface coverages of CO_2 and CO that desorbed from the surface, the time-integrated areas beneath the thermal desorption spectra of CO_2 ($A_{\mathrm{CO_2}}$) and CO (A_{CO}) in Fig. 1 must be divided by the corresponding mass spectrometric sensitivities, i.e.,

$$\theta_{\mathrm{CO_2}} : \theta_{\mathrm{CO}} = \frac{A_{\mathrm{CO_2}}}{\gamma_{\mathrm{CO_2}}} : \frac{A_{\mathrm{CO}}}{\gamma_{\mathrm{CO.}}} \tag{4}$$

The values of θ_{CO} and γ_{CO} were determined using a relative method in which A_{CO} was compared with that from a CO-staturated surface (**26**). The value of $\gamma_{\mathrm{CO_2}}$ was determined from Eq. (3) and $\theta_{\mathrm{CO_2}}$ was then determined from Eq. (4). For a saturation exposure of DCOOH at 130 K, the values of $\theta_{\mathrm{CO_2}}$ and θ_{CO} are 0.21 and 0.26, respectively, i.e., the maximum fractional coverage of dissociatively chemisorbed formic acid (θ_T) that can be obtained by the adsorption of DCOOH at 130 K is 0.47. The selectivity of the Ru(001) surface to the production of CO_2 and CO is shown in Fig. 2, in which θ_{CO} is plotted as a function of $\theta_{\mathrm{CO_2}}$ for each formic acid exposure in Fig. 1. The triangle data points in Fig. 2 correspond to θ_T that was obtained by adsorbing DCOOH on the surface at 310 K and will be discussed in Sec. 3.2.

The rate of production of CO_2 from the decomposition of DCOOH is limited by the decomposition of the surface intermediate, since CO_2 desorbs from the Ru(001) surface below 100 K. Hence, the rate of production of CO_2 is a direct measure of the rate of decomposition of the surface intermediate. As for the decomposition of formic acid on Ni(110) (**1-5**), the thermal desorption spectra of CO_2 are rather sharp with a full-width at half-maximum (FWHM) of 18 K at $\theta_T = 0.04$ [cf. curve 2 in Fig. 1 (a)] and 14 K at $\theta_T = 0.47$ [cf. curve 10 in Fig. 1 (a)]. By comparison, first-order kinetics with an activation energy of 26 kcal/mol and a preexponential factor of 10^{13} s^{-1} would have a FWHM of approximately 40 K. The peak temperatures increase with increasing θ_T from 320 K at $\theta_T = 0.02$ to 366 K at $\theta_T = 0.47$.

The rate of production of CO, on the other hand, is desorption limited. Kinetic information regarding the decomposition of the surface intermediates to form CO is obscured by the strong chemisorption of the product CO. The desorption spectra of

CO in Fig. 1 (b) are similar to those following adsorption of CO on a clean Ru(001) surface.

3.1.2 Production of H_2, HD and D_2

A *complete* recording of the thermal desorption spectra of H_2, HD and D_2 is very important since they provide valuable information concerning the reaction mechanism, specifically, the bond-cleavage sequence of the reaction intermediates. The thermal desorption spectra of H_2, HD and D_2 are shown in Fig. 3, following adsorption of DCOOH at 130 K at two quite different exposures, namely, low (a) and saturation (b) exposures that correspond to curves 4 and 10 in Fig. 1, respectively. At the low exposure, the thermal desorption spectra have the same shapes and peak temperatures (370 K), demonstrating that both hydrogen and deuterium atoms involved in the rate-limiting step of the desorption have the same chemical environment on the surface. After saturation exposure, however, the thermal desorption spectra of H_2, HD and D_2 differ not only in their shapes but also in their peak temperatures, indicating clearly that the hydrogen and the deuterium atoms involved in the rate-limiting step are in different chemical environments. Detectable desorption of H_2 was observed as low as 270 K, whereas *no* desorption of D_2 was detectable below 340 K. The thermal desorption spectrum of D_2, characterized by a rather sharp peak, bears a qualitative resemblence to that of CO_2 at the saturation exposure of DCOOH, cf. curve 10 in Fig. 1 (a). Quantitative differences between the thermal desorption spectra of D_2 and CO_2 are observed when a comparison of both spectra (scaled to the same peak height) is made as shown in Fig. 4. The desorption spectrum of HD has a relatively small component that is similar to that of H_2 and a rather large component that is similar to that of D_2.

3.1.3 Production of H_2O, HDO and D_2O

Thermal desorption spectra of H_2O, HDO and D_2O were measured following a saturation exposure of DCOOH on the Ru(001) surface at 130 K. The mass spectrometric intensities are rather low and noisy, and hence only a qualitative assessment can be made. There are three desorption peaks in the water desorption spectra. They are located at approximately 210, 275 and 370 K. The peak at 210 K is clearly visible for both H_2O and HDO but only barely for D_2O. The peak at 275 K is only visible for H_2O and HDO, with the former more intense. The peak at 370 K is visible for both HDO and D_2O. The desorption of water at 210 K is limited by the desorption kinetics of molecularly adsorbed water on the surface (**27**), whereas the desorption of water at 275 and 370 K is reaction limited.

3.1.4 Desorption of Molecular DCOOH

The two peaks in the thermal desorption spectra in Figs. 1 (a) and 1 (b) below 250 K are due to the molecular desorption of DCOOH from the surface. The high-temperature molecular desorption peak is attributable to the desorption of DCOOH from the second layer, i.e., the non-dissociatively adsorbed molecular DCOOH layer on top of first chemisorbed overlayer. The low-temperature peak, which does not saturate, results from desorption of condensed formic acid multilayer.

3.1.5 Kinetic Isotope Effect

The thermal desorption spectra of CO_2 from the decomposition of DCOOH and HCOOH on Ru(001) following the same exposure of 2.6 L at 130 K are shown in Fig. 5. The peak temperature of the desorption of CO_2 from HCOOH is 10 K lower than that from DCOOH. This kinetic isotope effect indicates that C-D bond cleavage is involved in the rate-limiting step in the production of CO_2.

3.1.6 Effects of the Preadsorbed CO

The decomposition of formic acid on a Ru(001) surface on which a quarter monolayer of CO was preadsorbed was studied to determine the effects of chemisorbed CO on the selectivity of the surface to the production of CO_2 and

CO and the reactivity of the reaction intermediate. After chemisorption of CO, the surface was exposed to 0.8 L of DCOOH, the same exposure as in curve 4 of Fig. 1. The coverage of the dissociatively chemisorbed formic acid θ_T and the selectivity of this surface to the formation of CO_2 and CO in the subsequent thermal decomposition experiment were determined. It was found that not only θ_T but also the selectivity were the same as when the surface was not preexposed with CO. The reactivity, however, is slightly modified by the preadsorbed CO: in the presence of the preadsorbed CO, the peak temperature of the CO_2 is 9 K higher than the initially clean surface, as may be seen in Fig. 6.

3.1.7 Effects of Annealing

The effects of annealing on the kinetics of decomposition of the surface intermediate that leads to the formation of CO_2 was investigated. Following an exposure of 3.8 L of HCOOH on the surface at 130 K, the surface was annealed to temperatures that were below those necessary for the formation of CO_2. The annealing was carried out in order to desorb hydrogen adatoms from the surface. The thermal desorption spectrum of H_2 resulting from the decomposition of HCOOH without any annealing is shown by curve (a) in Fig. 7. It is clearly composed of the three components of H_2, HD and D_2 in the earlier DCOOH experiment [cf. Fig. 3 (b)]. Curves (b) and (c) in Fig. 7 are the H_2 desorption spectra following an annealing of the surface to 298 and 310 K for 35 seconds. It is obvious that the annealing removes hydrogen adatoms that are adsorbed on the surface. The three corresponding desorption spectra of CO_2 are shown in Fig. 8, and they overlap completely. Hence, the annealing has no observable effect on the kinetics of decomposition of the surface intermediate in so far as the formation of CO_2 is concerned.

3.2 Adsorption of Formic Acid at 310 K

It was shown in Sec. 3.1.1 that the peak temperature of the CO_2 desorption spectra, which is a measure of the apparent activation energy for the surface intermediate to decompose to CO_2, increases continuously with the fractional surface coverage of the dissociatively chemisorbed formic acid θ_T, from 327 K at $\theta_T = 0.04$ to 366 K at $\theta_T = 0.47$. The latter is the maximum coverage that can be obtained following the adsorption of formic acid at 130 K. It would be very interesting to determine whether the peak temperature continues to increase if θ_T is increased further. It was shown in Sec. 3.1.7 that annealing the surface following the adsorption of DCOOH at 130 K desorbs hydrogen adatoms from the surface leaving vacant adsites for additional surface intermediates. We adsorbed DCOOH on the surface at 310 K at which temperature H_2 and trace amount of H_2O but not CO_2 desorb. The maximum value of θ_T in this case was found to be 0.89, following a saturation exposure of 12 L. The thermal desorption spectra of CO_2 following saturation exposures of DCOOH at 130 K (3.8 L) and 310 K (12 L) are shown in Fig. 9. The CO_2 peak temperature was observed to increase continuously beyond $\theta_T = 0.47$, reaching 395 K at $\theta_T = 0.89$. The peak temperatures are plotted as a function of θ_T in Fig. 10 for adsorption temperatures of 310 K (△) and 130 K (□). The FWHM of curve (b) in Fig. 9 is 8 K. The D_2 desorption spectrum overlaps that of CO_2 completely (cf. Fig. 4), indicating the production of D_2 is governed by the decomposition of the same surface intermediate that leads to the formation of CO_2.

4. DISCUSSION

4.1 Reaction Mechansim and Intermediates

The stable surface intermediates in the decomposition of formic acid on Ru(001) have been identified previously using electron energy loss spectroscopy after the adsorption of HCOOH at coverages up to slightly in execess of one monolayer at 80 K, followed by annealing to various surface temperatures (**10, 11**). Only bidentate formate and approximately 0.05 monolayer of CO were observed on the surface after annealing to 200 K. No vibrational features characteristic of a formic anhydride were observed.

Apparently, the surface formate is the reaction intermediate that leads to the formation of CO_2 via its C-D bond cleavage in the case of DCOOH. The rate of production of CO_2 is a direct measure of the rate of the decomposition of the surface formate via its C-D bond cleavage. Deuterium atoms from the formate are bonded directly to the surface following the formate decomposition. If the activation energy of the surface reaction that deposits hydrogen atoms on the surface is much lower than that for the recombinative desorption of the hydrogen adatoms, the H_2 production would be desorption limited. In that case no kinetic information concerning the surface reaction can be inferred from the rate of production of H_2. On the other hand, if the activation energy of the surface reaction is much greater than that for the desorption of hydrogen, the rate of production of H_2 would be reaction limited; and in this case it is a direct measure of the rate of the surface reaction.

Formic acid dissociatively chemisorbs on the surface via O-H bond cleavage at temperatures as low as 80 K to form surface formate and hydrogen adatoms (**10, 11**). Hence, following an exposure of 3.1 L of DCOOH on the Ru(001) surface at 130 K, the desorption of H_2, which became detectable at 270 K and peaked at 320 K, is desorption limited [cf. Fig. 3 (a)]. However, the desorption of D_2, unlike that of H_2 but similar to that of CO_2, is *mainly* controlled by the kinetics of decomposition of the formate. The apparent activation energy of the decomposition of the formate in this case is only slightly greater than that for the desorption of hydrogen. Note that after the decomposition of the formate and the desorption of CO_2, the hydrogen is more strongly bonded to the surface which has a lower concentration of adspecies. This slight overlap manifests itself in the differences in the thermal desorption spectra of D_2 and CO_2 that are shown in Fig. 4. The desorption of D_2 becomes detectable at a slightly higher temperature relative to that of CO_2 in the leading edge of the spectra, and decreases less rapidly in the trailing edge. The difference in the peak temperature is 4 K. The kinetics of D_2 formation in this case are *jointly* controlled by the decomposition reaction of the formate and the recombinative desorption of the deuterium adatoms, with the former predominant.

The apparent activation energy of decomposition of the surface formate can be lowered by reducing the coverage θ_T of the dissociatively chemisorbed formic acid [cf. Sec. **3.1.1** and Fig. 1 (a)], i.e., the peak temperature of the CO_2 formation decreases as θ_T decreases. We would then expect that the desorption spectra of H_2, HD, and D_2 should approach one another in both shape and peak temperature as θ_T is reduced. As may be seen in Fig. **3** (a), when $\theta_T \leq 0.17$ the desorption spectra of H_2, HD and D_2 become identical in both shape and peak temperature. In this case the production of H_2, HD and D_2 is *completely* desorption limited. On the other hand, when the apparent activation energy of the formate decomposition reaction is increased by increasing θ_T (cf. Sec. **3.2**), the difference between the desorption spectra of D_2 and CO_2 would decrease. In fact, following a 12 L exposure of DCOOH at 310 K, in which case θ_T is 0.89, the difference disappeared, and the production of D_2 is *completely* dictated by the kinetics of decomposition of the formate.

Compared to the mechanism of CO_2 production, that of CO is rather more complex. The kinetic information concerning the C-O bond cleavage that leads to CO formation is obscured completely by the strong chemisorption of CO. The desorption kinetics of H_2, HD, D_2, H_2O, HDO and D_2O, however, help to reveal the mechanism of CO formation in the case of the decomposition of DCOOH. It has been postulated that the production of CO on Ni(110) proceeds via a bimolecular dehydration reaction to generate a formate (DCOO), a deuterium adatom, CO and water (**3-5**). If the same mechanism were to apply to the decomposition of DCOOH on Ru(001), there would be no H_2 desorbing from the surface, and the production of at least half of the D_2 molecules would be desorption limited, neither of which was observed here, cf. Fig. **3** (b). Thus this mechanism can be ruled out.

In a previous EELS study (**10**), approximately 0.05 monolayer of CO was observed along with a bidentate formate following the adsorption of HCOOH at 80 K and subsequent annealing to 200 K. The intensity of the CO stretching mode increased slightly when the surface was annealed to 320 K followed by a rapid increase as the surface was annealed to 350 K. The latter annealing was accompanied by decomposition of the surface formate as indicated by the disappearance of the vibrational features of all the formate. The observed rapid increase in the intensity of the CO stretching mode near 350 K indicates that the *majority* of the CO is produced from the decomposition of the surface formate via C-O bond cleavage near the temperature where the formate decomposes to CO_2.

The small desorption-limited component in the desorption spectrum of HD in Fig. 3 (b) implies that some of the deuterium was deposited on the surface prior to C-D bond cleavage in the formate to form CO_2. Presumably this is correlated with C-O bond cleavage in some surface intermediate to produce CO. This observation agrees completely with the EELS observation of the presence of CO on the surface prior to the production of CO_2, and it also agrees with the observation of the reaction-limited formation of H_2O and HDO at 275 K (cf. Sec. **3.1.3**). Whether the reaction intermediate is a formate, or a formic acid molecule, or something else is not immediately clear.

Carbon monoxide formation via the C-O bond cleavage reaction at low temperatures deposits deuterium atoms on the surface. The majority of these deuterium adatoms do not desorb as water (cf. Sec. **3.1.3**). Rather, they desorb as HD at approximately 310 K in the desorption-limited component of the HD signal described in Fig. **3** (b). This makes it possible to estimate the amount of CO that is produced at low surface temperatures by estimating the amount of deuterium adatoms on the surface below approximately 330 K (where formate begins to decompose to CO_2, which also deposits deuterium atoms on the surface), since they are *approximately* equal rather than exactly equal because there is a very small amount of HDO desorption near 275 K. The amount of deuterium adatoms involved in the desorption-limited component of HD in Fig. **3** (b) is rather small, so small relative to the existing hydrogen adatoms on the surface that most deuterium adatoms recombine with hydrogen adatoms on the surface rather than with another deuterium. An estimation based on a comparison of areas in the thermal desorption spectra in Fig. **3** (b) indicates that the number of deuterium atoms involved in the desorption-limited component of HD is at most 8% of the total amount of deuterium on the surface, i.e., the approximate fractional coverage of CO below 330 K is 8% of 0.47, namely, 0.04 monolayer.

We have estimated the amount of CO on the surface below 330 K, and it agrees very well with the amount estimated by EELS. But what is the mechanism that leads to the formation of CO at a temperature as low as 200 K? It has been suggested that it is due to the onset of the decomposition of the surface formate via C-O bond cleavage reaction (**10**). The reaction-limited water desorption may result from the reaction of two hydroxyls to form a water and a surface oxygen adatom, from the recombinative desorption of an hydroxyl and a surface hydrogen adatom, or from the reaction between one oxygen and two hydrogen adatoms. There is no information available on the kinetics of these reactions, however. Considering that no water was detected following the coadsorption of hydrogen and oxygen on the Ru(001) surface (**28**), the first two mechanisms are more likely. Indeed, an hydroxyl (OD) was observed on the surface in EELS investigations of the adsorption of DCOOD on Ru(001) below 300 K (**11**). In the case of DCOOH, it is likely that it is this OH that leads to the formation of H_2O and HDO at 275 K via either recombinative desorption of the surface hydroxyls (OH) and the hydrogen (or deuterium) adatoms, or reaction between two hydroxyls. This implies that the intermediate that leads to the formation of CO at low surface temperature is the formic acid molecule via C-O bond cleavage, i.e.,

$$\mathrm{DCOOH(a)} \rightarrow \mathrm{D(a)} + \mathrm{CO(a)} + \mathrm{OH(a)}. \tag{5}$$

This reaction is competing with

$$\mathrm{DCOOH(a)} \rightarrow \mathrm{DCOO(a)} + \mathrm{H(a)}, \tag{6}$$

The concentration of CO(a) and DCOO(a) on the surface depends on the competing kinetics of Eqs. (5) and (6). For a saturation exposure of DCOOH, the coverage of CO is approximately 0.04 below 330 K. The coverage of hydroxyls (OH) and deuterium adatoms would also be approxiamtely 0.04 below 250 K. On the other hand, the surface coverage of hydrogen adatoms is approximately 0.43 $(0.47 - 0.04)$. This explains the relative amounts of H_2O, HDO and D_2O that are observed at 275 K.

A surface formate is the intermediate that leads to the production of CO_2 via C-D bond cleavage (in the case of DCOOH) and the production of CO via C-O bond cleavage above 320 K. The kinetics of the former can be probed directly by measuring the rate of CO_2 formation. It was shown in Sec. 3.1.1 that the apparent activation energy for C-D bond cleavage varies as the coverage of the dissociatively chemisorbed formic acid θ_T varies, cf. Fig. 10. Unless the apparent activation energy for the C-O bond cleavage reaction changes in exactly the same way as that for C-D bond cleavage reaction of the formate, the selectivity (the relative yield of CO_2 and CO), would vary when the initial coverage θ_T varies. As shown in Fig. 2, the relative yield is approximately unity, quite independent of θ_T, after considering the production of CO at low temperature (0.04 monolayer in the case of $\theta_T = 0.47$).

In addition, it was shown in Sec. 3.1.3 that for $\theta_T = 0.47$, the formation of water, which indicates C-O bond cleavage in the formate, appears at 370 K, approximately the same temperature as that of CO_2 formation of which the latter indicates C-D bond cleavage. The fact that the apparent activation energies for the production of CO_2 and CO from the decomposition of formate appear to vary in sympathy with θ_T, together with the fact that approximately equal numbers of CO_2 and CO are produced independent of θ_T, strongly suggest that the cleavage of C-O and C-D bonds of the surface formate may not act as two independent parallel reactions, but rather are coupled to each other. One possibility is that two formates form a surface complex which is the short-lived precusor for the cleavage of C-D and C-O bonds, and the decomposition of the complex leads to the formation of one CO_2 and one CO.

4.2 Kinetics of the Decomposition of Formate

The kinetics of CO_2 production from the decomposition of the surface formate are peculiar in that the widths of the CO_2 spectra are much narrower than that which would result from a 'normal' first-order decomposition reaction. Similar behavior has also been observed on Ni(110) (**1-5**) and Ni(100) (**6**). The FWHM decreases from 18 K at $\theta_T = 0.04$ to 8 K at $\theta = 0.89$, and is accompanied by an increase in the peak temperature from 326 to 395 K, which suggests a greater *apparent* activation energy for decomposition of the formate at higher θ_T. The presence of CO increases only slightly the apparent activation energy, as shown in Fig. 6. Hence, it is the coverage of formate itself on which the apparent activation energy mainly depends. This dependence of the apparent activation energy on the formate coverage is the reason behind the observed kinetic behavior: the formate is self-poisoning with respect to its decomposition to CO_2; as its coverage decreases, the apparent activation energy decreases, which accelerates the decomposition of the formate. The result is a sharp peak of CO_2 desorption. It is interesting to note that on Ru(100) the peak temperature of CO_2 formation (at approximately 390 K) is independent of surface coverage and the thermal desorption spectra of CO_2 do not have narrow peaks associated with them (**9**).

The increase in the apparent activation energy with formate coverage may be caused by one or both of two possibilities. The first is a true increase in the activation energy for the decomposition which results from an alteration in the electronic properties of the surface by virtue of the presence of the formate. The second possibility is that the activation energy for decomposition does not change significantly, but the formate requires vacant surface sites in its vacinity in order to decompose, which causes an increase in the *apparent* activation energy. The observed kinetic behavior of CO_2 formation from the decomposition of formic acid on Ru(001) can be described qualitatively by either of these two possibilities, since both result in an upward shift in the peak temperature and a smaller FWHM as the surface coverage of the formate increases. The second possibility, however, predicts a much broader peak associated with a 'normal' first-order surface reaction at low coverages than that which was observed. Thus, it is more likely that the observed kinetic behavior was mainly controlled by the first possibility, i.e., formate alters the surface catalytic property such that the activation energy of its decomposition increased with its coverage.

5. SYNOPSIS

The catalytic decomposition of formic acid on the Ru(001) surface was studied using thermal desorption mass spectrometry following the adsorption of DCOOH and HCOOH on the surface at 130 and 310 K. The results of this study may be summarized as follows:

1. Formic acid (DCOOH) chemisorbs dissociatively on the surface via both the

cleavage of its O-H bond to form a formate and a hydrogen adatom, and the cleavage of its C-O bond to form a CO, a deuterium adatom and an hydroxyl (OH). The former is the predominant reaction.

2. The rate of desorption of CO_2 is a direct measure of the kinetics of decomposition of the surface formate. It is characterized by a kinetic isotope effect, an increasingly narrow FWHM, and an upward shift in the peak temperature with the coverage θ_T of the dissociatively adsorbed formic acid. The FWHM and the peak temperature change from 18 K and 326 K at $\theta_T = 0.04$ to 8 K and 395 K at $\theta_T = 0.89$.
3. The increase in the apparent activation energy of the C-D bond cleavage is largely a result of self-poisoning by the formate, the presence of which on the surface alters the electronic properties of the surface such that the activation energy of the decomposition of the formate is increased. The coverage of CO was found to have little influence on the activation energy. The variation in the activation energy for CO_2 formation with θ_T results in the observed sharp thermal desorption spectra of CO_2.
4. The coverage of surface formate can be adjusted over a relatively wide range so that the activation energy for C-D bond cleavage in the case of DCOOH can be adjusted to be below, approximately equal to, or well above the activation energy for the recombinative desorption of the deuterium adatoms. Accordingly, the desorption of D_2 was observed to be governed completely by the desorption kinetics of the deuterium adatoms at low θ_T, jointly by the kinetics of deuterium desorption and C-D bond cleavage at intermediate θ_T, and solely by the kinetics of C-D bond cleavage at high θ_T.
5. The overall branching ratio of the formate to CO_2 and CO is approximately unity, regardless the initial coverage θ_T, even though the activation energy for the production of CO_2 varies with θ_T. The desorption of water, which

implies C-O bond cleavage of the formate, appears at approximately the same temperature as that of CO_2. These observations suggest that the cleavage of the C-D bond and that of the C-O bond of two surface formates are coupled, possibly via the formation of a short-lived surface complex that is the precursor to the decomposition.

Acknowledgment: This work was supported by The National Science Foundation under grant number CHE-8617826.

REFERENCES

1. J. McCarty, J. L. Falconer and R. J. Madix, *J. Catal.* **30**, 325 (1973).
2. J. L. Falconer and R. J. Madix, *Surface Sci.* **46**, 473 (1974).
3. (a) R. J. Madix and J. L. Falconer, *Surface Sci.* **51**, 547 (1975).
   (b) R. J. Madix, *Advan. Catal.* **29**, 1 (1980).
4. R. J. Madix, J. L. Gland, G. E. Mitchell and B. A. Sexton, *Surface Sci.* **125**, 481 (1983).
5. R. J. Madix, *Catal. Rev.-Sci. Eng.* **26**, 281 (1984).
6. J. B. Benziger and R. J. Madix, *Surface Sci.* **79**, 394 (1979).
7. J. B. Benziger and G. R. Schoofs, *J. Phys. Chem.* **88**, 4439 (1984).
8. J. B. Benziger and R. J. Madix, *J. Catal.* **65**, 49 (1980).
9. L. A. Larson and J. T. Dickenson, *Surface Sci.* **84**, 17 (1979).
10. (a) N. R. Avery, B. H. Toby, A. B. Anton and W. H. Weinberg, *Surface Sci.* **122**, L578 (1982).
    (b) N. R. Avery, B. H. Toby and W. H. Weinberg, *J. Electron Spec.* **29**, 233 (1983).
11. B. H. Toby, Ph.D. Thesis, California Institute of Technology, 1987.
12. Y. -K. Sun, J. J. Vajo, C. -Y. Chan and W. H. Weinberg, *J. Vac. Sci. Technol. A* **6**, 854 (1988).
13. Y. -K. Sun, J. J. Vajo and W. H. Weinberg, to be published.
14. B. A. Sexton, *Surface Sci.* **88**, 319 (1979).
15. D. H. S. Ying and R. J. Madix, *J. Catal.* **61**, 48 (1980).
16. N. R. Avery, *Appl. Surface Sci.* **11/12**, 774 (1981).
17. B. A. Sexton and R. J. Madix, *Surface Sci.* **105**, 177 (1981).
18. S. L. Miles, S. L. Bernasek and G. L. Gland, *Surface Sci.* **127**, 271 (1983).
19. A. B. Anton, J. E. Parmeter and W. H. Weinberg, *J. Am. Chem. Soc.* **108**,

1823 (1986).

20. Y. -K. Sun, C. -Y. Chan and W. H. Weinberg, *J. Vac. Sci. Technol. A* **7**, 1983 (1989).
21. T. E. Madey, H. A. Engelhardt and D. Menzel, *Surface Sci.* **48**, 304 (1975).
22. J. R. Engstrom and W. H. Weinberg, *Rev. Sci. Instru.* **55**, 404 (1984).
23. C. T. Campbell and S. M. Valone, *J. Vac. Sci. Technol. A* **3**, 408 (1985).
24. P. Feulner and Menzel, *J. Vac. Sci. Technol.* **17** 662 (1980).
25. Y. -K. Sun and W. H. Weinberg, *Surface Sci.* **214**, L246 (1989).
26. Y. -K. Sun and W. H. Weinberg, *J. Vac. Sci. Technol.* (in press).
27. D. Doering and T. E. Meday, *Surface Sci.* **123**, 305 (1982).
28. J. Hrbek, *J. Phys. Chem.* **90**, 6217 (1986).

Figure Captions

Fig. 1 : Mass spectrometric intensities of masses 44 (a) and 28 (b) vs. the surface temperature following the adsorption of DCOOH on the Ru(001) surface at 130 K for various exposures. Only alternate labels on the curves are shown. The exposures (in Langmuirs) and the fractional coverage θ_T of dissociatively chemisorbed formic acid are (1) 0.0 and 0.00, (2) 0.2 and 0.04, (3) 0.4 and 0.11, (4) 0.8 and 0.17, (5) 1.1 and 0.28, (6) 1.5 and 0.36, (7) 2.6 and 0.42, (8) 3.1 and 0.47, (9) 3.8 and 0.46, and (10) 5.6 and 0.47, respectively. The heating rate is 3.0 K-s^{-1}. The origin of each peak is properly indicated.

Fig. 2 : Selectivity of the Ru(001) surface to the formation of CO_2 and CO in the decomposition of DCOOH adsorbed at 130 K (□) and 310 K (△), respectively. The *effective* fractional coverage of CO is plotted as a function of that of CO_2 for each exposure in Fig. 1. The solid line represents a unity relative yield of production of CO_2 and CO. The heating rate is 3.0 K-s^{-1}.

Fig. 3 : Thermal desorption spectra of H_2, HD and D_2 following adsorption of DCOOH on the Ru(001) surface at 130 K for low (a) and saturation (b) exposures that correspond to curves 4 and 10 in Fig. 1. The heating rate is 3.0 K-s^{-1}.

Fig. 4 : A comparison of the thermal desorption spectra of CO_2 and D_2 following the adsorption of DCOOH on the Ru(001) surface at 130 K for 3.8 L. The difference in the peak temperature is 4 K. The heating rate is 3.0 K-s^{-1}.

Fig. 5 : The thermal desorption spectra of CO_2 due to the decomposition of DCOOH (dots) and HCOOH (solid line) on Ru(001) following the same exposure of formic acid of 3.8 L at 130 K. The difference in the peak temperatures is approximately 11 K. The heating rate is 3.0 K-s^{-1}.

Fig. 6 : Comparison of the thermal desorption of CO_2 due to the decomposition of

DCOOH at 130 K for 0.8 L on the clean (a) and the CO precovered (b) Ru(001) surfaces. The fractional coverage of CO is 0.25. The peak temperature of (b) is 9 K higher than that of (a).

Fig. 7 : Thermal desorption spectra of H_2 following adsorption of 3.8 L of HCOOH on the Ru(001) surface at 130 K without annealing (a) and with annealing to 298 K (b) and 310 K (c) for 35 seconds. The heating rate is 8.0 K-s^{-1}.

Fig. 8 : The thermal desorption spectra of CO_2 corresponding the (a), (b) and (c) in Fig. 7, they overlap completely with a peak temperature at 362 K.

Fig. 9 : Comparison of the thermal desorption spectra of CO_2 following the adsorption of DCOOH on the Ru(001) surface at 130 (a) and 310 K (b). The exposure was 3.8 L at 130 K and 12 L at 310 K. The FWHM is 14 K for (a) and 8 K for (b).

Fig. 10 : The peak temperatures of the thermal desorption spectra of CO_2, $T_P^{CO_2}$, determined following the adsorption of DCOOH on the Ru(001) surface at 130 K (□) and 310 K (△) are plotted as a function of the fractional coverage θ_T of the dissociatively chemisorbed DCOOH.

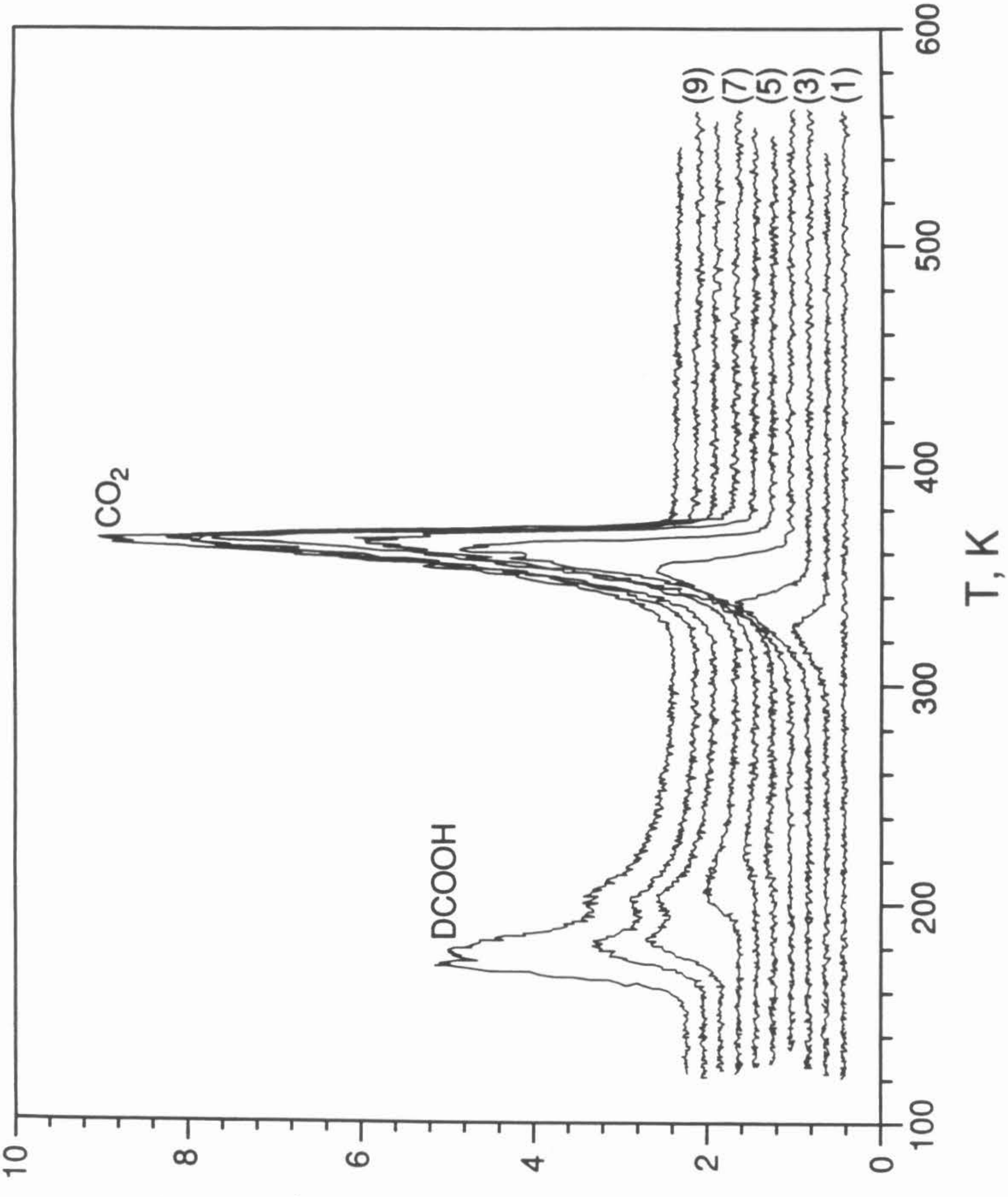
DCOOH
CO2
(9)
(7)
(5)
(3)
(1)
T, K
100
200
300
400
500
600
m/e = 44 Ion Current, 10-9 A
0
2
4
6
8
10

Figure 1 (a)

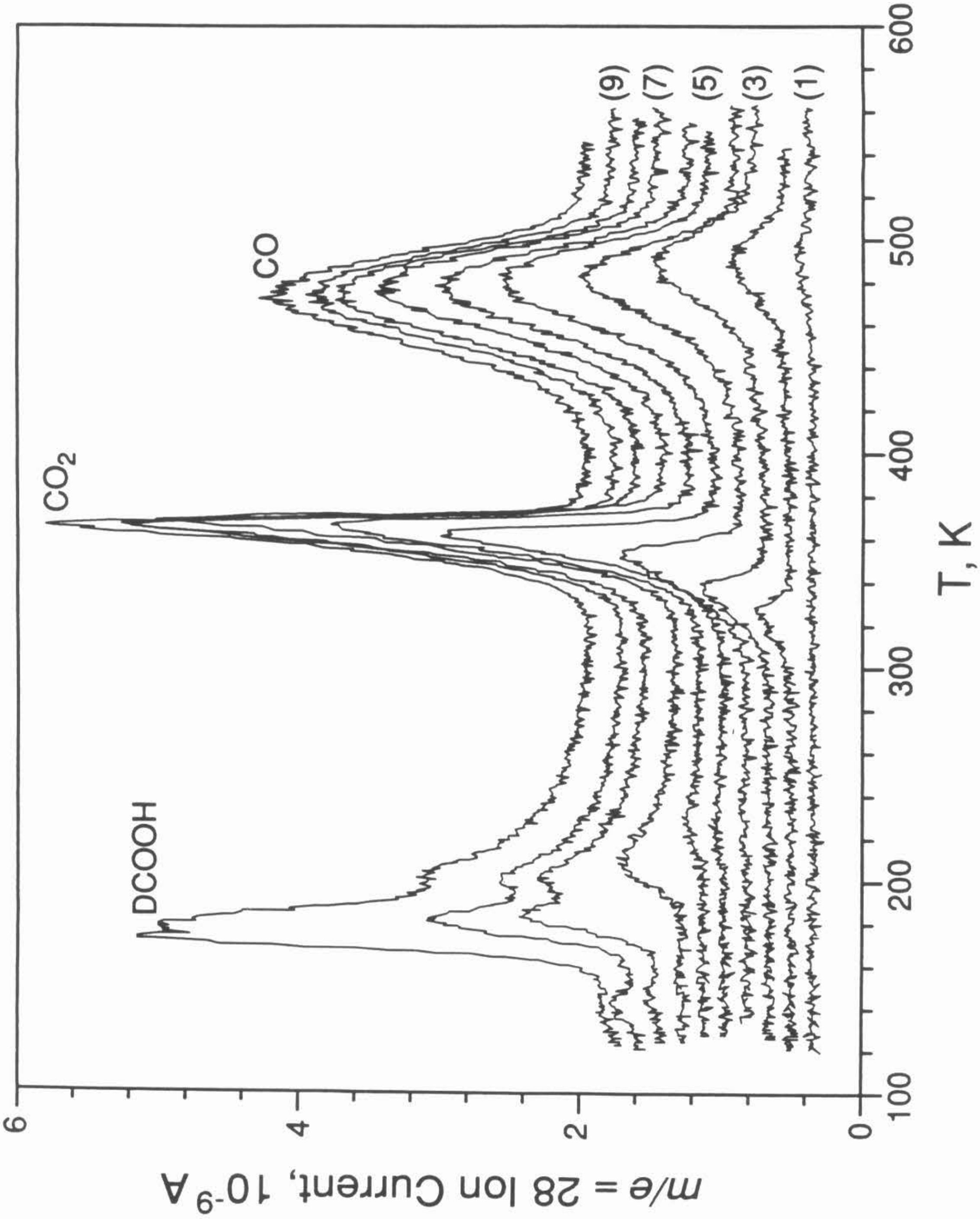
DCOOH
CO$_2$
CO
(9)
(7)
(5)
(3)
(1)
m/e = 28 Ion Current, 10^{-9} A
0
2
4
6
T, K
100
200
300
400
500
600

Figure 1 (b)

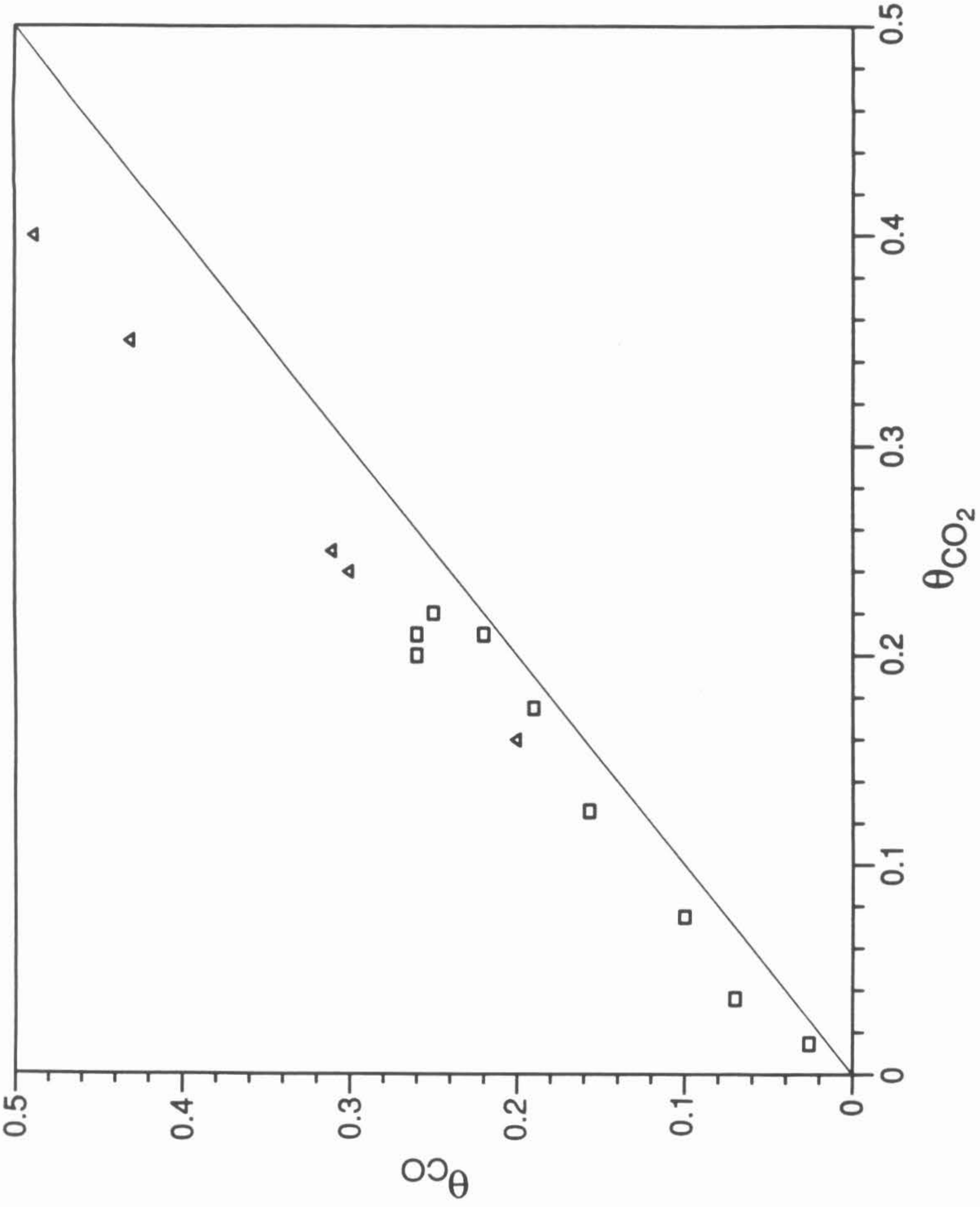

Figure 2

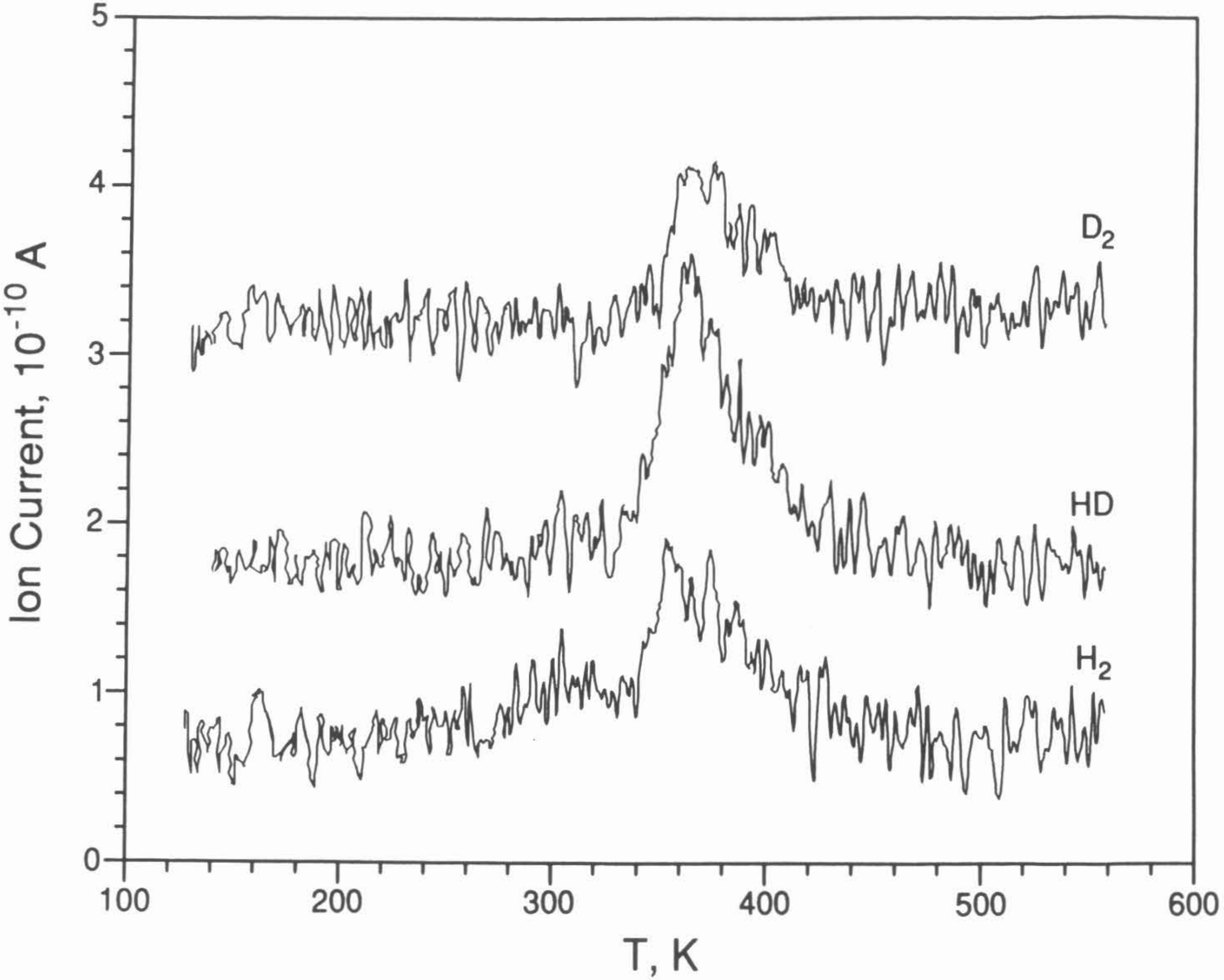

Figure 3 (a)

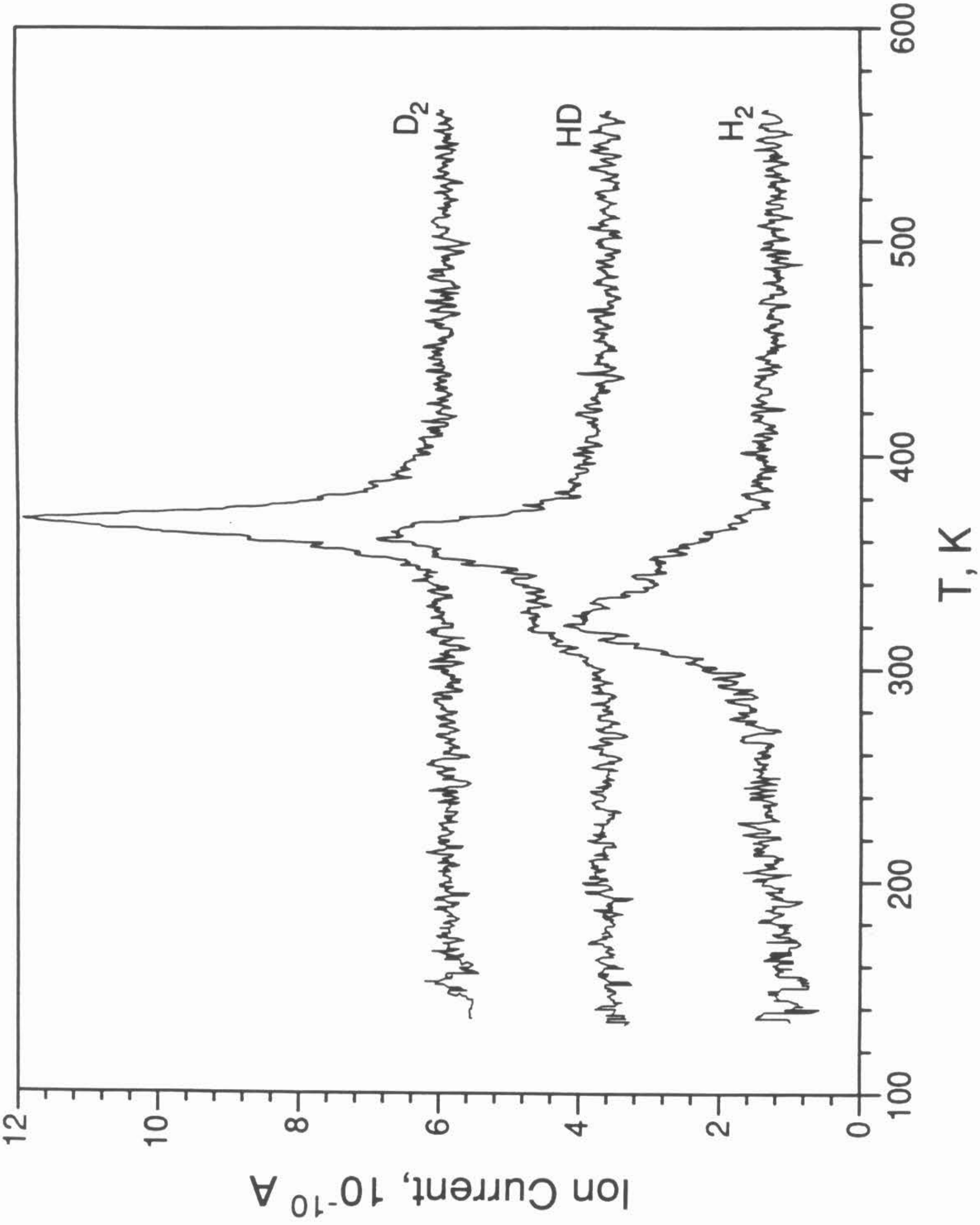
D$_2$
HD
H$_2$
Ion Current, 10^{-10} A
0
2
4
6
8
10
12
T, K
100
200
300
400
500
600

Figure 3 (b)

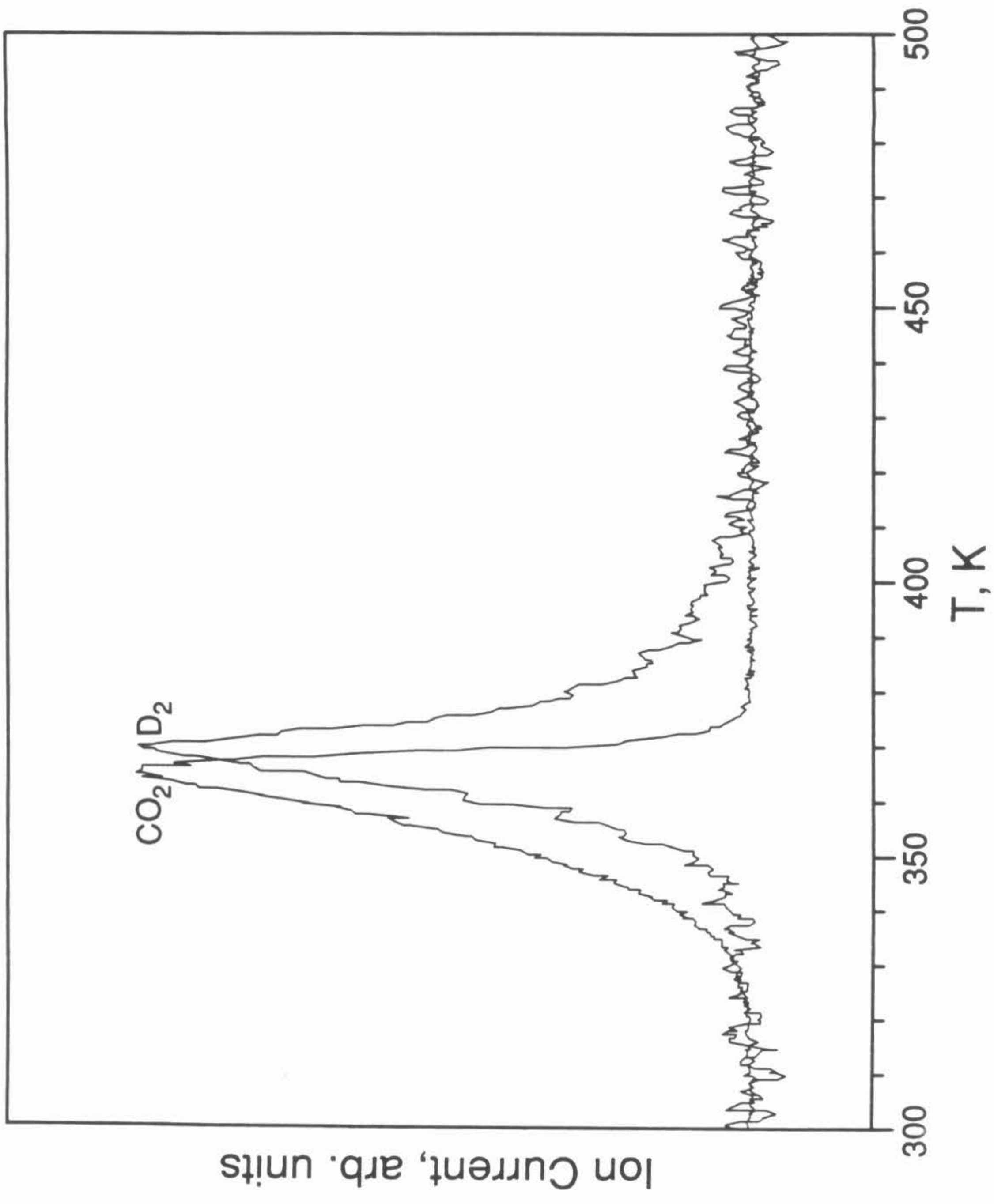

Figure 4

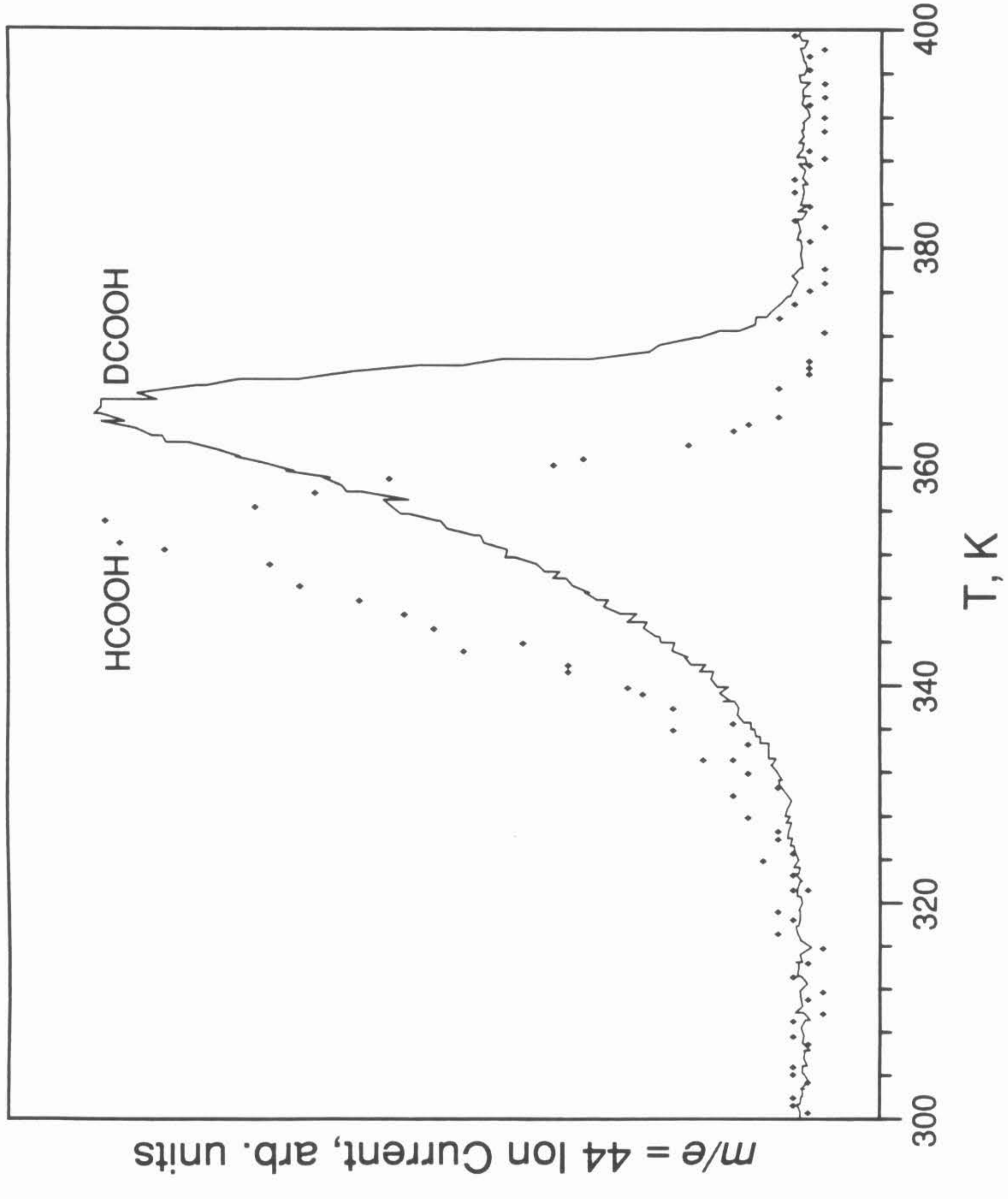
m/e = 44 Ion Current, arb. units
T, K
300
320
340
360
380
400
HCOOH
DCOOH

Figure 5

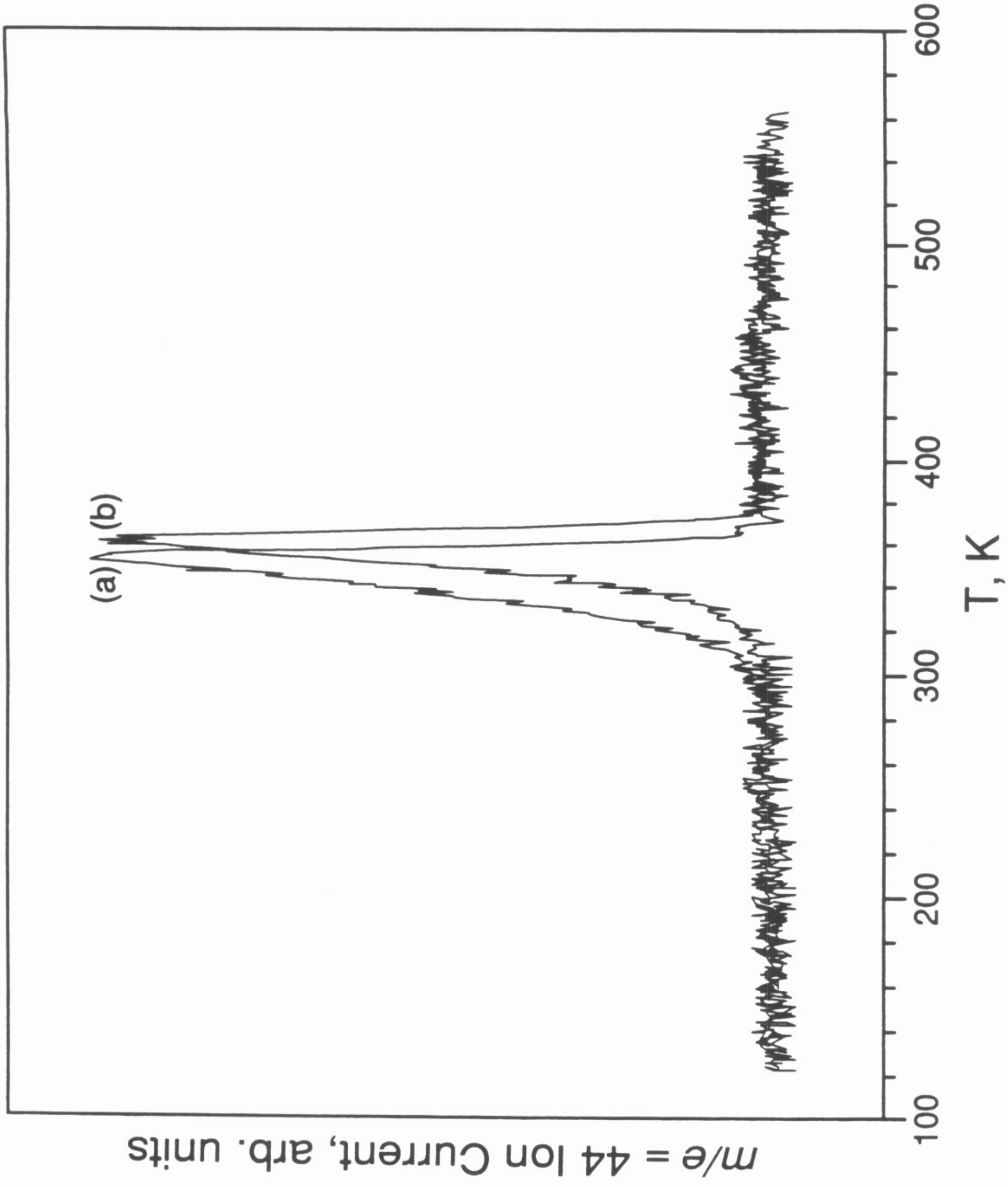

Figure 6

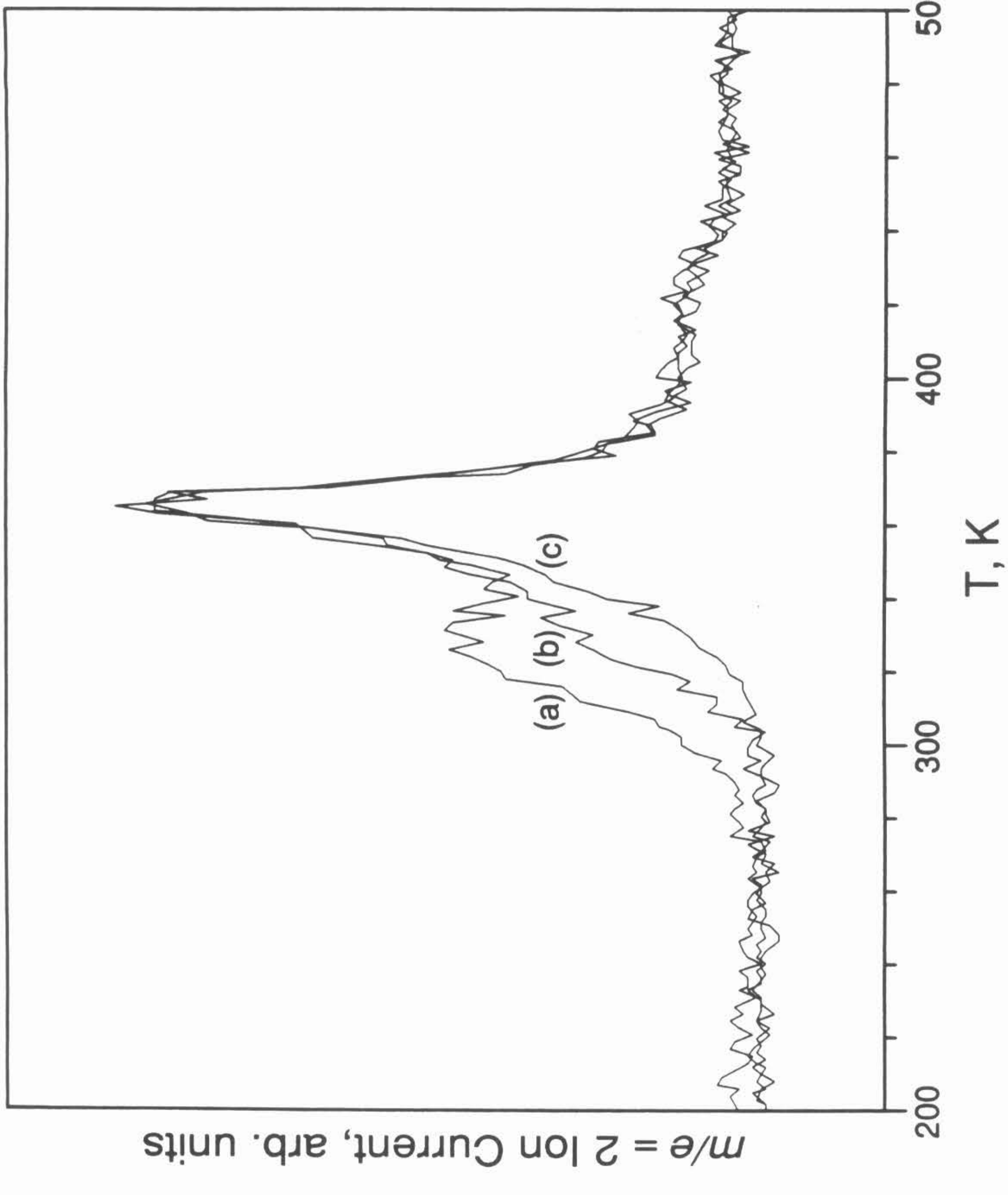

Figure 7

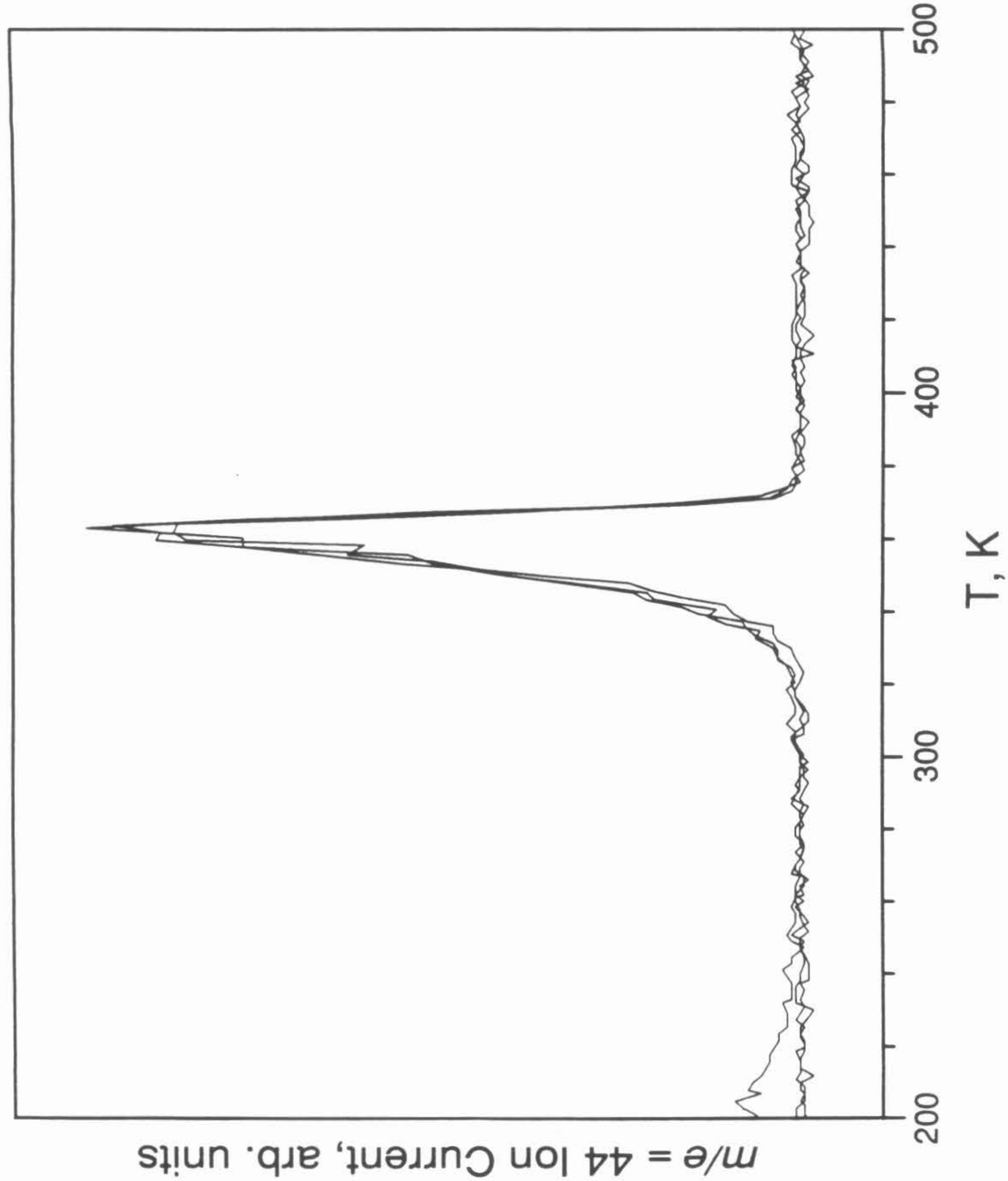

Figure 8

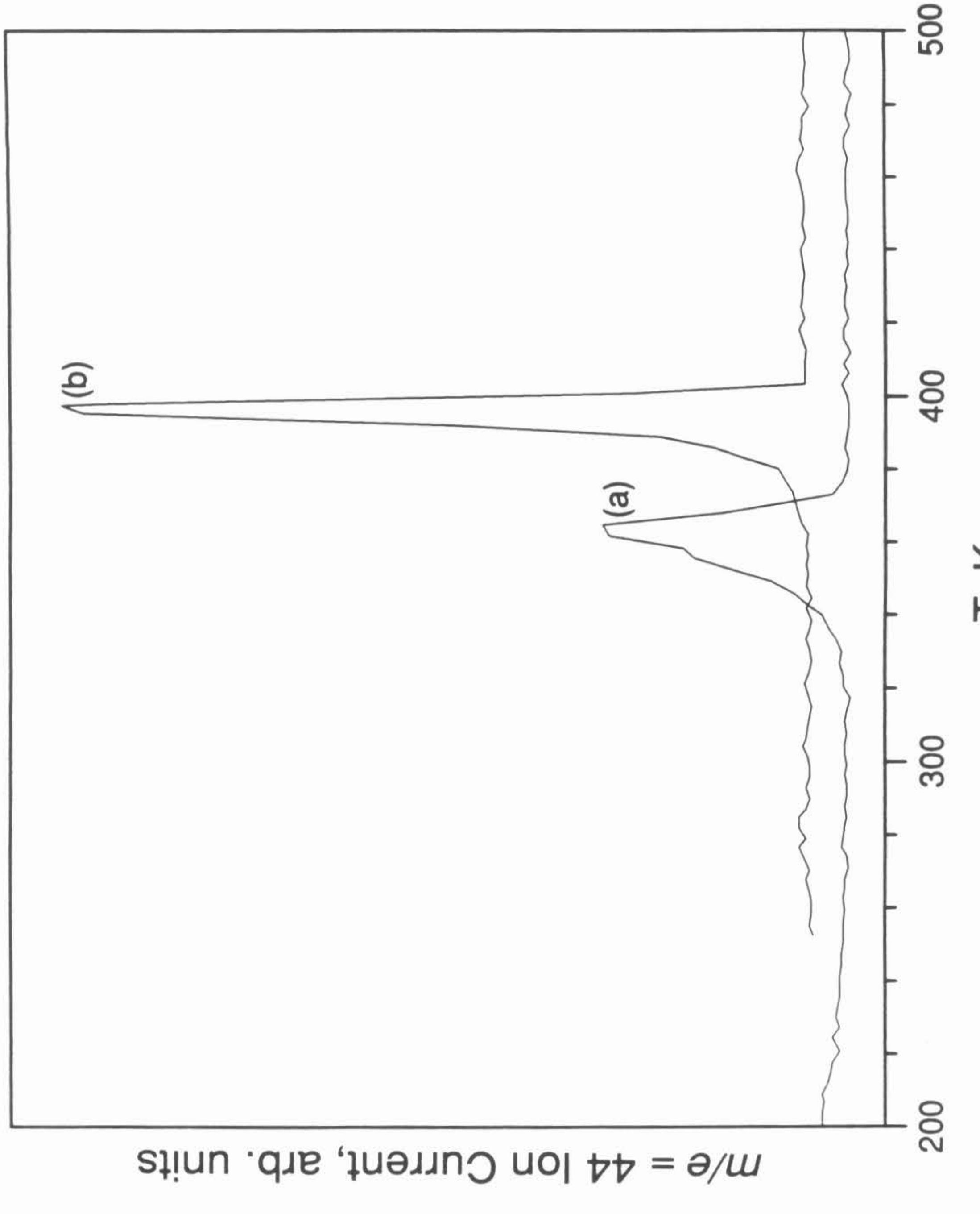

Figure 9

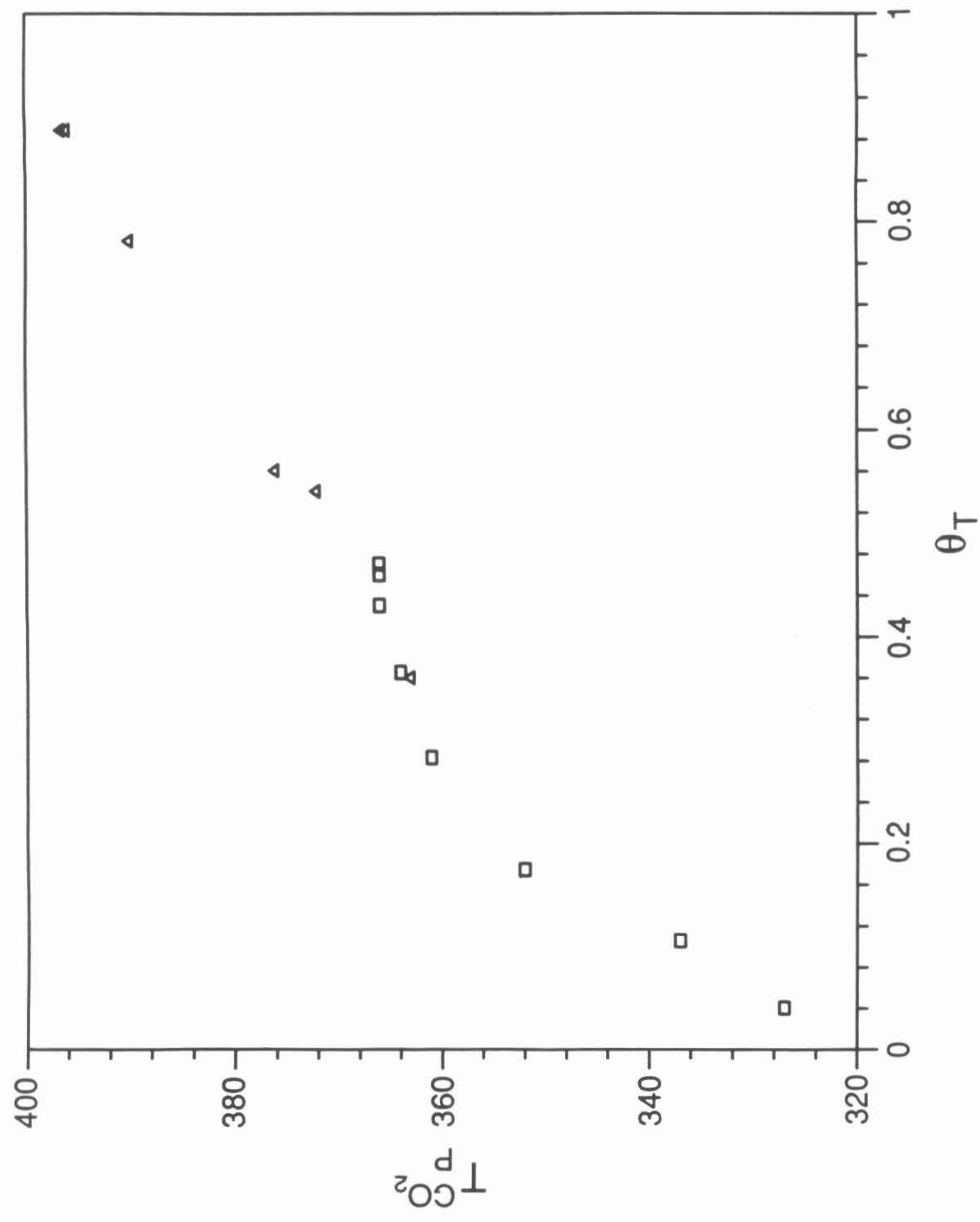

Figure 10

CHAPTER 5.

Steady-State Rate of Decomposition of Formaldehyde on Ru(001)

[This chapter was published as a paper by Y. -K. Sun, C. -Y. Chan and W. H. Weinberg in *Journal of Vacuum Science and Technology A* **7**, 1983 (1989).]

Steady-state rate of decomposition of formaldehyde on Ru(001)

Y.-K. Sun, C.-Y. Chan, and W. H. Weinberg
Division of Chemistry and Chemical Engineering, California Institute of Technology, Pasadena, California 91125

(Received 3 October 1988; accepted 5 December 1988)

The steady-state, absolute rate of decomposition of formaldehyde on the Ru(001) surface has been measured as a function of surface temperature from 310 to 750 K and for reactant pressures between 9.7×10^{-8} and 1.6×10^{-6} Torr. The only observed reaction products were carbon monoxide and hydrogen. Postreaction Auger spectroscopic analysis revealed a clean surface. Two distinct kinetic regimes are observed. At relatively low surface temperatures (and/or high formaldehyde pressures), the rate is zero order in formaldehyde pressure with an apparent activation energy of 23 ± 0.5 kcal/mol and an apparent preexponential factor of $4\times10^{11}\ \mathrm{s}^{-1}$. The rate becomes flux limited and first order in formaldehyde pressure with an apparent activation energy of zero at relatively high surface temperatures (and/or low formaldehyde pressures). Perdeutero-formaldehyde decomposes on Ru(001) with the same kinetic parameters as HCHO. The lack of a kinetic isotope effect indicates that C–H bond cleavage is not the rate-limiting step under these experimental conditions. In the low-temperature regime, the surface is saturated with CO, and the rate is CO desorption limited. Dissociative chemisorption of formaldehyde is irreversible since no isotopic exchange products were observed by reacting a mixture of HCHO and D_2 with a molar ratio of 1:4 at a total pressure of 1×10^{-6} Torr.

I. INTRODUCTION

The decomposition of formaldehyde has been studied on a number of transition-metal surfaces including W(111) and W(100),[1] Ru(110),[2,3] Ru(001),[4] Ni(110),[5,6] clean and sulfided Pt(111),[7] clean and oxygen precovered Cu(110),[8] and oxygen precovered Ag(110).[9] The possibility that the methanation reaction may proceed via HCHO or HCHO-derived intermediates[10] makes a study of the chemistry of formaldehyde on transition-metal surfaces quite relevant. Carbon monoxide and hydrogen are the major reaction products of formaldehyde decomposition, as determined by temperature progammed desorption. Small quantities of other products were also observed on these surfaces, however, including CH_4,[1,2] CH_3OH,[5–7] CO_2,[1–7] and H_2O.[2,5,6] The presence of impurities in the formaldehyde sample (methyl formate, for example) may account for the observation of CO_2 and CH_4 in some cases. On the Ru(001) surface, stable reaction intermediates including η^1-formaldehyde, η^2-formaldehyde, and η^1-formyl have been identified by electron energy-loss spectroscopy following formaldehyde adsorption at 80 K.[4] In this study, we have made mass spectrometric measurements of the steady-state and transient isothermal rate of decomposition of formaldehyde on an initially clean Ru(001) surface as a function of surface temperature, parametric in the formaldehyde pressure. We have determined the kinetics and mechanism of the formaldehyde decomposition reaction, as well as the surface coverages of carbon monoxide and hydrogen during the steady-state reaction.

II. EXPERIMENTAL DETAILS

The experiments were carried out in an ion-pumped (200 l/s) stainless-steel, ultrahigh vacuum chamber equipped with quadrupole mass spectrometry, Auger electron spectroscopy, low-energy electron diffraction, and x-ray photoelectron spectroscopy.[11] The base pressure of the belljar was below 8×10^{-11} Torr of reactive gases. The Ru(001) surface (8 mm in diameter and 0.8 mm thick) was cut from a single-crystalline ruthenium boule by spark erosion. It was polished to within 0.5° of the (001) orientation and mounted on a manipulator by two 0.010-in. tantalum wires spotwelded on the back of the crystal. The Ru(001) crystal could be heated resistively, and cooled conductively by liquid nitrogen. The temperature of the Ru(001) surface was measured by a 0.003-in. W/5% Re–W/28% Re thermocouple spotwelded to the back of the crystal. Oxygen cleaning was routinely performed prior to each measurement by cycling the temperature of the Ru(001) crystal between 400 and 1100 K in 7×10^{-8} Torr of oxygen backfilled into the belljar. Chemisorbed oxygen was removed by annealing the crystal to over 1600 K.[12] The cleanliness of the surface was verified by Auger electron spectroscopy.

An IBM PC/XT microcomputer with a Data Translation 2805 board was utilized as a temperature controller,[13] which controls a programmable dc power supply. The emf of the thermocouple was measured with a Hewlett–Packard 3455A digital voltmeter at a rate of 25 readings/s, and the readings are transferred to the computer though a general purpose interface bus (GPIB) interface. This controller allows the crystal temperature to follow a predefined temperature profile, a staircase function in the case of the steady-state decomposition rate measurements. The software performs temperature control, mass spectrometric multiplexing, and mass spectrometric signal measurements simultaneously.

Deuterated paraformaldehyde (99.6 at.% D) was obtained from MSD Isotopes and paraformaldehyde (with $H_2O<1\%$) from Fluka. They were transferred in powder form into a preevacuated 50-ml Pyrex flask in a plastic bag purged with dry nitrogen gas. The flask with the paraformaldehyde sample was evacuated in a gas manifold which is pumped by a Varian M-2 diffusion pump and has a base pressure of 6×10^{-6} Torr. Formaldehyde in monomer form was prepared in a similar way to that described by Yates *et al.*,[1] and was stored at room temperature in a 500-ml Pyrex bulb at pressures from 0.2 to 8 Torr. A mass spectrum of the HCHO sample exhibits *m/e* peaks only at 30, 29, 28, 16, 14, 13, 12, and 2 with peak height ratios of 0.73:1.00:0.34:0.02:0.04:0.03:0.05; that of the DCDO sample exhibits *m/e* peaks at 32, 30, 28, 16, 14, 12, and 4 with intensity ratios of 0.80:1.00:0.36:0.07:0.05:0.04:0.05, in reasonable agreement with the reported values.[14] Most importantly, there are no peaks at masses 44 and 60, indicating that the samples were free of methyl formate.[1] The mass spectra remain unchanged for up to one week following storage at room temperature.

The formaldehyde was introduced from the storage bulb onto the Ru(001) surface though a directional beam doser consisting of a type 304 stainless-steel plate with collimated hole structures (Brunswick Corporation). The hole diameters are 0.1 mm; the thickness of the plate is 1.3 mm; and the open area of the plate is 50%. The diameter of the plate is 9 mm, slightly larger than that of the Ru(001) single crystal, in order to improve the pressure profile across the Ru(001) surface. The Ru(001) surface is parallel to and 3 mm away from the doser when the crystal is in front of the beam doser. The crystal so positioned intercepts ~ 50% of the formaldehyde flowing through the doser.[15]

The absolute HCHO beam flow rate through the doser was determined by the rate of pressure drop in the formaldehyde storage bulb, measured by a Baratron manometer. The cryopanal in the UHV system was cooled by liquid nitrogen, and the ion gauge was turned off during the steady-state rate measurements in order to decrease the background pressure. The ratio of the formaldehyde "beam pressure" to the background formaldehyde pressure was determined to be greater than 40:1 by measuring the formaldehyde decomposition rate when the crystal was in and out of the formaldehyde beam at high surface temperatures (where the reaction kinetics are first order).

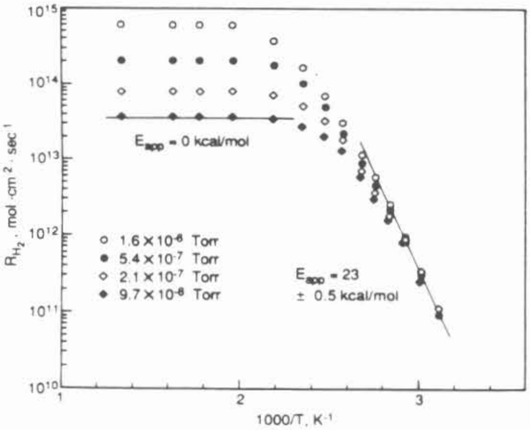

FIG. 1. Arrhenius plots of the steady-state rate of decomposition of formaldehyde on Ru(001). Note that the reaction is zero order in the low-temperature regime and first order in the high-temperature regime.

During steady-state rate measurements, formaldehyde flowed steadily through the gas doser. The temperature of the Ru(001) surface was programmed to follow a staircase function. Each time the surface temperature became constant, mass spectrometric signals of masses 2 and 29 were monitored as the Ru(001) surface was positioned in and out of the formaldehyde beam. The Ru(001) surface remained in the beam for a sufficiently long time that steady state was achieved. The difference in the mass spectrometric signal of mass 2 (in the case of HCHO) when the surface was in and out of the beam serves as a measure of the decomposition rate. Since the beam-to-background pressure ratio is > 40, both the reaction rate when the Ru(001) surface was out of the beam and the reaction rate from the rear of the crystal when the Ru(001) was in the beam were negligible. The absolute rate of hydrogen production was calculated by calibrating the mass spectrometer with a known leak of hydrogen into the UHV system. The leak rate of hydrogen was determined in the same way as that of formaldehyde discussed above. Similar techniques have been employed in studying the kinetics of formic acid decomposition on the Ru(001) surface.[16]

III. RESULTS AND DISCUSSION

The measurement of the steady-state, absolute rate of formaldehyde decomposition on the Ru(001) surface was carried out at surface temperatures ranging from 310 to 750 K and pressures ranging from 9.7×10^{-8} to 1.6×10^{-6} Torr. The decomposition products are CO and H_2. No detectable quantities of CH_4, H_2O, or CO_2 were observed, unlike on the Ru(110) surface.[2] The temperature and pressure dependence of the reaction rate is presented in Arrhenius plots in Fig 1. Two distinct kinetic regimes are observed. At relatively low surface temperatures and/or high formaldehyde pressures, the reaction rate is nearly zero order in the formaldehyde pressure with an apparent activation energy of 23 ± 0.5 kcal/mol and an apparent preexponential factor of $4 \times 10^{11}\ s^{-1}$. The rate levels off and becomes first order in the formaldehyde pressure with an apparent activation energy of zero at relatively high temperatures and/or low formaldehyde pressures. The reaction probability in this regime is essentially unity, i.e., the reaction rate becomes flux limited. The steady-state, absolute rate of DCDO decomposition was also measured under the same conditions. The kinetic parameters and absolute decomposition rates are the same as those for HCHO. The lack of a kinetic isotope effect indicates that C–H bond cleavage is not involved in the rate limiting step of the reaction under these experimental conditions. This observation also suggested a better way to measure the steady-state rate in the low surface temperature regime where the reaction rate is low. Instead of pure HCHO or DCDO, an equimolar mixture of both reagents was used. The intensity of mass 3 was monitored rather than mass 2 (or 4) in the case of pure HCHO (or DCDO). Since the background intensity of mass 3 in the UHV system is extremely low, the sensitivity of the rate measurements was increased by a factor of 10.

The fact that the reaction rate is nearly zero order in formaldehyde pressure in the low-temperature regime and the absense of an isotope effect imply that the Ru(001) surface is saturated with the reaction product(s), carbon monoxide, and/or hydrogen. A determination of surface coverages of these species during the steady-state reaction is essential to a confirmation of the mathematical model describing the reaction. The coverages of carbon monoxide and hydrogen during the steady-state reaction were determined by temperature programmed thermal desorption. When the reaction reached steady state, the Ru(001) surface was swung rapidly away from the formaldehyde beam and positioned in front of the mass spectrometer, the temperature of the crystal was increased linearly at 3 K/s, and mass spectrometric signals of masses 2 and 28 were monitored. It took ~0.2 s from swinging the surface away from the doser to the start of the temperature ramp. The area under the thermal desorption spectra of CO and H_2 serves as a measure of the surface coverages of CO and hydrogen during the steady-state reaction. The mass spectrometer was enclosed in a glass envalope with an aperture of 3.7 mm in diameter during the coverage determination experiments, in order to reduce the contribution from any change in the background partial pressures and desorption from the rear of the crystal.[17] The relative mass spectrometric sensitivities of CO and H_2 were determined from the thermal desorption spectra of CO and H_2 following the adsorption of HCHO on the Ru(001) surface at or below 200 K, when the ratio of the coverages of CO and hydrogen is 1:2. The results are shown in Fig. 2 for the decomposition of formaldehyde at 7×10^{-8} Torr. The surface is saturated with CO, whereas the coverage of hydrogen is only $\frac{1}{30}$ that of CO in the low-temperature regime. Furthermore, the coverage of CO remains essentially constant in the low-temperature regime. This demonstrates that the measured decomposition rate in the low-temperature regime corresponds to the rate of CO desorption. The activation energy of the desorption of CO is given by

$$\frac{E_{d,\mathrm{CO}}}{k_B} = -\frac{d(\ln R)}{d(1/T)} + \frac{d(\ln \theta_{\mathrm{CO}})}{d(1/T)},$$

where R is the reaction rate, and the first term on the right-hand side of the equation is the apparent activation energy determined from the Arrhenius plots. Since the second term on the right-hand side is essentially zero in the low-temperature regime (cf. Fig. 2), the apparent activation energy (23 ± 0.5 kcal/mol) determined in this regime is the desorption energy of CO at saturation coverage.

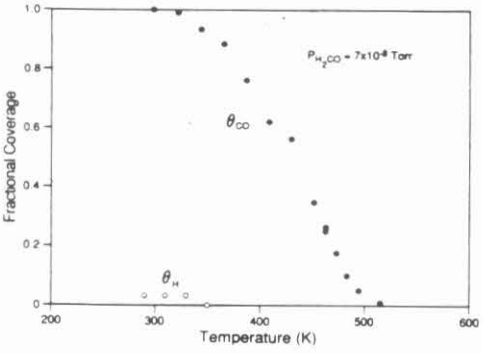

FIG. 2. The coverages of CO and hydrogen during the steady-state decomposition of formaldehyde on Ru(001) at an effective pressure of 7×10^{-8} Torr, determined by temperature programmed thermal desorption.

A mixture of HCHO and D_2 with a molar ratio of 1:4 at a total pressure of 1.0×10^{-6} Torr was reacted on the Ru(001) surface, in order to determine if there are any isotopic exchange or reduction products. No DCHO, DCDO, or methanol was observed at any temperature from 300 to 750 K. Our detection sensitivity would allow us to have observed a rate of 1×10^{11} mol cm^{-2} s^{-1}.

IV. SUMMARY

The decomposition kinetics of formaldehyde on the Ru(001) surface have been studied by measuring the steady-state, absolute rate of the reaction as a function of surface temperature from 310 to 750 K, parametric in the formaldehyde pressure from 9.7×10^{-8} to 1.6×10^{-6} Torr. Formaldehyde dissociates irreversibly on the Ru(001) surface, and only one reaction channel is observed, decomposition to CO and H_2. There are two distinct kinetic regimes in the Arrhenius plots, a low-temperature regime characterized by a Ru(001) surface which is essentially saturated with CO (the coverage of hydrogen is only $\frac{1}{30}$ of that of CO), and a high-temperature regime where the surface is essentially clean. In the low-temperature regime, the rate is nearly zero order in the formaldehyde pressure and has an apparent activation energy of 23 ± 0.5 kcal/mol and an apparent preexponential factor of 4×10^{11} s^{-1}. In the high-temperature regime, the rate is first order in the formaldehyde pressure, the apparent activation energy is zero, and the reaction probability is unity. No kinetic isotope effect is observed, indicating that C–H bond cleavage is not involved in the rate limiting step under these experimental conditions.

ACKNOWLEDGMENT

This work was supported by The National Science Foundation under Grant No. DMR-8500789.

[1] J. T. Yates, T. E. Madey, and M. J. Dresser, J. Catal. **30**, 260 (1973).
[2] D. W. Goodman, T. E. Madey, M. Ono, and J. T. Yates, J. Catal. **50**, 279 (1977).
[3] G. B. Fisher, T. E. Madey, and J. T. Yates, J. Vac. Sci. Technol. **15**, 543 (1978).
[4] A. B. Anton, J. E. Parmeter, and W. H. Weinberg, J. Am. Chem. Soc. **108**, 1823 (1986).
[5] J. T. Dickinson and R. J. Madix, Int. J. Chem. Kinet. **10**, 871 (1978).
[6] L. J. Richter and W. Ho, J. Chem. Phys. **83**, 2165 (1985).
[7] N. M. Abbas and R. J. Madix, Appl. Surf. Sci. **7**, 241 (1981).
[8] B. A. Sexton, A. E. Hughes, and N. R. Avery, Surf. Sci. **155**, 366 (1985).
[9] E. M. Stuve, R. J. Madix, and B. A. Sexton, Surf. Sci. **119**, 279 (1982).
[10] M. A. Vannice, Catal. Rev. Sci. Eng. **14**, 153 (1976).
[11] J. L. Taylor, D. E. Ibbotson, and W. H. Weinberg, J. Chem. Phys. **69**, 4298 (1978).
[12] T. E. Madey, H. A. Engelhardt, and D. Menzel, Surf. Sci. **48**, 304 (1975).
[13] J. R. Engstrom and W. H. Weinberg, Rev. Sci. Instrum. **55**, 404 (1984).
[14] A. Cornu and R. Massot, *Compilation of Mass Spectral Data*, 2nd ed. (Heyden, 1975), Vol. 1A.
[15] C. T. Campbell and S. M. Valone, J. Vac. Sci. Technol. A **3**, 408 (1985).
[16] Y.-K. Sun, J. J. Vajo, C.-Y. Chan, and W. H. Weinberg, J. Vac. Sci. Technol. A **6**, 854 (1988).
[17] P. Feulner and D. Menzel, J. Vac. Sci. Technol. **17**, 662 (1980).

CHAPTER 6.

Kinetics of Decomposition of Formaldehyde on Ru(001)

[This chapter consists of an article coauthored with W. H. Weinberg.]

ABSTRACT

Both steady-state and transient isothermal rates of decomposition of formaldehyde on the Ru(001) surface have been measured as a function of surface temperature. When the reaction reaches steady state at a reactant pressure between 9.7×10^{-8} and 1.6×10^{-6} Torr and at a surface temperature between 310 and 750 K, the only observed reaction products are carbon monoxide and hydrogen. The rate of the decomposition at low surface temperatures (below 360 K) is nearly zero order in formaldehyde pressure since the surface is nearly saturated with carbon monoxide. The rate is governed by the rate of desorption of carbon monoxide. Hence, the apparent activation energy of 23 ± 0.5 kcal/mol and the apparent preexponential factor of 4×10^{11} s^{-1} at low surface temperature are the kinetic parameters associated with desorption of carbon monoxide at saturation coverage. As the surface temperature is increased to above 500 K, the reaction occurs on a essentially clean surface. The rate becomes flux-limited and first order in the formaldehyde pressure. No kinetic isotope effect was observed under these experimental conditions. The unity reaction probability, together with the lack of a kinetic isotope effect, indicates that the rate coefficient for the formaldehyde molecules on the surface to dissociate is much greater than that for them to desorb back to the gas phase. The decomposition of formaldehyde results in coadsorption of hydrogen and carbon monoxide. It is shown that the presence of carbon monoxide on the surface reduces the binding energy of hydrogen adatoms.

1. INTRODUCTION

The decomposition of formaldehyde has been studied on a number of transition metal surfaces including W(111) and W(100) (**1**), Ru(110) (**2, 3**), Ru(001) (**4, 5**), Ni(110) (**6, 7**), clean and sulfided Pt(111) (**8**), clean and oxygen precovered Cu(110) (**9**), and oxygen precovered Ag(110) (**10**). The possibility that the methanation reaction may proceed via H_2CO or H_2CO-derived intermediates (**11**) makes a study of the chemistry of formaldehyde on transition metal surfaces quite relevant. Carbon monoxide and hydrogen are the major reaction products of formaldehyde decomposition, as determined by thermal desorption mass spectrometry. Small quantities of other products were also observed on these surfaces, including CH_4 (**1, 2**) CH_3OH (**6-8**), CO_2 (**1, 6-8**) and H_2O (**2, 6, 7**). The presence of impurities in the formaldehyde sample (methyl formate, for example) may account for the observation of CO_2 and CH_4 in some cases. On the Ru(001) surface, stable reaction intermediates including η^1-formaldehyde, η^2-formaldehyde, and η^1-formyl have been identified by electron energy loss spectroscopy following the adsorption of formaldehyde at 80 K and subsequent annealing to various surface temperatures (**4**). In this study, we have made mass spectrometric measurements of the steady-state and transient isothermal rate of decomposition of formaldehyde on the Ru(001) surface as a function of surface temperature, parametric in the formaldehyde pressure. The observed kinetic behavior is explained on the basis of a proposed reaction mechanism in terms of elementary surface reactions.

EXPERIMENTAL DETAILS

The experiments were carried out in an ion-pumped (200 *l*/s) stainless steel, ultrahigh vacuum chamber equipped with quadrupole mass spectrometry and Auger electron spectroscopy, low-energy electron diffraction (**5**). The base pressure of the belljar was below 8×10^{-11} Torr of reactive gases. Details concerning the preparation and cleaning of the Ru(001) surface were presented previously (**5**). The crystal was mounted on a manipulator by two 0.001 in. tantalum wires spotwelded on the back of the crystal. The Ru(001) crystal could be heated resistively, and cooled conductively by liquid nitrogen. The temperature of the Ru(001) surface was measured by a 0.003 in. W/5%Re – W/26%Re thermocouple spotwelded to the back of the crystal.

Deuterated paraformaldehyde (99.6 atom %D) was obtained from MSD Isotopes and paraformaldehyde (with $H_2O < 1\%$) from Fluka. They were transferred in powder form into a preevacuated 50 ml pyrex flask in a plastic bag purged with dry nitrogen gas. The flask with the paraformaldehyde sample was evacuated in a gas manifold which is pumped by a Varian M-2 diffusion pump and has a base pressure of 6×10^{-6} Torr. Formaldehyde in monomer form was prepared in a similar way to that described by Yates *et al.* (**1**), and was stored at room temperature in a 500 ml Pyrex bulb at pressures from 0.2 to 8 Torr. A mass spectrum of the HCHO sample exhibits m/e peaks only at 30, 29, 28, 16, 14, 13, 12 and 2 with peak height ratios of 0.73 : 1.00 : 0.34 : 0.02 : 0.04 : 0.03 : 0.05; that of the DCDO sample exhibits m/e peaks at 32, 30, 28, 16, 14, 12 and 4 with intensity ratios of 0.80 : 1.00 : 0.36 : 0.07 : 0.05 : 0.04 : 0.05, in reasonable agreement with the reported values (**12**). Most importantly, there are no peaks at masses 44 and 60, indicating that the samples were free of methyl formate (**1**). The mass spectra remain unchanged for up to one week following storage at room temperature.

The formaldehyde was introduced from the storage bulb onto the Ru(001) surface through a directional beam doser consisting of a type 304 stainless steel plate with collimated hole structures (Brunswick Corporation). The hole diameters are 0.1 mm; the thickness of the plate is 1.3 mm; and the open area of the plate is 50%. The diameter of the plate is 9 mm, slightly larger than that of the Ru(001) single crystal, in order to improve the pressure profile across the Ru(001) surface.

The Ru(001) surface is parallel to and 3 mm away from the doser when the crystal is in front of the beam doser. The crystal so positioned intercepts approximately 50% of the formaldehyde flowing through the doser (**13**).

The absolute flow rate of the formaldehyde through the doser was determined by the rate of pressure drop in the formaldehyde storage bulb, measured by a Baratron manometer. The cryopanel in the UHV system was cooled by liquid nitrogen, and the ion gauge was turned off during both the steady-state and transient rate measurements in order to decrease the background pressure. The ratio of the formaldehyde 'beam pressure' to the background formaldehyde pressure was determined to be greater than 40 : 1 by measuring the formaldehyde decomposition rate when the crystal was in and out of the formaldehyde beam at high surface temperatures where the reaction kinetics are first order.

During steady-state rate measurements, formaldehyde flowed steadily through the gas doser. The temperature of the Ru(001) surface was programmed to follow a staircase function. Each time the surface temperature became constant, mass spectrometric signals of the products (H_2 and CO) and reactant (H_2CO) were monitored as the Ru(001) surface was positioned in and out of the formaldehyde beam. The Ru(001) surface remained in the beam for a sufficiently long time that steady state was achieved. Since H_2CO and D_2CO were observed to react on the Ru(001) surface with exactly the same rate (*vide infra*), an equimolar mixture of H_2CO and D_2CO was used as reactant and the mass spectrometric intensity of mass 3 (HD^+) was monitored. Since the background intensity of mass 3 in the UHV system is extremely low, the sensitivity of the measurements of the rate of the decomposition was increased by a factor of ten, compared with the case in which pure H_2CO or D_2CO was used. Typical data are shown in Fig. 1 in which the surface temperature and the mass spectrometric intensity of mass 3 (HD^+) when the surface was in and out of the reactant beam are plotted vs. time. The difference in the mass spectrometric signal of mass 2 (ΔI_{H_2}) in the case of H_2CO when the surface was in and out of the beam is directly proportional to the decomposition rate. Since the beam-to-background pressure ratio is greater than 40, both the reaction rate when the Ru(001) surface was out of the beam and the reaction rate from the rear of the crystal when the Ru(001) was in the beam were negligible. In the high pumping speed limit, the absolute rate R of the decomposition and ΔI_{H_2} are related by

$$R = \frac{S_{H_2}}{k_B T_g} \eta_{H_2} \Delta I_{H_2}, \tag{1}$$

where S_{H_2} is the pumping speed of H_2, T_g is the gas temperature, k_B is the Boltzmann constant, and η_{H_2} is the mass spectrometric sensitivity of H_2 defined in such a way that the partial pressure P_{H_2} is given by $P_{H_2} = \eta_{H_2} I_{H_2}$. The product $S_{H_2}\eta_{H_2}$ was calculated using Eq. 1 following the determination of ΔI_{H_2} with a known leak of H_2 into the UHV system from the doser. The leak rate of H_2 (R_{H_2}) was determined in the same way as that of formaldehyde discussed above.

2. RESULTS AND DISCUSSION

The measurement of the steady-state, absolute rate of formaldehyde decomposition on the Ru(001) surface was carried out at surface temperatures ranging from 310 to 750 K and pressures ranging from 9.7×10^{-8} to 1.6×10^{-6} Torr. The decomposition products are CO and H_2. No detectable quantities of CH_4, H_2O or CO_2 were observed, unlike on the Ru(110) surface (**2**). The temperature and pressure dependence of the reaction rate is presented in the form of Arrhenius plots in Fig 2. At relatively low surface temperatures, the reaction rate is nearly zero order in the formaldehyde pressure with an apparent activation energy of 23 ± 0.5 kcal/mol and an apparent preexponential factor of 4×10^{11} s^{-1}. The rate levels off and becomes first order in the formaldehyde pressure with an apparent activation energy of zero at relatively high temperatures. The reaction probability in this regime is essentially unity, *i.e.*, the reaction rate is flux-limited. The steady-state, absolute rate of D_2CO decomposition was also measured under the same conditions. The kinetic parameters and absolute decomposition rates are the same as those for H_2CO. The lack of a kinetic isotope effect indicates that C-H bond cleavage is not involved in the rate limiting step of the reaction under these experimental conditions. This observation also suggested a better way to measure the steady-state rate in the low surface temperature regime where the reaction rate is low. Instead of pure H_2CO or D_2CO, an equimolar mixture of both reagents was used. The intensity of mass 3 was monitored rather than mass 2 (or 4) in the case of pure H_2CO (or D_2CO). Since the background intensity of mass 3 in the UHV system is extremely low, the sensitivity of the rate measurements was increased by a factor of ten.

The fact that the reaction rate is nearly zero order in formaldehyde pressure in the low-temperature regime and the absence of a kinetic isotope effect imply that the Ru(001) surface is saturated with the reaction product(s), carbon monoxide and/or hydrogen adatoms. A determination of surface fractional coverages of CO and the hydrogen adatoms during the steady-state reaction at 320 K reveals that the surface is saturated with CO, whereas the coverage of hydrogen adatoms is only 1/30 of that of CO in the low-temperature regime (**5**). Furthermore, the coverage of CO remains essentially constant in the low-temperature regime, whereas that of the hydrogen adatoms decreases to near zero by 340 K (**5**). The rate of decomposition is completely limited by the rate of desorption of CO. The activation energy of desorption of CO in this case is given by

$$\frac{E_{d,\mathrm{CO}}}{k_B} = -\frac{\mathrm{d}(\ln R)}{\mathrm{d}(1/T)} + \frac{\mathrm{d}(\ln \theta_{CO})}{\mathrm{d}(1/T)},$$

where R is the measured rate of decomposition and θ_{CO} is the surface coverage of CO. The first term on the right-hand-side of the equation is the apparent activation energy determined from the Arrhenius plots. Since the second term on the right-hand-side is essentially zero in the low-temperature regime, the apparent activation energy (23 ± 0.5 kcal/mol) determined in this regime is the desorption energy of CO at saturation coverage.

The decomposition of the formaldehyde can be expressed mechanistically as

$$\mathrm{H_2CO(g)} \overset{\zeta \mathrm{f}}{\underset{\mathrm{k_{d,H_2CO}}}{\rightleftharpoons}} \mathrm{H_2CO(a)} \tag{2}$$

$$\mathrm{H_2CO(a)} \xrightarrow{\mathrm{k_r}} \mathrm{CO(a)} + \mathrm{2H(a)} \tag{3}$$

$$\mathrm{CO(a)} \xrightarrow{\mathrm{k_{d,CO}}} \mathrm{CO(g)} \tag{4}$$

$$\mathrm{2H(a)} \xrightarrow{\mathrm{k_{d,H_2}}} \mathrm{H_2(g)} \tag{5}$$

where ζ is a thermal average of the Maxwell Boltzmann gas of H_2CO at 300 K and is taken to be unity here, f is the impingement frequency of H_2CO per surface site, and k_i's are rate constants associated with each step. In Eq. (3) the dissociation of H_2CO is taken as irreversible since no isotopic exchange products were observed when reacting a mixture of H_2CO and D_2 of a molar ratio of 1 : 4 at a total pressure of 1.0×10^{-6} Torr on the Ru(001) surface at any temperature from 310 to 750 K. The readsorption of the reaction products CO and H_2 was neglected in Eqs. (4) and (5) since they were pumped away rapidly. To calculate the reaction rate based on this mechanism, the following material balances for adsorbed H_2CO, CO and H_2 were used:

$$\frac{\mathrm{d}\theta_{\mathrm{H_2CO}}}{\mathrm{d}t} = \zeta f_{\mathrm{H_2CO}} f(\theta) - k_{d,\mathrm{H_2CO}} \theta_{\mathrm{H_2CO}} - k_r \theta_{\mathrm{H_2CO}} f(\theta) \tag{6}$$

$$\frac{\mathrm{d}\theta_{\mathrm{CO}}}{\mathrm{d}t} = k_r \theta_{\mathrm{H_2CO}} f(\theta) - k_{d,\mathrm{CO}} \theta_{\mathrm{CO}} \tag{7}$$

$$\frac{\mathrm{d}\theta_{\mathrm{H}}}{\mathrm{d}t} = 2k_r \theta_{\mathrm{H_2CO}} f(\theta) - k_{d,\mathrm{H_2CO}} \theta_{\mathrm{H_2CO}} - k_{d,\mathrm{H_2}} \theta_{\mathrm{H}}, \tag{8}$$

where θ's are the fractional coverage of surface species and $f(\theta)$ is the density of vacant sites on the surface

$$f(\theta) = 1 - \theta_{\mathrm{CO}} - \theta_{\mathrm{H}}. \tag{9}$$

Two assumptions were made in the above material balances concerning the kinetics associated with each step in this mechanism, namely, only the intrinsic precursor of H_2CO exists on the surface (**14**); and the reaction represented by Eq. 3 requires two neighboring vacant sites to proceed.

When steady state is achieved all three derivatives in Eqs. 6 to 8 become zero. Given the function $f(\theta)$, one can solve the algebraic equations for θ_{CO}. The overall rate of the decomposition at steady state is given by

$$R = k_{d,\mathrm{CO}}\theta_{\mathrm{CO}}.$$

It was shown experimentally that the coverage of hydrogen is negligibly small compared to that of CO during the steady-state reaction (**5**), hence,

$$f(\theta) = 1 - \theta_{\mathrm{CO}}. \tag{10}$$

Insert Eq. 10 into Eq. 6 and 7, and solve for θ_{CO}, we find

$$\theta_{\mathrm{CO}} = \frac{2f_{\mathrm{H_2CO}} + k_{d,\mathrm{CO}} - [4f_{\mathrm{H_2CO}}k_{d,\mathrm{CO}}(1/P_r^{(0)} - 1) + k_{d,\mathrm{CO}}^2/(P_r^{(0)})^2]^{1/2}}{2(f_{\mathrm{H_2CO}} + k_{d,\mathrm{CO}})} \tag{11}$$

where $P_r^{(0)}$, given by

$$P_r^{(0)} = \frac{k_r}{k_r + k_{d,\mathrm{H_2CO}}}, \tag{12}$$

is the probability of decomposition on a clean Ru(001) surface and has been shown experimentally to be unity, since the reaction rate is flux limited at high surface temperatures when the surface is essentially clean. The expression for the surface coverage of CO (Eq. 11) during the steady-state decomposition of the formaldehyde then becomes very simple:

$$\theta_{\mathrm{CO}} = \frac{f_{\mathrm{H_2CO}}}{f_{\mathrm{H_2CO}} + k_{d,\mathrm{CO}}}, \tag{13}$$

and the reaction rate is

$$R = \frac{k_{d,\mathrm{CO}}f_{\mathrm{H_2CO}}}{f_{\mathrm{H_2CO}} + k_{d,\mathrm{CO}}}. \tag{14}$$

Eq. 14 can successfully describe the observed kinetic behavior shown in Fig. 2. At low surface temperatures and/or high formaldehye pressures, the rate of formaldehyde impingement on the surface is much higher than the rate constant of CO desorption, i.e., $f_{H_2CO} \gg k_{d,CO}$, Eqs. 13 and 14 become

$$\theta_{CO} \rightarrow 1,$$

$$R = k_{d,CO}.$$

The surface is saturated with CO, and the overall reaction rate is governed by that of CO desorption. At high surface temperatures and/or low formaldehyde pressure, however, the rate constant of CO desorption is much greater than the impingement rate of the formaldehyde, i.e., $f_{H_2CO} \ll k_{d,CO}$, Eqs. 13 and 14 then become

$$\theta_{CO} \rightarrow 0,$$

$$R = f_{H_2CO}.$$

The reaction is occurring on a virtually clean Ru(001) surface and the reaction probability is unity.

The fact that the reaction probability at high surface temperatures is unity, together with the lack of a kinetic isotope effect, implies that the activation energy for the thermally accommodated formaldehyde molecules on the surface to dissociate is much lower than that for them to desorb back to the gas phase, i.e., $E_r \ll E_d$. The rate coefficient k_r is always much greater than k_{d,H_2CO} in Eq. 12 and hence disappears from the overall rate expression, cf. Eq. 14. No information concerning k_r, the rate constant of the dissociation of molecularly adsorbed formaldehyde on Ru(001), can be evaluated from the measured steady-state rate. This is in contrast with the case of the decomposition of formaldehyde on Pt(110)-(1×2) surface at 8.1×10^{-8} Torr (**15**), where the activation energy E_r is also lower than E_{d,H_2CO}

(by 3 kcal/mol), but not as overwhelmingly as it does on Ru(001). On the Pt(110)-(1×2) surface the steady-state rate is also limited by the desorption rate of CO at low surface temperatures. At high surface temperatures the steady-state rate passes a maximum at 540 K and decreases with increasing surface temperature. Rather than limited by the flux of formaldehyde, the rate is limited by the competing kinetics of the thermally accommodated, molecularly adsorbed formaldehyde on the surface to its dissociation and its desorption from the surface (**15**).

The decomposition of the formaldehyde results in the coadsorption of CO and hydrogen adatoms on the Ru(001) surface, which can be conveniently utilized to study the effect of CO on the kinetics of the recombinative desorption of hydrogen adatoms on the surface. The dissociative chemisorption of the formaldehyde was carried out at 200 K, slightly below the temperature at which H_2 desorption becomes detectable during the adsorption of H_2CO. Thus, this is equivalent to adsorb equimolar of H_2 and CO on the surface. The thermal desorption spectra of H_2 and CO from this surface following an exposure of 13 L are plotted in Figs. **3** and **4**, together with the thermal desorption spectra of H_2 and CO from Ru(001) following saturation exposures of H_2 and CO, respectively. Note that a small fraction of the surface species would be η^2-H_2CO following the saturation exposure of H_2CO at 200 K, since it was observed that approximately 0.03 monolayer of η^2-H_2CO, together with 0.25 monolayer of CO, remained on the surface following adsorption of H_2CO at 80 K and subsequently annealed to 275 K, above which temperature the η^2-H_2CO decomposed rapidly (**4**). Since the coverage of the η^2-H_2CO is small and the bonding of the η^2-H_2CO to the surface is similar to that of CO (**4**), the small fraction of the η^2-H_2CO would behave qualitatively similar to CO in far as the modification of the surface is concerned. It is apparent from Fig. **3** that the chemisorbed CO on the surface decreases the desorption temperature of H_2, indicating a decreases in the binding energy of hydrogen adatoms due to the presence of approximately 0.31 monolayer of CO on the surface (**16**).

The reduction of the binding energy of hydrogen adatoms on Ru(001) in the presence of CO is also manifested in transient isothermal desorption spectra of H_2 resulted from the decomposition of H_2CO on a initially clean Ru(001) surface. During each measurement, formaldehyde flowed steadily into the UHV system through the doser when the *clean* Ru(001) surface, held at a constant temperature, was positioned in the beam rapidly and the mass spectrometric intensity of H_2 was monitored. The results are shown in Figs. 5 and 6, in which the rate of desorption of H_2 was plotted as a function of time. The time zero corresponds to when the surface was positioned in the H_2CO beam. The effective pressure of H_2CO was 2.6×10^{-8} Torr when the Ru(001) surface was facing the doser. At 455 K, the production of H_2 was immediately observed and reached steady state as the Ru(001) surface was exposed to H_2CO, cf. curve 4 in Fig. 5 (note that it is offset horizontally by 290 seconds for clarity). As can be seen from Fig. 2, the steady-state rate at 455 K for a H_2CO pressure of 2.6×10^{-8} Torr is the same as the formaldehyde flux, which is 9.5×10^{12} cm^{-2}-s^{-1}. There is, however, a induction period associated with the rest of curves in Figs. 5 and 6 prior to the observation of H_2 production. During this induction period, hydrogen atoms and CO resulted from the decomposition chemisorb on the surface. As CO and hydrogen adatoms accumulate on the surface, the activation energy for the recombinative desorption of the hydrogen adatoms is reduced. Eventually, desorption of H_2 occurs. The rate of desorption of H_2 increases with time at beginning, reaches a maximum and decreases to the steady-state rate, as hydrogen adatoms become depleted from the surface. The steady-state rate is undetectable for temperatures below 315 K. Each of the curves in Fig. 5 has exactly the same area, indicating that the resulted surfaces are saturated with CO with its coverage being the same. The induction period becomes shorter as the surface temperature increases. The peak rate of H_2

desorption increases with the surface temperature and reaches a maximum at 325 K. Note that the peak rate at 325 K is 28% higher than the flux of formaldehyde, or the maximum rate of H_2 production at steady state, cf. curve 5 in Fig. 6.

Each of the curves in Fig. 5 is similar to a thermal desorption spectrum (**17**). Only in this case the decrease in activation energy for the recombinative desorption of hydrogen adatoms is the driving force for the increasing rate constant with time. The physical picture behind the reduction of the activation energy could be repulsive interactions between CO and hydrogen adatom and between hydrogen adatoms (**18**), or more importantly, perhaps, a complete segregation of hydrogen and CO (**19**) that would lead to higher local density of hydrogen adatoms and hence a lower binding energy.

SUMMARY

The decomposition kinetics of formaldehyde on the Ru(001) surface have been studied by measuring the steady-state, absolute rate of the reaction as a function of surface temperature from 310 to 750 K, parametric in the formaldehyde pressure from 9.7×10^{-8} to 1.6×10^{-6} Torr. Formaldehyde dissociates irreversibly on the Ru(001) surface with unity reaction probability on a clean surface with CO and H_2 as products. There are two distinct kinetic regimes in the Arrhenius plots, a low-temperature regime characterized by a Ru(001) surface which is essentially saturated with CO (the coverage of hydrogen is only 1/30 of that of CO), and a high-temperature regime where the surface is essentially clean. In the low-temperature regime, the rate is nearly zero order in the formaldehyde pressure and has an apparent activation energy of 23 ± 0.5 kcal/mol and an apparent preexponential factor of 4×10^{11} s^{-1}. In the high-temperature regime, the rate is first order in the formaldehyde pressure. No kinetic isotope effect is observed, indicating that C-H bond cleavage is not involved in the rate-limiting step under these experimental conditions. The dissociation of the formaldehyde leads to the coadsorption of CO and hydrogen adatoms. The presence of CO on the surface reduces the activation energy of the recombinative desorption of the hydrogen adatoms.

Acknowledgment: This work was supported by The National Science Foundation under grant number DMR-8500789.

REFERENCES

1. J. T. Yates, T. E. Madey and M. J. Dresser, J. Catal. **30**, 260 (1973).
2. D. W. Goodman, T. E. Madey, M. Ono and J. T. Yates, . *J. Catal.* **50**, 279 (1977).
3. G. B. Fisher, T. E. Madey and J. T. Yates, *J. Vac. Sci. Technol.* **15**, 543 (1978).
4. A. B. Anton, J. E. Parmeter and W. H. Weinberg, *J. Am. Chem. Soc.* **108**, 1823 (1986).
5. Y. -K. Sun, C. -Y. Chan and W. H. Weinberg, *J. Vac. Sci. Technol. A* **7** 854 (1988).
6. J. T. Dickinson and R. J. Madix, *Int. J. Chem. Kinet.* **10**, 871 (1978).
7. L. J. Richter and W. Ho, *J. Chem. Phys.* **83**, 2165 (1985).
8. N. M. Abbas and R. J. Madix, *Appl. Surface. Sci.* **7**, 241 (1981).
9. B. A. Sexton, A. E. Hughes and N. R. Avery, . *Surface Sci.* **155**, 366 (1985).
10. E. M. Stuve, R. J. Madix and B. A. Sexton, *Surface Sci.* **119**, 279 (1982).
11. M. A. Vannice, *Catal. Rev.-Sci. Eng.* **14**, 153 (1976).
12. A. Cornu and R. Massot, *Compilation of Mass Spectral Data*, Heyden, 2nd ed. 1A (1975).
13. C. T. Campbell and S. M. Valone, *J. Vac. Sci. Technol. A* **3**, 408 (1985).
14. W. H. Weinberg, in *Kinetics of Interface Reactions*, Eds., M. Grunze and H. J. Kreuzer, Springer-Verlag, Heidelberg, 1987, p. 94.
15. Y. -K. Sun and W. H. Weinberg, *Surface Sci.* submitted.
16. D. E. Peebles, J. A. Schreifels and J. M. White, *Surface Sci.* **116**, 117 (1982).
17. P. A. Redhead, *Vacuum* **12**, 203 (1962).
18. P. Feulner and D. Menzel, *Surface Sci.* **154**, 465 (1985).
19. E. D. Williams, P. A. Thiel, W. H. Weinberg and J. Y. Yates, Jr., *J. Chem. Phys.* **72**, 3496 (1980).

Figure Captions

Fig. 1: Temperature profile of the Ru(001) surface and the mass spectrometric intensity of HD when the surface was positioned in and out of a beam of an equimolar mixture of H_2CO and D_2CO at constant surface temperatures.

Fig. 2: Arrhenius plots of the steady-state rate of decomposition of formaldehyde on Ru(001) at different formaldehyde pressures.

Fig. 3: Comparison of the thermal desorption spectra of H_2 from the Ru(001) surface following dissociative adsorption of H_2CO on the Ru(001) surface at 200 K and that of H_2 from a Ru(001) surface saturated with hydrogen adatoms.

Fig. 4: Comparison of the thermal desorption spectra of CO from the Ru(001) surface following dissociative adsorption of H_2CO on the Ru(001) surface at 200 K and that of CO from a CO-saturated Ru(001) surface.

Fig. 5: Rate of desorption of H_2 in transient isothermal decomposition of H_2CO on a initially clean Ru(001) surface as a function of time. The flux of H_2CO is $9.5 \times 10^{12}\ cm^{-2}\text{-}s^{-1}$. The surface temperatures are (1) 210 K, (2) 273 K, (3) 284 K, (4) 295 and (5) 315 K.

Fig. 6: The same as Fig. 5 except that the surface temperatures are (1) 325 K, (2) 356 K, (3) 400 K, and (4) 455 K.

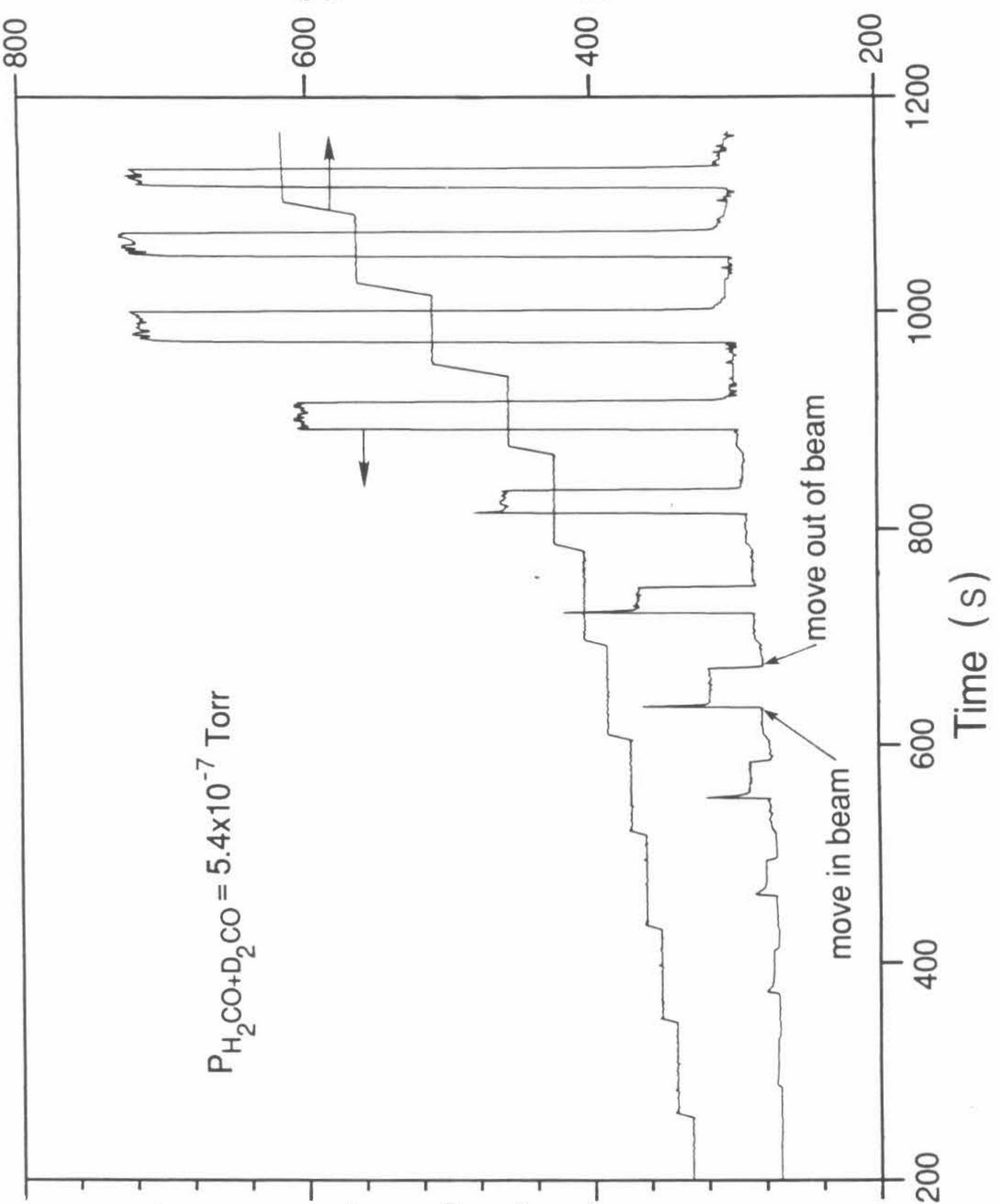
$P_{H_2CO+D_2CO} = 5.4\times10^{-7}$ Torr
move in beam
move out of beam
Time (s)
200
400
600
800
1000
1200
Mass 3 (HD) Signal (Arb. units)
Temperature (K)
200
400
600
800

Figure 1

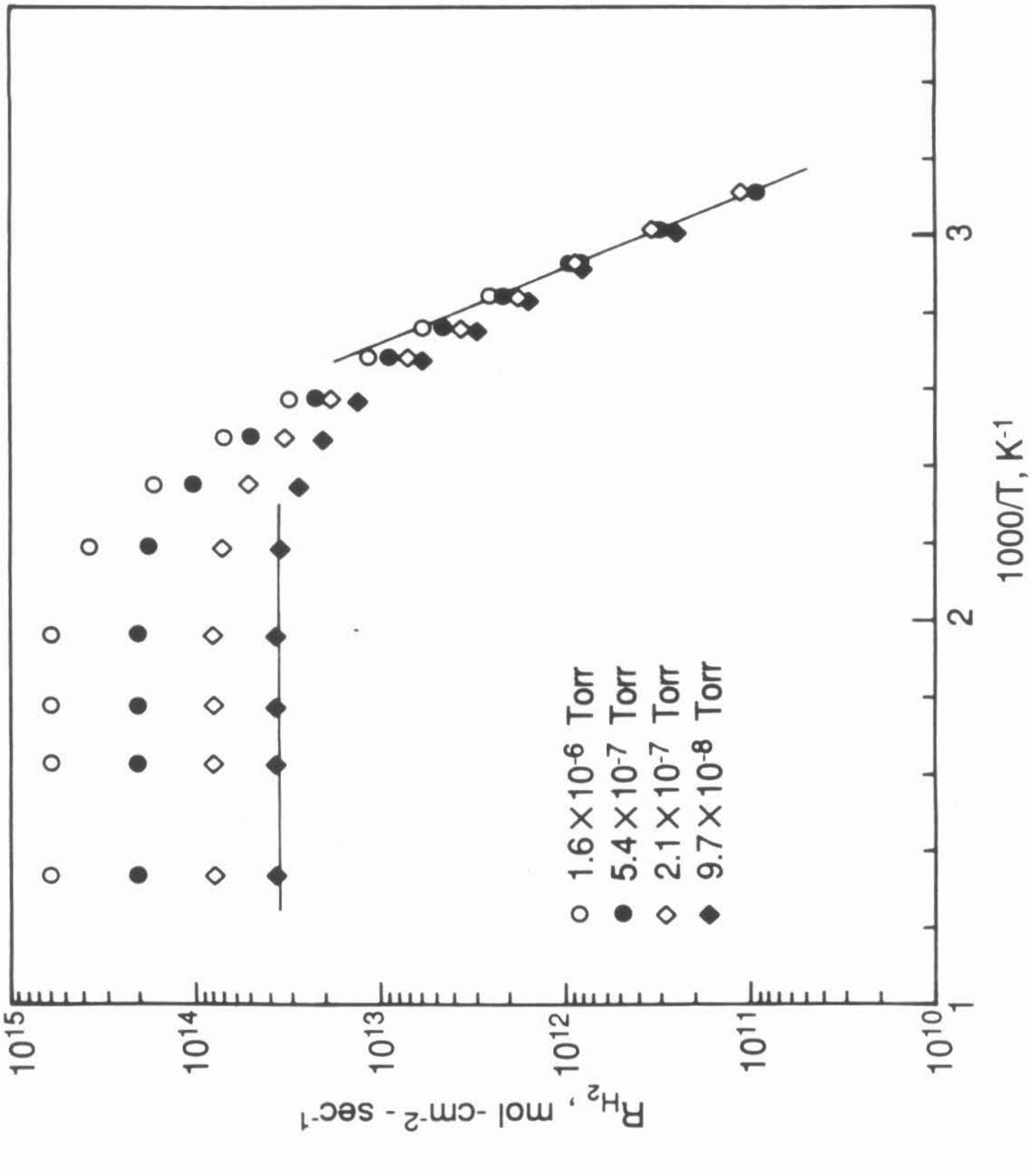
R_{H_2}, mol -cm^{-2} - sec^{-1}
10^{15}
10^{14}
10^{13}
10^{12}
10^{11}
10^{10}
1
2
3
1000/T, K^{-1}
○ 1.6×10^{-6} Torr
● 5.4×10^{-7} Torr
◇ 2.1×10^{-7} Torr
◆ 9.7×10^{-8} Torr

Figure 2

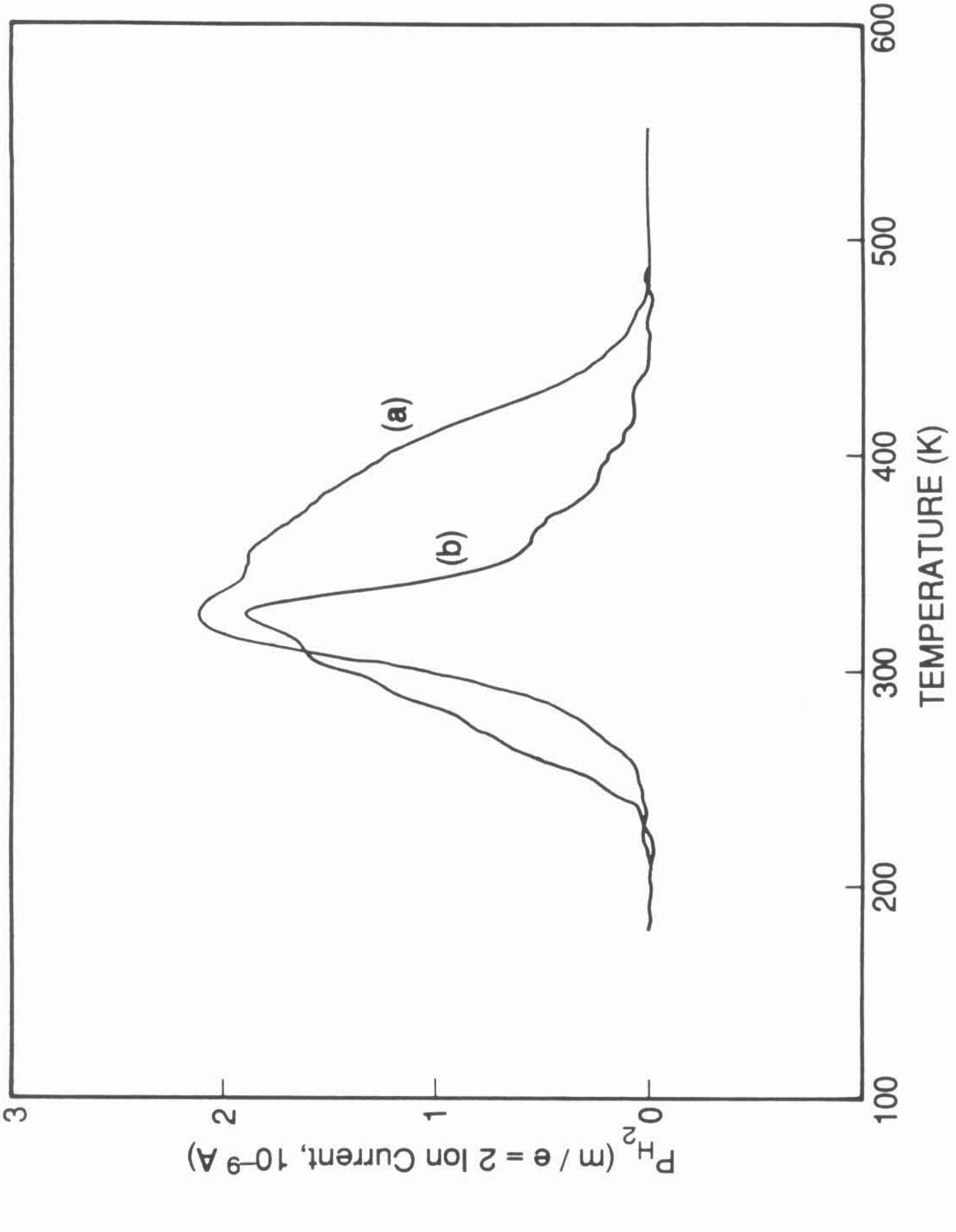

P_{H_2} (m / e = 2 Ion Current, 10^{-9} A)
0
1
2
3
TEMPERATURE (K)
100
200
300
400
500
600
(a)
(b)

Figure 3

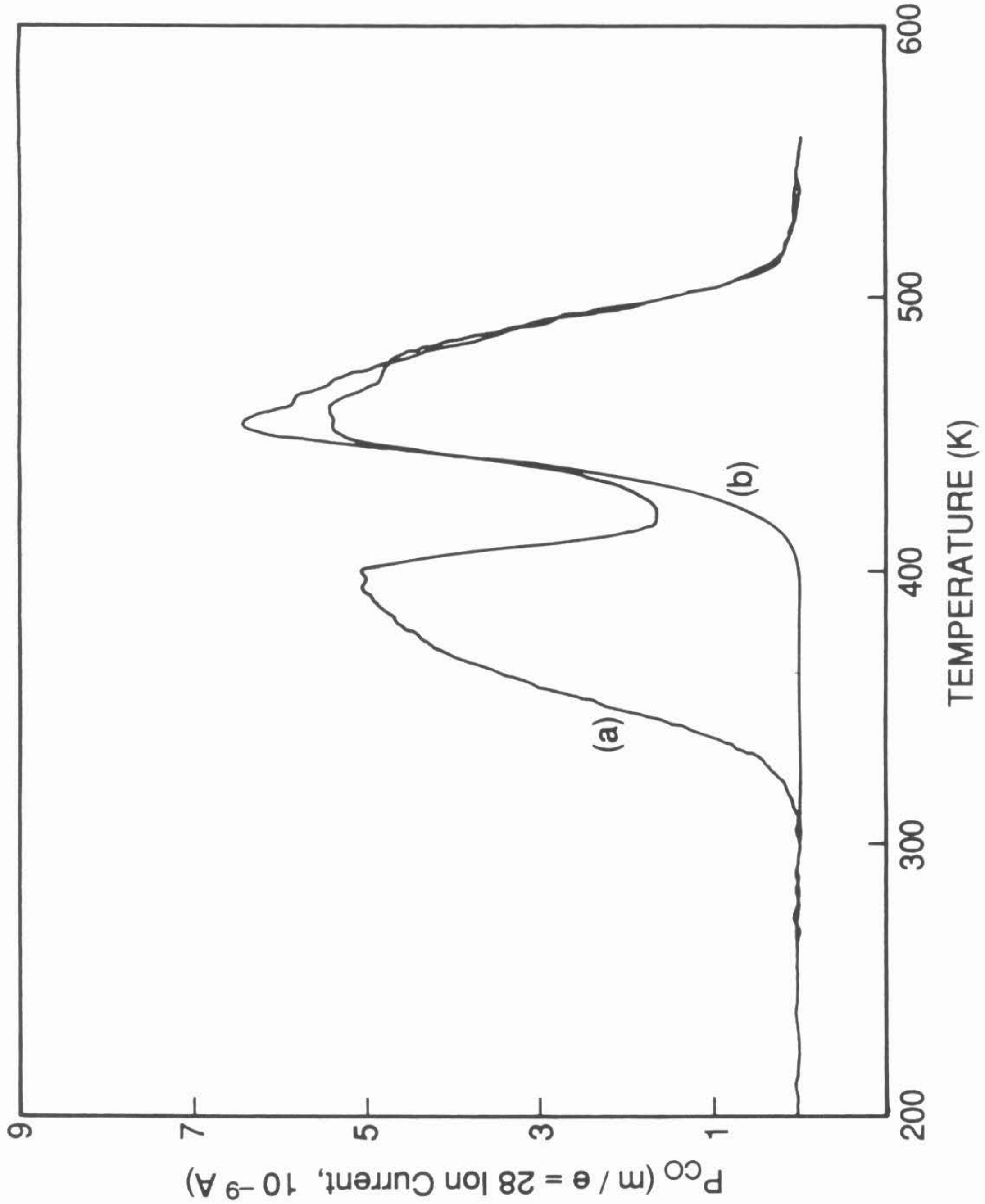
(a)
(b)
TEMPERATURE (K)
200
300
400
500
600
P_{CO} (m / e = 28 Ion Current, 10⁻⁹ A)
1
3
5
7
9

Figure 4

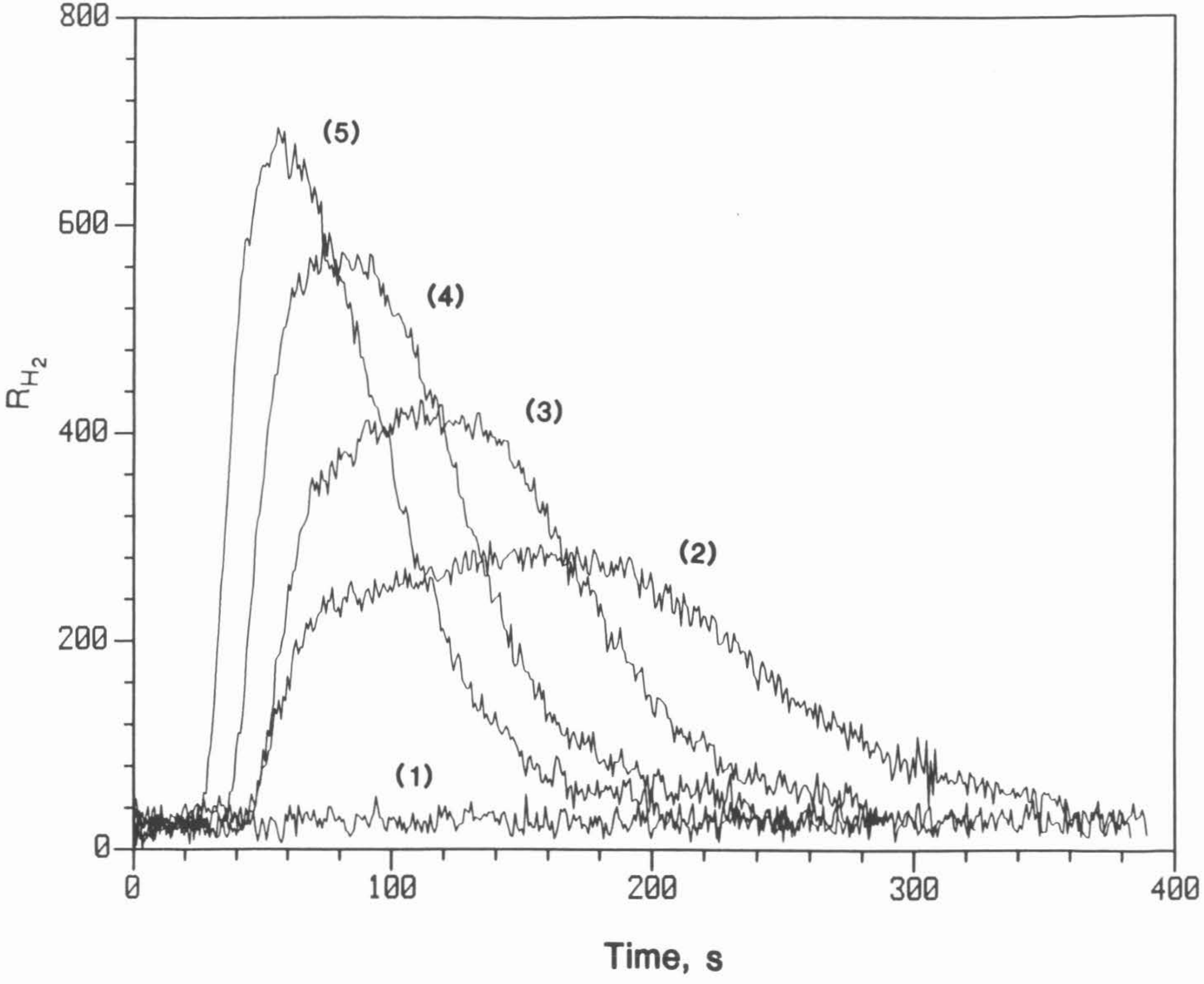

Figure 5

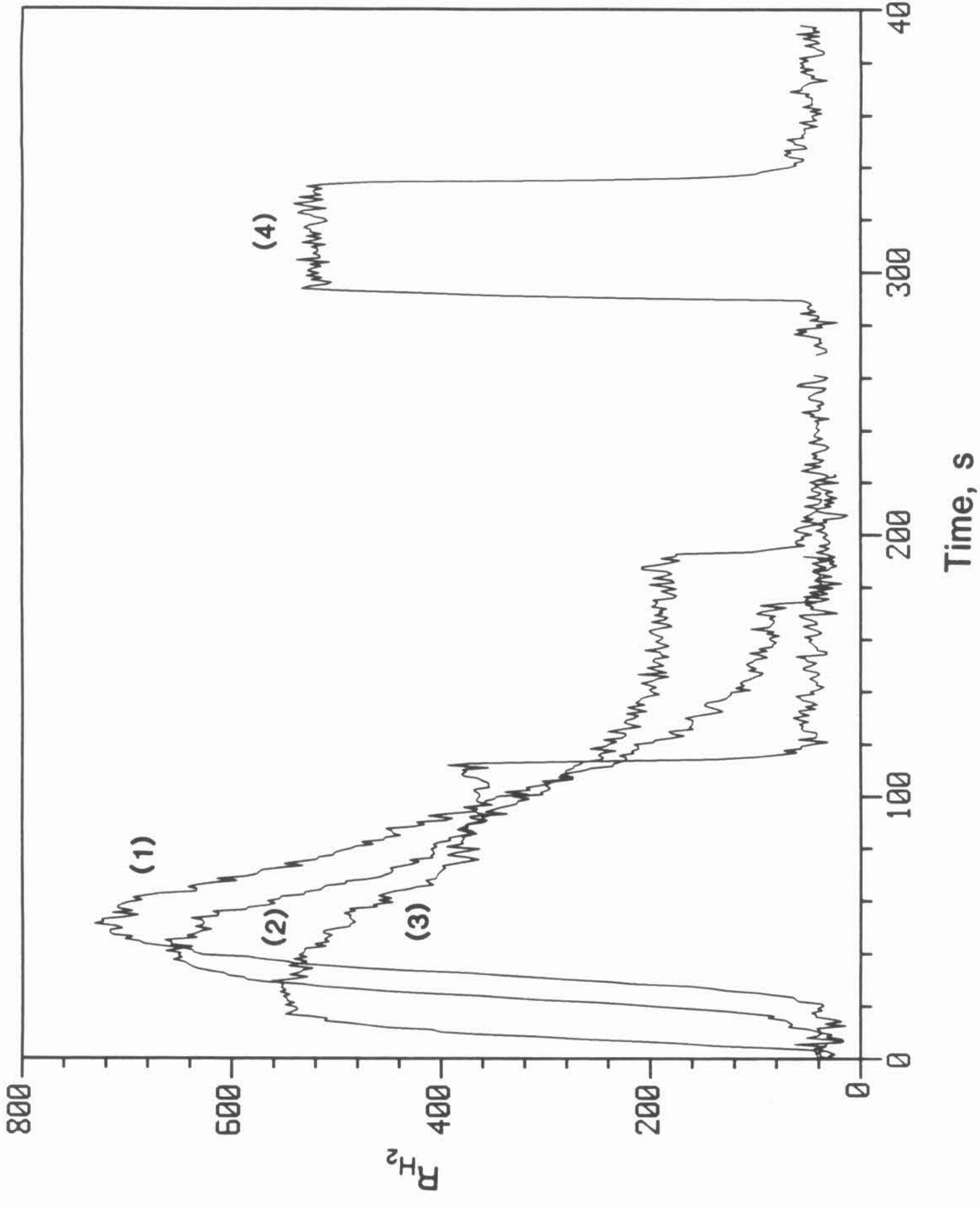

Figure 6

CHAPTER 7.

Steady-State Kinetics of Formaldehyde Decomposition on Pt(110)-(1×2): Probing Precursors

[This chapter was submitted as a paper by Y. -K. Sun and W. H. Weinberg to *Surface Science.*]

Abstract

We have carried out measurements of the steady-state rate of decomposition of formaldehyde on the Pt(110)-(1 × 2) surface, and we have interpreted these measurements in such a way as to permit an incisive probe of the molecular precursor to dissociation. The rate coefficient of the decomposition reaction of molecularly adsorbed formaldehyde (H_2CO) was found to be $2 \times 10^{12} \exp[(-13.4\, kcal/mol)/k_B T] s^{-1}$.

Although they are generally present in concentrations that are too low to be measured directly, transient intermediates which are frequently termed "precursors" play an extremely important role in a wide variety of surface reactions (**1**). In favorable circumstances, however, the rate coefficient describing the elementary surface reaction experienced by the precursor may be extracted from overall kinetic data, even though the precursor intermediate is not itself isolated. We describe in this Letter how this has been accomplished in the particular case of the decomposition of formaldehyde on the Pt(110)-(1 × 2) surface.

The formaldehyde decomposition reaction is an especially useful vehicle to illustrate how surface precursor states may be probed. On the Pt(110)-(1 × 2) surface, formaldehyde decomposes exclusively to a hydrogen molecule and a carbon monoxide molecule in the gas phase (*vide infra*). The intermediates in the decomposition reaction are molecularly adsorbed formaldehyde, a formyl (HCO) species, hydrogen adatoms and chemisorbed carbon monoxide (**2**). Of these intermediates the chemisorbed carbon monoxide is the most stable, and the chemisorbed formyl is the least stable (**3**). Indeed, the formyl is sufficiently unstable that its reactivity cannot be probed employing the methodology we describe here. The chemisorbed formaldehyde, however, may be probed at high surface temperatures at which its fractional surface coverage is approximately 10^{-9} to 10^{-12} (*vide infra*).

The set of reactions that we consider in the overall decomposition of formaldehyde is the following:

$$\mathrm{H_2CO}(g) \underset{k_{d,f}}{\overset{FP_g}{\rightleftarrows}} \mathrm{H_2CO}(a)\,, \tag{1}$$

$$\mathrm{H_2CO}(a) \xrightarrow{k_r} 2\mathrm{H}(a) + \mathrm{CO}(a)\,, \tag{2}$$

$$\mathrm{CO}(a) \xrightarrow{k_{d,CO}} \mathrm{CO}(g)\,, \tag{3}$$

and

$$2\mathrm{H}(a) \xrightarrow{k_{d,H_2}} \mathrm{H}_2(g)\,, \tag{4}$$

where (g) and (a) denote gas phase and adsorbed phase, respectively, F is the flux of formaldehyde onto the surface (per site), P_a is the probability of molecular adsorption of formaldehyde, and the k_i are rate coefficients of the indicated reactions. The latter are assumed to be of the Arrhenius form, *i.e.*, $k_i = k_i^{(o)} e^{-E_i \beta}$, where $\beta \equiv 1/k_B\mathrm{T}$. There is no need to consider the presence of the formyl explicitly because the decomposition reaction is irreversible, and the cleavage of the C-H bond in formaldehyde is considerably slower than cleavage of the C-H bond in formyl. Technically, the rate coefficient k_r applies to the formation of a formyl, but in the steady-state decomposition reaction it can be considered to apply to the formation of hydrogen adatoms and chemisorbed carbon monoxide without loss of generality.

At steady state the rate of decomposition of the formaldehyde is given by

$$R = k_r \theta_{H_2CO} = k_{d,CO}\theta_{CO} = k_{d,H_2}\theta_H^2\,, \tag{5}$$

where the θ_i are fractional surface coverages of species i. Recognizing that chemisorbed CO inhibits the adsorption of formaldehyde (4), we find that the steady-state surface coverages of formaldehyde and carbon monoxide are given by

$$\theta_{H_2CO} = \frac{FP_a/k_r}{FP_a/k_{d,CO} + k_r(1 + k_{d,f}/k_r)}\,, \tag{6}$$

and

$$\theta_{CO} = \frac{FP_a}{FP_a + k_{d,CO}(1 + k_{d,f}/k_r)}\,. \tag{7}$$

This implies that the rate of the decomposition reaction is given by

$$R = \frac{FP_a\, k_{d,CO}}{FP_a + k_{d,CO}(1 + k_{d,f}/k_r)}\,. \tag{8}$$

This, in turn, implies that one would expect the decomposition rate at "low" surface temperatures to be dictated solely by the desorption of carbon monoxide and to be zero order in the pressure (flux) of formaldehyde, *i.e.*, in this case $FP_a >> k_{d,CO}(1 + k_{d,f}/k_r)$. Likewise, one would expect the decomposition rate at "high" surface temperatures to be given by

$$R \cong FP_a\left(\frac{k_r}{k_r + k_{d,f}}\right), \tag{9}$$

and hence to be first order in formaldehyde pressure. As discussed below, this is precisely the behavior that we observed experimentally. It is very important to note that since k_r appears in Eq. (9), it is possible to determine the rate coefficient for C-H bond cleavage in the formaldehyde under conditions at which its surface concentration is far too low to be measured spectroscopically.

The experiments were carried out in a microreactor, which is described in detail elsewhere (**5**, **6**). Briefly, the microreactor consists of a small "high pressure cell" that can be isolated from an ultrahigh vacuum section by a right-angle valve. The base pressure of the reactor is below 3×10^{-10} Torr. The right-angle valve is linked to one port of a $2\frac{3}{4}''$-six-way cross, which is connected to the UHV chamber. An ion gauge and a quadrupole mass spectrometer are attached to two other ports on the six-way cross. Since the probability of the formaldehyde decomposition reaction is quite high, the right-angle valve to the reactor cell was kept completely open in order to maintain low conversions of the formaldehyde (**4**).

The pressure of the formaldehyde in the reactor was measured by a properly calibrated ion gauge.

The Pt(110) crystal with a total oriented surface area of 1.0 cm^2 was supported by two high purity platinum wires (0.010″ diameter and 0.2″ in length) which were spot welded on the edges of the crystal. These wires were clamped onto two copper leads (0.10″ diameter) which were used both to support and to heat the crystal. The Pt(110) crystal was heated resistively and its temperature was measured with a 0.003″ diameter W-5% Re/W-26% Re thermocouple that was spotwelded on the edge of the crystal. The Pt(110) surface was cleaned by argon ion bombardment and oxidation-reduction cycles (5×10^{-4} Torr of flowing oxygen for 5 min at 900 K followed by 5×10^{-4} Torr of flowing hydrogen also for 5 min at 900 K). The cleanliness of the surface was verified by thermal desorption spectra of carbon monoxide.

Paraformaldehyde with below 1% water was obtained from Fluka, and deuterated paraformaldehyde (99.6 atom % D) was obtained from MSD Isotopes. The preparation of monomeric formaldehyde was effected as described previously (**7**). The *absolute* rate of the decomposition reaction was determined by calibrating the quadrupole mass spectrometer with a known leak of hydrogen into the UHV reactor.

The steady-state rate of decomposition of formaldehyde on the Pt(110)-(1×2) surface was measured at formaldehyde pressures of 8.1×10^{-8} and 4.0×10^{-8} Torr, and at surface temperatures between 400 and 1100 K. As noted earlier, the only products of the reaction are hydrogen and carbon monoxide. This is shown clearly in Fig. 1, which is a *difference* mass spectrum for $2 \leq m/e \leq 60$ AMU, *i.e.*, the measured partial pressures during the steady-state reaction at 8.1×10^{-8} Torr of formaldehyde (H_2CO) and 715 K minus the partial pressures at 300 K (at which temperature the rate is negligibly slow). The positive peaks at 2 and 28 AMU are due to the products of the reaction (hydrogen and carbon monoxide), and the negative peaks at 29 and 30 AMU are due to the consumption of formaldehyde.

Below approximately 475 K, the rate of decomposition is zero order in formaldehyde pressure and increases with increasing temperature, *i.e.*, the low-temperature regime discussed earlier in which the desorption of carbon monoxide is rate limiting. Above approximately 550 K, the rate of decomposition is first order in formaldehyde pressure and decreases with increasing temperature, *i.e.*, the high-temperature regime discussed earlier which is described by Eq. (9). Between 475 and 550 K, the rate of the reaction increases with increasing temperature with an order in the formaldehyde pressure that varies between zero and unity. This is a "transition" regime that is described by the general expression of Eq. (8). The steady-state rate of formaldehyde (H_2CO and D_2CO) decomposition is shown in Fig. 2 between 400 and 1100 K for a formaldehyde pressure of 8.1×10^{-8} Torr. The rate is maximized at approximately 580 K where the reaction probability, $P_r \equiv R/F$, is approximately 0.75.

The data in Fig. 2 may be analyzed most easily by rewriting Eq. (9) in the following way (**1**):

$$\frac{P_a}{P_r} - 1 = \frac{k_{d,f}}{k_r}\,. \tag{10}$$

The value of P_a for formaldehyde on Pt(110) at 300 K is unity. Since the adsorption of *molecular* formaldehyde is unactivated, we expect that the probability of molecular adsorption will be equal to the probability of trapping into the physically adsorbed well, which is a weak function of surface temperature (**8**, **9**). Hence, we shall assume P_a maintains the constant value of unity, which allows us to plot $\ell n(\frac{P_a}{P_r} - 1)$ as a function of reciprocal temperature. We would expect to find a straight line from this construction with a slope of $-(E_{d,f} - E_r)/k_B$ and an intercept of $k_{d,f}^{(o)}/k_r^{(o)}$. Such a plot is shown in Fig. 3 from which we deduce that $E_{d,f} - E_r = 3.2 \pm 0.5\, kcal/mol$ and $k_{d,f}^{(o)}/k_r^{(o)} = 5.2$. This means that the activation energy of the decomposition reaction (C-H bond cleavage) lies 3.2 $kcal/mol$ *below* the energy level of the gas-phase formaldehyde far from the platinum surface.

Since we were unable to cool our crystal below room temperature, we were unable to obtain an experimental estimate of $k_{d,f}$, the rate coefficient of desorption of formaldehyde. However, on the Pt(111) surface, Abbas and Madix (**10**) evaluated $k_{d,f}$ and found it to be equal to $10^{13}\exp[(-16.6\, kcal/mol)/k_BT]s^{-1}$. We expect a similar value for Pt(110) since the bonding of the molecular formaldehyde will presumably be via lone pair electron donation to a single platinum atom on both surfaces. This implies that the elementary rate coefficient for the C-H bond cleavage reaction of the molecularly adsorbed precursor state is approximately $2 \times 10^{12}\exp[(-13.4\, kcal/mol)/k_BT]s^{-1}$. Note that this measurement was made at temperatures at which the fractional coverage of the molecularly adsorbed formaldehyde was between approximately 10^{-9} and 10^{-12}, *i.e.*, we have provided a *kinetic* measurement under conditions where a *spectroscopic* measurement would not be possible. Indeed, our measurements apply to an essentially clean Pt(110) surface since the fractional coverage of carbon monoxide, the most abundant surface species, varies between approximately 10^{-3} and 10^{-9}.

The experimentally measured steady-state decomposition of D_2CO at 8.1×10^{-8} Torr is also shown in Fig. 2, and, as expected, its rate of decomposition lies consistently below that of H_2CO. The ratio of the rates at 580 K is approximately 1.11 which implies, assuming the same value of $k_r^{(o)}$ for H_2CO and D_2CO, a difference in the difference of the zero-point energies of H_2CO and D_2CO between the transition state and the reactants of approximately $120\,cal/mol$. This, in turn, implies that for D_2CO, $k_r^{(o)} = 2 \times 10^{12} s^{-1}$ and $E_r = 13.5\,kcal/mol$. Note that this small kinetic isotope effect is hardly visible in the experimental data at temperatures above approximately 800 K.

To summarize, we have carried out measurements of the steady-state rate of decomposition of formaldehyde on the Pt(110) surface, and we have interpreted these measurements in such a way as to permit an incisive probe of the molecular precursor to dissociation. The rate coefficient of the decomposition reaction of molecularly adsorbed formaldehyde (H_2CO) was found to be $2 \times 10^{12} \exp[(-13.4\,kcal/mol)/k_BT] s^{-1}$.

Acknowledgment:

This work was supported by the National Science Foundation via Grant CHE-8617826. Additional support was provided by the Donors of the Petroleum Research Fund of the American Chemical Society (Grant PRF 19819-AC5-C).

References

1. W. H. Weinberg, in *Kinetics of Interface Reactions*, Eds. H. J. Kreuzer and M. Grunze, Springer-Verlag, Heidelberg, 1987, p. 94.
2. A. B. Anton, J. E. Parmeter and W. H. Weinberg, *J. Am. Chem. Soc.* **108**, 1823 (1986).
3. A. B. Anton, J. E. Parmeter and W. H. Weinberg, *J. Am. Chem. Soc.* **107**, 5558 (1985).
4. We made measurements at surface temperatures above 400 K, where the fractional coverages of formyl, formaldehyde and hydrogen are all much less than those of carbon monoxide.
5. J. J. Vajo, W. Tsai and W. H. Weinberg, *Rev. Sci. Instrum.* **56**, 1439 (1985).
6. Y.-K. Sun and W. H. Weinberg, to be published.
7. Y.-K. Sun, C.-Y. Chan and W. H. Weinberg, *J. Vac. Sci. Technol.* **A7**, 1983 (1989).
8. C. T. Rettner, H. Stein and E. K. Schweizer, *J. Chem. Phys.* **89**, 3337 (1988).
9. C. T. Rettner, E. K. Schweizer, H. Stein and D. J. Auerbach, *Phys. Rev. Letters* **61**, 986 (1988).
10. N. M. Abbas and R. J. Madix, *Appl. Surface Sci.* **7** , 241 (1981).

Figure Captions

Figure 1: Difference mass spectrum of the contents of the reactor at surface temperatures of 715 and 300 K during the steady-state decomposition of formaldehyde (H_2CO) on Pt(110)-(1 × 2) at a formaldehyde pressure of 8.1×10^{-8} Torr.

Figure 2: Rate of decomposition of H_2CO and D_2CO at pressures of 8.1×10^{-8} Torr on Pt(110)-(1 × 2) as a function of the surface temperature.

Figure 3: A plot of $\ell n(\frac{P_a}{P_r} - 1)$ as a function of reciprocal temperature for the data of Fig. 2 (H_2CO) above 600 K. The slope of the line implies that $E_{d,f} - E_r = 3.2 \pm 0.5\, kcal/mol$, and the intercept implies that $k_{d,f}^{(o)}/k_r^{(o)} = 5.2$.

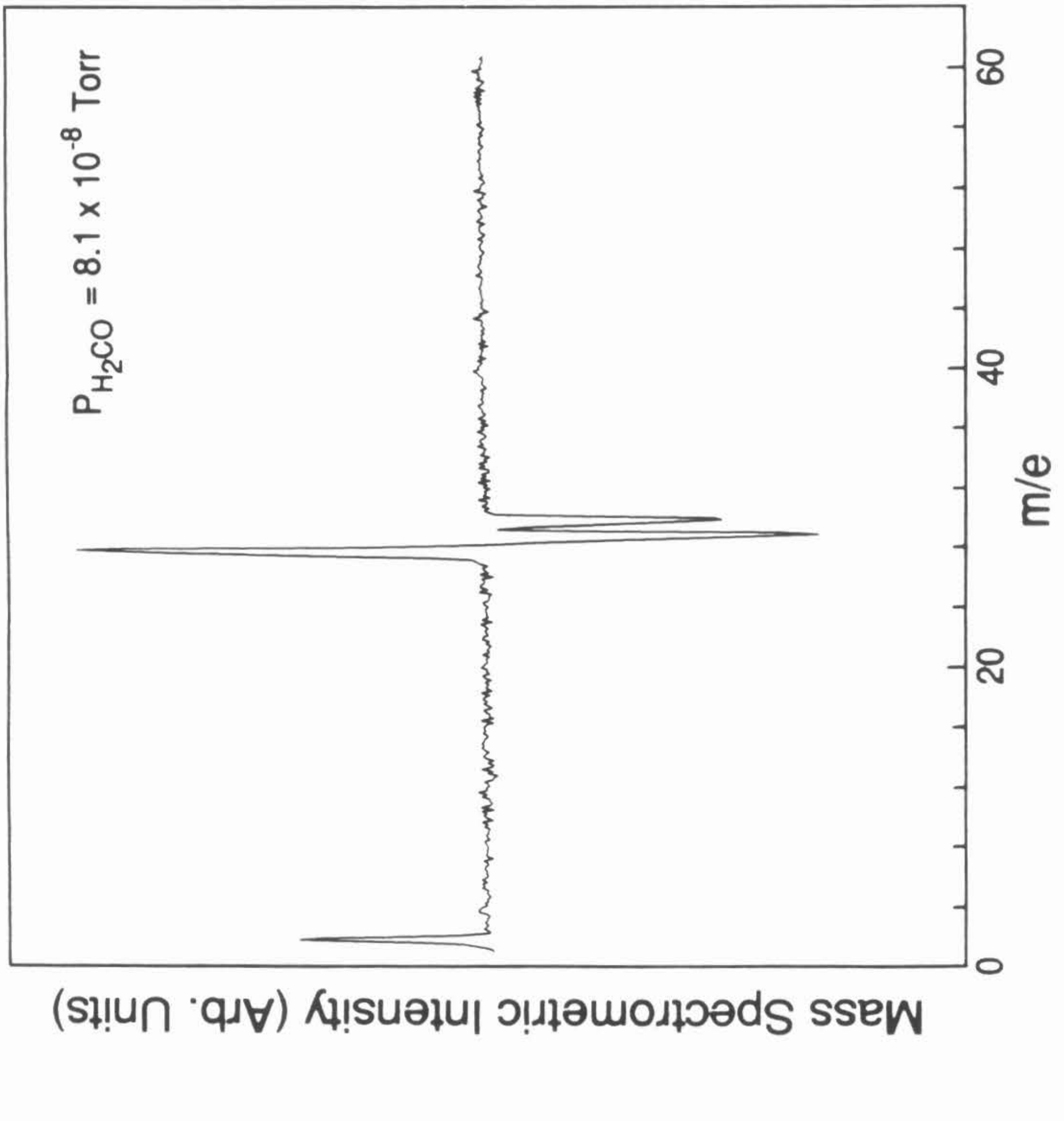
$P_{H_2CO} = 8.1 \times 10^{-8}$ Torr
0
20
40
60
m/e
Mass Spectrometric Intensity (Arb. Units)

Figure 1

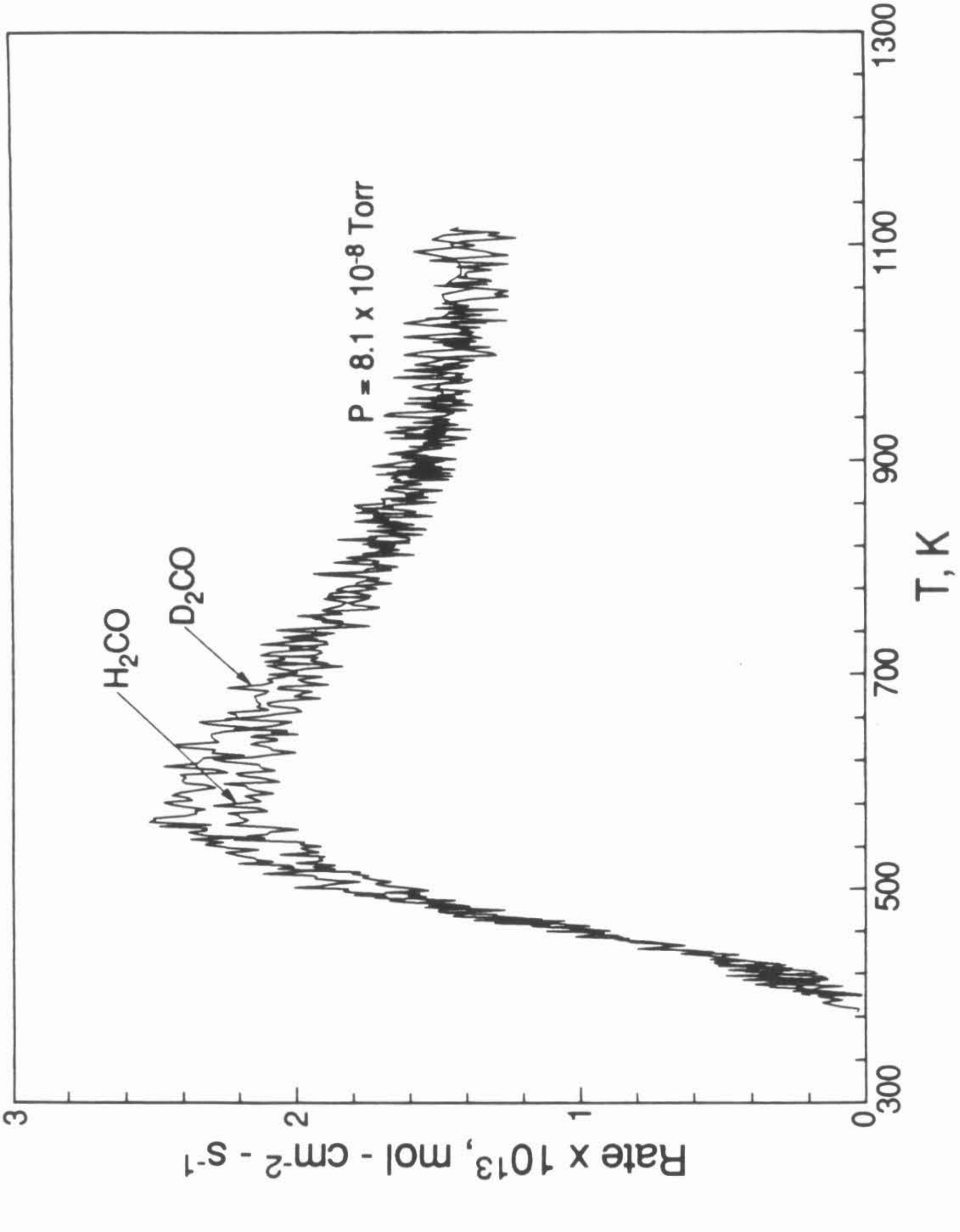
H$_2$CO
D$_2$CO
P = 8.1 x 10^{-8} Torr
Rate x 10^{13}, mol - cm^{-2} - s^{-1}
0
1
2
3
300
500
700
900
1100
1300
T, K

Figure 2

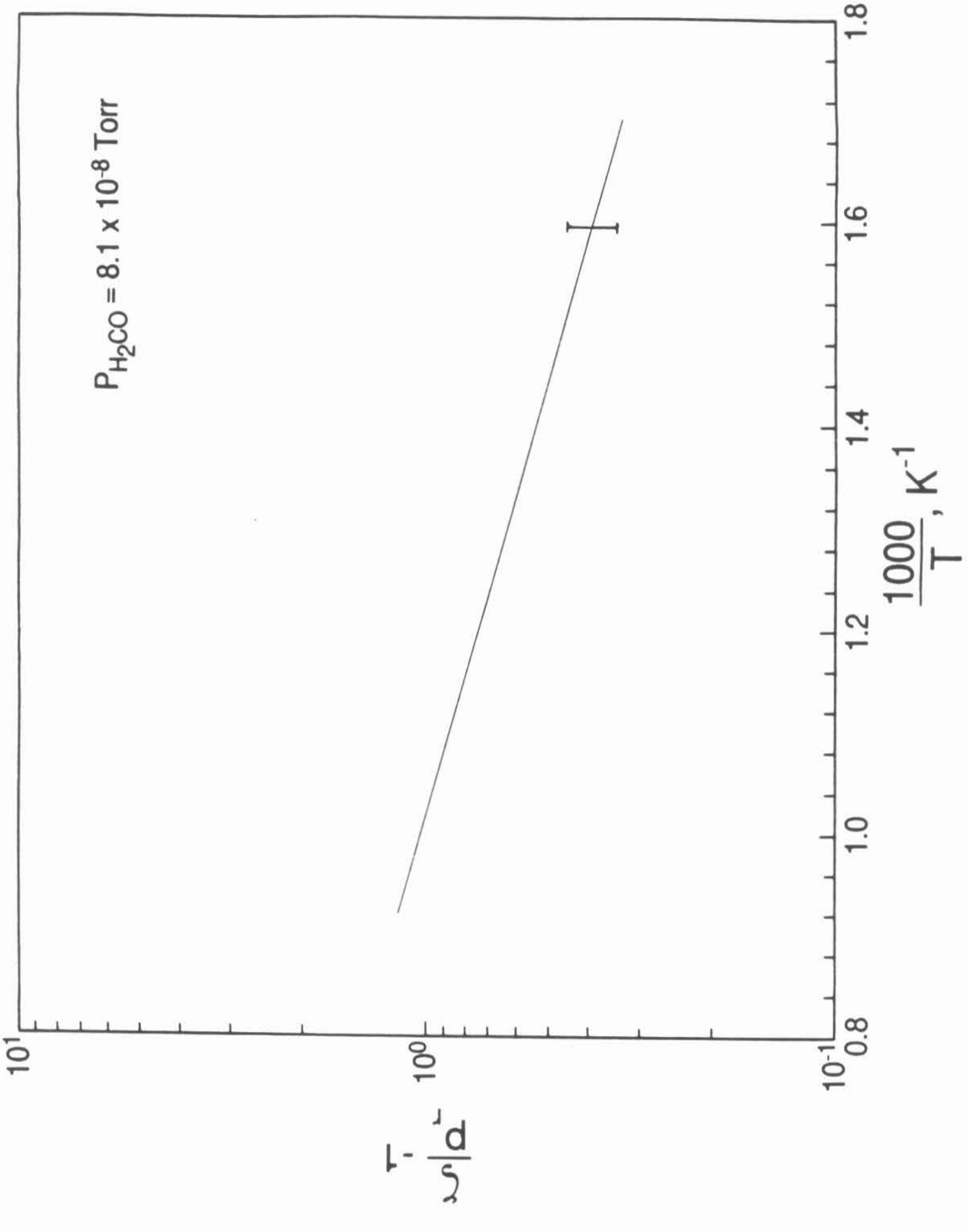
$P_{H_2CO} = 8.1 \times 10^{-8}$ Torr
$\frac{1000}{T}$, K^{-1}
0.8
1.0
1.2
1.4
1.6
1.8
10^{-1}
10^{0}
10^{1}
$\frac{\zeta}{p_r} - 1$

Figure 3

CHAPTER 8.

An Accurate and Simple Method of Measuring Relative Mass Spectrometric Sensitivities

[This chapter has been accepted as a shop note by Y. -K. Sun and W. H. Weinberg to *Journal of Vacuum Science and Technology A*.]

ABSTRACT

We describe an accurate and convenient method of determining the relative mass spectrometric sensitivities of various species by using surface decomposition reactions to generate these species in known stoichiometric ratios *in situ* in vacuum systems. In particular, we have used the decomposition reactions of formaldehyde and formic acid on Ru(001) to determine the relative mass spectrometric sensitivities of H_2, HD, D_2 and CO.

It is often necessary to determine the relative or absolute mass spectrometric sensitivities of various molecules in rate measurements of heterogeneously catalyzed reactions, as well as in other applications. For example, in studying the kinetics and mechanism of formic acid decomposition on the Ru(001) surface in order to determine the selectivity of this surface for dehydration (decomposition to CO and H_2O) and dehydrogenation (decomposition to CO_2 and H_2), knowledge of the relative mass spectrometric sensitivities of CO and H_2 was required (**1**). The absolute mass spectrometric sensitivities of H_2, HD and D_2 must be known in order to calculate the absolute rate of HD production and the reaction probability in measurements of the kinetics of isotopic exchange of H_2 and D_2 (**2**), and in order to perform mass balance studies of the coadsorption of D_2 and C_2H_4 (**3, 4**).

In the high pumping speed limit, the absolute rate of production of species x (R_{x}) and its mass spectrometric intensity (I_{x}) are related by

$$R_{\mathrm{x}} = \frac{S_{\mathrm{x}}}{k_B T_g} \eta_{\mathrm{x}} I_{\mathrm{x}}, \tag{1}$$

where S_{x} is the pumping speed of species x, T_g is the gas temperature, and k_B is the Boltzmann constant. The quantity η_{x} is a proportionality *constant* defined in such a way that the partial pressure P_{x} is given by $P_{\mathrm{x}} = \eta_{\mathrm{x}} I_{\mathrm{x}}$. It is often termed the mass spectrometric sensitivity. Since we are concerned with the relation between the absolute rate and the mass spectrometric intensity in kinetic studies of heterogeneously catalyzed reactions, we *define* the *absolute* mass spectrometric sensitivity β_{x} as

$$\beta_{\mathrm{x}} \equiv \frac{k_B T_g}{S_{\mathrm{x}} \eta_{\mathrm{x}}}. \tag{2}$$

In the following discussion, we also *define* the *relative* mass spectrometric sensitivity of species x as

$$\gamma_{\mathrm{x}} \equiv \beta_{\mathrm{x}} / \beta_{\mathrm{H_2}}; \tag{3}$$

thus γ_{H_2} is unity. The choice of hydrogen as a reference here is completely arbitrary. From Eqs. (1)-(**3**), we find that

$$\gamma_{\mathrm{x}} = \frac{S_{\mathrm{H}_2}}{S_{\mathrm{x}}} \frac{\eta_{\mathrm{H}_2}}{\eta_{\mathrm{x}}}, \tag{4}$$

$$\gamma_{\mathrm{x}} = \frac{R_{\mathrm{H}_2}}{R_{\mathrm{x}}} \frac{I_{\mathrm{x}}}{I_{\mathrm{H}_2}} \tag{5}$$

and

$$R_{\mathrm{x}} = \frac{I_{\mathrm{x}}}{\gamma_{\mathrm{x}} \beta_{\mathrm{H}_2}}. \tag{6}$$

To compare the relative production rates of species x and y, one has to divide the mass spectrometric intensities of x and y (I_{x} and I_{y}) by their relative mass spectrometric sensitivities, *i.e.* $R_{\mathrm{x}} : R_{\mathrm{y}} = I_{\mathrm{x}}/\gamma_{\mathrm{x}} : I_{\mathrm{y}}/\gamma_{\mathrm{y}}$ [cf. Eq. (**6**)].

The relative mass spectrometric sensitivity of species x (γ_{x}) is proportional to the ratio of pumping speeds of hydrogen and species x ($S_{\mathrm{H}_2}/S_{\mathrm{x}}$) and the ratio of the proportionality constants of hydrogen and species x ($\eta_{\mathrm{H}_2}/\eta_{\mathrm{x}}$), cf. Eq. (4). The proportionality constant η_{x} is a function of the ionization probability of species x in the ionizer of the mass spectrometer (**5**), the transmission probability of the ions through the mass spectrometer (which remains relatively constant up to AMU 20 and then falls off by approximately one decade per 150 AMU for our UTI 100C quadrupole mass spectrometer), and the electron multiplier gain of the ions generally considered to have an $M^{-1/2}$ dependence, where M is the ion mass. The ratio $\eta_{\mathrm{H}_2}/\eta_{\mathrm{x}}$ is obviously independent of the system configuration since it is an intrinsic property of the mass spectrometer. The ratio of pumping speeds $S_{\mathrm{H}_2}/S_{\mathrm{x}}$, however, depends upon the system configuration. For example, for an ion pumped vacuum system with a poppet valve separating the vacuum chamber and the ion pump, the ratio of the pumping speeds $S_{\mathrm{H}_2}/S_{\mathrm{x}}$ would be different for a system configuration with the poppet valve wide open and for a system configuration with the poppet valve partially closed. *Each time one changes the system configuration in any way,* *the relative mass spectrometric sensitivities must be remeasured.* Thus, an accurate yet simple method of determining the relative mass spectrometric sensitivity would be very helpful. We present here such a method of determining the relative mass spectrometric sensitivities, particularly those of H_2, HD, D_2 and CO by introducing into the vacuum system $CO+H_2$, or $CO+D_2$, or H_2+HD+D_2+CO stoichiometrically (*i.e. with known rate ratios)* via chemical decomposition reactions on the Ru(001) surface.

The system we have employed in the measurement of rates of catalytic reactions is an ion pumped ultrahigh vacuum (UHV) system, equipped with quadrupole mass spectrometry and a directional beam doser (**1, 6**). In the steady-state rate measurements, the reactant is introduced into the UHV system through the directional beam doser. The Ru(001) surface is positioned in and out of the reactant beam at a constant surface temperature, and the increase in the intensities of the products and the decrease in intensity of the reactant are monitored mass spectrometrically.

Formaldehyde (H_2CO) decomposes on the Ru(001) surface only to H_2 and CO (**6**). Hence the steady-state decomposition of H_2CO is equivalent to leaking an equimolar mixture of CO and H_2 into the UHV system. The relative mass spectrometric sensitivity of CO (γ_{co}) can be determined simply by taking the ratio of the mass spectrometric intensities of CO (I_{CO}) to H_2 (I_{H_2}), measured during the steady-state decomposition of H_2CO since $R_{H_2} = R_{CO}$, *i.e.* $\gamma_{CO} = I_{CO}/I_{H_2}$ [cf. Eq. (5)]. The increase in the intensity of mass 28 (ΔI_{28}) is the sum of an increase of CO intensity and a decrease in the partial pressure of H_2CO, due to the H_2CO decomposition (measured by the decrease in the mass 29 intensity, ΔI_{29}; the peak at m/e=29 is the most intense one in the mass spectrum of H_2CO). The cracking pattern of H_2CO can be measured easily, and in our UHV system the H_2CO exhibits m/e peaks at 30, 29 and 28 with intensity ratios of 0.73 : 1.00 : 0.34, in good agreement with previously reported values (**7**). Thus, the mass spectrometric intensity of CO is given by $I_{\mathrm{CO}} = \Delta I_{28} + 0.34|\Delta I_{29}|$. The determination of the true mass spectrometric intensity of H_2 is straightforward. It is simply the increase in the intensity of mass 2 (ΔI_2) when the Ru(001) surface is positioned in the H_2CO beam, since the H_2CO molecule has no mass 2 cracking fragment. The result is $\gamma_{\mathrm{CO}} = I_{\mathrm{CO}}/I_{\mathrm{H_2}} = 0.98$. Similarly, the relative mass spectrometric sensitivity of D_2 was determined by using D_2CO. We find in this case

$$\gamma_{\mathrm{D_2}} : \gamma_{\mathrm{CO}} = I_{\mathrm{D_2}} : I_{\mathrm{CO}} = 0.65 : 0.98.$$

It is known that during the steady-state decomposition of DCOOH on Ru(001) at high surface temperatures, the production rates of H_2, HD and D_2 have a ratio of 1 : 2 : 1 (**1**). The steady-state decomposition of DCOOH on Ru(001) at high surface temperatures is equivalent to leaking H_2, HD and D_2 with a stoichiometry of 1 : 2 : 1 into the UHV system (**8**). The relative mass spectrometric sensitivities of H_2, HD and D_2 may be determined easily by taking the ratio of the properly weighted mass spectrometric intensities of H_2 ($I_{\mathrm{H_2}}$), HD (I_{HD}) and D_2 ($I_{\mathrm{D_2}}$) according to Eq. (5), *i.e.* $\gamma_{\mathrm{H_2}} : \gamma_{\mathrm{HD}} : \gamma_{\mathrm{D_2}} = I_{\mathrm{H_2}} : 0.5 I_{\mathrm{HD}} : I_{\mathrm{D_2}}$. The relative mass spectrometric sensitivities thus determined are $\gamma_{\mathrm{H_2}} : \gamma_{\mathrm{HD}} : \gamma_{\mathrm{D_2}} = 1.00 : 0.80 : 0.60$. Note that the relative mass spectrometric sensitivity of D_2 is in good agreement with the value determined from the formaldehyde experiments described above. We conclude that the relative mass spectrometric sensitivities of H_2, HD, D_2 and CO is

$$\gamma_{\mathrm{H_2}} : \gamma_{\mathrm{HD}} : \gamma_{\mathrm{D_2}} : \gamma_{\mathrm{CO}} = 1.00 : 0.80 : 0.63 : 0.98.$$

for our system configuration. Note that the relative mass spectrometric sensitivity of D_2 is an average of the two results obtained from D_2CO and DCOOH.

The relative mass spectrometric sensitivities of H_2, HD, D_2 and CO can also be determined by decomposing an equimolar mixture of H_2CO and D_2CO on Ru(001), assuming statistical mixing of H and D on the surface. When steady state is achieved,

$$\gamma_{\mathrm{H_2}} : \gamma_{\mathrm{HD}} : \gamma_{\mathrm{D_2}} : \gamma_{\mathrm{CO}} = I_{\mathrm{H_2}} : 0.5 I_{\mathrm{HD}} : I_{\mathrm{D_2}} : 0.25 I_{\mathrm{CO}},$$

and the experimentally measured mass spectrometric sensitivities in this case are

$$\gamma_{\mathrm{H_2}} : \gamma_{\mathrm{HD}} : \gamma_{\mathrm{D_2}} : \gamma_{\mathrm{CO}} = 1.00 : 0.83 : 0.60 : 0.95,$$

in good agreement with the values determined above. To obtain the absolute mass spectrometric sensitivities of these species, one needs merely evaluate it for any one of them.

In summary, we have presented a convenient method of determining the relative mass spectrometric sensitivities of various species (and those of H_2, HD, D_2 and CO in particular), by introducing them into an UHV system stoichiometrically via surface chemical reactions. One may, of course, use calibrated sources to determine the relative and absolute mass spectrometric sensitivities. The method we have described is much easier, however. This method is obviously not limited to the decomposition of formaldehyde and formic acid on a Ru(001) surface. The concept of using surface decomposition reactions to generate various species in known stoichiometric ratios *in situ* in an UHV system to calibrate mass spectrometers is very useful.

Acknowledgment: This work was supported by the National Science Foundation under grant number CHE-8617826.

REFERENCES

1. Y. -K. Sun, J. J. Vajo, C. -Y. Chan and W. H. Weinberg, *J. Vac. Sci. Technol. A* **6**, 854 (1988).
2. K. E. Lu and R. R. Rye, *Surface Sci.* **45**, 677 (1974).
3. P. G. Cartier and R. R. Rye, *J. Chem. Phys.* **56**, 5316 (1972).
4. M. M. Hills, J. E. Parmeter and W. H. Weinberg, *J. Am. Chem. Soc.* **108**, 7215 (1986).
5. T. A. Flaim and P.D. Ownby, *J. Vac. Sci. Technol.* **8**, 661 (1971).
6. Y. -K. Sun, C. -Y. Chan and W. H. Weinberg, *J. Vac. Sci. Technol. A* **7**, 1983 (1989).
7. A. Cornu and R. Massot, Compilation of Mass Spectral Data, Heyden, 2nd Ed., 1A, 1975.
8. High surface temperature here implies above 500 K, where the rate of decomposition of formic acid is first order in pressure. Usually, a surface temperature above that at which hydrogen desorbs will be sufficiently high to ignore kinetic isotope effects (hydrogen vs. deuterium), but this issue must be considered for each system employed.

CHAPTER 9.

Determination of the Absolute Saturation Coverage of Hydrogen on Ru(001)

[This chapter was published as a paper by Y. -K. Sun and W. H. Weinberg in *Surface Science* **214**, L246 (1989).]

ABSTRACT

We describe here a general methodology for the *indirect* relative determination of absolute fractional surface coverages. The saturation fractional coverage of hydrogen on Ru(001) has been evaluated in particular. In this case, we used H_2CO as a bridge to lead us from the known reference point of the saturation fractional coverage of CO to the unknown reference point of the fractional coverage of hydrogen on Ru(001), which is then used to determine accurately the saturation fractional coverage of hydrogen. We find that $\theta_{\mathrm{H}}^{sat} = 1.02\ (\pm 0.05)$ *i.e.* the surface stoichiometry is $\mathrm{Ru} : \mathrm{H} = 1 : 1$. The relative nature of the method, which cancels systematic errors, together with the utilization of a glass envelope around the mass spectrometer, which reduces spurious contributions in the thermal desorption spectra, results in high accuracy in the determination of absolute fractional coverages.

In spite of the large number of studies concerning hydrogen adsorption on the Ru(001) surface (**1-9**), the fundamental question of what is the saturation fractional coverage of hydrogen is yet to be answered accurately and unambiguously. The fractional coverage is defined here as the number of hydrogen adatoms per surface Ru atom in the topmost layer. Knowledge of the absolute saturation fractional coverage is necessary for a quantitative assessment of the adsorption kinetics, and specifically, a determination of the value of the initial probability of adsorption. The fractional coverage of hydrogen at saturation on Ru(001) has been measured to be both 0.86 (±20%) (**2**), and approximately unity (**1**), and has been assumed to be two (**3**). Difficulties in determining the fractional hydrogen coverage accurately are partly due to the fact that no superstructures are observed in LEED studies on the Ru(001) surface following hydrogen adsorption (**2**), unlike hydrogen adsorption on Ni(111) (**10**), W(100) (**11**) and Pd(100) (**12**), for example. For hydrogen adsorption on Pd(100), a $(\sqrt{2}\times\sqrt{2})$R45° hydrogen superstructure is observed below 250 K (**12**). Maximum intensity of the fractional order LEED beams corresponds to a surface on which the fractional coverage of hydrogen is 0.5. The thermal desorption spectrum of hydrogen from this surface (with $\theta_{\mathrm{H}} = 0.5$) serves as a *reference point* from which any other fractional coverage of hydrogen on Pd(100) can be calculated. In the absence of LEED (or other) information, thermal desorption mass spectrometry is commonly employed to estimate the fractional surface coverages.

An absolute determination of the fractional surface coverage of species x may be achieved by numerical integration of the *absolute* desorption rate R_x in a thermal desorption measurement, *i.e.*

$$\theta_x = \frac{1}{nA}\int_0^{\infty} R_x dt, \qquad (1)$$

where n is the surface density of substrate atoms, and A is the area of the surface.

The absolute desorption rate is given by

$$R_x = \frac{S_x}{k_B T_g} \eta_x I_x, \tag{2}$$

where S_x is the pumping speed of the system for species x, T_g is the gas temperature, I_x is the mass spectrometric intensity of species x, and η_x is the mass spectrometric sensitivity of species x defined in such a way that the partial pressure P_x is given by $P_x = \eta_x I_x$. Both an accurate measurement of the thermal desorption spectrum of species x and an accurate experimental determination of the absolute values of $S_x \eta_x$ are required in order to calculate the absolute rate in thermal desorption measurements and, therefore, the fractional coverage. In practice, however, to accomplish both is somewhat difficult for reasons discussed below. For a vacuum system in which the mass spectrometer is not enclosed in a glass envelope (**13**), the product $\eta_x S_x$ can be evaluated according to Eq. (2) by measuring the mass spectrometric intensity of species x when leaking into the vacuum system species x with a calibrated flow rate. In this case, however, the mass spectrometer measures desorption from both the well-defined surface and undefined areas such as the rear and edge of the single crystal, and the manipulator assembly for example. This introduces errors into the fractional surface coverage determination. If the thermal desorption spectra are measured as described by Menzel, *et al.* (**13**) with the mass spectrometer enclosed in a glass envelope, the accuracy of the thermal desorption spectra is quite high. The quantity $S_x \eta_x$ in this case, however, is not trivial to determine if there is no accurate reference point available (as is the case of hydrogen on Ru(001), for example). Compared to the case discussed above in which the mass spectrometer is not enclosed in a glass envelope, the mass spectrometric sensitivity η_x is the same since it is an intrinsic property of the mass spectrometer; the pumping speed of species x out of the glass envelope, however, would be quite different. In addition, the area A of the well-defined surface from which the molecules desorb and enter the glass envelope is not known with certainty, in general.

A more accurate method of determining the fractional coverage is via a relative determination, *i.e.* calibrating the thermal desorption spectra relative to the thermal desorption spectrum of a known coverage (a reference point). For example, the saturation coverage of CO on Ru(001) at 300 K is 0.65 (**14**). Hence the fractional coverage of CO at any coverage may be determined by employing the known coverage as a reference point, *i.e.*

$$\theta_{\mathrm{CO}} = \left(\int_0^\infty I_{\mathrm{CO}}\,dt \Big/ \int_0^\infty I_{\mathrm{CO}}^{sat}\,dt\right)\theta_{\mathrm{CO}}^{sat}. \tag{3}$$

This method is more accurate than the absolute determination described above since the mass spectrometer may be enclosed in a glass envelope and knowledge of the absolute values of S_{CO}, η_{CO} and A is not required. This technique for determining fractional coverages is referred to here as a *direct* relative determination since the fractional coverage is determined by directly calibrating the thermal desorption spectrum of an unknown coverage relative to that of a known coverage (a reference point). Such a reference point, however, is not known for hydrogen on Ru(001).

We present here the methodology for an *indirect* relative determination of fractional coverages that allows us to determine the fractional coverage of hydrogen on Ru(001) at saturation accurately. In this method, one adsorbs CO and hydrogen on Ru(001) ***with an accurately known ratio*** α ($\equiv \theta_{\mathrm{H}}/\theta_{\mathrm{CO}}$). Measuring the thermal desorption spectra of CO and hydrogen and calculating the fractional coverage of CO using the direct relative determination method, one can calculate the fractional coverage of hydrogen on this surface. This supplies the reference point for hydrogen that leads to the determination of the saturation coverage of hydrogen via

$$\theta_{\mathrm{H}}^{sat} = \left(\int_0^\infty I_{\mathrm{H_2}}^{sat}\,dt \Big/ \int_0^\infty I_{\mathrm{H_2}}\,dt\right)\left(\alpha\int_0^\infty I_{\mathrm{CO}}\,dt \Big/ \int_0^\infty I_{\mathrm{CO}}^{sat}\,dt\right)\theta_{\mathrm{CO}}^{sat}, \tag{4}$$

where I_{CO} and $I_{\mathrm{H_2}}$ are the mass spectrometric intensities in the thermal desorption spectra of CO and H_2 from the surface with the known ratio of CO and hydrogen adsorbed, and I_{CO}^{sat} and $I_{\mathrm{H_2}}^{sat}$ are the mass spectrometric intensities in the thermal desorption spectra from a Ru(001) surface saturated with CO and hydrogen, respectively. Rather than calibrating against a known coverage of the same species directly, as implied by Eq. (3), we relate the unknown fractional coverage of one species (hydrogen) to a known reference coverage of another species (CO). That is why this technique is referred to here as an *indirect* relative determination of fractional coverages.

The key point is to prepare a Ru(001) surface on which CO and hydrogen are adsorbed with a precisely known stoichiometry. The best way to achieve this goal is to adsorb a molecule which dissociates to CO and hydrogen below the desorption temperature of either CO or H_2. Formaldehyde is a perfect candidate. Formaldehyde dissociates to CO and hydrogen upon adsorption on Ru(001) near 200 K, at which temperature neither CO nor hydrogen desorbs (**15**). Independent of the formaldehyde coverage, the measured thermal desorption spectra of CO and H_2 represent a molar ratio of $\mathrm{CO} : \mathrm{H_2} = 1 : 1$, *i.e.* $\alpha = 2$ in Eq. (4) since there are two hydrogen adatoms per CO admolecule. This allows us to use the method embodied in Eq. (4) to measure the value of $\theta_{\mathrm{H}}^{sat}$.

The experiments were carried out in previously described UHV system (**16**). The base pressure of the belljar was below 5×10^{-11} Torr of reactive gases. The Ru(001) surface was mounted on a manipulator by two 0.01 in. tantalum wires spotwelded on the back of the crystal. The Ru(001) crystal could be heated resistively, and cooled conductively by liquid nitrogen. The temperature of the Ru(001) surface was measured by a 0.003 in. W/5%Re – W/26%Re thermocouple that was spotwelded to the back of the crystal. Oxygen cleaning was routinely performed prior to each measurement by cycling the temperature of the Ru(001) crystal between 400 and 1100 K in 7×10^{-8} Torr of oxygen backfilled into the belljar. Chemisorbed oxygen was removed by annealing the crystal to over 1600 K. The cleanliness of the surface was verified by Auger electron spectroscopy. The mass spectrometer was enclosed in a glass envelope which has a orifice with a diameter of 3 mm, in order to limit contributions to the thermal desorption spectra to the well-characterized front face of the crystal (**13**). The monomer gas of formaldehyde was prepared in the same way as has been described previously (**16**). The formaldehyde and hydrogen were introduced onto the Ru(001) surface through a directional beam doser that has also been described previously (**16**). The saturation coverage of CO on Ru(001) was achieved by exposing the surface to 13 L of formaldehyde at 295 K. The coverage of hydrogen on the surface is less than 1/30 of that of CO (**16**), and thermal desorption spectrum of CO from this surface has an identical peak area, shape and position as the thermal desorption spectrum following saturation exposure to molecular CO. It is convenient to employ H_2CO to saturate the surface with CO (rather than molecular CO), since this results in a lower background partial pressure of CO following the adsorption. The hydrogen saturated surface was prepared by exposing the Ru(001) surface to 230 L of H_2 at 178 K (**3**), further exposure to hydrogen shows no additional increase in the integrated area of the thermal desorption of H_2.

The thermal desorption spectrum of CO from the Ru(001) surface saturated with CO and the Ru(001) surface after exposure to 13 L of H_2CO at 200 K are shown in Fig. 1. The ratio of the areas under the peaks of the spectra is $\int_0^\infty I_{\mathrm{CO}} dt / \int_0^\infty I_{\mathrm{CO}}^{sat} dt = 0.48$ (± 0.01). The fractional coverage of CO following exposure to 13 L of H_2CO at 200 K is 0.31 (± 0.01), *i.e.* 0.48×0.65 via Eq. (3). The fractional coverage of hydrogen is twice that of CO, *i.e.* $\theta_{\mathrm{H}} = \alpha \theta_{\mathrm{CO}} = 0.62$ (± 0.02). The thermal desorption spectrum of H_2 from this surface, together with the spectrum from a hydrogen saturated Ru(001) surface are shown in Fig. 2. The measured ratio of the areas under the peaks of the spectra is $\int_0^\infty I_{\mathrm{H}_2}^{sat} dt / \int_0^\infty I_{\mathrm{H}_2} dt = 1.64$ (± 0.03). The uncertainties here are the standard deviation from a statistical analysis of five sets of experimental data measured under the same conditions. Now that we have a reference point for hydrogen, the fractional coverage of hydrogen on Ru(001) at saturation can be easily calculated from Eq. (4), *i.e.*

$$\theta_{\mathrm{H}}^{sat} = (\int_0^\infty I_{\mathrm{H}_2}^{sat} dt \Big/ \int_0^\infty I_{\mathrm{H}_2} dt)\theta_{\mathrm{H}} = 1.64 \times 0.62 = 1.02.(\pm 0.05).$$

In conclusion, we have unambiguously determined the fractional coverage of hydrogen on Ru(001) at saturation to be 1.02 (±0.04), *i.e.* the surface stoichiometry is Ru : H = 1 : 1. We have used H_2CO as a bridge to lead us from the known reference point of the saturation fractional coverage of CO to the unknown reference point of the fractional coverage of hydrogen, which is then used to determine accurately the saturation fractional coverage of hydrogen. Employing a glass envelope around the mass spectrometer reduces spurious contributions in the thermal desorption spectra, and the relative nature of the method cancels systematic errors allowing high accuracy in the coverage determination.

Acknowledgment: This work was supported by the National Science Foundation under grant number CHE-8617826.

REFERENCES

1. J. A. Schwarz, *Surface Sci.* **87**, 525 (1979).
2. H. Shimizu, K. Christmann and G. Ertl, *J. Catal.* **61**, 412 (1979).
3. P. Feulner and D. Menzel, *Surface Sci.* **154**, 465 (1985).
4. M. A. Barteau, J. Q. Broughton and D. Menzel, *Surface Sci.* **133**, 443 (1983).
5. H. Conrad, R. Scala and R. Unwin, *J. Chem. Phys.* **81**, 6371 (1983).
6. C. H. F. Peden, D. W. Goodman, J. E. Houston and J. T. Yates, Jr., *Surface Sci.* **194**, 92 (1988).
7. P. Feulner, H. Pfnür, P. Hofmann and D. Menzel, *Surface Sci.* **173**, L576 (1986).
8. C. H. F. Peden, D. W. Goodman, J. E. Houston and J. T. Yates, Jr., *Surface Sci.* **184**, L405 (1987).
9. P. Feulner, H. Phnür, P. Hofmann and D. Menzel, *Surface Sci.* **184**, L411 (1987).
10. K. Christmann, R. J. Behm, G. Ertl, M. A. Van Hove and W. H. Weinberg, *J. Chem. Phys.* **70**, 4168 (1979).
11. P. J. Estrup and J. Anderson, *J. Chem. Phys.* **45**, 2254 (1966).
12. R. J. Behm and G. Ertl, *Surface Sci.* **99**, 320 (1980).
13. P. Feulner and D. Menzel, *J. Vac. Sci. Technol.* **17**, 662 (1980).
14. E. D. Willians and W. H. Weinberg, *Surface Sci.* **82**, 93 (1979).
15. A. B. Anton, J. E. Parmeter and W. H. Weinberg, *J. Am. Chem. Soc.* **108**, 1823 (1986).
16. Y. -K. Sun, C. -Y. Chan and W. H. Weinberg, *J. Vac. Sci. Technol. A* **7**, 1983 (1989).

Figure Captions

Fig. 1: Thermal desorption spectra of CO from the Ru(001) surface saturated with CO, (a), and after exposure to 13 L of formaldehyde at 200 K, (b). The heating rate is 2 K/s. The ratio of the areas under the spectra is $\int_0^\infty I_{\mathrm{CO}}\,dt / \int_0^\infty I_{\mathrm{CO}}^{sat}\,dt =$ 0.48 (±0.01).

Fig. 2: Thermal desorption spectra of hydrogen from a hydrogen-saturated Ru(001) surface, (a), and from a Ru(001) surface after exposure to 13 L of formaldehyde at 200 K, (b). The heating rate is 5 K/s. The ratio of the areas under the spectra is $\int_0^\infty I_{\mathrm{H}_2}^{sat}\,dt / \int_0^\infty I_{\mathrm{H}_2}\,dt = 1.64$ (±0.03).

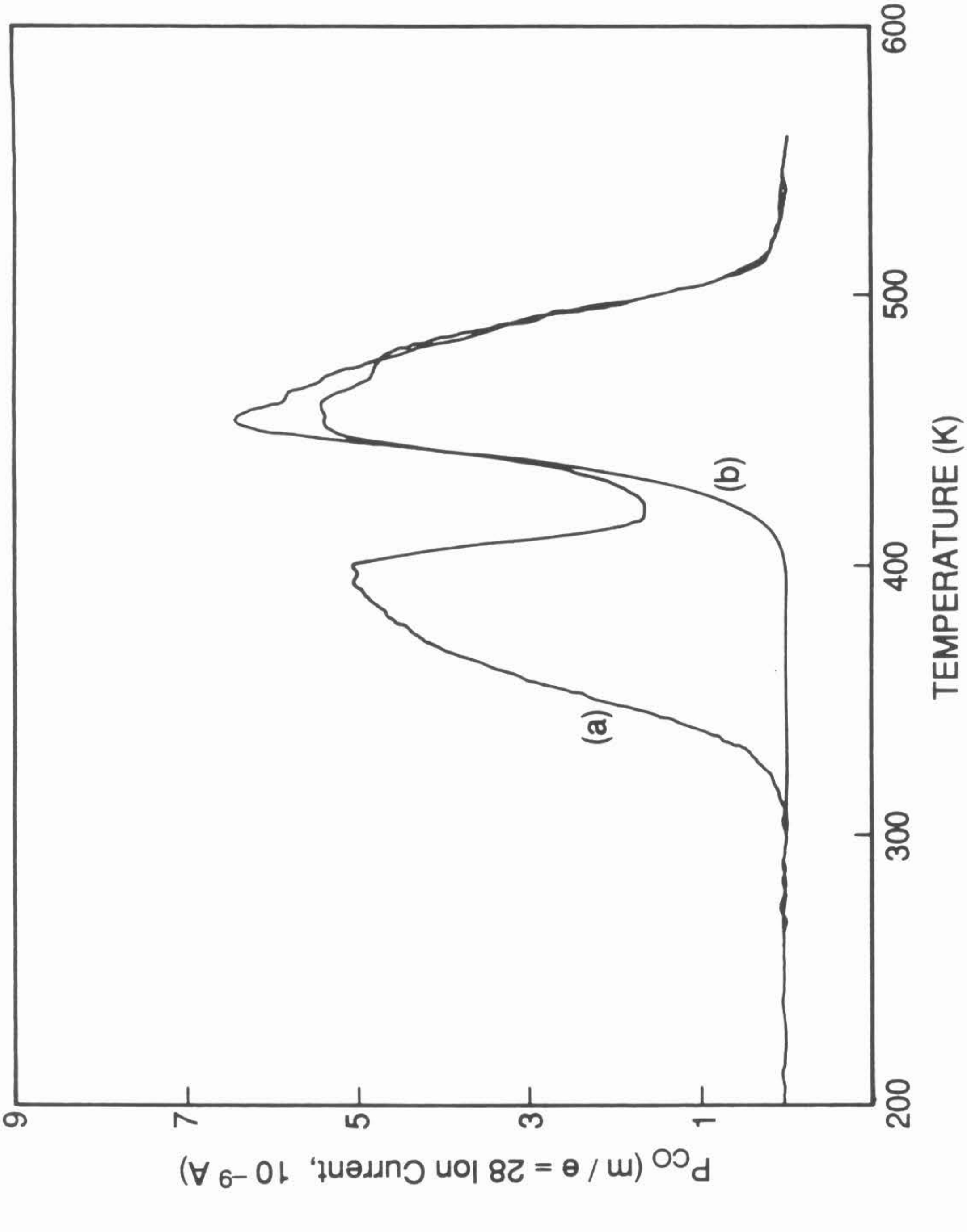
9
7
5
3
1
P_{CO} (m / e = 28 Ion Current, 10^{-9} A)
200
300
400
500
600
TEMPERATURE (K)
(a)
(b)

Figure 1

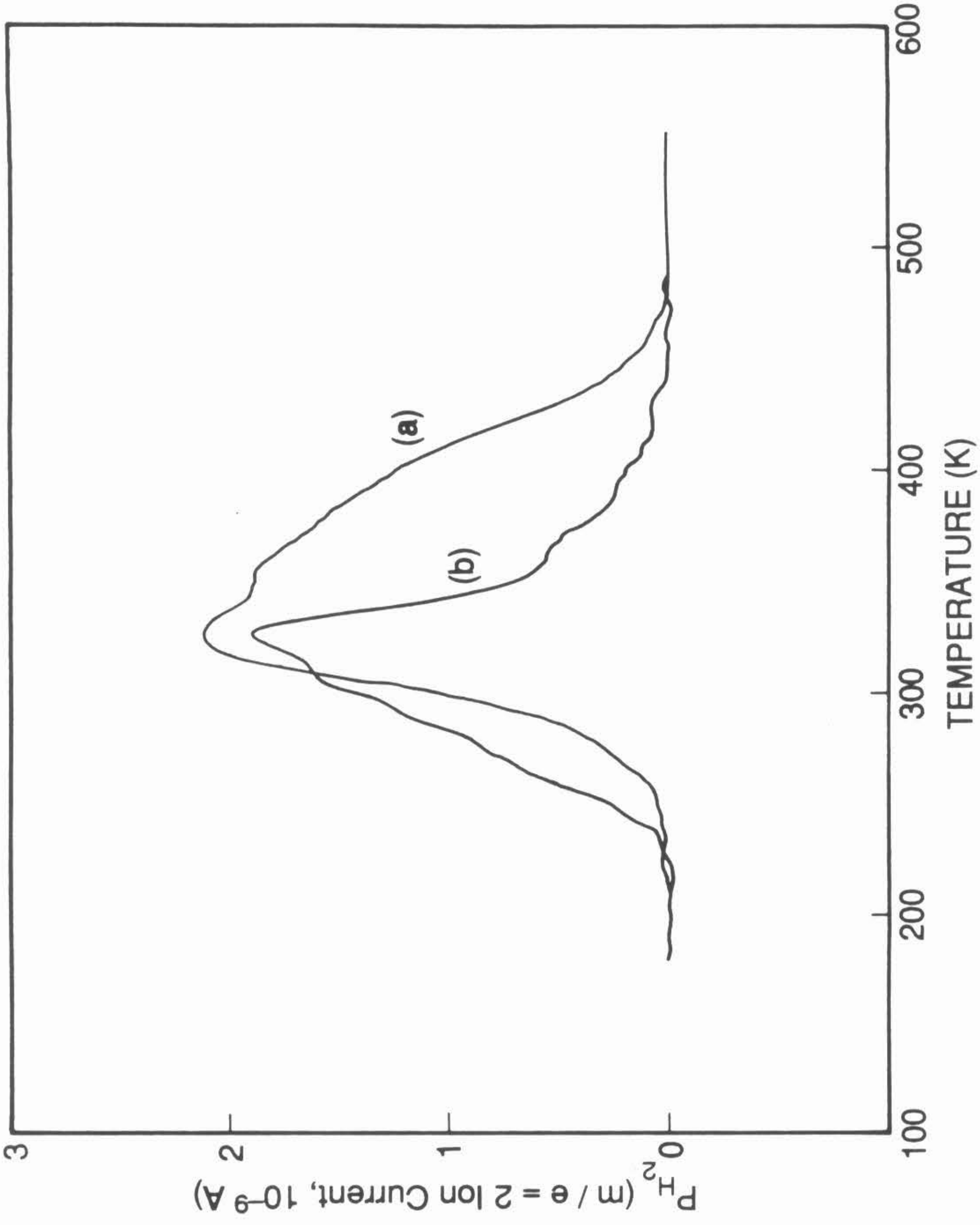

P_{H_2} (m / e = 2 Ion Current, 10^{-9} A)
0
1
2
3
TEMPERATURE (K)
100
200
300
400
500
600
(a)
(b)

Figure 2

CHAPTER 10.

Characterization of Nitrogen-Adatom Overlayers on Ru(001)

[This chapter was submitted as a paper by Y. -K. Sun and W. H. Weinberg to *Surface Science.*]

ABSTRACT

Overlayers of nitrogen adatoms on Ru(001) have been characterized both by thermal desorption mass spectrometry and low-energy electron diffraction, as well as chemically via the postadsorption and desorption of ammonia and carbon monoxide. The nitrogen-adatom overlayer was prepared by decomposing ammonia thermally on the surface at a pressure of 2.8×10^{-6} Torr and a temperature of 480 K. The saturated overlayer prepared under these conditions has associated with it a $(\frac{\sqrt{247}}{10} \times \frac{\sqrt{247}}{10})R22.7°$ LEED pattern, has two peaks in its thermal desorption spectrum, and has a fractional surface coverage of 0.40. Annealing the overlayer to approximately 535 K results in a rather sharp $(\sqrt{3} \times \sqrt{3})R30°$ LEED pattern with an associated fractional surface coverage of one third. Annealing the overlayer further to 620 K results in the disappearance of the low-temperature thermal desorption peak and the appearance of a rather fuzzy p(2×2) LEED pattern with an associated fractional surface coverage of approximately one fourth. The presence of the $(\sqrt{3} \times \sqrt{3})R30°$-N overlayer affects the surface in such a way that the binding energy of ammonia is increased relative to the clean surface, whereas that of carbon monoxide is decreased.

1. INTRODUCTION

The catalytic properties of clean transition metal surfaces can be altered significantly by the presence of both electropositive (**1**) and electronegative (**2**) adsorbates, including sulfur (**2-10**), oxygen (**11, 12**), phosphorus (**8**) and nitrogen (**13, 14**). A characterization of the geometrical structure of overlayers of these adatoms on a variety of different catalytically active surfaces is clearly important. Of even more importance, perhaps, is a determination of how the chemical properties of the surface are modified by the presence of overlayers of these adatoms. For example, quantifying how the binding energies of electron-donor and electron-acceptor probe molecules are influenced by the surface modification should be essential for a better understanding of catalysis and an improvement in catalyst design.

We are concerned specifically here with the influence of nitrogen adatoms on catalytic surfaces and reactions, three important examples of which include the synthesis of ammonia (**15-17**), the reduction of nitric oxide (**18-21**), and the synthesis of hydrogen cyanide (**22-24**). Nitrogen adatoms have been found to be the most abundant surface species in a number of catalytic reactions (**17, 21, 25**). The presence of the nitrogen adatoms will influence the catalytic properties of the metal surfaces either via geometric blocking of "active sites" or via an alteration in the electronic structure of the surface. In studying the kinetics of adsorption and desorption of hydrogen on the Pt(110)-1x2 surface, nitrogen adatoms were found to block selectively hydrogen adsorption into the high-temperature β_2-state prior to poisoning the low-temperature β_1-state (**14**). Furthermore, nitrogen adatoms also reduce the binding energy of hydrogen adatoms on this surface in such a way that the binding energy decreases linearly with the fractional coverage of atomic nitrogen in the limit of low-fractional coverages of hydrogen (**14**). Despite its importance, little is currently known concerning the nature of overlayers of nitrogen adatoms on the Ru(001) surface (**25-27**), including the chemical effects of the overlayer on postadsorbed probe molecules. We describe here a characterization by thermal desorption mass spectrometry and low-energy electron diffraction (LEED) of overlayers of nitrogen adatoms on Ru(001) that were prepared by the thermal decomposition of ammonia. We also clarify the nature of the chemical modification of the surface by these overlayers via the postadsorption of both ammonia and carbon monoxide.

2. EXPERIMENTAL DETAILS

The experiments were carried out in an ion-pumped (200 l/s) stainless steel, ultrahigh vacuum chamber equipped with quadrupole mass spectrometry, Auger electron spectroscopy, and LEED (**28**). The base pressure of the belljar was below 1×10^{-10} Torr of reactive gases. The Ru(001) crystal was mounted on a manipulator by two 0.010 in. tantalum wires spotwelded on the back of the crystal, which can be heated resistively, and cooled conductively by liquid nitrogen. The temperature of the Ru(001) surface was measured by a 0.003 in. W/5%Re – W/26%Re thermocouple spotwelded to the back of the crystal. Oxygen cleaning was routinely performed by cycling the temperature of the Ru(001) crystal between 400 and 1100 K in 7×10^{-8} Torr of oxygen backfilled into the belljar. Chemisorbed oxygen was removed by annealing the crystal to over 1600 K, and the cleanliness of the surface was verified by Auger electron spectroscopy.

Ammonia, obtained from Matheson (99.99%), was introduced into the UHV chamber through a directional beam doser. During exposure to ammonia, the surface was positioned four mm from the gas doser, which effectively reduced the amount of ammonia that must be leaked into the UHV system to reach the same ammonia exposure as compared to backfilling the belljar: with the manipulator cooled by liquid nitrogen, the increase in the background pressure was less than 2×10^{-11} Torr, i.e., the cold manipulator acted as a very effective ammonia getter.

The mass spectrometer was enclosed in a glass envelope, which has a orifice with a diameter of three mm, in order to limit contributions to the thermal desorption spectra to the well-characterized front face of the crystal (**29**). During measurements of the thermal desorption spectra of nitrogen, the mass spectrometric intensity of mass 14 (N^+) was monitored, while the Ru(001) surface was positioned three mm from the orifice. Enclosure of the mass spectrometer in the glass envelope also effectively reduced the stray electron current from the mass spectrometer to the manipulator assembly including the Ru(001) surface to less than 5 nA. Without the glass envelope, the stray current was 4 μA at a mass spectrometric emission current of 2 mA. This could cause electron-stimulated processes such as dissociation of the ammonia (**27**). All LEED observations were made after cooling the crystal to below 150 K. Readsorption of ammonia from the background was negligible during the cooling due to the low background partial pressure of ammonia.

3. RESULTS AND DISCUSSION

The overlayers of nitrogen adatoms on the Ru(001) surface were synthesized by exposing the surface to an effective pressure of 2.8×10^{-6} Torr of NH_3 at a temperature of 480 K. The reasons for choosing this particular temperature are twofold, namely, it is sufficiently low that the desorption rate of nitrogen adatoms is negligible, and it is sufficiently high that the rate of thermal decomposition of NH_3 is reasonably high. Note that the thermal decomposition of NH_3 on Ru(001) is activated, and a high surface temperature favors decomposition (**25**). Thermal desorption spectra of nitrogen due to adatom-adatom recombination following various exposures of NH_3 are shown in Fig. 1. At low exposures, only one peak is observed; whereas a second peak appears at higher exposures. Curve (*f*) in Fig. 1, obtained following a 600 s exposure to 2.8×10^{-6} Torr of NH_3, corresponds to the saturation coverage of nitrogen adatoms on Ru(001) with this method of thermal decomposition of NH_3 used to generate the overlayer. Further exposure (at the same pressure for 840 s) to NH_3 at 480 K did not increase the integrated area of the nitrogen thermal desorption spectrum.

Since the thermal decomposition of NH_3 is activated and high surface temperatures favor the decomposition of molecularly adsorbed NH_3, an overlayer of nitrogen adatoms was also prepared by exposing the Ru(001) surface to 2.8×10^{-6} Torr of NH_3 for a total of 840 s with the surface temperature profile shown in Fig. 2, in an attempt to increase the surface coverage of nitrogen adatoms. The thermal desorption spectrum of nitrogen from this nitrogen overlayer was found to be exactly the same as that of curve (*f*) in Fig. 1. The relative coverages of nitrogen adatoms associated with each thermal desorption spectrum in Fig. 1 were obtained by numerically integrating the area beneath each spectrum and then normalizing to curve (*f*). In the low-coverage limit, the coverage of nitrogen adatoms increases linearly with the NH_3 exposure with a slope of $P_r^{(0)} f_{\mathrm{NH_3}} / \theta_{\mathrm{N}}^{sat}$, where $P_r^{(0)}$ is the initial reaction probability of NH_3 on the Ru(001) surface, $f_{\mathrm{NH_3}}$ is the impingement flux of NH_3 per surface site, and $\theta_{\mathrm{N}}^{sat}$ is the saturation fractional coverage of the nitrogen adatoms on the surface. the latter was determined to be approximately 0.4 (*vide infra*). The plot of the relative coverage of the nitrogen adatoms as a function of the NH_3 exposures for curves (*a*) to (*c*) results in a straight line with a slope of $1.9 \times 10^{-2}\ s^{-1}$. Since $\theta_{\mathrm{N}}^{sat} = 0.40$ and $f_{\mathrm{NH_3}} = 0.86\ s^{-1}$, we find that $P_r^{(0)} = 8.8 \times 10^{-3}$, which is in fair agreement with the previously reported value of 3×10^{-3} in the zero-coverage limit at this temperature (**25**).

The temperature of the high-temperature peak in the thermal desorption spectra shifts from 880 K at a relative coverage of 0.22 (absolute coverage of 0.09) to 745 K at saturation. We evaluated the activation energy E_d and the preexponential factor $k_d^{(0)}$ of the desorption rate coefficient independently as a function of surface coverage, using the methods described by Taylor and Weinberg (**30**) and Falconer and Madix (**31**). The results of this analysis are shown in Figs. 3 (a) and 3 (b). At low coverage of nitrogen, the activation energy of desorption is approximately 32 kcal/mol, and the preexponential factor of the desorption rate coefficient is approximately 10^{-8} cm^2-s^{-1}. The latter is rather low compared to a typical preexponential factor of a second-order surface reaction, 10^{-3} cm^2-s^{-1}, and may well be due to the fact that the *adsorption* reaction is activated. This will impose rather more severe entropy restrictions on the transition state for desorption via the substantial "corrugation" of the potential energy surface. Note that the preexponential factor for desorption of nitrogen from the Pt(110)-(1×2) surface is also approximately 10^{-8} cm^2-s^{-1}, and the adsorption reaction is activated on platinum as well (**32, 33**). At relative coverages near half of saturation, both the activation energy and the preexponential factor decrease precipitously; the former to approximately 20 kcal/mol, and the latter to approximately 10^{-11} cm^2-s^{-1}. This could be due to a decrease in the binding energy of the nitrogen which effectively imposes further entropy restrictions on the transition state to desorption, e.g. the "concentration" of transition states that are available to surmount the *lowest* energy barrier to desorption (and adsorption) is substantially reduced.

The $(\frac{\sqrt{247}}{10} \times \frac{\sqrt{247}}{10})R22.7^\circ$ LEED pattern shown in Fig. 4 (*a*) was observed for this nitrogen-saturated Ru(001) surface. The LEED observation was made after momentarily annealing the surface to 480 K, cf. Fig. 4 (*e*), which results in neither molecular ammonia, NH_x species nor atomic hydrogen remaining on the surface (**25**). The two outermost fractional-order LEED spots in Fig. 4 (*a*) are due to first-order diffraction of the nitrogen adatoms, whereas the innermost one is not. The vectors corresponding to the first-order diffraction spots differ from the $(\sqrt{3} \times \sqrt{3})R30^\circ$ vector by $\pm 7.3^\circ$, and the ratio of their vector lengths to that of the $(\sqrt{3} \times \sqrt{3})R30^\circ$ vector was measured to be 1.10. This implies that the unit vector of the overlayer of nitrogen adatoms is rotated by $\pm 7.3^\circ$ with respect to the unit vector of a $(\sqrt{3} \times \sqrt{3})R30^\circ$ overlayer, and that the length of the unit vector of this nitrogen-saturated overlayer is 0.91 times that corresponding to the $(\sqrt{3} \times \sqrt{3})R30^\circ$ superstructure. Based upon this analysis, the structure of the saturated overlayer of the nitrogen adatoms is shown in Fig. 4 (*i*). The unit cell of this coincidence structure, which is determined to be $(\sqrt{247} \times \sqrt{247})R22.7^\circ$-100N, is not shown completely since it is too large. However, the primitive unit cell which obtains when one ignores the substrate, a $(\frac{\sqrt{247}}{10} \times \frac{\sqrt{247}}{10})R22.7^\circ$, can be seen clearly in Fig. 4 (*i*). The fractional coverage of the nitrogen adatoms corresponding to the $(\frac{\sqrt{247}}{10} \times \frac{\sqrt{247}}{10})R22.7^\circ$ superstructure is 0.40. Annealing the surface briefly to a temperature between 515 and 540 K, as indicated in Fig. 4 (*f*), resulted in a rather sharp $(\sqrt{3} \times \sqrt{3})R30^\circ$ LEED pattern, shown schematically in Fig. 4 (*b*). The $(\sqrt{3} \times \sqrt{3})R30^\circ$ LEED pattern became progressively less sharp following further annealing. After momentary annealing to 575 K, cf., Fig. 4 (*g*), a streaked (2×2) LEED pattern was observed which is depicted schematically in Fig. 4 (*c*). This LEED pattern persisted up to approximately 600 K. Further annealing of the surface to 620 K resulted in a fuzzy (2×2) LEED pattern, shown schematically in Fig. 4 (*d*). Annealing to 660 K caused the disappearance of the (2×2) LEED pattern, and no other ordered superstructures were observed after annealing to higher temperatures. We conclude from the above observations that the saturation coverage of nitrogen adatoms on Ru(001) following thermal decomposition of NH_3 at 2.8×10^{-6} Torr and 480 K is approximately 0.40, which is associated with the $(\frac{\sqrt{247}}{10} \times \frac{\sqrt{247}}{10})R22.7^\circ$ LEED pattern of Fig. 4 (*a*). The nitrogen overlayers with $(\sqrt{3} \times \sqrt{3})R30^\circ$ and (2×2) superstructures patterns correspond to coverages of 0.33 and 0.25, respectively.

A (2×2) LEED pattern has been reported previously following the steady-state thermal decomposition of NH_3 at an effective NH_3 pressure of 2×10^{-6} Torr and surface temperatures from 750 to 450 K (**25**). A saturation fractional coverage of nitrogen adatoms of 0.47 was estimated, and it was suggested that the observed (2×2) LEED pattern corresponded to three independent p(1×2) domains rotated 120° with respect to one another. The experimental conditions under which this nitrogen adatom overlayer on Ru(001) was prepared overlaps with the experimental conditions in this study. The failure to observe the $(\frac{\sqrt{247}}{10} \times \frac{\sqrt{247}}{10})R22.7°$ and $(\sqrt{3} \times \sqrt{3})R30°$ LEED patterns could have been caused by readsorption of NH_3 on the nitrogen-saturated surface, which also has an apparent (2×2) LEED pattern (**34**).

The adsorption of NH_3 and CO on the Ru(001)-$(\sqrt{3} \times \sqrt{3})R30°$-N overlayer was used as a chemical probe to investigate the effect of the nitrogen adatoms on the chemical properties of the Ru(001) surface. The reason for choosing these two particular probe molecules is that they interact qualitatively differently with the surface. The adsorption of NH_3 causes a decrease in the work function (**35**), whereas adsorption of CO has the opposite effect (**36**). In the case of NH_3, the binding is via donation of the lone pair of electrons on the nitrogen to unoccupied density of states on the metal, which results in a net transfer of charge to the surface and hence a decrease in the work function. The work function decreases rapidly by 1.7 eV as the fractional coverage of NH_3 reaches 0.20, and then less rapidly by an additional 0.6 eV when the surface coverage reaches 0.7 monolayer (**35**). In the case of CO, the binding involves a combination of donation from the 5σ orbital localized on the carbon atom to the metal and backdonation from the metal into the 2π orbital of the CO, with the latter dominant (**37-40**). The work function of the Ru(001) surface increases upon CO adsorption by 0.5 eV at saturation coverage (**36**).

We found that the presence of the $(\sqrt{3} \times \sqrt{3})R30°$-N overlayer strengthens the bonding of NH_3 but reduces the binding energy of CO to the Ru(001) surface. Thermal desorption spectra of NH_3 on clean Ru(001) and on the Ru(001)-$(\sqrt{3} \times$

$\sqrt{3})R30°$-N surface following various exposures of NH_3 at 120 K are shown in Figs. 5 and 6, respectively. The results for the clean Ru(001) surface agree very well with those reported by Benndorf and Madey (**35**). The peak temperatures of the thermal desorption spectra at low and approximately the same coverages are 320 K on clean Ru(001) and 385 K on Ru(001)-($\sqrt{3} \times \sqrt{3})R30°$-N, cf. curve (*a*) in Figs. 5 and 6, indicating clearly an increase in the binding energy of NH_3 to the Ru(001) surface of approximately 4 kcal/mol due to the overlayer of nitrogen adatoms. Thermal desorption spectra of CO at a fractional coverage of approximately 0.05 from both clean Ru(001) and the Ru(001)-($\sqrt{3} \times \sqrt{3})R30°$-N surface are shown in Fig. 7 (*a*) and (*b*), respectively. In this case the presence of the nitrogen adatoms reduces the peak temperature from approximately 520 to 440 K, indicating a weakening of CO bonding to the Ru(001) surface by approximately 5 kcal/mol. Assuming the same preexponential factors of the desorption rate coefficients on both surfaces, the binding energy of NH_3 is increased by 20% and that of CO is reduced by 15% on the Ru(001)-($\sqrt{3} \times \sqrt{3})R30°$-N surface relative to the clean surface. Note that the peak temperatures of the thermal desorption spectra are compared in the low coverage limit in order to avoid complication due to NH_3-NH_3 and CO-CO interactions.

A reduction in the binding energy of CO has also been observed on other surfaces modified by nitrogen adatoms, including Ni(100) (**13**) and Rh(100) (**41**), and also on surfaces modified by other electronegative elements such as sulfur, chlorine and phosphorus (**8**). In addition to possible direct electrostatic interactions (**2, 42**) between the nitrogen adatoms and CO, the decrease in the binding energy of the CO can be caused by indirect, surface-mediated interactions between the nitrogen adatoms and the chemisorbed CO. The presence of the nitrogen causes a reduction in the local density of states near the Fermi level (**10**), which could cause a decrease in the coupling of the 2π orbitals with the Ru(001) surface. Ammonia, on the other hand, due to the nature of its bonding to the surface (donation of a lone pair of electrons to the metal surface), increases its binding energy to the surface in the presence of the electronegative nitrogen adatoms. One would expect qualitatively similar and quantitatively stronger effects on the binding energies of NH_3 and CO on oxygen-modified Ru(001) surfaces, since oxygen is more electronegative than nitrogen. These expectations have been confirmed experimentally on the Ru(001)-p(2×2)-O and Ru(001)-p(1×2)-O surfaces (**34**).

5. SUMMARY

Overlayers of nitrogen adatoms on the Ru(001) surface were prepared by thermal decomposition of ammonia at a pressure of 2.8×10^{-6} Torr and a surface temperature of 480 K, and characterized both by thermal desorption mass spectrometry and low-energy electron diffraction, as well as chemically via the postadsorption and desorption of ammonia and carbon monoxide. The maximun fractional coverage of nitrogen adatoms obtainable under these experimental conditions is 0.40. The saturated overlayer has associated with it a $(\frac{\sqrt{247}}{10} \times \frac{\sqrt{247}}{10})R22.7°$ LEED pattern and two peaks in the thermal desorption spectrum. Annealing the overlayer to approximately 535 K results in a rather sharp $(\sqrt{3} \times \sqrt{3})R30°$ LEED pattern with an associated fractional surface coverage of one third. Annealing the overlayer further to 620 K, however, results in the disappearance of the low-temperature thermal desorption peak and the appearance of a rather fuzzy p(2×2) LEED pattern with an associated fractional surface coverage of approximately one fourth. The presence of the $(\sqrt{3} \times \sqrt{3})R30°$-N overlayer affects the surface such that the binding energy of ammonia is increased relative to the clean surface, whereas that of carbon monoxide is decreased.

Acknowledgment: This work was supported by the National Science Foundation under grant number CHE-8617826.

REFERENCES

1. H. P. Bonzel, *Surface Sci. Reports* **8**, 43 (1988), and references therein.
2. M. P. Kiskinova, *Surface Sci. Reports* **8**, 359 (1987).
3. D. W. Goodman and J. E. Houston, *Science* **236**, 403 (1987).
4. J. Oudar, *Catal. Rev.-Sci. Eng.* **22**, 171 (1980).
5. C. H. Bartholomew, P. K. Agrawal and J. R. Katzer, *Advan. Catal.* **31**, 135 (1982).
6. R. J. Madix, M. Thornburg and S. -B. Lee, *Surface Sci.* **133**, L447 (1983).
7. M. Kiskinova and D. W. Goodman, *Surface Sci.* **105**, L265 (1981).
8. M. Kiskinova and D. W. Goodman, *Surface Sci.* **108**, 64 (1981).
9. R. J. Madix, M. Thornburg and S. -B. Lee, *Surface Sci.* **133**, L447 (1983).
10. P. J. Feibelman and D. R. Hamann, *Phys. Rev. Letters* **52**, 61 (1984).
11. J. E. Parmeter, U. Schwalke and W. H. Weinberg, *J. Am. Chem. Soc.* **109**, 5083 (1987).
12. A. B. Anton, N. R. Avery, T. E. Madey and W. H. Weinberg, *J. Chem. Phys.* **85**, 507 (1986).
13. M. Kiskinova and D. W. Goodman, *Surface Sci.* **109**, L555 (1981).
14. W. Tsai and W. H. Weinberg, *J. Phys. Chem.* **92**, 1245 (1988).
15. M. Boudart, *Catal. Rev.-Sci. Eng.* **23**, 1 (1981).
16. G. Ertl, *Catal. Rev.-Sci. Eng.* **21**, 201 (1980).
17. J. J. Vajo, W. Tsai and W. H. Weinberg, *J. Phys. Chem.* **89**, 3243 (1985).
18. S. E. Oh, G. B. Fisher, J. E. Carpenter and D. W. Goodman *J. Catal.* **100**, 360 (1986).
19. W. F. Egelhoff Jr., in *The Chemical Physics of Solid Surfaces*, Eds., D. A. King and D. P. Woodruff, Vol. 4, Elsevier, Amsterdam, (1982).
20. T. W. Root, L. D. Schmidt and G. B. Fisher, *Surface Sci.* **150**, 173 (1985).

21. C. H. F. Peden, D. W. Goodman, D. S. Blair, P. J. Berlowitz, G. B. Fisher and S. H. Oh, *J. Phys. Chem.* **92**, 1563 (1988).
22. D. Hasenberg, and L. D. Schmidt, *J. Catal.* **104**, 441 (1987).
23. D. Hasenberg, and L. D. Schmidt, *J. Catal.* **97**, 156 (1986).
24. D. Hasenberg, and L. D. Schmidt, *J. Catal.* **91**, 116 (1985).
25. W. Tsai and W. H. Weinberg, *J. Phys. Chem.* **91**, 5302 (1987).
26. L. R. Danielson, M. J. Dresser, E. E. Donaldson and J. T. Dickinson, *Surface Sci.* **71**, 599 (1978).
27. L. R. Danielson, M. J. Dresser, J. T. Dickinson and D. R. Sandstrom, *Surface Sci.* **71**, 615 (1978).
28. Y. -K. Sun, C. -Y. Chan and W. H. Weinberg, *J. Vac. Sci. Technol. A* **7**, 4298 (1989).
29. P. Feulner and Menzel, *J. Vacuum Sci. Technol.* **17**, 662 (1980).
30. J. L. Taylor and W. H. Weinberg, *Surface Sci.* **78**, 259 (1978).
31. J. L. Falconer and R. J. Madix, *J. Catal.* **48**, 262 (1977).
32. A. Ozaki and K. I. Aika, in *A Treatise on Dinitrogen Fixation*, Eds., R. W. Hardy, F. Bottomley and R. C. Burns, Wiley, N. Y., 1979, Chap. 4.
33. Y. -K. Sun and W. H. Weinberg, to be published.
34. Y. -K. Sun and W. H. Weinberg, to be published.
35. C. Benndorf and T. E. Madey, *Surface Sci.* **135**, 164 (1983).
36. T. E. Madey and D. Menzel, *Japan J. Appl. Phys. Suppl.* **2**, 229 (1974).
37. P. S. Bagus, C. J. Nelin and C. W. Bauschlicher, Jr., *Phys. Rev. B* **28**, 5423 (1983).
38. G. Blyholder, *J. Phys. Chem.* **68**, 2772 (1968).
39. C. W. Bauschlicher Jr., S. R. Langhoff and L. A. Barnes, Chem. Phys. **129**, 431 (1989).
40. R. C. Baetzold, *Phys. Rev. B* **29**, 4211 (1984).

41. W. M. Daniel and J. M. White, *Surface Sci.* **171**, 289 (1986).

42. N. D. Lang, S. Holloway and J. K. Norskov, *Surface Sci.* **150**, 24 (1985).

43. C. Benndorf and T. E. Madey, *Surface Sci.* **135**, 164 (1983).

Figure Captions

Fig. 1: Thermal desorption spectra of nitrogen due to adatom-adatom recombination following thermal decomposition of NH_3 on Ru(001) at 480 K and at ammonia pressure of 2.8×10^{-6} Torr for various durations (in seconds): (a) 10, (b) 30, (c) 60, (d) 195, (e) 300, (f) 600 and 840. The *absolute* coverages of nitrogen adatoms are (a) 0.09, (b) 0.15, (c) 0.22, (d) 0.29, (e) 0.35 and (f) 0.40, respectively. The heating rate is 10.0 K-s^{-1}. The small peak near 400 K in curve (e) is caused by NH_3 desorption from the nitrogen-adatom covered surface.

Fig. 2: Surface temperature profile during the decomposition of NH_3.

Fig. 3: The desorption energy (a) and the preexponential factor (b) of the rate coefficient of recombinative desorption of nitrogen from Ru(001) as a function of the absolute fractional coverage of nitrogen adatoms. The solid line in each diagram serves as a visual guide.

Fig. 4: LEED patterns (a)-(d) observed below 150 K following annealing the nitrogen adatom-saturated Ru(001) surface to the temperatures indicated by a line marker on the thermal desorption spectra (e)-(h), along with structures proposed for the observed LEED patterns (i)-(k). In the schematics of the LEED patterns (a)-(d), the filled and the shaded circles have approximately the same intensities, whereas the intensity of the open circles is less. The diameter of the ruthenium atoms is 2.71 Å and that of the nitrogen adatoms (filled circles) is taken to be 0.75 Å. The nitrogen adatoms are assumed to reside in the high coordination three-fold sites in Figs. (j) and (k), which is not possible in Fig. (i).

Fig. 5: Thermal desorption spectra of NH_3 from Ru(001) following increasing NH_3 exposures from (a) to (d). The low-temperature peak does not saturate with

increasing exposure. The heating rate is 3.0 K-s^{-1}.

Fig. 6: Thermal desoption spectra of NH_3 from Ru(001)-($\sqrt{3} \times \sqrt{3}$)$R30°$-N at increasing NH_3 exposures from (a) to (d). The low-temperature peak does not saturate with increasing exposure. The heating rate is 3.0 K-s^{-1}.

Fig. 7: Thermal desorption of CO with a fractional coverage of approximately 0.05 from (a) Ru(001)-($\sqrt{3} \times \sqrt{3}$)$R30°$-N, and (b) Ru(001). The two spectra are displaced vertically for clarity. The heating rate is 10.0 K-s^{-1}.

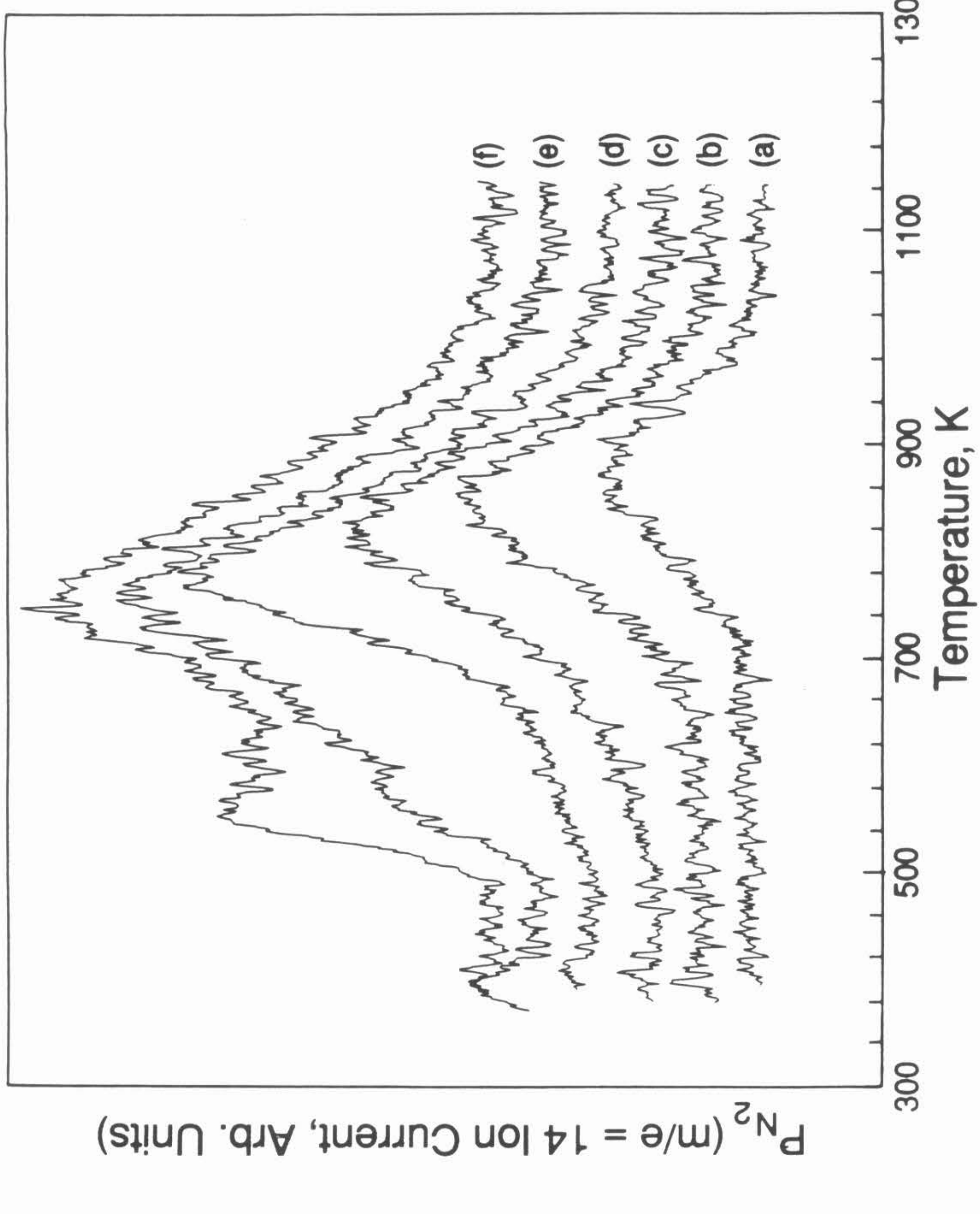
(f)
(e)
(d)
(c)
(b)
(a)
300
500
700
900
1100
1300
Temperature, K
P_{N_2} (m/e = 14 Ion Current, Arb. Units)

Figure 1

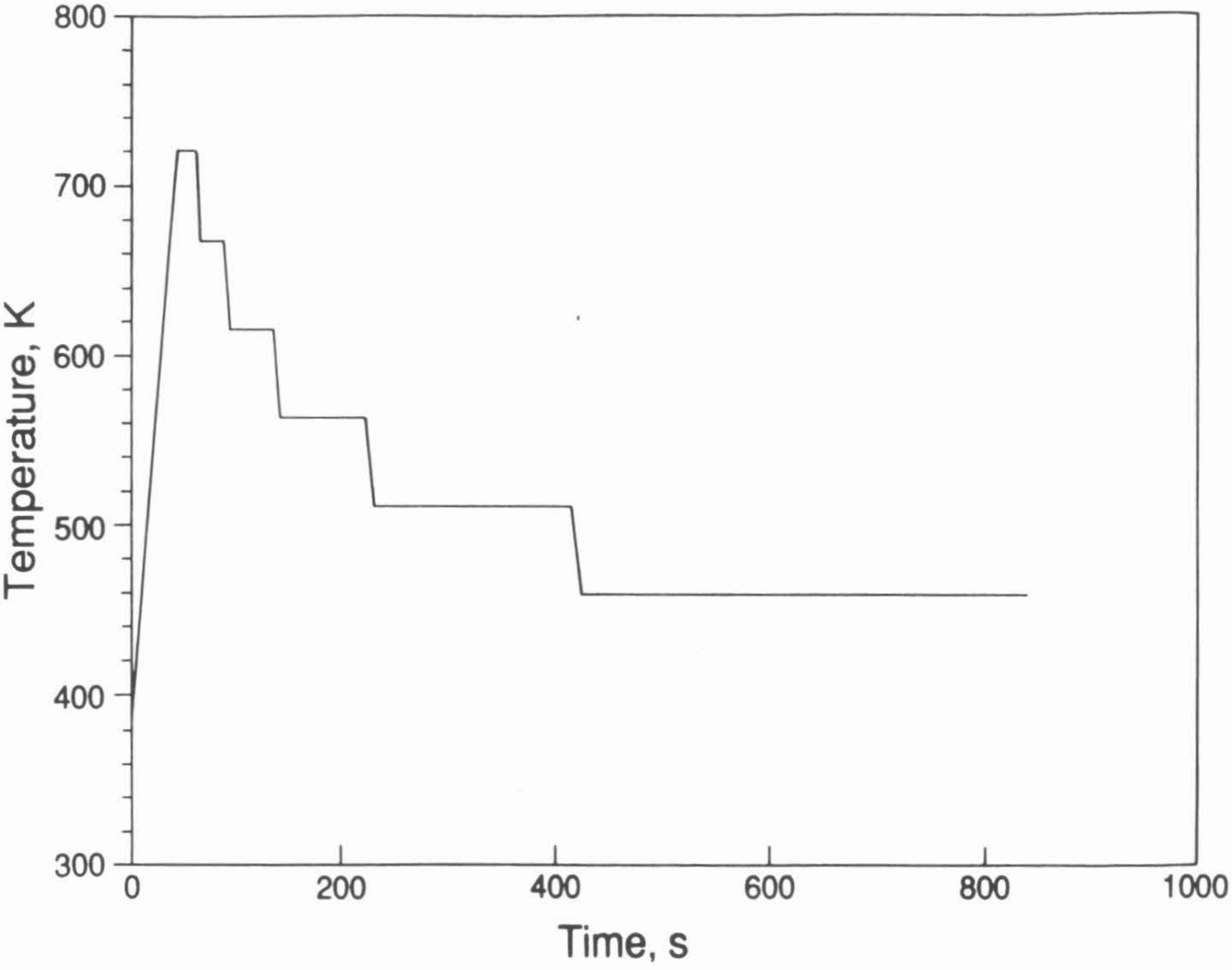
800
700
600
500
400
300
Temperature, K
0
200
400
600
800
1000
Time, s

Figure 2

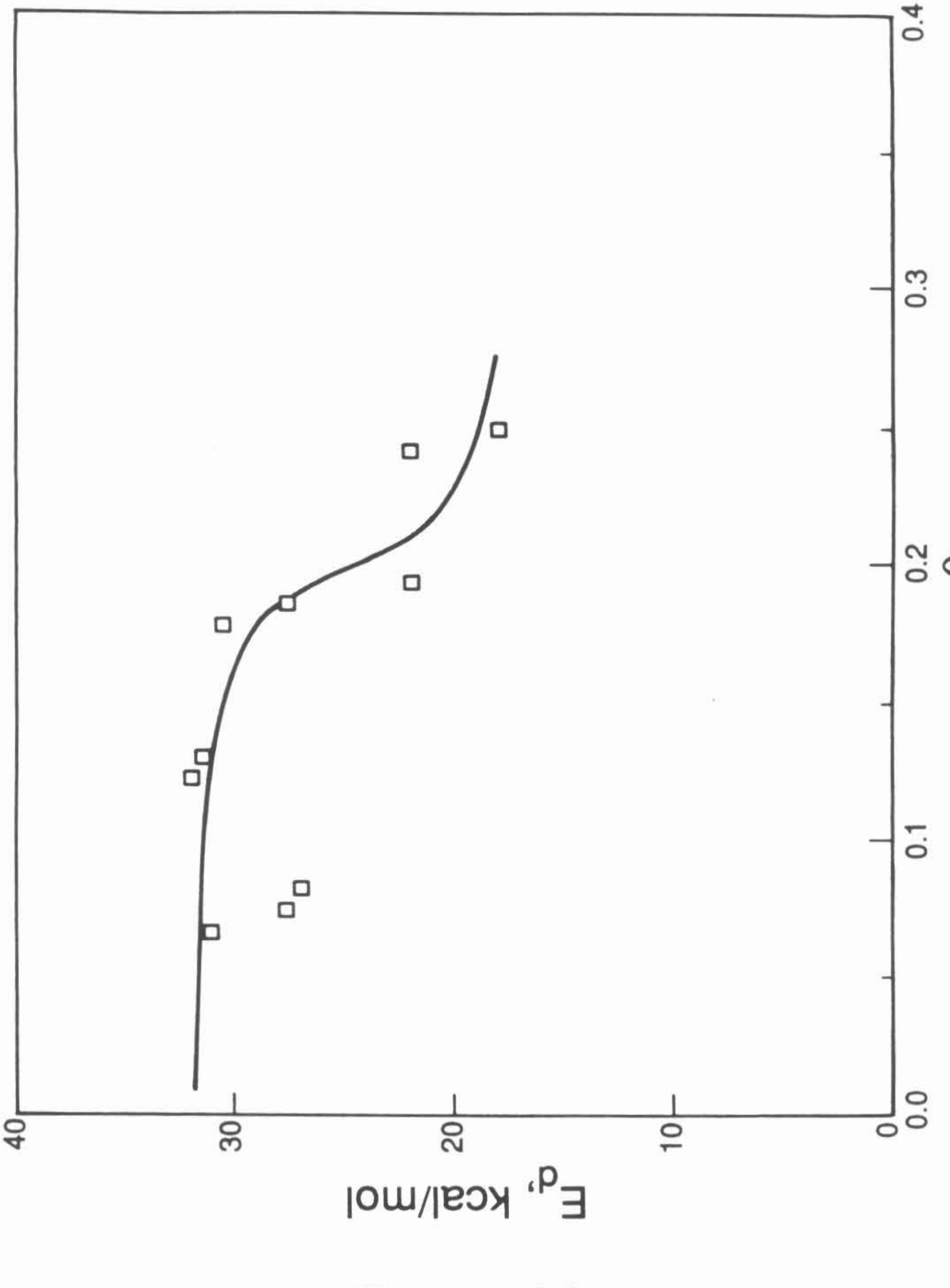

Figure 3 (a)

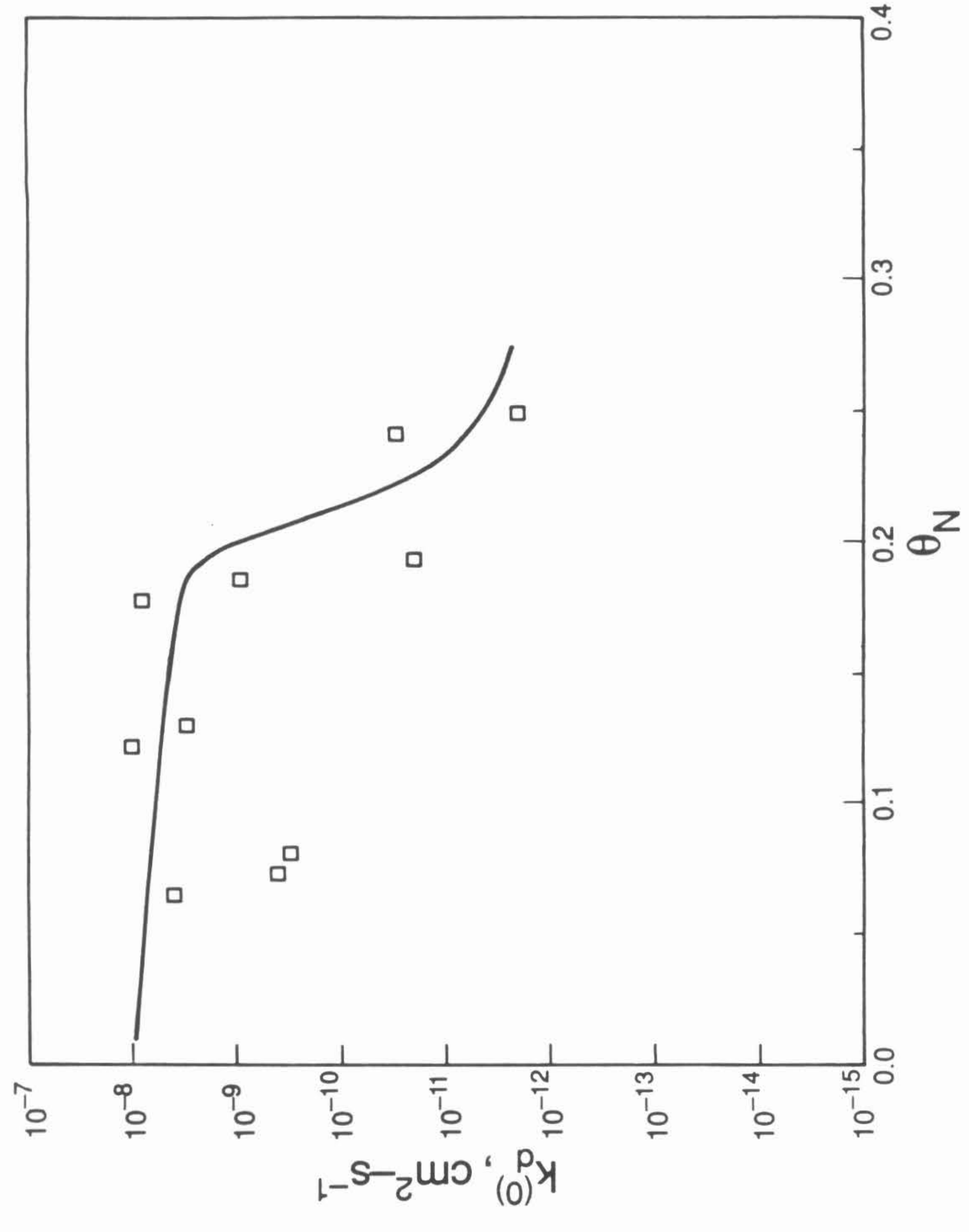
0.0
0.1
0.2
0.3
0.4
θN
10−7
10−8
10−9
10−10
10−11
10−12
10−13
10−14
10−15
K(0)d, cm2–s−1

Figure 3 (b)

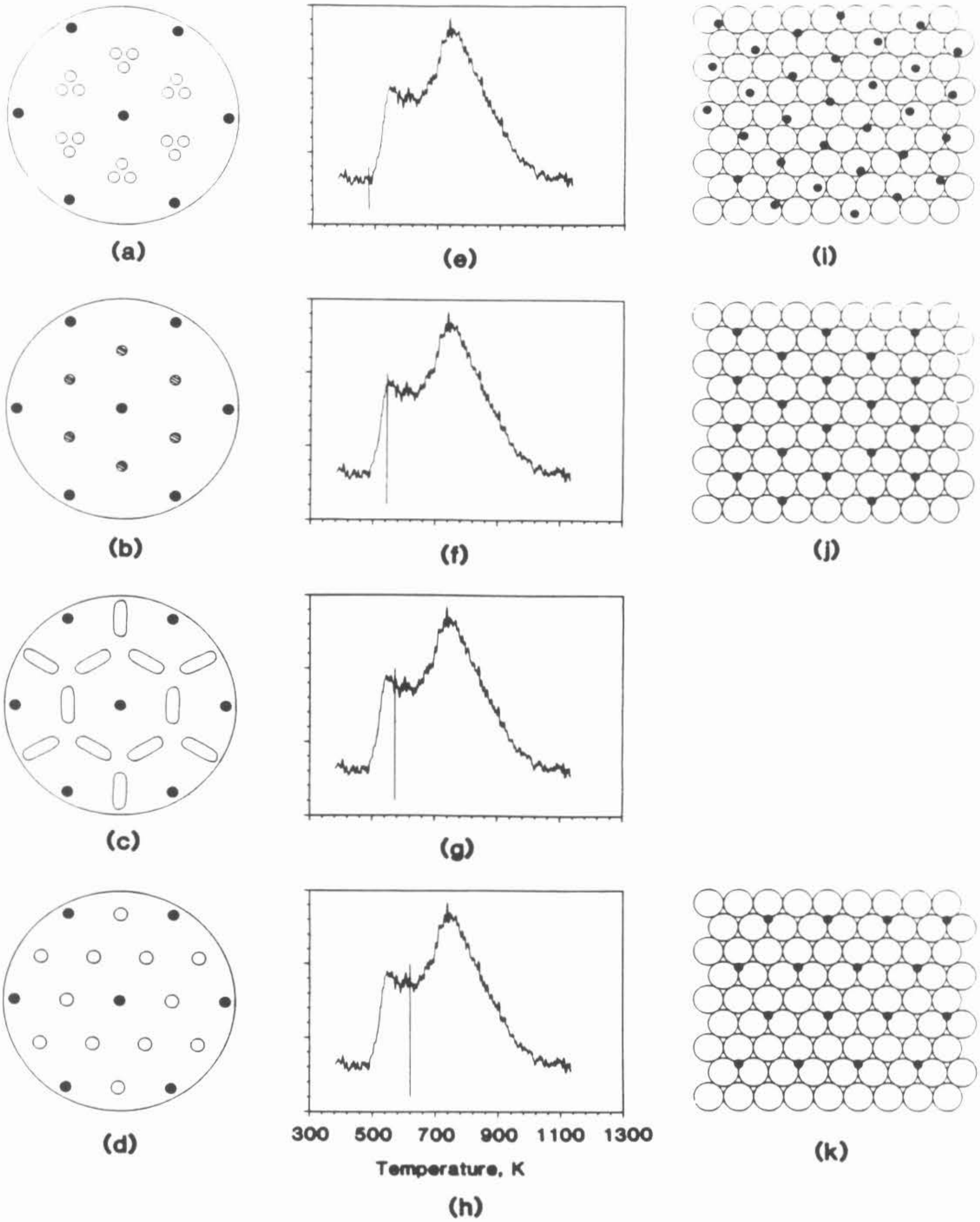

Figure 4

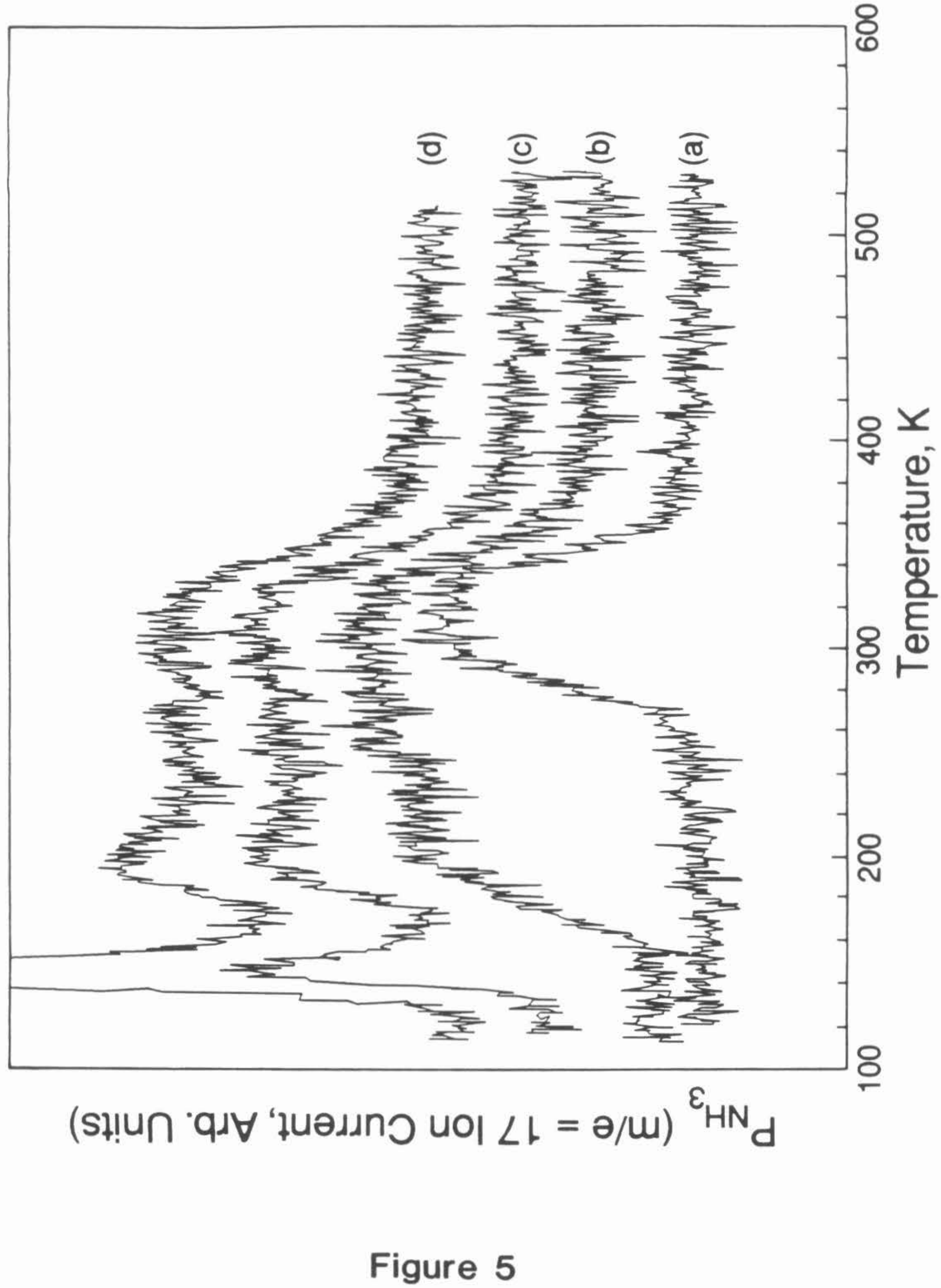
(d)
(c)
(b)
(a)
100
200
300
400
500
600
Temperature, K
P_{NH_3} (m/e = 17 Ion Current, Arb. Units)

Figure 5

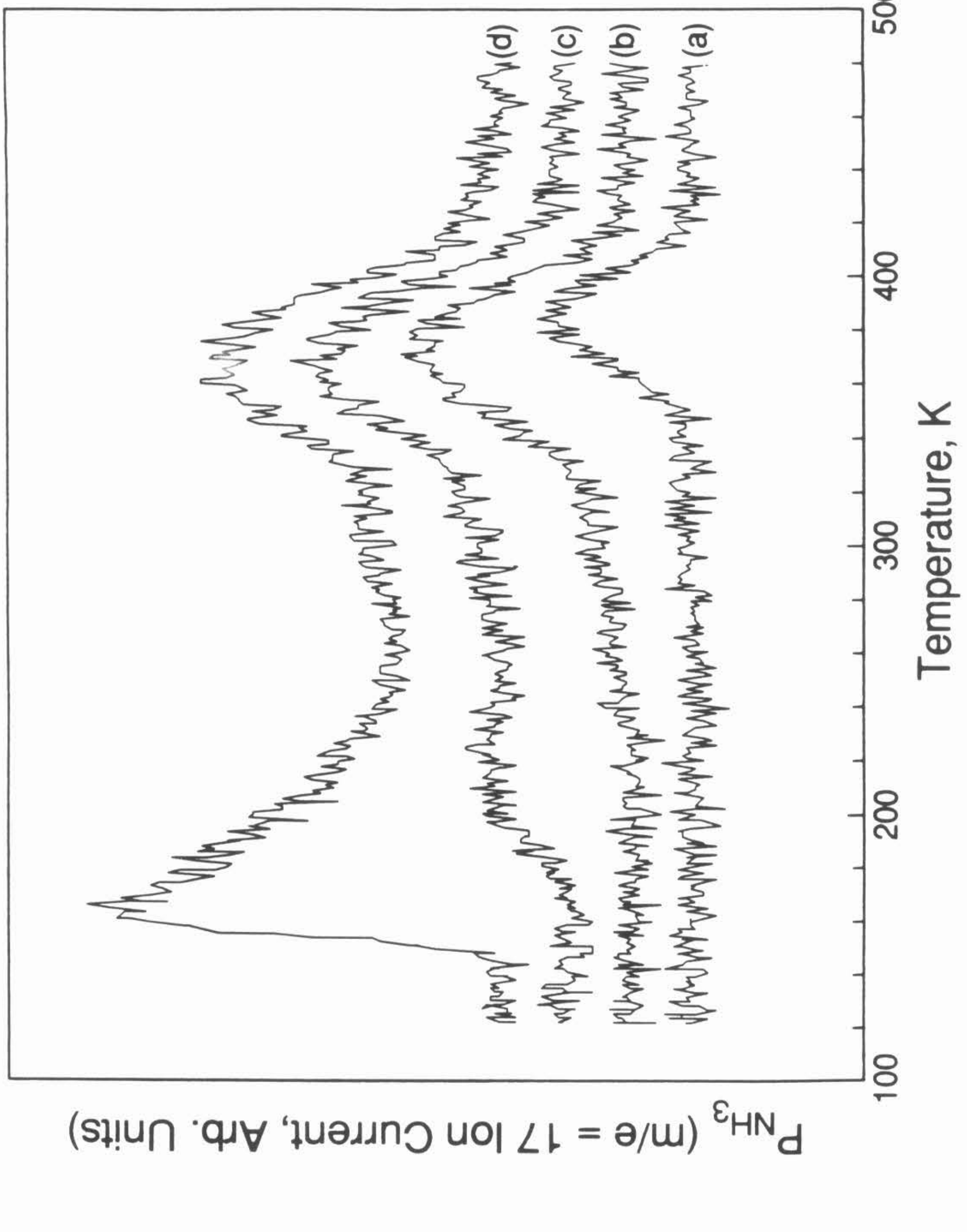
(d)
(c)
(b)
(a)
100
200
300
400
500
Temperature, K
P_{NH_3} (m/e = 17 Ion Current, Arb. Units)

Figure 6

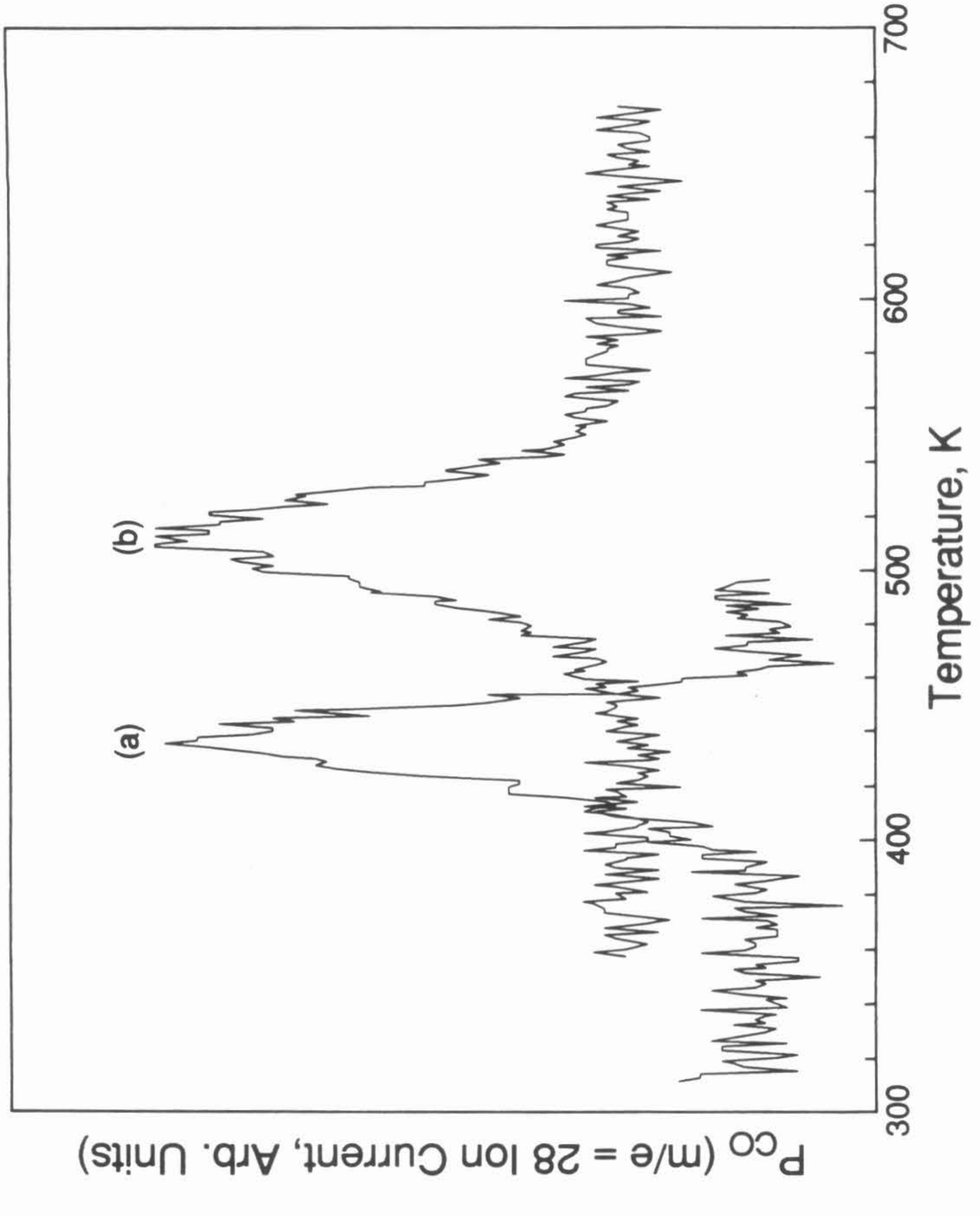
(a)
(b)
300
400
500
600
700
Temperature, K
P_{CO} (m/e = 28 Ion Current, Arb. Units)

Figure 7

CHAPTER 11.

Conclusions

The principal conclusions of the research presented in this thesis may be summarized as follows:

Chapter 2

1. The activated dissociative chemisorption of methane and ethane on Pt(110)-(1×2) is studied under such conditions that the dissociation reactions proceed via a trapping-mediated mechanism that is manifested by the strong dependence of probabilities of dissociation of methane and ethane on the surface temperature while the gas temperature remains at 300 K.
2. Dissociative chemisorption is activated for both methane with an apparent activation energy of 14.4 kcal/mol, and ethane with an apparent activation energy of 2.8 kcal/mol. These activation energies are measured with respect to the alkane in the gas phase. The activation energies measured with respect to the bottom of the physically adsorbed well (i.e., the activation energies of the elementary surface reactions) are approximately 18.4 kcal/mol for methane and 10.3 kcal/mol for ethane.

Chapters 3-7

1. The catalytic decomposition on the Ru(001) surface was examined with thermal desorption mass spectrometry. Formic acid (DCOOH) chemisorbs dissociatively on the Ru(001) surface not only via the cleavage of O-H bond to form a formate and a hydrogen adatom, but also via the cleavage of C-O bond to form a CO, a deuterium adatom and an hydroxyl (OH) on the surface. The former is the predominant reaction.
2. The kinetics of the thermal desorption of CO_2 resulted from the decomposition of the formate via C-D bond cleavage is characterized by a kinetic isotope effect, an increasingly narrow FWHM, and an upward shift in the peak temperature

with the coverage of the formate. These kinetic features are attributed to an increase in the activation energy for the C-D bond cleavage of the formate with increasing formate coverage, which results from an alteration of the electronic properties of the surface by the presence of the formate.

3. The overall probability of the C-D bonf cleavage and C-O bond cleavage reactions of the formate is approximately equal, regardless the initial formate coverage, which causes variation in the activation energy for C-D bond cleavage reaction. The desorption of water, which implies C-O bond cleavage of the formate, appears at approximately the same temperature as that of CO_2, indicating that the activation energies for the C-O and C-D bond cleavage reactions of the formate are approximately the same and change in sympathy with the initial formate coverage. It is suggested that formate might decompose via the formation of a short-lived surface complex, which is composed of two formate and is the precursor to the decomposition.
4. The presence of CO on the surface does not change the relative yields of the decomposition of the formate to the formation of CO_2 and CO, and was found to influence the reactivity of the formate slightly. The presence of oxygen adatoms on the surface, however, enhances the relative yield of CO_2.
5. The measurement of steady-state rate is demonstrated to be especially valuable in determining kinetics of the elementary reaction associated with short-lived, molecularly adsorbed precursor to decomposition on the surface. In particular, The kinetic parameters of the molecular precursor of formaldehyde to its dissociation on the Pt(110)-(1×2) surface are determined.

Chapters 9 and 10

1. Overlayers of nitrogen adatoms on Ru(001) have been synthesized and characterized by thermal desorption mass spectrometry and low-energy electron

diffraction, as well as chemically via the postadsorption and desorption of ammonia and carbon monoxide. A series of ordered overlayer structures are observed. They are $(\frac{\sqrt{247}}{10} \times \frac{\sqrt{247}}{10})R22.7°$, $(\sqrt{3} \times \sqrt{3})R30°$ and p(2×2) with associated with them fractional surface coverage of 0.40, 0.33 and 0.25. In the low coverage limit, the presence of the $(\sqrt{3} \times \sqrt{3})R30°$-N overlayer alters the Ru(001) surface in such a way that the binding energy of ammonia is increased by 20 % relative to the clean surface, whereas that of carbon monoxide is reduced by 15 %.

2. A general methodology for the *indirect* relative determination of the absolute fractional surface coverages is described and was utilized to determine the saturation fractional coverage of hydrogen on Ru(001). Formaldehyde was employed as a bridge to lead us from the known reference point of the saturation fractional coverage of carbon monoxide to unknown reference point of the fractional coverage of hydrogen on Ru(001), which was then used to determine accurately the saturation fractional coverage of hydrogen. It was determined that $\theta_{\mathrm{H}}^{sat} = 1.02\ (\pm 0.05)$ *i.e.* the surface stoichiometry is Ru : H = 1 : 1. The relative nature of the method, which cancels systematic errors, together with the utilization of a glass envelope around the mass spectrometer, which reduces spurious contributions in the thermal desorption spectra, results in high accuracy in the determination of absolute fractional coverages.

APPENDIX A

Catalytic Dehydration of Acetic Acid on a Graphitized Platinum Surface

[This Appendix consists of an article coauthored with J. J. Vajo and W. H. Weinberg, which appeared in *The Journal of Physical Chemistry* **91**, 1153 (1987).]

Reprinted from The Journal of Physical Chemistry, 1987, *91*, 1153.
Copyright © 1987 by the American Chemical Society and reprinted by permission of the copyright owner.

Catalytic Dehydration of Acetic Acid on a Graphitized Platinum Surface

J. J. Vajo, Y.-K. Sun, and W. H. Weinberg*

Division of Chemistry and Chemical Engineering, California Institute of Technology, Pasadena, California 91125 *(Received: July 18, 1986; In Final Form: October 17, 1986)*

Absolute reaction rates have been measured in a continuous flow microreactor for the steady-state, catalytic dehydration of acetic acid to ketene at pressures between 8×10^{-7} and 7×10^{-4} Torr and temperatures between 500 and 800 K. The catalyst was a polycrystalline platinum wire containing approximately a monolayer of graphitic carbon. At 675 K or above, for the entire range of pressures studied, the order of the dehydration reaction is unity with respect to acetic acid pressure. In this regime, the apparent activation energy is 1 ± 1 kcal/mol, and the extrapolated reaction probability at $1/T = 0$ is $(2.5-10) \times 10^{-4}$. Under these conditions, the rate of dehydration is determined by a competition between the rates of desorption and surface reaction of molecularly adsorbed acetic acid. For temperatures below 540 K and pressures of 3.5×10^{-4} Torr and above, the reaction rate is independent of acetic acid pressure, and the apparent activation energy is 27 ± 2 kcal/mol. Under these conditions, the rate of decomposition of a surface intermediate controls the rate of reaction. A mechanistic model is developed and discussed which describes accurately both the temperature and the pressure dependence of the rate of dehydration.

I. Introduction

It is well-known that carbon overlayers on transition-metal surfaces can affect both the reactivity and the selectivity of many heterogeneously catalyzed surface reactions.[1-11] These effects may have several origins. For example, carbon adatoms may physically occupy specific surface sites that are necessary for a particular reaction to occur, and they may chemically modify unoccupied sites by altering the electronic structure of the surface.[12-14] Both of these phenomena can change the reactivity and/or the selectivity of a heterogeneous catalyst. The effect of adsorbed carbon on both the reactivity and the selectivity of a catalytic reaction may be illustrated by considering the decomposition of formic acid on the Ni(110) surface.[6] Since formic acid decomposition may produce either CO or CO_2, the relative rates of these competing reactions provide a measure of selectivity. On the clean Ni (110) surface, the CO_2 to CO product ratio observed upon heating a saturation coverage of formic acid at 315 K is 1:1. On a carbided Ni(110) surface, formed by the dissociative adsorption of ethylene at 600 K, the product ratio is 10 ± 5:1, whereas the total quantity of formic acid which decomposed is unchanged compared to the clean surface. However, a shift in the temperature corresponding to the maximum rate of CO_2 production from 390 to 440 K indicates that the activation energy for CO_2 production is greater on the carbon-covered surface compared to the clean surface. Upon exposing the Ni(110) surface to ethylene at 800 K, a graphitic overlayer was formed. Decomposition of formic acid on this surface produced only 0.1 as much as on the clean and carbided surfaces, and the product ratio was near unity.

Recently, the decomposition of acetic acid over a polycrystalline platinum wire was studied in our laboratory at a pressure of 7×10^{-4} Torr and at temperatures between 300 and 900 K.[11] Two disparate kinetic regimes were observed. On the initially clean platinum surface, acetic acid decomposed to yield CO, CO_2, H_2, and adsorbed carbon. No water was observed during this transient production of CO, CO_2, and H_2. The adsorbed carbon ultimately poisoned the reaction channels producing CO, CO_2, and H_2, while simultaneously initiating the steady-state, catalytic dehydration of acetic acid to ketene and water. Similar to the results described above for formic acid decomposition on nickel, both the reaction rate and the CO_2 to CO product ratio were found to be dependent on the carbon adatom concentration in the first regime. Since graphitic overlayers on platinum surfaces are formed readily from carbon adatoms at temperatures above 750 K,[15-17] the carbon-covered surface which dehydrates acetic acid and which is formed at 900 K is graphitic.[11] Moreover, the carbon adatom concentration, determined from oxygen titration measurements, corresponds to approximately one monolayer of the basal plane of graphite.

In the work described here, we shall focus on the steady-state dehydration of acetic acid to ketene and water which occurs only on the graphitized platinum surface. Absolute reaction rates have been measured for reactant pressures between 8×10^{-7} and 7×10^{-4} Torr and at temperatures between 500 and 800 K. The steady-state reactivities of acetic anhydride, acetone, methyl acetate, and isopropyl alcohol on the graphitized surface also have been investigated briefly. On the basis of these results, together with those of thermal desorption measurements, a consistent mechanism of the acetic acid dehydration reaction is developed. For completeness, the decomposition of acetic acid on the clean platinum surface is described briefly, whereas a detailed discussion of both this reaction and the nature of the carbon overlayer is presented elsewhere.[11]

The organization of this paper is as follows. In section II the experimental details are described, and the experimental data are presented in section III. The reaction mechanism is developed and discussed in section IV. Finally, the major results of this work are summarized in section V.

II. Experimental Procedures

The experiments were performed over a range of pressures from 8×10^{-7} to 7×10^{-4} Torr in a steady-state flow microreactor that has been described previously.[18,19] The catalyst was a 20-cm

---

(1) Ollis, D. F.; Boudart, M. *Surf. Sci.* **1970**, *23*, 320.
(2) Worley, S. D.; Yates, Jr., J. T. *J. Catal.* **1977**, *48*, 385.
(3) Ko, E. I.; Benziger, J. B.; Madix, R. J. *J. Catal.* **1980**, *62*, 264.
(4) Barteau, M. A.; Madix, R. J. *J. Catal.* **1980**, *62*, 329.
(5) Davis, S. M.; Zaera, F.; Somorjai, G. A. *J. Catal.* **1982**, *77*, 439.
(6) McCarty, J. G.; Madix, R. J. *J. Catal.* **1975**, *38*, 402.
(7) McCarty, J. G.; Madix, R. J. *J. Catal.* **1976**, *54*, 210.
(8) Wittrig, T. S.; Szuromi, P. D.; Weinberg, W. H. *J. Chem. Phys.* **1982**, *76*, 3305.
(9) Szuromi, P. D.; Engstrom, J. R.; Weinberg, W. H. *J. Chem. Phys.* **1984**, *80*, 508.
(10) Szuromi, P. D.; Engstrom, J. R.; Weinberg, W. H. *J. Chem. Phys.* **1984**, *89*, 2497.
(11) Vajo, J. J.; Sun, Y.-K.; Weinberg, W. H., in preparation.
(12) Kiskinova, M.; Goodman, D. W. *Surf. Sci.* **1981**, *108*, 64.
(13) Lang, N. D.; Holloway, S.; Norskov, J. K. *Surf. Sci.* **1985**, *150*, 24.
(14) Feibelman, P. J.; Hamann, D. R. *Phys. Rev. Lett.* **1984**, *52*, 61.
(15) Netzer, F. P.; Willie, R. A. *J. Catal.* **1978**, *51*, 18.
(16) Smith, D. L.; Merrill, R. P. *J. Chem. Phys.* **1970**, *52*, 5861
(17) Abon, M.; Billy, J.; Bertulini, J. C.; Tardy, B. *Surf. Sci.* **1986**, *167*, 1.
(18) Vajo, J. J.; Tsai, W.; Weinberg, W. H. *Rev. Sci. Instrum.* **1985**, *56*, 1439.
(19) Vajo, J. J.; Tsai, W.; Weinberg, W. H. *J. Phys. Chem.* **1985**, *89*, 3243

0022-3654/87/2091-1153$01.50/0

length of 0.0125-cm-diameter high-purity (99.99%) polycrystalline platinum wire. All reagents were either reagent or research grade and were purified further by freeze–thaw–pump cycles in liquid nitrogen. Isotopically labeled ethylene, $^{13}C_2H_4$ (98 atom % ^{13}C from MSD Isotopes), was used without further purification.

The reaction products, which were sampled via a capillary tube from the main chamber of the reactor, were monitored continuously by a microcomputer-interface EAI 1200 quadrupole mass spectrometer, located in a high-vacuum chamber of the reactor of which the base pressure is below 10^{-8} Torr. Absolute reaction rates for the steady-state dehydration of acetic acid were determined by monitoring the change in the parent ion signal at 60 amu and using the appropriate continuous stirred tank reactor (CSTR) formalism.[18,19] The reactor was well characterized as a CSTR by a series of step-response experiments.[18] Average conversions were below 5% except for temperatures above 600 K at 7×10^{-4} Torr, where average conversions were ≤20%. However, separate measurements in which the average conversions were below 8% for all conditions gave identical results.[20]

For thermal desorption measurements, the bellows valve separating the main reaction chamber from the high-vacuum section was opened, and the sample was translated into the high-vacuum section (see Figure 2 of ref 18). Heating was accomplished with a constant-current power supply which produced a nearly linear temperature ramp of 20 K/s over the temperature range 350–650 K. Temperatures were measured with a W–5% Re/W–26% Re thermocouple which was spot-welded near the center of the platinum wire.

Two different platinum wires were used in this study. Initially, each one was heated in 0.1 Torr of oxygen (99.99%) at 1000 K for 3 h and then reduced in 0.1 Torr of hydrogen (99.995%) under the same conditions. Approximately ten cycles of this procedure led to reproducible, steady-state rates of acetic acid dehydration. A single oxidation–reduction cycle at 10^{-3} Torr and 1000 K for 30 min was conducted prior to each experiment to remove carbon that had been deposited during previous acetic acid decomposition. This treatment was found to produce a clean platinum surface, as judged by the reproducible rates of the acetic acid decomposition reactions which occur on the initially clean surface[11] and the steady-state rates of dehydration of acetic acid after formation of the graphitic overlayer. After the initial cleaning treatment at 0.1 Torr, longer oxidation–reduction cycles at 10^{-3} Torr did not change the measured rates.

III. Experimental Results

1. Acetic Acid Decomposition. Relative rates of production of CO, CO_2, H_2, H_2O, and CH_2CO (ketene), uncorrected for mass spectrometric sensitivities and pumping speeds, from an initially clean platinum surface are shown in Figure 1 as a function of time during a constant flow (average residence time of 3.6 s) of acetic acid at a pressure of 7×10^{-4} Torr and a surface temperature of 900 K. It is apparent that the rates of production of CO, CO_2, and H_2 pass through a maximum and decline nearly to their respective background values. Coincident with the decrease in the CO, CO_2, and H_2 signals, the rates of formation of both ketene and water rise to steady-state values.[21] These steady-state rates have been observed for more than 2 h, corresponding to well over 100 catalytic "turnovers" per surface site, without significant change. Under these steady-state conditions, no reaction products were detected other than ketene and water. The minimum in the ketene signal, which coincides with the maximum for CO, CO_2, and H_2 in Figure 1, is a consequence of the fact that mass 42 is also a fragmentation product of acetic acid. The minimum, therefore, is associated with the decomposition of acetic acid to CO, CO_2, and H_2, and it is unrelated to ketene.

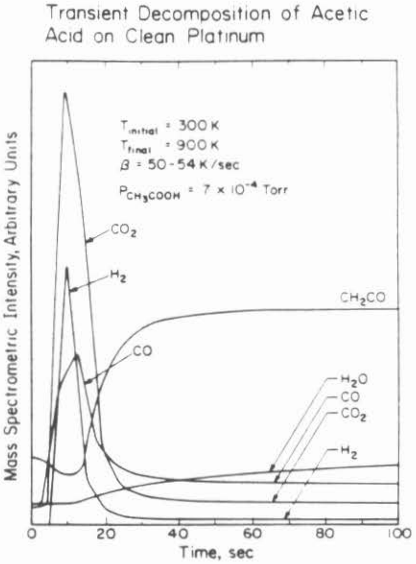

Figure 1. Time evolution curves for the production of CO, CO_2, H_2, H_2O, and CH_2CO (42 amu) during the constant exposure of an initially clean platinum surface to acetic acid at 7×10^{-4} Torr. At $t = 0$, the surface temperature was increased at a rate of 50–54 K/s from 300 to 900 K and thereafter held constant at 900 K. The data are uncorrected for fragmentation, mass spectrometric sensitivities, and pumping speeds.

The relatively slow rise in the water signal, compared with the ketene signal, is due to adsorption of water on the walls of the vacuum system. This has been confirmed by independent step-response experiments. After correction for mass spectrometric sensitivities and pumping speeds, the mass 42 and mass 18 steady-state signals shown in Figure 1 correspond to a 1:1 molar ratio of ketene to water.

After exposure to acetic acid, the platinum surface contains a substantial concentration of carbon adatoms, as judged from oxygen titration experiments in which predominantly CO_2 is formed.[11] The concentration of surface carbon atoms following a 90-s exposure to acetic acid at 7×10^{-4} Torr and a temperature of 900 K was $(2.6\text{–}3.5) \times 10^{15}$ cm^{-2}. Exposure of the platinum surface to acetic acid at 1000 K for 5 min did not alter the carbon adatom concentration. Although the surface that results from exposure to acetic acid at temperatures below 900 K was not examined extensively, it appears that for surface temperatures above 700 K an identical surface may be prepared with a sufficiently long exposure (annealing) time. The carbon adatom concentration produced from exposure to acetic acid at 0.1 Torr for 90 s at 900 K was 5.9×10^{15} cm^{-2}. Other pressures were not investigated in detail. A similar concentration of carbon, 2.4×10^{15} cm^{-2}, was produced from a 90-s exposure of the surface at 900 K to 7×10^{-4} Torr of ethylene. For comparison, the surface atom densities of Pt(111) and of the basal plane of graphite are 1.5×10^{15} cm^{-2} and 3.8×10^{15} cm^{-2}, respectively.[22]

To summarize, on an initially clean platinum surface, acetic acid decomposes to CO, CO_2, and H_2 and produces a graphitic overlayer. The surface becomes poisoned to these decomposition reactions, and subsequently, on the graphitic surface, acetic acid dehydrates catalytically to ketene and water.

2. Steady-State Dehydration Kinetics. Absolute steady-state reaction rates for the dehydration of acetic acid to ketene and water over the graphitized platinum surface are shown in Figure

---

[20] For these experiments, the conversion was lowered by placing an additional pump on the outlet of the reactor, thereby decreasing the residence time of the acetic acid.

[21] The existence of ketene was confirmed by monitoring the parent ion signal at 42 amu and the fragmentation products at 41, 28, and 14 amu. Water was monitored at 18 amu. For the fragmentation intensities of ketene, see: Cornu, A.; Masut, R. *Compilation of Mass Spectral Data*, 2nd ed.; Heydon and Son: New York, 1975; Vol. 1.

[22] These values result from assuming a hexagonally close-packed surface and an atom–atom distance of 2.746 and 1.42 Å for platinum and graphite, respectively.

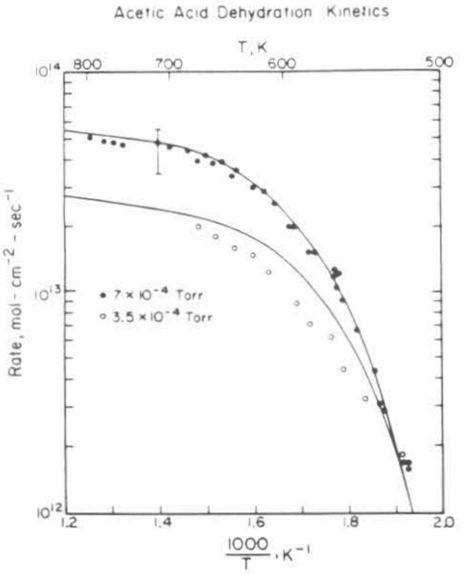

Figure 2. Arrhenius plots of the rate of dehydration of acetic acid at 7 × 10^{-4} and 3.5 × 10^{-4} Torr. For each pressure, a graphitic overlayer was first prepared by exposing a clean platinum surface to 7 × 10^{-4} Torr of acetic acid at 900 K for 90 s. The error bar at $10^3/T = 1.4$ indicates the variation in the rate observed by repeatedly removing and depositing the graphitic overlayer. The lines are the results of model calculations which are described in the text.

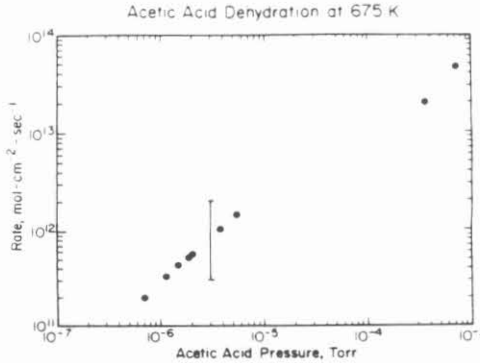

Figure 3. Absolute reaction rates for the dehydration of acetic acid at 675 K as a function of acetic acid pressure. The error bar at 3 × 10^{-6} Torr indicates the systematic error in calibration of the rates for all pressures below 10^{-5} Torr.

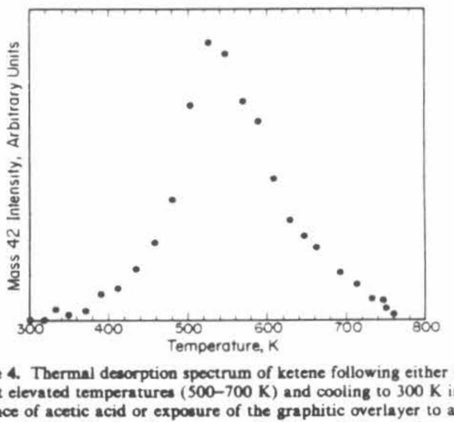

Figure 4. Thermal desorption spectrum of ketene following either reaction at elevated temperatures (500–700 K) and cooling to 300 K in the presence of acetic acid or exposure of the graphitic overlayer to acetic acid at 300 K. The heating rate was 20 K/s, and the maximum desorption rate occurs at 520 K.

2 as a function of reciprocal temperature for pressures of 7 × 10^{-4} and 3.5 × 10^{-4} Torr. The kinetics displayed in Figure 2 are essentially identical for all the methods that were used to prepare the graphitic overlayer, including graphite formation from ethylene (cf. section III.1). In addition, annealing the graphitized surface under vacuum at 1000 K did not change the observed kinetics. For the data presented explicitly here, however, each of the graphitic overlayers was prepared by exposing the initially clean platinum surface to 7 × 10^{-4} Torr of acetic acid for 90 s at 900 K. At low temperatures (≲540 K), the steady-state reaction rate is independent of acetic acid pressure. Under these conditions, the apparent activation energy is 27 ± 2 kcal/mol, with an extrapolated intercept at $1/T = 0$ of (0.2–1.6) × 10^{24} molecules/(cm^2 s). At higher temperatures (≳675 K), the reaction rate scales linearly with the acetic acid pressure, and the activation energy decreases to 1 ± 1 kcal/mol. In this regime, the extrapolated intercept at high temperatures is (0.7–2.8) × 10^{17} molecules/(cm^2 s Torr). This corresponds to a reaction probability per surface collision of acetic acid of (2.5–10) × 10^{-4}. The error bar at $10^3/T = 1.4$ in Figure 2 indicates the variation in the measured rate after repeatedly cleaning the surface and redepositing the graphitic overlayer. The dehydration of perdeuterioacetic acid showed no detectable isotope effect under any conditions, although the uncertainty in the measured activation energy would have obscured any change in the activation energy that is less than 1–2 kcal/mol. Thus, a primary isotope effect involving cleavage of a C–H bond with a vibrational frequency of 3000 cm^{-1} would not be observed, since the expected increase in the activation energy is only 1.1 kcal/mol for C–D bond cleavage.

At the lowest temperatures studied (≲540 K), the steady-state CO signal, which is a fragmentation product of ketene, increased relative to the ketene mass spectrometric intensity. Since the mass spectrometric intensities at these low temperatures are approaching our detection limit, it was not possible to quantify this behavior. However, this may represent another steady-state decomposition mechanism which competes with dehydration to ketene at low temperatures where the overall rate of decomposition is very small (e.g., the reaction probability at 540 K and 7 × 10^{-4} Torr is approximately 10^{-5}).

Figure 3 shows the steady-state rate of dehydration of acetic acid as a function of pressure from 8 × 10^{-7} to 7 × 10^{-4} Torr at 675 K. The reaction order with respect to acetic acid pressure, measured from the data that were recorded below 10^{-5} Torr, is 0.95 ± 0.05. While the *relative* rates determined at these low pressures are quite accurate, the calibration that is necessary to calculate absolute rates is difficult at low pressures. The error bar at 3 × 10^{-6} Torr indicates the absolute error present in all the data at pressures below 10^{-5} Torr. Considering this rather large absolute error and the much smaller uncertainties for measurements at higher pressures, a first-order dependence of the rate on pressure is suggested at 675 K over the entire range of pressures studied, i.e., for pressures below 10^{-3} Torr.

Steady-state dehydration of acetic acid was also conducted on a graphitic surface composed of ^{13}C to ascertain the stability of the graphitic overlayer. The ^{13}C-labeled surface was prepared by exposing the clean platinum surface to 7 × 10^{-4} Torr of $^{13}C_2H_4$ for 90 s at 900 K. Comparison of the ^{13}C surface concentration, determined by oxygen titration, following dehydration of acetic acid at 7 × 10^{-4} Torr and 675 K for 20 min with the ^{13}C surface concentration measured without reaction revealed that the ^{13}C atoms remain on the surface during the dehydration of acetic acid. Hence, the dehydration of acetic acid over graphitized platinum is a "catalytic" reaction in the strictest sense; i.e., no component of the "catalyst" is incorporated into the reaction product.

3. Thermal Desorption Measurements. A thermal desorption spectrum of ketene following exposure of the graphitized platinum surface to 7×10^{-4} Torr of acetic acid for 240 s at 300 K is shown in Figure 4. A single peak occurs at a temperature of 520 K. The desorption spectrum is independent of the delay time associated with transferring the sample from the reaction chamber to the high-vacuum chamber. Moreover, the desorption spectrum is independent of exposure time (>4 min) and surface temperature (between 300 and 700 K), provided the surface is cooled to 300 K before the acetic acid is evacuated. Exposures at pressures below 7×10^{-4} Torr were not investigated. An approximate calibration using the mass spectrometric sensitivity and the pumping speed for CO_2 indicates the desorption of $(0.1-5) \times 10^{13}$ molecules/cm^2 of ketene. Although the desorption of neither acetic acid nor H_2O was observed, these species would not be detected for surface concentrations below approximately 5×10^{13} cm^{-2} due to the adsorption of acetic acid and H_2O on the system walls.

Carbon monoxide was also observed to desorb from the graphitized platinum surface following exposure to acetic acid. The peak temperature was approximately 540 K and showed the same independence of surface temperature and delay time in transfer as ketene. The amount of CO that desorbed corresponded to approximately half the amount of ketene that desorbed and (as verified by independent measurements) was not due to adsorption from the background. This desorption of CO may be related to the increase in the mass 28:mass 42 ratio observed at low temperatures during the steady-state reaction (cf. section III.2). Due to the lack of quantitative steady-state data concerning this reaction pathway, however, the origin of the CO was not investigated further.

4. Steady-State Reaction of Related Compounds. To gain further insight into the mechanism of the steady-state dehydration of acetic acid, the reactions of four functionally related model compounds, namely, acetic anhydride, isopropyl alcohol, acetone, and methyl acetate, were investigated briefly. In each case, the graphitic overlayer was prepared in a manner identical with that used for the steady-state measurements of acetic acid dehydration, i.e., an exposure of 7×10^{-4} Torr f acetic acid for 90 s at 900 K. The rates of decomposition of each compound were measured at a pressure of 7×10^{-4} Torr. Acetic anhydride decomposed predominantly to ketene and acetic acid, with an activation energy of 12–15 kcal/mol which was constant over the temperature range 420–650 K. A minor amount of water, <1% of the acetic acid signal, was observed above 535 K. Isopropyl alcohol dehydrated to propylene and water, with an activation energy decreasing from approximately 16 kcal/mol at temperatures between 450 and 500 K to approximately 3 kcal/mol at 625 K. Qualitatively, the observed steady-state kinetics for the dehydration of isopropyl alcohol are similar to those for acetic acid dehydration. Acetone and methyl acetate showed no reaction at any temperature studied ($\leq$700 K).

IV. Discussion

1. Reaction Kinetics and Adsorbed Intermediates. For temperatures below approximately 570 K and pressures between 10^{-3} and 10^{-4} Torr, the steady-state rate of dehydration of acetic acid to ketene on graphitized platinum exhibits a linear Arrhenius behavior and a diminishing dependence on acetic acid pressure as the temperature decreases (cf. Figure 2). These observations suggest that under these conditions the catalytic surface is nearly saturated with either acetic acid, a reaction intermediate, or a reaction product. Since the heat of adsorption of acetic acid, water, and ketene on graphitized platinum is expected to be $\leq$5 kcal/mol,[23] a mechanism in which the surface is saturated with an intermediate in the dehydration reaction species is implicated. For example, the intramolecular elimination of water from molecularly adsorbed acetic acid is not a viable mechanism of dehydration, since *molecular* acetic acid would be adsorbed reversibly at 300 K. Moreover, the thermal desorption of ketene at 520 K following both exposure of the surface to acetic acid at 300 K and the reaction of acetic acid at elevated temperatures is identical, provided the surface is cooled in the presence of acetic acid. This result implies that the adsorbed intermediate in the reaction is stable and readily formed at 300 K.

Information concerning the reaction intermediate is provided by the observed reactivities of methyl acetate, acetone, and isopropyl alcohol. On the basis of both these results and those pertaining to acetic acid, we suggest that the physically most reasonable intermediate which leads to ketene from acetic acid dehydration is a monodentate acetate, designated η^1-$CH_3COO(a)$, formed by the dissociation of the oxygen–hydrogen bond of acetic acid. As discussed below, this intermediate is consistent with the observed reactivity (or lack thereof) of methyl acetate, acetone, and isopropyl alcohol, as well as that of acetic acid on the graphitized platinum surface. The observed lack of reactivity of methyl acetate in which the hydroxyl hydrogen of acetic acid is replaced with a methyl group indicates the importance of the acidic hydrogen. Since the oxygen–carbon bond is substantially more difficult to cleave than the oxygen–hydrogen bond, dissociation of the acidic hydrogen is implicated in the formation of the surface intermediate. Note that since the heats of reaction for both the dehydration of acetic acid and the elimination of methanol from methyl acetate are approximately 34 kcal/mol,[24] arguments based solely on thermochemistry cannot account for the observed differences in reactivity. Similarly, acetone, in which the hydroxyl group is replaced with a methyl group, is unreactive.

The relative importance of the acidic hydrogen is also illustrated by the dehydration of isopropyl alcohol, which exhibits kinetics that are qualitatively similar to those of acetic acid. Although much less acidic than that of acetic acid, the hydroxyl hydrogen or 2-propanol can dissociate, forming an alkoxy intermediate. This alkoxy intermediates that is formed by cleavage of the oxygen–hydrogen bond of 2-propanol is analogous to the monodentate acetate intermediate that is formed from cleavage of the acidic hydrogen from acetic acid. Since the intermediates are analogous similar kinetics may be expected. In addition, the measured apparent activation energies at low temperatures of 27 and 16 kcal/mol for the dehydration of acetic acid and 2-propanol vary consistently with the C–OH bond energies of 107 and 92 kcal/mol for acetic acid and isopropyl alcohol, respectively.[25] Assuming the same relative C–O bond energies in the adsorbed intermediates, the observed activation energies indicate that the cleavage of the C–O bond can be important in controlling the rate of decomposition of the surface intermediate.

In contrast to the kinetics observed at low temperatures ($\leq$570 K), at high temperatures ($\geq$675 K) the rate of dehydration of acetic acid is first-order in acetic acid pressure, and the reaction probability approaches $(2.5-10) \times 10^{-4}$. This low reaction probability indicates that the vast majority of acetic acid molecules which adsorb (weakly) on the surface subsequently desorb without reacting. Hence, the steady-state surface coverage of acetic acid is essentially equal to the equilibrium value in the absence of any decomposition. A low reaction probability of acetic acid is also consistent with our measurements of the decomposition of acetic anhydride. Although acetic anhydride decomposes readily to ketene and acetic acid, only a small fraction (<1%) of the acetic acid that is formed on the surface reacts further via dehydration.

2. Mechanistic Modeling. The steady-state reaction kinetics and the thermal desorption measurements, taken together, imply that the dehydration of acetic acid proceeds via an irreversibly adsorbed intermediate. Although the mechanistic model described below postulates that this adsorbed intermediate is a monodentate acetate, *the numerical results are insensitive to the structure of the intermediate provided it is readily formed at 300 K and stable*

---

[23] Kouznetzov, A. V.; Shcherbakova, K. D. *J. Chromatogr.* **1970**, *49*, 21.

[24] This result is based on the following values for the various heats of formation: ΔH_f(acetic acid) = −106.7, ΔH_f(methyl acetate) = −98, ΔH_f(ketene) = −14.6, ΔH_f(water) = −57.8, and ΔH_f(methyl alcohol) = −48.1. All quantities are in kcal/mol for the gas phase at 298 K.

[25] *Handbook of Chemistry and Physics*, 51st ed.; Weast, R. C., Ed.; Chemical Rubber Co.: Cleveland, OH, 1970; p F-166.

TABLE I: Model Parameters for the Dehydration of Acetic Acid on a Graphitized Platinum Surface

S^0	1	E_3	0 kcal/mol[a]
$k_2^{(0)}$	1×10^{10} s^{-1}	$E_1 - E_d$	2 kcal/mol
E_2	27.5 kcal/mol	$k_1^{(0)}/k_d^{(0)}$	10^{-3}
$k_3^{(0)}$	7×10^{-10} cm^2/s[a]	n_s	10^{14} cm^{-2}[b]

[a] Reference 27. [b] Reference 26.

upon heating to approximately 520 K.

Assuming a monodentate acetate intermediate, the dehydration of acetic acid may be written mechanistically as follows

$$CH_3COOH(g) \underset{k_d}{\overset{S(\theta)F}{\rightleftharpoons}} CH_3COOH(a) \tag{1}$$

$$CH_3COOH(a) \xrightarrow{k_1} \eta^1\text{-}CH_3COO(a) + H(a) \tag{2}$$

$$\eta^1\text{-}CH_3COO(a) \xrightarrow{k_2} CH_2CO(g) + OH(a) \tag{3}$$

$$OH(a) + H(a) \xrightarrow{k_3} H_2O(g) \tag{4}$$

where $S(\theta)$ represents the functional dependence of the probability of adsorption of acetic acid on the fractional coverage of each surface species; F is the molecular flux of acetic acid to the surface; and k_d, k_1, k_2, and k_3 are the reaction rate coefficients for the desorption of acetic acid and the three surface reactions. The probability of adsorption of acetic acid may be written as

$$S(\theta) = S^0(1 - \sum_i \theta_i) \tag{5}$$

where S^0 is the probability of adsorption on the graphitized platinum surface in the limit of zero adsorbate coverage, θ_i is the fractional surface coverage of species i, and the sum is over all surface species. Each of the reaction rate coefficients may be written as $k_i = k_i^{(0)} \exp(-E_i/k_BT)$ with (assumed) coverage-independent preexponential factors $k_i^{(0)}$ and activation energies E_i. To calculate the steady-state rate of acetic acid dehydration via this mechanism, the steady-state material balance equations for each surface species were solved. Since only three of the mass balance equations are linearly independent, the additional assumption that $\theta_{\eta^1\text{-}CH_3COO}$ is equal to θ_H was invoked. As discussed below, the rate of reaction 4 is rapid compared to that of reaction 3, validating this assumption. The probability of molecular adsorption of acetic acid on the clean graphitic surface S^0 was taken to be unity, and the surface site density n_s, which is necessary to calculate absolute rates, was taken to be 10^{14} cm^{-2}.[26] For the recominative desorption of water, reaction 4, the preexponential factor and the activation energy have been determined from a molecular beam investigation of the $H_2O + D_2O$ exchange reaction on pyrolytic graphite.[27,28] Thus, the model described by the elementary reactions 1–4 contains four parameters, namely $k_2^{(0)}$ and E_2 and the composite quantities $E_1 - E_d$ and $k_1^{(0)}/k_d^{(0)}$. These parameters were adjusted until the best description of the experimental data was obtained. The values for each of the variables used in the model calculations are given in Table I, and the model results for the dehydration of acetic acid at 7×10^{-4} and 3.5×10^{-4} Torr are compared with the experimental data in Figure 2. Obviously, the model accurately describes both the temperature and the pressure dependence of the reaction rate.

Although the model contains four adjustable parameters, a consideration of the analytic form of the reaction rate in the limits of high and low temperature illustrates that the values of these "adjustable" parameters are actually quite severely constrained by the data. In the limit of high temperature, where the coverage of all surface species approaches zero, the reaction rate becomes

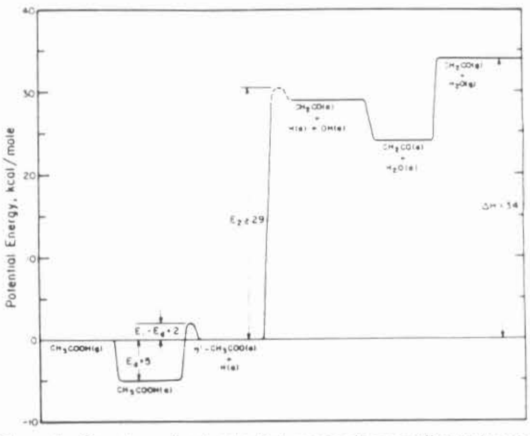

Figure 5. One-dimensional potential energy diagram illustrating the catalytic dehydration of acetic acid to ketene over a graphitized platinum surface. The energy levels have been calculated by choosing acetic acid in the gas phase as the reference level and using the bond energies listed in Table II.

$$R = \frac{S^0 F k_1^{(0)}}{k_d^{(0)}} \exp[-(E_1 - E_d)/k_BT] \tag{6}$$

Thus, the activation energy observed at high temperature, 1 ± 1 kcal/mol, is equal to $E_1 - E_d$, and the reaction probability at $1/T = 0$ is $S^0k_1^{(0)}/k_d^{(0)}$. At low temperature, the surface becomes saturated with the reaction intermediates η^1-$CH_3COO(a)$ and $H(a)$. Since for all the reaction conditions studied the fractional surface coverages of molecular acetic acid, ketene, and water are negligible, $\theta_{\eta^1\text{-}CH_3COO} = \theta_H = 0.5$, and the reaction rate at low temperature may be written as

$$R = 0.5 n_s k_2^{(0)} \exp(-E_2/k_BT) \tag{7}$$

The observed activation energy, 27 ± 2 kcal/mol, is therefore equal to E_2, and the extrapolated intercept at $1/T = 0$, $(0.2\text{–}1.6) \times 10^{24}$ molecules/(cm^2 s), is equal to $0.5 n_s k_2^{(0)}$.

An analysis of the thermal desorption measurements provides *independent* determinations of $k_2^{(0)}$ and E_2. Calibration of the ketene thermal desorption spectrum indicates the desorption of $(0.1\text{–}5) \times 10^{13}$ molecules/cm^2, $0.5n_s$, of ketene. Using this range of values together with the measured result $n_s k_2^{(0)} = (0.4\text{–}3.2) \times 10^{24}$ molecules/(cm^2 s) yields $k_2^{(0)} = (0.04\text{–}16) \times 10^{11}$ s^{-1}. Since we are postulating that ketene originates from the unimolecular decomposition of an adsorbed intermediate, a first-order Redhead analysis[29] applied to the thermal desorption spectrum of ketene using $T_p = 520$ K and $k_2^{(0)} = (0.04\text{–}16) \times 10^{11}$ s^{-1} is appropriate. This gives $E_2 = 23\text{–}29$ kcal/mol, which agrees well with the value of E_2 determined independently from the steady-state kinetics.

In order for the mechanism embodied by reactions 1–4 to describe the experimental data correctly, the rate coefficient for the recombinative desorption of molecular hydrogen must be small compared to that for the production of water. The desorption of molecular hydrogen following both the adsorption of atomic hydrogen and the dissociative adsorption of water has been studied on pyrolytic graphite.[27,28] These results indicate that hydrogen is produced from dissociatively adsorbed water only at temperatures above 2000 K, and even under these conditions, the rate of production of water is an order of magnitude larger than that of hydrogen desorption.[27] An analysis of our model indicates that $k_3 n_s^2 >> k_2 n_s$ for all conditions studied; e.g., a "worst" case occurs

---

(26) Based on the excluded area of an acetic acid molecule, the saturation surface density is approximately 10^{14} cm^{-2}.

(27) Olander, D. R.; Acharya, T. R.; Ullman, A. Z. *J. Chem. Phys.* **1977**, *67*, 3549.

(28) Balooch, M.; Olander, D. R. *J. Chem. Phys.* **1975**, *63*, 4772.

(29) Redhead, P. A. *Vacuum* **1962**, *12*, 203.

(30) McMillen, D. F.; Golden, D. M. *Annu. Rev. Phys. Chem.* **1982**, *33*, 493.

TABLE II: Bond Energies for the Dehydration of Acetic Acid on a Graphitized Platinum Surface

bond	bond energy, kcal/mol	note
$CH_3COO–H$	107	*a*
$CH_3CO–OH$	107	*b*
$CH_3COOH–S$	5	*c*, *d*
$CH_2CO–S$	5	*d*
$H_2O–S$	5	*d*
H–S	61	*e*
HO–S	58	*f*
η^1-$CH_3COO–S$	52	*g*
η^1-$CH_3CO–O(a)$	101	*g*

[a] See ref 30. [b] See ref 25. [c] "S" denotes bonding to the graphitized platinum surface. [d] The adsorbate–surface bond energy for each physically adsorbed species is *estimated* to be 5 kcal/mol. [e] The activation energy for the recombinative desorption of hydrogen from the basal plane of graphite is 18 kcal/mol,[28] which implies a bond energy of 61 kcal/mol. [f] The activation energy for the recombinative desorption of water from the basal plane of graphite is 0 kcal/mol.[27] Given an H–S bond energy of 61 kcal/mol, this implies an HO–S bond energy of 58 kcal/mol. [g] Typically, substitution of the hydrogen in an alcohol or a carboxylic acid with an alkyl group reduces the C–O bond energy by 10 kcal/mol, from approximately 90 to 80 kcal/mol.[25] Given the reduced HO–S (carbon) bond energy of 58 kcal/mol, linear scaling implies that the reduction here is approximately 6 kcal/mol.

at 800 K for which $k_3 n_s^2 > 100 k_2 n_s$. Consequently, the steady-state coverages of η^1-$CH_3COO(a)$ and H(a) are equal, since water is produced rapidly after the decomposition of η^1-$CH_3COO(a)$ into ketene and OH(a).

3. Potential Energy Diagram for Acetic Acid Dehydration. A mechanistic model was developed in section IV.2 which describes the observed kinetics for the dehydration of acetic acid to ketene over a graphitized platinum surface. The energetics of this reaction implied by this model are shown in Figure 5 in the form of a potential energy diagram along the "reaction coordinate". The reference energy level of acetic acid in the gas phase is defined to be zero.

To evaluate the energy levels for each of the other points along the reaction coordinate, the bond energies tabulated in Table II were utilized. Note that the predicted energy levels are consistent with the known endothermicity of the overall reaction, namely, 34 kcal/mol.[24] In addition, for temperatures above 675 K, the observed activation energy is 1 ± 1 kcal/mol, which is consistent with the potential energy level for η^1-$CH_3COO(a) + H(a)$. The measured value for E_2 is 27 ± 2 kcal/mol, which is in good agreement with the predicted value of $E_2 \gtrsim 29$ kcal/mol.

Although carbon–hydrogen bond energies in hydrocarbons are typically 100 kcal/mol, following Balooch and Olander,[28] a hydrogen–surface bond energy of 61 kcal/mol was used to construct the potential energy diagram shown in Figure 5. However, identical energy levels would be calculated by assuming that the hydrogen–surface bond energy is 100 kcal/mol with a concurrent reduction of approximately 80 kcal/mol in the carbon–carbon bond energy of the graphite overlayer for each dissociatively adsorbed acetic acid molecule. In this case, the HO–surface and η^1-CH_3COO-surface bond energies would become approximately 90 and 80 kcal/mol, respectively. This alternate formulation is equally consistent with the measured activation energies for both the desorption of hydrogen and the recombinative desorption of water from the basal plane of graphite.[27,28]

V. Synopsis

The results of this study may be summarized as follows:

1. On a polycrystalline platinum surface containing approximately a monolayer of graphitic carbon, the catalytic dehydration of acetic acid to ketene and water proceeds at steady state.

2. For reactant pressures above 3.5×10^{-4} Torr and temperatures below 540 K, the reaction rate is independent of acetic acid pressure, and the apparent activation energy is 27 ± 2 kcal/mol. Under these conditions the rate of decomposition of an irreversibly adsorbed intermediate controls the rate of reaction.

3. The reaction intermediate is formed from acetic acid on the graphitized platinum surface at 300 K and, upon heating, decomposes at 520 K with the accompanying desorption of ketene. Dissociation of the acidic hydrogen of acetic acid appears to be important in the formation of the intermediate.

4. For reactant pressures below 7×10^{-4} Torr and at temperatures above 675 K, the reaction rate is linearly dependent on acetic acid pressure, and the apparent activation energy is 1 ± 1 kcal/mol. In this regime, the reaction rate is determined by a competition between the rates of desorption and surface reaction of molecularly adsorbed acetic acid.

Acknowledgment. This work was supported by the National Science Foundation under Grant No. DMR-8500789

Registry No. Acetic acid, 64-19-7; carbon, 7440-44-0; platinum, 7440-06-4.

APPENDIX B

Acetic Acid Decomposition on a Polycrystalline Platinum Surface

[This Appendix consists of an article coauthored with J. J. Vajo and W. H. Weinberg, which appeared in *Applied Surface Science* **29**, 165 (1987).]

Applied Surface Science 29 (1987) 165–178
North-Holland, Amsterdam

ACETIC ACID DECOMPOSITION ON A POLYCRYSTALLINE PLATINUM SURFACE

J.J. VAJO, Y.-K. SUN and W.H. WEINBERG

Division of Chemistry and Chemical Engineering, California Institute of Technology, Pasadena, CA 91125, USA

Received 10 March 1987; accepted for publication 9 June 1987

The decomposition of $CH_3{}^{13}COOH$ on a polycrystalline platinum surface has been examined at temperatures between 300 and 900 K during continuous exposure to $CH_3{}^{13}COOH$ at 7×10^{-4} Torr. On an initially clean platinum surface ^{13}CO, CO, $^{13}CO_2$, H_2 and adsorbed carbon-12 are the major reaction products. The adsorbed carbon eventually poisons completely the reactions that produce these products. For temperatures above approximately 800 K, the carbon overlayer that is formed is graphitic and saturates at a carbon adatom concentration of $(2.6–3.5) \times 10^{15}$ cm^{-2}. The reaction quantities of ^{13}CO and $^{13}CO_2$ that are produced depend both on the surface temperature and the carbon coverage. Lower temperatures and higher carbon coverages favor the production of ^{13}CO. On the graphitized platinum surface, the catalytic dehydration of acetic acid to ketene and water proceeds at steady-state.

1. Introduction

Although the catalytic decomposition of formic acid on transition metal surfaces has been studied extensively using both conventional catalytic measurements [1–5] and surface science techniques [6–7], this is not the case for the decomposition of acetic acid [18–20]. Formic acid decomposition can produce CO, CO_2, H_2 and H_2O with no self-poisoning of the surface. This reaction is therefore of interest as a prototypical branching surface reaction and as a measure of catalytic selectivity [4]. The investigation of acetic acid decomposition offers the possibility of clarifying the kinetic and mechanistic changes which occur upon introducing a carbon–carbon bond into the carboxylic acid. In addition, the decomposition of acetic acid may produce adsorbed carbon atoms which can chemically modify the catalytic surface and the mechanism of decomposition.

The decomposition of both acetic acid and formic acid has been investigated on the Ni(111) [11,19] and Ni(110) [9,10,18] surfaces, and the results of these studies may be used to compare the reactivities of acetic acid and formic acid. On the Ni(111) surface, acetic acid and formic acid decompose via their respective carboxylate intermediates [11,19]. However, thermal desorption

0169-4332/87/$03.50

measurements indicate that the surface formate is less stable than the surface acetate, the latter of which was observed to decompose to CO_2 with the simultaneous production of H_2 at 460 K when employing a linear heating rate β of 7.1 K/s. For the surface formate, decomposition to CO_2 and H_2 occured at 404 K with $\beta = 20$ K/s. In each case, desorption of CO was observed near 450 K, which is typical of CO desorption following adsorption on a clean Ni(111) surface [11]. In addition to the differences in the stability of the adsorbed intermediates, the observed CO to CO_2 product ratios of 0.3 [11] and 1.6 [19] for formic acid and acetic acid decomposition on Ni(111) indicate considerably more CO production during the decomposition of acetic acid. The preponderance of CO during the decomposition of acetic acid might be due partly to oxidation of the methyl carbon. Similar results have been obtained on Ni(110).

While the decomposition of acetic acid on platinum has not been investigated in detail, a similar sequence of stabilities was observed for formate and acetate on Pt(111) using electron energy loss spectroscopy (EELS) [20]. Formic acid decomposition on Pt(111) has been studied, however, using thermal desorption mass spectrometry [14], modulated molecular beam scattering [17] and EELS [15,16]. In all cases it was found that formic acid decomposes almost completely to CO_2 and H_2 with only minor amounts of CO and H_2O produced. The product ratio for acetic acid decomposition on any platinum surface has not been determined. Electron energy loss measurements following adsorption of acetic acid on Pt(111) at 100 K and annealing to 380 K revealed the presence of adsorbed CO [20]. However, CO_2 and H_2 were observed with reaction-limited kinetics near 450 K. Assuming surface acetate is the common intermediate, these results indicate that the reaction producing CO proceeds at a lower temperature (with a lower activation energy) than the reaction producing CO_2.

Similar results have been obtained for the decomposition of formic acid on the Ru(001) surface [12,13]. Chemisorbed carbon monoxide has been detected via EELS following the adsorption of formic acid with annealing to 200 K. Carbon dioxide is produced between 310 and 340 K, depending on the initial surface coverage, with a heating rate of 10 K/s. These results clearly imply that the reaction producing CO is favorable compared with the reaction producing CO_2, for the initial decomposition of chemisorbed formate on the Ru(001) surface.

In the present study, the decomposition of acetic acid on a polycrystalline platinum surface has been examined at temperatures between 300 and 900 K during continuous exposure to acetic acid at 7×10^{-4} Torr. The effects of temperature and of adsorbed carbon on the decomposition mechanism are discussed. Briefly, two disparate kinetic regimes are observed for the decomposition of acetic acid. Initially, CO, CO_2, H_2 and adsorbed carbon are the major reaction products. However, the adsorbed carbon eventually poisons completely the reaction that produce these products. On this graphitized platinum surface, the dehydration of acetic acid to ketene (CH_2CO) and water is the only reaction observed. Here we will focus on the transient decomposition reaction on the (initially) clean surface, whereas the steady-state dehydration reaction on the graphitized surface is discussed separately [21].

2. Experimental procedures

The experiments were performed in a continuous flow microreactor that has been described previously [22,23]. The catalyst was a 20 cm length of 0.0125 cm diameter high-purity (99.99%) polycrystalline platinum wire. Acetic acid (reagent grade, 99.7%) and $CH_3{}^{13}COOH$ (99 at% ^{13}C, MSD isotopes) were purified further by several freeze–thaw–pump cycles. Prior to each experiment, the surface was cleaned in oxygen and hydrogen, as described elsewhere [21].

The reaction products, which were samples via a capillary tube from the main chamber of the reactor, were monitored continuously by a microcomputer-interfaced EAI 1200 quadrupole mass spectrometer located in a high vacuum section of the reactor of which the base pressure is below 10^{-8} Torr. The capillary is replaced by a metal tube (1/4 inch OD and 3/16 inch ID) for pressures in the micron regime. The time lag due to the flow of reaction products through this tube is negligible in the results presented here. The absolute quantities of CO, CO_2 and H_2 produced during acetic acid decomposition (and of CO_2 and CO produced during oxygen titration measurements) were determined by calibrating the mass spectrometer using feeds with known concentrations of CO, CO_2 and H_2 and using the appropriate continuous stirred tank reactor formation. Average conversions of acetic acid were below 10% for all conditions, studied, thus eliminating any significant contributions from secondary reactions.

For the thermal desorption measurements, the bellows valve separating the main chamber of the reactor from the high vacuum section was opened, and the sample was translated into the high vacuum section (see fig. 2 of ref. [22]). Heating was accomplished with a constant current power supply, which produced a nearly linear temperature ramp with a heating rate β of 20 K/s. For the decomposition experiments, the same power supply was used to provide temperature ramps with β between 2 and 54 K/s and final temperatures between 500 and 900 K. Temperatures were measured with a W–5%Re/W–26%Re thermocouple, which was spot-welded near the center of the wire.

3. Experimental results

3.1. Decomposition of acetic acid

Relative reaction rates for the production of CO, CO_2, H_2, CH_4, H_2O and ketene (uncorrected for mass spectrometric sensitivities) as shown in fig. 1 as a function of time during a continuous flow (average residence time of 3.6 s) of acetic acid at 7×10^{-4} Torr. At $t = 0$, the temperature of the platinum surface is increased from 300 to 900 K with a heating rate of 50–54 K/s. As illustrated in Fig. 1, the rates of production of CO, CO_2, H_2 and CH_4 pass through maxima and then decline to their background values. Coincident with the decrease in the rate of production of CO, CO_2, H_2 and CH_4, the production of water and ketene is observed which reaches a steady-state rate. When the platinum surface, treated as in fig. 1, is cooled to 300 K and then related to 900 K, only water and ketene are produced with the same steady-state

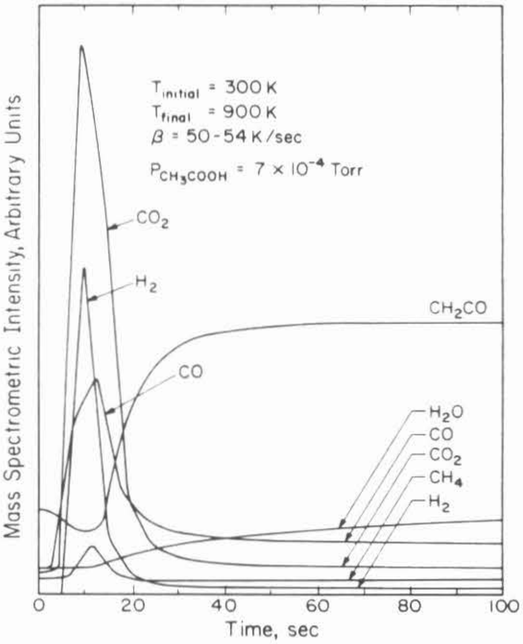

Fig. 1. Time evolution curves for the production of CO, CO_2, H_2, CH_4, H_2O and CH_2CO (ketene) during constant exposure of an initially clean platinum surface to acetic acid at 7×10^{-4} Torr. At $t = 0$, the surface temperature was increased linearly at a rate of 50–54 K/s from 300 to 900 K, and thereafter held constant at 900 K. The parent ion mass spectrometric signal was monitored in each case. The data are uncorrected for relative mass spectrometric sensitivities, fragmentation and pumping speeds.

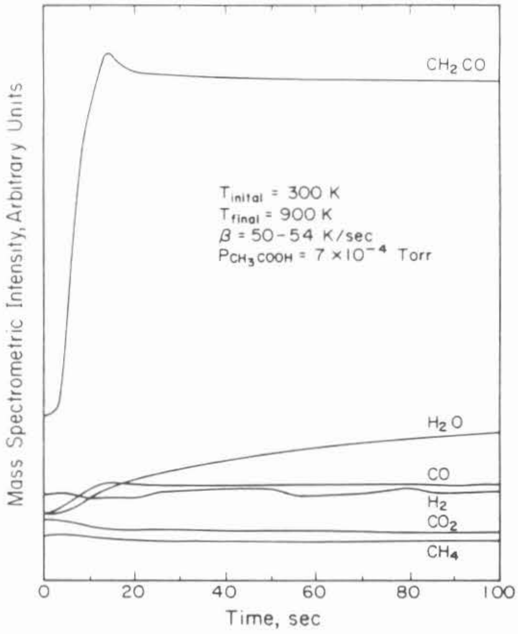

Fig. 2. Time evolution curves for the production of CO, CO_2, H_2, CH_4, H_2O and ketene during continuous exposure to acetic acid at 7×10^{-4} Torr. The platinum surface was first exposed to acetic acid at 900 K, as in fig. 1, and then cooled to 300 K. The final temperature was 900 K, and the linear heating rate was 50–54 K/s. The apparent increase in the CO signal is due entirely to a fragmentation product of the parent ketene.

rate, as is shown in fig. 2. The reactivities displayed in figs. 1 and 2 indicate that the surface has been altered chemically by the initial decomposition reaction, and that a different surface is created that gives rise to a steady-state rate of dehydration of acetic acid.

Thermal desorption measurements from the platinum surface, exposed to acetic acid as in fig. 1, shows only ketene desorption. Although the desorption of water was not detected, adsorption on the walls of the vacuum system would have precluded its detection under these conditions. Furthermore, as described in detail in section 3.4, the reaction with oxygen of a surface exposed to acetic acid at temperatures above 500 K produced CO_2 and CO with an approximate ratio of 5 : 1. This indicates that after the transient decomposition of acetic acid, the platinum surface contains substantial quantities of adsorbed carbon.

3.2. Decomposition of $CH_3{}^{13}COOH$

In order to investigate further the surface reactions of acetic acid which produce CO, CO_2, H_2 and adsorbed carbon, continuous flow decomposition measurements were made with $CH_3{}^{13}COOH$ employing a range of heating rates between 2 and 54 K/s with corresponding final surface temperatures between 500 and 900 K. Figs. 3 and 4 show the rate of production of ^{13}CO, CO, $^{13}CO_2$ and H_2 during exposure of the initially clean platinum surface at 300 K to 7×10^{-4} Torr of $CH_3{}^{13}COOH$ with heating rates of 50–54 and 4–6 K/s, respectively. The results shown in fig. 3, which are similar to those in fig. 1, indicate that $^{13}CO_2$ and H_2 are the major decomposition products. In addition, both ^{13}CO and CO are produced, indicating the occurrence of oxidation of the carbon atom of the methyl group of acetic acid [24]. On the other hand, when the surface is heated at a rate of 4–6 K/s, CO, ^{13}CO and H_2 are the major reaction products, as may be seen in fig. 4. Although the product signals shown in fig. 4 have declined to their background values, additional CO, CO_2 and H_2 can be produced by increasing the surface temperature. However, surfaces heated to 800 K or higher are deactivated completely with respect to the formation of CO, CO_2 and H_2.

An absolute calibration of the areas under the $^{13}CO_2$ curves indicates the production of increasing amounts of $^{13}CO_2$ with increasing final surface temperatures (for temperatures below 800 K). A maximum of $(2.5–3.1) \times 10^{15}$ molecules cm^{-2} is produced for surface temperatures above 800 K. Calibration of the quantities of H_2 and ^{13}CO that are produced indicates a molar ratio of H_2 to total ^{13}C (i.e. $^{13}CO_2 + + {}^{13}CO$) of approximately two, independent of final temperature.

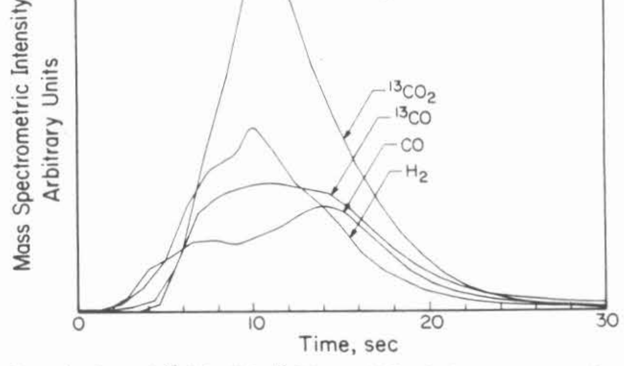

Fig. 3. Rates of production of ^{13}CO, CO, $^{13}CO_2$ and H_2 during exposure of an initially clean platinum surface to $CH_3{}^{13}COOH$. At $t = 0$, the temperature was increased from 300 to 900 K with a linear heating rate of 50–54 K/s.

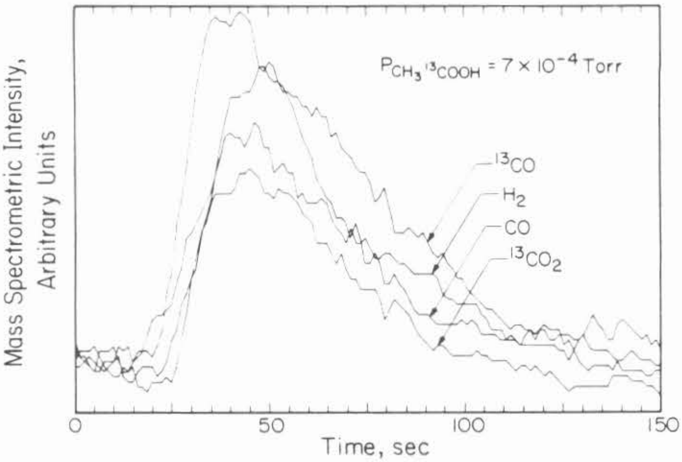

Fig. 4. As for fig. 3, except that the heating rate is 4–6 K/s and the final surface temperature is 545 K.

The fraction of acetic acid which decomposes to ^{13}CO, determined by the ratio of the area of ^{13}CO to the total area of ^{13}CO and $^{13}CO_2$, is shown in fig. 5 as a function of heating rate. Fig. 5 quantifies the qualitative trend observed in figs. 3 and 4. For low heating rates, ^{13}CO is the major product with respect

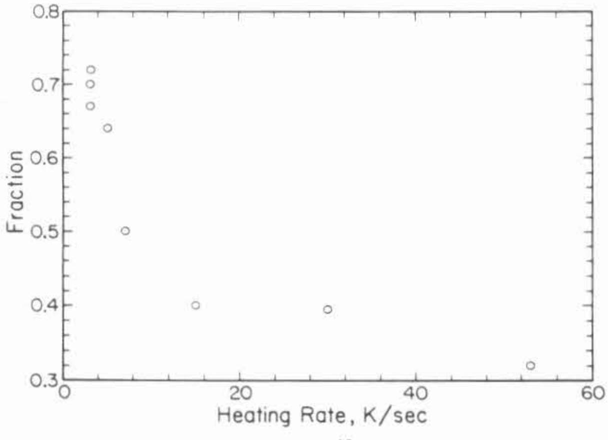

Fig. 5. Fraction of acetic acid that decomposes to ^{13}CO as a function of the heating rate. This fraction is defined as the ratio of the area under the ^{13}CO evolution curve to the total areas of the ^{13}CO and $^{13}CO_2$ curves. The areas were corrected for relative mass spectrometric sensitivities, fragmentation and pumping speeds.

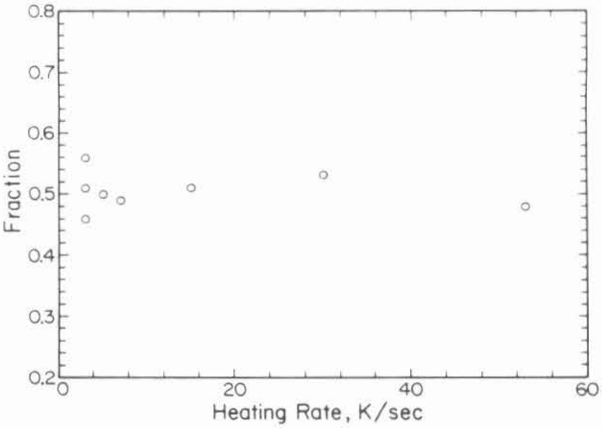

Fig. 6. Fraction of the total number of carbon monoxide molecules produced during the decomposition of $CH_3{}^{13}COOH$ which is ^{13}CO as a function of the heating rate.

to $^{13}CO_2$. As the heating rate increases, the fraction of acetic acid that decomposes to ^{13}CO decreases to a limiting value of 0.35 ± 0.05. The ratio of the amount of ^{13}CO produced to the total mount of carbon monoxide produced ($^{13}CO + CO$) is independent of heating rate, as shown in fig. 6. Moreover, this ratio is 0.5 ± 0.05, indicating that, independent of heating rate, equal quantities of CO and ^{13}CO are produced.

3.3. Thermal desorption mass spectrometry

Thermal desorption spectra following large exposures (approximately 0.1 Torr · s) of unlabeled acetic acid on the initially clean platinum surface at 300 K were recorded by transferring the sample into the high vacuum section of the microreactor, as described in section 2. Carbon monoxide desorbed in a single, broad peak with a maximum at 435–450 K. Similarly, CO_2 and H_2 desorbed with peak maxima at 425 and 440 K, respectively. No other products (e.g. acetic acid or water) were observed. However, since there was no line-of-slight between the mass spectrometer and the platinum surface, the sensitivity to small concentrations of acetic acid and water is poor. Calibrations of the thermal desorption spectra for CO_2 and CO indicate the desorption of approximately 3×10^{13} and 4×10^{14} molecules cm^{-2}, respectively.

3.4. Oxygen titration measurements

Carbon adatom concentrations, determined by the CO and CO_2 mass spectrometric intensities during reaction in 3×10^{-4} Torr of oxygen at 900 K,

Table 1
Surface carbon atom concentrations ρ_C

Decomposed species	Pressure [a] (Torr)	ρ_C (10^{15} cm^{-2})
Acetic acid	1×10^{-6}	1.5 [b]
	7×10^{-4}	2.6–3.5 [c]
	0.1	5.9 [b]
Ethylene	7×10^{-4}	2.4 [b]
$CH_3{}^{13}COOH$	7×10^{-4}	3.0 [b] (^{12}C) 0.15[b] (^{13}C)

[a] All exposures were for 90 s at 900 K.

[b] Value determined from a single measurement.

[c] Values indicate the range of six measurements.

are shown in table 1 (following 90 s exposures to acetic acid at pressures of 10^{-6}, 7×10^{-4} and 0.1 Torr at 900 K). The concentrations of surface carbon from ethylene decomposition and both ^{13}C and ^{12}C from $CH_3{}^{13}COOH$ decomposition are also shown in table 1. The concentrations of surface carbon vary only slightly with pressure and are nearly identical for acetic acid and ethylene. In addition, for the decomposition of acetic acid, more than 95% of the surface carbon originates from the methyl group. For comparison, the surface atom densities of Pt(111) and of the basal plane of graphite are 1.5×10^{15} and 3.8×10^{15} cm^{-2}, respectively.

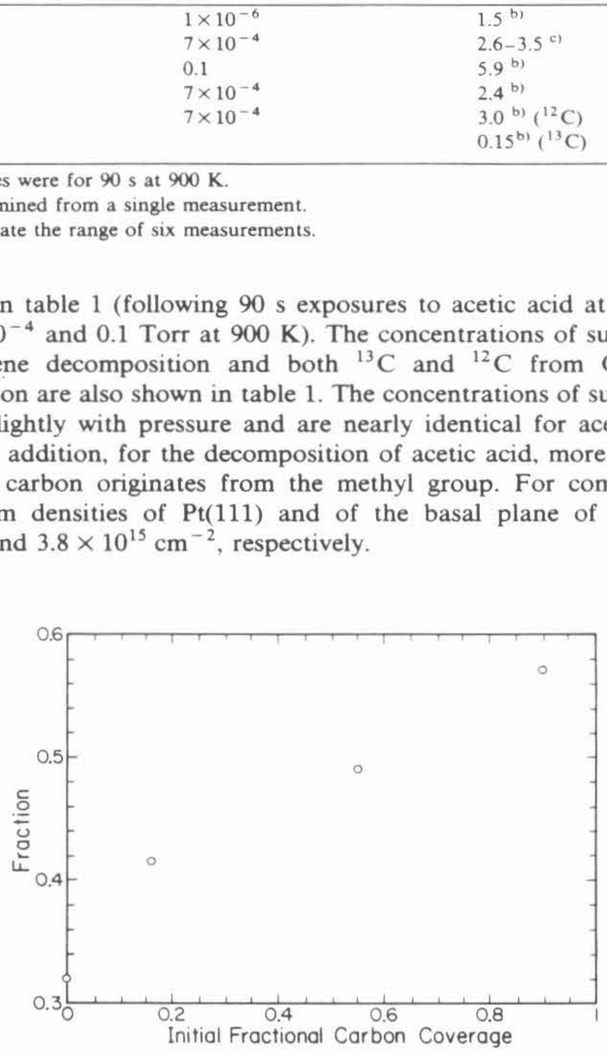

Fig. 7. Fraction of the $CH_3{}^{13}COOH$ which decomposes to ^{13}CO relative to $^{13}CO + {}^{13}CO_2$ as a function of initial fractional carbon coverage. In each case the heating rate was 50–54 K/s, and the initial and final temperatures were 300 and 900 K. The surfaces were prepared by exposure to acetic acid, and the initial carbon coverages were determined by oxygen titration in separate measurements.

3.5. Effects of surface carbon

The effects of adsorbed carbon on the decomposition of acetic acid were investigated by determining the fraction of acetic acid ($CH_3{}^{13}COOH$) which decomposes to ^{13}CO on surfaces with varying initial fractional coverages of ^{12}C. In these measurements, a clean platinum surface was heated to various temperatures between 500 and 700 K during exposure to acetic acid to deposit a known concentration of carbon adatoms, and then cooled to 300 K. Subsequently, the surface was heated to 900 K ($\beta = 50$–54 K/s), and the fraction of acetic acid which decomposes to ^{13}CO was determined. The initial concentration of carbon adatoms was determined from oxygen titration measurements, in which an identical exposure of acetic acid was used, followed by evacuation at 300 K and annealing for 30 s to 900 K to remove or decompose any adsorbed acetic acid. The results, shown in fig. 7, indicate that the fraction of acetic acid which decomposes to ^{13}CO increases with increasing initial carbon coverage. Note that the *final* carbon coverage in each case is identical, as verified by subsequent oxygen titration measurements. In addition, the temperature corresponding to the maximum rate of decomposition is shifted upward for both ^{13}CO and $^{13}CO_2$ on the carbon-covered surfaces, compared to the initially clean surface.

4. Discussion

4.1. Reaction stoichiometry

The decomposition of $CH_3{}^{13}COOH$ on an initially clean polycrystalline platinum surface yields predominantly ^{13}CO, CO, $^{13}CO_2$, H_2 and adsorbed carbon [C(a)]. Small quantities of $^{13}C(a)$ and CH_4 are also produced. Two *overall* reactions can account for the major products, namely,

$$CH_3{}^{13}COOH \rightarrow {}^{13}CO_2 + 2\,H_2 + C(a), \tag{1}$$

$$CH_3{}^{13}COOH \rightarrow {}^{13}CO + CO + 2\,H_2. \tag{2}$$

the adsorbed carbon from reaction (1) poisons both of these reactions, as shown in fig. 1, producing a surface on which the steady-state dehydration of acetic acid to ketene occurs.

Although water was not detected mass spectrometrically, adsorption on the walls of the vacuum chamber might have masked observation of the transient production of water. The following arguments, however, demonstrate clearly that water is not a major reaction product. As illustrated in fig. 6, equal quantities of ^{13}CO and CO are produced, independent of surface temperature (and heating rate). If any acetic acid decomposed to form water via

$$CH_3{}^{13}COOH \rightarrow {}^{13}CO + H_2 + H_2O + C(a), \tag{3}$$

then more ^{13}CO than CO would necessarily have been produced. Furthermore, the saturation carbon adatom density of $(2.6–3.5) \times 10^{15}$ atoms cm^{-2}, determined from oxygen titration measurements, is equal to the total number of $^{13}CO_2$ molecules that are produced, $(2.5–3.1) \times 10^{15}$ adatoms cm^{-2}. This confirms that reaction (1) is only significant source of surface carbon and that little, if any, water is produced. Moreover, a material balance indicates a 2 : 1 molar ratio of H_2 to the total amount of ^{13}C that is produced, which is inconsistent with the stoichiometry of reaction (3). Furthermore, CO_2 is not a major reaction product. This conclusion follows from the observation that equal quantities of ^{13}CO and CO and negligible quantities of $^{13}C(a)$ are produced. The production of CO_2 is, therefore, inconsistent with the stoichiometries of reactions (1) and (2).

4.2. Production of carbon dioxide versus carbon monoxide

Electron energy loss measurements have established that acetic acid dissociates upon adsorption on Pt(111) at 225 K to form a bidentate acetate species [20]. Moreover, a bidentate formate species has been identified with EELS on many transition metal surfaces, including the Pt(111) [15,16], Ni(110) [10] and Ru(001) [12,13] surfaces. Since a similar species on the polycrystalline surface studied here is likely, the following discussion presumes that a bidentate acetate species is formed upon dissociative adsorption of $CH_3{}^{13}COOH$. The acetate may decompose by either $C–{}^{13}C$ or $^{13}C–O$ bond cleavage. Since surface reaction(s) of $^{13}CO_2(a)$ do not occur due to its short residence time [25], $C–{}^{13}C$ bond cleavage in the acetate leads directly to the desorption of $^{13}CO_2$ and the formation of $CH_{3-x}(a) + xH(a)$, where x can be 0, 1, 2 or 3, depending on the surface temperature. Ultimately, C(a) is formed, and the hydrogen desorbs as H_2. Decomposition of the adsorbed acetate via $^{13}C–O$ bond cleavage followed by $C–{}^{13}C$ bond cleavage produces $^{13}CO(a)$, O(a) and $CH_{3-x}(a) + xH(a)$. Subsequent surface reactions of these species could lead to either $^{13}CO_2$ and C(a) or ^{13}CO and CO depending on the relative rates of oxidation of $^{13}CO(a)$ and C(a). However, as discussed below, the oxidation of $^{13}CO(a)$ was found not bo be a major reaction pathway. Since water is not a reaction product, all of the hydrogen desorbs as H_2.

The peak temperatures of 425 and 440 K, observed for the desorption of CO_2 and H_2 following adsorption of unlabeled acetic acid, are indicative of reaction-limited kinetics. The small difference in peak temperatures observed for CO_2 and H_2 is due to the decomposition of CH_x species on this surface. In addition, H_2 production during the continuous flow transient decomposition experiments is coincident with the production of $^{13}CO_2$, as shown in figs. 3 and 4. These results imply that the reaction step which controls the overall rate of production of $^{13}CO_2$ is the decomposition of the surface acetate. The desorption of CO, which occurs by oxidation of C(a), occurs earlier than the desorption of either ^{13}CO or $^{13}CO_2$, as may be seen in fig. 4 at $t = 20$ s [26]. Since $^{13}CO_2$ would desorb immediately upon formation at these temperatures, the C(a) which ultimately appears as CO is necessarily produced together with $^{13}CO(a)$ and O(a), i.e. via ^{13}C–O bond cleavage in the adsorbed acetate. Furthermore, CO(a) is produced on the surface before the desorption of carbon monoxide occurs. Both CO(a) and $^{13}CO(a)$ are present on the surface and, therefore, have equal probabilities of being oxidized to CO_2 and $^{13}CO_2$, respectively. Since CO_2 was shown not to be a reaction product, the oxidation of $^{13}CO(a)$ to $^{13}CO_2$ may also be excluded. Consistent with these results, the peak temperature observed for the desorption of carbon monoxide agrees with the results of carbon monoxide desorption from polycrystalline platinum [27,28].

As the heating rate is increased from 2 to 54 K/s, the fraction of acetic acid which decomposes to ^{13}CO on the platinum wire declines, as shown in fig. 5. This dependence implies that the reaction channels which produce $^{13}CO_2$ and ^{13}CO have different activation energies. For two competing reactions, the temperature dependence of the relative rates is given by $\exp[-(E_1 - E_2)/k_BT]$, where E_1 and E_2 are the activation energies for the two reactions. Thus, the fraction of the reactant that reacts via the lower activation energy pathway will decrease at higher temperatures (i.e. higher heating rates). Decomposition of acetic acid via C–^{13}C bond cleavage produces $^{13}CO_2$, whereas initial ^{13}C–O bond cleavage leads to the production of ^{13}CO. Therefore, the dependence shown in fig. 5 indicates that the apparent activation energy for the formation of $^{13}CO_2$ is larger than the apparent activation energy for the production of ^{13}CO. As discussed in section 1, similar behavior has been observed for acetic acid decomposition on the Pt(111) surface [20] and for formic acid decomposition on Ni(111), Ni(110) and Ru(001) surfaces [9,11,13].

4.3. Effects of surface carbon

For carbon adatom concentrations of approximately 3×10^{15} cm^{-2}, the reactions producing ^{13}CO, CO, $^{13}CO_2$ and H_2 from $CH_3{}^{13}COOH$ are poisoned completely. However, for lower carbon coverages, these reactions are not poisoned totally, and the fraction of the $CH_3{}^{13}COOH$ which decomposes to ^{13}CO is shown as a function of the initial fractional carbon coverage in fig. 7. As the initial carbon coverage increases, the fraction of acetic acid which decomposes to ^{13}CO increases. This result implies that while both reactions are ultimately poisoned by adsorbed carbon, the reaction producing $^{13}CO_2$ is poisoned selectively. Since the reaction pathways producing $^{13}CO_2$ also produce additional adsorbed carbon, unoccupied surface sites must be available for these reactions to occur. Thus, on a surface containing a partial overlayer of carbon adatoms, the selective poisoning of reaction (1) with respect to reaction (2) is reasonable.

4.4. Nature of the saturated carbon overlayer

The surface atom density of carbon produced by the decomposition of acetic acid, $(2.6-3.5) \times 10^{15}$ cm^{-2}, corresponds to approximately one monolayer of the basal plane of graphite, 3.8×10^{15} cm^{-2}. While the carbon overlayer could not be examined spectroscopically in the present work, other studies of carbon deposition on platinum [29–33] and nickel [34,35] surfaces strongly support the conclusion that the carbon overlayer produced from acetic acid decomposition at the elevated temperatures of interest here is graphitic. For example, exposure of the Ni(110) surface to ethylene at temperatures above 600 K led to the formation of an overlayer with a surface carbon atom concentration of 3.35×10^{15} cm^{-2} and a carbon Auger peak with a graphitic shape [35]. A graphitic overlayer has also been prepared on Pt(111) by exposing the surface to ethylene at 300 K and annealing briefly to 873 K [32]. On the basis of these results and considering the reaction conditions of our experiments, it appears certain that the carbon overlayer formed both from acetic acid and from ethylene, which yield similar carbon adatom concentrations, is graphitic.

5. Synopsis

The results of this study may be summarized as follows:

(1) On an initially clean polycrystalline platinum surface, $CH_3{}^{13}COOH$ at 7×10^{-4} Torr decomposes at temperatures above approximately 400 K to ^{13}CO, CO, $^{13}CO_2$, CH_4, H_2 and adsorbed carbon. The adsorbed carbon eventually poisons the reactions that produce these products.

(2) At temperatures above approximately 800 K, the carbon overlayer is graphitic with a carbon adatom concentration of $(2.6-3.5) \times 10^{15}$ cm^{-2}.

(3) On the graphitized platinum surface, the steady-state dehydration of acetic acid to ketene is the only reaction that is observed.

(4) The fraction of acetic acid which decomposes to ^{13}CO relative to $^{13}CO_2$ depends both on the surface temperature and the carbon adatom concentration. The production of ^{13}CO is favored at lower temperatures and higher carbon coverages.

Acknowledgment

This work was supported by the National Science Foundation under Grant No. DMR-8500789.

References

[1] K. Fukuda, S. Nagashima, Y. Noto, T. Onishi and K. Tamaru, Trans. Faraday Soc. 64 (1968) 522.
[2] E.M.A. Willhoft and A.J.B. Robertson, J. Catalysis 9 (1967) 358.
[3] G.M. Schwab and A.M. Watson, Trans. Faraday Soc. 60 (1964) 1833.
[4] P. Mars, J. Schloten and P. Zwietering, Advan. Catalysis 14 (1963) 35.
[4] P. Mars, J. Schloten and P. Zwitering, Advan. Catalysis 14 (1963) 35.
[5] J. Block and J. Vogl, Z. Elektrochem. 63 (1959) 3.
[6] B.A. Sexton, Surface Sci. 88 (1979) 319.
[7] S.L. Miles, S.L. Bernasek and J.L. Gland, Surface Sci. 127 (1983) 271.
[8] M. Chtaib, P.A. Thirty, J.P. Delrue, J.J. Pireaux and R. Caudano, J. Electron Spectrosc. 29 (1983) 293.
[9] R.J. Madix and J.L. Falconer, Surface Sci. 51 (1975) 546.
[10] R.J. Madix, J.L. Gland, G.E. Mitchell and B.A. Sexton, Surface Sci. 125 (1983) 481.
[11] J.B. Benziger and G.R. Schoofs, J. Phys. Chem. 88 (1984) 4439.
[12] B.H. Toby, N.R. Avery, A.B. Anton and W.H. Weinberg, J. Electron Spectrosc. 29 (1983) 318.
[13] B.H. Toby, N.R. Avery, M.M. Hills and W.H. Weinberg, in preparation.
[14] N. Abbas and R.J. Madix, Appl. Surface Sci. 16 (1983) 424.
[15] N.R. Avery, Appl. Surface Sci. 11/12 (1982) 774.
[16] N.R. Avery, Appl. Surface Sci. 14 (1982–83) 149.
[17] G.E. Gdowski, J.A. Fair and R.J. Madix, Surface Sci. 127 (1983) 541.
[18] R.J. Madix, J.L. Falconer and A.M. Suszko, Surface Sci. 54 (1976) 6.
[19] G.R. Schoofs and J.B. Benziger, Surface Sci. 143 (1984) 359.
[20] N.R. Avery, J. Vacuum Sci. Technol. 20 (1982) 592.
[21] J.J. Vajo, Y.-K. Sun and W.H. Weinberg, J. Phys. Chem. 91 (1987) 1153.
[22] J.J. Vajo, W. Tsai and W.H. Weinberg, Rev. Sci. Instr. 56 (1985) 1439.
[23] J.J. Vajo, W. Tsai and W.H. Weinberg, J. Phys. Chem. 89 (1985) 3243.
[24] The complete oxidation of the methyl group carbon atom to CO_2 could not be monitored due to an overlap with a major fragmentation product of $CH_3{}^3COOH$ at 44 amu.
[25] G. Ertl, in: Catalysis Science and Technology, Vol. 4, Eds., J.R. Anderson and M. Boudart (Springer, New York, 1983) p. 209.
[26] This result indicates that CO is produced by the oxidation of C(a) at temperatures below the desorption temperature of carbon monoxide and that at least a fraction of this CO desorbs at a slightly lower temperature than would be expected for desorption of carbon monoxide. This may not be particularly surprising in view of the large carbon–oxygen bond energy in carbon monoxide, which renders the surface oxidation reaction highly exothermic leading to the production of "activated" CO(a).
[27] R.A. Shigeishi and D.A. King, Surface Sci. 58 (1976) 379.
[28] Y. Nishiyama and H. Wise, J. Catalysis 32 (1974) 50.
[29] D.L. Smith and R.P. Merrill, J. Chem. Phys. 52 (1970) 5861.
[30] W.H. Weinberg, H.A. Deans and R.P. Merrill, Surface Sci. 41 (1974) 312.
[31] B. Lang, Surface Sci. 53 (1975) 317.
[32] M. Abon, J. Billy, J.C. Bertolini and B. Tardy, Surface Sci. 167 (1986) 1.
[33] F.P. Netzer and R.A. Wille, J. Catalysis 51 (1978) 18.
[34] R. Sau and J.B. Hudson, Surface Sci. 102 (1981) 239.
[35] R. Sau and J.B. Hudson, Surface Sci. 95 (1980) 465.